

# Operational Multi-Scale Environment Model with Grid Adaptivity, Version 4.0, Volume 1 - Model Enhancements

Approved for public release; distribution is unlimited.

September 2000



Prepared for:  
Defense Threat Reduction Agency  
45045 Aviation Drive  
Dulles, VA 20166-7517

**20010320 079**

DNA 001-95-C-0130

David P. Bacon, et. al.

Prepared by: Science Applications International Corporation  
P.O. Box 1303  
McLean, VA 22102

*Technical Report*

**DESTRUCTION NOTICE:**

Destroy this report when it is no longer needed. Do not return to sender.

PLEASE NOTIFY THE DEFENSE THREAT REDUC-  
TION AGENCY, ATTN: ADM, 45045 AVIATION  
DRIVE, DULLES, VA 20166-7517, IF YOUR ADDRESS  
IS INCORRECT, IF YOU WISH IT DELETED FROM  
THE DISTRIBUTION LIST, OR IF THE ADDRESSEE IS  
NO LONGER EMPLOYED BY YOUR ORGANIZATION.

# DISTRIBUTION LIST UPDATE

This mailer is provided to enable DTRA to maintain current distribution lists for reports. (We would appreciate you providing the requested information.)

- Add the individual listed to your distribution list.
- Delete the cited organization/individual.
- Change of address.

**Note:**  
Please return the mailing label from the document so that any additions, changes, corrections or deletions can be made easily. For distribution cancellation or more information call DTRA/ADM (703) 325-1036.

NAME: \_\_\_\_\_

ORGANIZATION: \_\_\_\_\_

**OLD ADDRESS**

**NEW ADDRESS**

\_\_\_\_\_  
\_\_\_\_\_  
\_\_\_\_\_

\_\_\_\_\_  
\_\_\_\_\_  
\_\_\_\_\_

TELEPHONE NUMBER: (    ) \_\_\_\_\_

**DTRA PUBLICATION NUMBER/TITLE**

**CHANGES/DELETIONS/ADDITIONS, etc.)**  
*(Attach Sheet if more Space is Required)*

\_\_\_\_\_  
\_\_\_\_\_  
\_\_\_\_\_

\_\_\_\_\_  
\_\_\_\_\_  
\_\_\_\_\_

DTRA or other GOVERNMENT CONTRACT NUMBER: \_\_\_\_\_

CERTIFICATION of NEED-TO-KNOW BY GOVERNMENT SPONSOR (if other than DTRA):

SPONSORING ORGANIZATION: \_\_\_\_\_

CONTRACTING OFFICER or REPRESENTATIVE: \_\_\_\_\_

SIGNATURE: \_\_\_\_\_

CUT HERE AND RETURN

**DEFENSE THREAT REDUCTION AGENCY  
ATTN: ADM  
45045 AVIATION DRIVE  
DULLES, VA 20156-7517**

**DEFENSE THREAT REDUCTION AGENCY  
ATTN: ADM  
6801 TELEGRAPH ROAD  
ALEXANDRIA, VA 22310-3398**

# REPORT DOCUMENTATION PAGE

*Form Approved*  
OMB No. 0704-0188

Public reporting burden for this collection of information is estimated to average 1 hour per response, including the time for reviewing instructions, searching existing data sources, gathering and maintaining the data needed, and completing and reviewing the collection of information. Send comments regarding this burden estimate to any other aspect of this collection of information, including suggestions for reducing this burden, to Washington Headquarters Services, Directorate for Information Operations and Reports, 1215 Jefferson Davis Highway, Suite 1204, Arlington, VA 22202-4302, and to the Office of Management and Budget, Paperwork Reduction Project (0704-0188), Washington, DC 20503.

<b>1. AGENCY USE ONLY (Leave blank)</b>		<b>2. REPORT DATE</b>		<b>3. REPORT TYPE AND DATES COVERED</b> Technical 950615 - 980930	
<b>4. TITLE AND SUBTITLE</b> Operational Multi-scale Environment Model with Grid Adaptivity, Version 4.0, Volume 1 - Model Enhancements			<b>5. FUNDING NUMBERS</b> C DNA001-95-C-0130 PE - 62715H PR - AC TA - BA WU - DH50464, DH52120		
<b>6. AUTHOR(S)</b> David P. Bacon, Christopher Agritellis, Nash'at Ahmad, Zafer Boybeyi, Thomas J. Dunn, Mary Hall, Yi Jin, Pius Lee Rangarao Madala, Douglas E. Mays, Ananthakrishna Sarma,					
<b>7. PERFORMING ORGANIZATION NAME(S) AND ADDRESS( ES)</b> Science Applications International Corporation P.O. Box 1303 McLean, VA 22102			<b>8. PERFORMING ORGANIZATION REPORT NUMBER</b>  SAIC-99/1051		
<b>9. SPONSORING /MONITORING AGENCY NAME(S) AND ADDRESS( ES)</b> Defense Threat Reduction Agency 45045 Aviation Drive Dulles, VA 20166-7517 CPWT / Smith			<b>10. SPONSORING /MONITORING AGENCY REPORT NUMBER</b>  DTRA-TR-98-82-V1		
<b>11. SUPPLEMENTARY NOTES</b> This work was sponsored by Defense Threat Reduction Agency under RDT&E RMC code B 4662 D AC BA 50464 4400 A BA 25904D.					
<b>12a. DISTRIBUTION/AVAILABILITY STATEMENT</b> Approved for public release; distribution is unlimited				<b>12b. DISTRIBUTION CODE</b>	
<b>13. ABSTRACT (Maximum 200 words)</b> This report details the status of the Operational Multi-scale Environment model with Grid Adaptivity (OMEGA). OMEGA is a nonhydrostatic atmospheric simulation system, which includes a graphical user interface (GUI), a grid generator, a data preprocessor, the atmospheric forecast model, and visualization postprocessor. It also includes terrain, land-water, and climatological surface datasets, and scripts that allow the model to be setup and run operationally. This report discusses the primary features of OMEGA with special emphasis to the improvements made under this contract. The improvements include a time-splitting scheme which groups the grid cells into masks that can use similar timesteps resulting in considerable computational savings; air-surface interaction routines that take into account nonhomogeneous surface properties; a Lagrangian particle model that takes into account turbulent fluctuations in the momentum of air; and scripts which allow the automatic execution of the model from data ingest to results postprocessing. A major improvement to the system has been the dynamic adaptation capability by which the model grid adapts to runtime flow-characteristics to maintain the accuracy of solution and yet save computational cycles. Another modification to improve runtime performance is the addition of Message Passing Interface (MPI) calls to implement parallelization.					
<b>14. SUBJECT TERMS</b> Hazard Prediction                      Atmospheric Dispersion Unstructured Grid                      Numerical Weather Prediction Adaptive Grid                            Atmospheric Prediction				<b>15. NUMBER OF PAGES</b>	
				<b>16. PRICE CODE</b>	
<b>17. SECURITY CLASSIFICATION OF REPORT</b> UNCLASSIFIED	<b>18. SECURITY CLASSIFICATION OF THIS PAGE</b> UJNCLASSIFIED	<b>19. SECURITY CLASSIFICATION OF ABSTRACT</b> UNCLASSIFIED	<b>20. LIMITATION OF ABSTRACT</b> SAR		

SECURITY CLASSIFICATION OF THIS PAGE

**CLASSIFIED BY:**

N/A since Unclassified

**DECLASSIFY ON:**

N/A since Unclassified

6. AUTHOR(S) (Continued)

Mark Turner, Timothy Wait (SAIC)

Pam E. Price, Steven Young, Kenneth Waight and John Zack (MESO, Inc.)

7. PERFORMING ORGANIZATION NAME(S) AND ADDRESS(ES) (Continued)

MESO, Inc.

185 Jordan Road

Troy, NY 12180

## Preface

This marks the culmination of about six years of very exciting and fast-paced research. Science Applications International Corporation (SAIC) feels very privileged to work on the “Hazard Predication and Assessment Capability/Weather” project and to provide the Defense Special Weapons Agency (DSWA) a landmark capability to accurately predict the transport and dispersion of hazardous materials in air. This capability is manifested in the Operational Multiscale Environment Model with Grid Adaptivity (OMEGA) which significantly advances the state-of-the-art in numerical weather prediction. OMEGA integrates into one model the advances in the fields of computational fluid dynamics, numerical algorithms, atmospheric dynamics and physics, and atmospheric dispersion and transport; most of these advances have been the results of prior DSWA programs. The work presented in this report and its companion “The Operational Multiscale Environment Model with Grid Adaptivity, Volume 2 – Model Validation and Verification” represents the work performed by a team forming the Center of Atmospheric Physics of SAIC, with the support and guidance of several individuals at DSWA and SAIC. The SAIC’s OMEGA modeling team has enjoyed the constant support and inspiration of Dr. George Ullrich, Mr. Clifton McFarland and Dr. Leon Wittwer of DSWA, and the expert guidance of Lt.Col. James Hodge, PhD., who served as the DSWA’s technical monitor for this contract and his successor in that role Maj. Thomas Smith.

## Table of Contents

Section	Page
Preface	iii
Figures	vii
Tables	xi
1 Introduction	1
2 Program Philosophy: The OMEGA Architecture	3
2.1 Unstructured Adaptive Grids	4
2.2 Embedded Atmospheric Dispersion Model	9
2.3 Operational Considerations	10
3 Solution of Governing Equations	12
3.1 Fundamental Equation Set	12
3.2 Hydrodynamic Solver	14
4 Model Physics	25
4.1 Turbulence and the Planetary Boundary Layer	25
4.2 Air Surface Interactions	29
4.3 Microphysics	36
4.4 Radiation	51
5 Grid Generation and Adaptation	54
5.1 Grid Definition	54
5.2 Grid Generation	56
5.3 Surface Characteristics Databases	61
5.4 Static Grid Adaptation	63
5.5 Grid Editor	66
5.6 Dynamic Grid Adaptation	67
6 Initial and Boundary Conditions	69
6.1 Data Ingestion	71
6.2 Processing of Surface Characteristics Databases	73
6.3 Processing of Real-Time Hydrology Data	74
6.4 PREPDAT Module	75
6.5 GENINIT Module	77
6.6 ANALYSIS Module	78
6.7 Preparation of Lateral Boundary Conditions	86



## Table of Contents (Continued)

Section		Page
7	Model Boundary Conditions	87
7.1	Lower Boundary Conditions	87
7.2	Lateral Boundary Conditions	88
7.3	Upper Boundary Conditions	89
8	Atmospheric Dispersion Model Structure	91
8.1	Overview	91
8.2	Eulerian Model	91
8.3	Lagrangian Particle Model	91
8.4	Probabilistic Puff Model	96
8.5	Lagrangian Model Modes of Operation	100
9	Dynamic Grid Adaptation	101
9.1	Introduction	101
9.2	Methodology	102
9.3	Adaptation Criteria	102
9.4	Pseudo-Laplacian Interpolation	103
9.5	Adaptation to Atmospheric Dispersion	104
9.6	Effects of Improving the Underlying Terrain	105
9.7	Adaptation to Velocity Deformation	108
10	Parallelization	111
11	XOMEGA Graphical User Interface	117
11.1	Overview	117
11.2	OMEGA Shell Script Interface	118
11.3	XOMEGA	120
11.4	Set Time Domain	126
11.5	Set Spatial Domain	128
11.6	Set ADM Sources	134
11.7	Run Grid Generator	138
11.8	Set Meteorology	140
11.9	Fetch Meteorology	143
11.10	Run Preprocessor	145
11.11	Run OMEGA Model	147

## Table of Contents (Continued)

Section		Page
12	OMEGA Output and Visualization	150
	12.1 OMEGA Output	150
	12.2 X-Grid - OMEGA Visualization Tool	150
	12.3 OMEGA Simulation Image Maker (OSM)	154
13	Conclusions	160
14	References	161
	Distribution List	DL-1

## Figures

Figure		Page
1	OMEGA grid element	5
2	OMEGA coordinate system and vertical alignment of OMEGA grid	5
3	Vertex addition and reconnection	7
4	Vertex deletion and reconnection	7
5	Vertex relaxation and edge bifurcation	8
6	OMEGA represents a balance of physical, numerical, and operational considerations	11
7	Arrangement of the variables on a 2-dimensional unstructured-grid. The generic advected variable, $\psi$ , is placed at cell centroids. The subscripts L and R designates their left-hand-side and right-hand-side cell placements. The velocity is decomposed into normal and parallel components (not to scale). The flux $F$ is co-located with $V_n$ at the face centers, and points only in the normal direction	14
8	Rotating cone advection test	17
9	Rotating cone advection test after five rotations	18
10	Error scaling with grid resolution. Three measurements of deviation from the original cone are used: root-mean-square error over the whole mesh, root-mean-square error over an area extended by the original cone, and deviation in the height of the cone	19
11	The ghost triangle used in the calculation of the Laplacian	21
11	A local coordinate system defines the horizontal plane passing through the centroid of each triangle.	21
13	Advection test consisting of a passive scalar in a steady-state flow field composed of six counter-rotating vortices (left). The analytic solution at a given scaled time (from Staniforth) is shown (center); along with the second order solution at the for the OMEGA advection solver (right)	23
14	Coarse and two finer sub-domains for testing time splitting technique	24
15	Initial and final positions of the cone	24

## Figures (Continued)

Figure		Page
16	Microphysical processes parameterized in OMEGA	37
17	Using an appropriately chosen set of criteriz, OMEGA can generate a grid that captures the important physical features	55
18	Initial rectangular grid	57
19	Grid refinement	58
20	Grid after reconnection. The deleted edges are shown as dashed lines and the new edges are shown as thin lines	59
21	The vertical levels of the OMEGA grid are constructed by extending radials through each of the surface vertices. A set of stretchable layers exists near the surface with constant thickness layers above	60
22	Datasets used to initialized OMEGA	64
23	OMEGA grid for the Middle-East region used for gulf war analysis. The grid has been refined around data sources	65
24	Refined to regional interim emissions inventory	66
25	Test of the dynamic adaptation routine. The adaptation was to the presence of test particles (shown in red) initialized in the southwest corner of the grid and traveling on a prescribed trajectory	68
26	Data flow between the preprocessor and other OMEGA components	70
27	A particle $X_1$ , located in one element of the OMEGA unstructured grid, is evaluated using $A \times B$ . The cross product between the vector formed from the first vertex location to the current particle location, $\vec{A}$ , and the first vertex location to the second vertex location, $\vec{B}$ indicates a positive value of area with respect to $\vec{B}$ .	94
28	A particle, $X_1$ , located in one element of the OMEGA unstructured grid, is evaluated using $A \times B$ . The cross product between the vector formed from the first vertex location to the current location to the current particle location, $\vec{A}$ , and the vector formed from the first vertex location to the second vertex location, $\vec{B}$ indicates a negative value of area with respect to $\vec{B}$ .	94

## Figures (Continued)

Figure		Page
29	Computational grid for Case A simulation (left) and Case B simulation (right)	105
30	Particle locations for Case A simulation (left) and Case B simulation (right)	106
31	Time evolution of pressure perturbation field for the growing mountain case. Vertical cross sections at initialization (left), 8 minutes (center), and 15 minutes (right)	107
32	Pressure perturbation fields for 1000m static mountain case (left) and 350m-1000m growing mountain case (right) after 30 minutes into the simulation	107
33	Particle locations for 350m static mountain simulation (left); 1000m static simulation (center) and 350-1000m growing mountain simulation (right)	108
34	Simulations for the Four Corners, USA. Static (Case A) simulation results after 12 hours into the simulation are shown in the left panel and dynamically adapting simulation (Case B) results after 12 hours into the simulation are shown in the right panel	109
35	Adaptation to velocity deformation. Initial grid (left) and sea level pressure (right) at the start of the simulation	110
36	Adaptation to velocity deformation. Final grid (left) and sea level pressure (right) after 12 hours into the simulation	110
37	Speedup projection of the OMEGA code by a power Fortran compiler	112
38	File structure for the parallelized OMEGA code	113
39	The k10m model with one domain, 9 sub-domains and 16 sub-domains	114
40	Run time plotted as a function of processor allocation	115
41	Run time and parallel efficiency plotted as a function of processor allocation	115
42	Run time and parallel efficiency plotted as a function of processor allocation for a mainframe and a workstation cluster	116
43	Select Case	119
44	View Case	119

## Figures (Continued)

Figure		Page
45	XOMEGA	121
46	Set preferences dialog box	122
47	Map operations dialog box	124
48	Draw area features	125
49	Set time domain dialog box	127
50	Set spatial domain dialog box	129
51	Set refinement disks dialog box	133
52	Set ADM sources dialog box	135
53	Run grid generator dialog box	139
54	Set meteorology dialog box	142
55	Fetch meteorology dialog box	144
56	Run preprocessor dialog box	146
57	Run model dialog box	148
58	XGRID terrain view upon initial data load	151
59	Display of map and contour options	152
60	Zoomed in, with wind arrows	152
61	XGRID vertical cross section	153
62	XGRID profile	153
63	XGRID skewT-logP diagram	155
64	Field of regard and particle trajectories	156
65	Concentration values computed from the ADM Lagrangian tracers	156

## Figures (Continued)

Figure		Page
66	OSIM stage one	157
67	OSIM stage two	158
68	OSIM stage three	159

## Tables

Table		Page
1	Soil parameters of the USDA (United States Department of Agriculture) textural classes	34
2	High-resolution OMEGA terrain and land/water databases	56
3	Datasets used to determine surface characteristics	61
4	Summary of NCEP GRIB and BUFR data files ingested by PREPDAT	73
5	Summary of FNMOC data files ingested by PREPDAT	73
6	Summary of data types which can be ingested by PREPDAT	76
7	Observation increment error thresholds	80
8	Recommended values for user specified OI variables	83



## Section 1

### Introduction

The Operational Multiscale Environment model with Grid Adaptivity (OMEGA) and its embedded Atmospheric Dispersion Model (ADM) was designed to support critical studies and forecasts of hazardous atmospheric dispersal. OMEGA is a multi-scale, non-hydrostatic atmospheric simulation model with an adaptive grid that permits a variable spatial resolution that ranges from 100 km to 1 km without wave-reflecting internal boundaries. The model contains a 2.5 level explicit boundary layer formulation, surface layer physics with multiple soil layers and 12 soil types, a sophisticated explicit microphysics package with five water species and a four dimensional data analysis scheme based on the optimum interpolation technique. ADM is an atmospheric dispersion model that computes the dispersion of aerosols and gases. This report is split into two volumes. Volume 1 contains the OMEGA/ADM atmospheric forecast and dispersion system. Model validations against analytic and idealized test problems, and against meteorological and dispersion datasets are described in Volume 2.

This report is intended to replace the documentation of OMEGA v. 1.0 (Bacon, *et al.*, 1996). This report documents OMEGA v. 4.0, which includes capabilities for dynamic grid adaptation and a version, which has been parallelized via domain decomposition using the Message Passing Interface (MPI). Since the first report, many modifications, which are listed below, have been made to the model and its operational system. The major changes in the OMEGA system are:

- Multiple layer cell masking to improve model execution speed,
- Automatic incorporation of heterogeneous surface properties from archived databases,
- Improved boundary conditions (top, bottom, and lateral),
- Expanded data pre-processor options to permit a wider variety of input data,
- Splitting and merging of puffs and the development of a probabilistic transport model,
- Improved and expanded user interface,
- Development of scripts to support hands-free automated daily model execution including automatic generation of a standard graphics package,
- Explicit boundary layer formulation using a 2.5 level K-E scheme,
- Improved surface energy physics for improving surface forecasts with two soil layers and a canopy layer. Twelve soil types are allowed in the model,
- Inclusion of microphysics allowing five species of water and a cumulus parameterization for coarser resolution areas,
- Dynamic grid adaptation to increase resolution wherever and whenever needed,
- A faster time-split solver to reduce the OMEGA run time,
- User friendly data ingest routines,
- XGRID system visualization tool,
- Packed Binary data format to reduce the storage requirement without sacrificing data accuracy, and,
- Model parallelization to run on multi-processor computer systems.

The basic OMEGA grid architecture is described in Section 2. Section 3 describes governing equations and hydrodynamics solvers. Model physics is presented in Section 4. The OMEGA grid generator and dynamic adaptation for heterogeneous surface properties are presented in Section 5. Sections 6 and 7 describe model boundary conditions, data quality control methods and optimum interpolation data analysis technique. The atmospheric dispersion model used for particle and plume dispersion is described in Section 8. Dynamic adaptation for moving meteorological systems or for dispersing plumes is described in Section 9. Section 10 describes our recent progress in parallelizing the OMEGA code for massively parallel computers. A detailed description of the user friendly XOMEGA Graphical User Interface (GUI) is presented in Section 11. Section 12 describes the XGRID visualization package for OMEGA/ADM. It also contains a machine independent data storage technique (Packed Binary Format) developed for OMEGA; this technique substantially reduces data storage requirements for the system. As mentioned above, Volume 2 of this report contains model validation against analytic and idealized test problems, and against meteorological and dispersion data sets.

## Section 2

### Program Philosophy: The OMEGA Architecture

In order to improve the fidelity of hazardous transport models, it is essential that the meteorological forecast itself be improved. This is because the modeling of atmospheric dispersion involves virtually all scales of atmospheric motion from microscale turbulence to planetary scale waves. The current operational atmospheric simulation systems (Hoke, *et al.*, 1989; Janjic, 1990; Mesinger, *et al.*, 1988) are scale specific and cannot resolve the full spectrum required for the accurate forecast of local scale phenomena. Even with recent advances in computational power (McPherson, 1991), the current architecture and physics of today's generation of atmospheric models cannot fully simulate the scale interaction of the atmosphere. Recently, several groups have started the development of non-hydrostatic, nested (multiply nested in some cases) atmospheric models (Dudia, 1993; Skamarock and Klemp, 1992); however these represent an incremental evolutionary path in atmospheric simulation.

A capability such as OMEGA/ADM has been desirable for many years. Had it existed, it would have found broad use in the Defense Nuclear Agency (DNA) Global Effects Program that was mounted to study Nuclear Winter related issues. It would also have proven useful in forecasting the trajectories of the dust and ash injected into the atmosphere by numerous recent volcanoes including Mt. St. Helens, El Chichon, Mt. Pinatubo, Mt. Redoubt, and Mt. Spur. OMEGA/ADM did not exist primarily because of a perception that there is no present and continuing need for a permanent forecast capability. This perception changed during OPERATION DESERT SHIELD/STORM (hereafter referred to as DESERT STORM). Science Applications International corporation (SAIC) proposed the creation of OMEGA/ADM as a method for providing hazardous aerosol and gas dispersion prediction support for future US military operations.

OMEGA/ADM was conceived as an operational tool to support US forces in the field. It was to form the kernel of an Operations Center. As in DESERT STORM, the Operations Center would be centrally located and would receive worldwide meteorological information. As will be seen, however, the rapid increase in computational power available in high performance workstations has led to the concept of using OMEGA in the field as well, albeit at a degraded performance level from that available from supercomputers.

The major advantages of OMEGA/ADM over the current state-of-the-art include the ability to resolve the surface terrain down to scales of 1 km and along with that the local perturbations on the larger scale wind field. This local wind field perturbation is of extreme importance in determining the trajectory of an aerosol release. In order to calculate this local perturbation, however, it is important to include all of the physical parameters and processes that affect the local flow. These include not only the topography, but the land use, the land/water composition, the vegetation, the soil moisture, the snow cover (if appropriate), and the surface moisture and energy budgets. The inclusion of this additional physics, some of, which is only appropriate because of the increased spatial resolution, represents an additional advance in the state-of-the-art.

OMEGA, with its embedded ADM was conceived to advance the state-of-the-art in predicting the transport and diffusion of hazardous releases. The bulk of hazardous releases occur near the surface, are dispersed primarily in the PBL, and are strongly influenced by surface features (Sherman, 1978; Paegle, *et al.*, 1984). These hazardous releases often require emergency response. Effective emergency response, in turn, requires the highest possible resolution of both the atmospheric state as well as the aerosol concentration. OMEGA is based upon an adaptive unstructured grid technique (AGARD, 1992) that makes possible a continuously varying horizontal grid resolution ranging from 100 km down to 1 km and a vertical resolution from a few tens of meters in the boundary layer to 1 km in the free atmosphere. This feature allows one to obtain the highest possible resolution of the atmosphere as well as the hazardous aerosol/gas concentration.

The basic philosophy of the OMEGA/ADM model development has been the creation of an operational tool for real-time hazard prediction. The model development has been guided by two basic design considerations in order to meet the operational requirements: (1) the application of an unstructured mesh numerical technique to atmospheric simulation; and (2) the use of an embedded atmospheric dispersion algorithm. For many years, SAIC has been developing new algorithms and techniques in computational fluid dynamics (CFD); SAIC has also been studying cloud scale and mesoscale dynamics, thermodynamics, and microphysics, and atmospheric transport at cloud scale and mesoscale. OMEGA/ADM represents the marriage of these efforts.

The use of an unstructured mesh in OMEGA permits the use of variable grid resolution in a natural fashion, as well as providing a relatively straightforward basis for the introduction of dynamic grid adaptivity. The use of an embedded dispersion model eliminates the input/output (I/O) restrictions that would otherwise dominate the operational system at 1 km resolution. In this section, we discuss first the unique unstructured grid used in OMEGA. We then discuss the important considerations that led to the development of ADM. Finally, we discuss the necessary balance between physical fidelity, numerical accuracy, and operational constraints that affected the overall design of the OMEGA system.

## **2.1 Unstructured Adaptive Grids.**

We will discuss the OMEGA model grid structure in more detail in Section 3; however, it is so intricately enmeshed in the overall design that it is important to set the stage for our discussion here. The flexibility of unstructured grids facilitates the gridding of arbitrary surfaces and volumes in three dimensions. In particular, unstructured grid cells in the horizontal dimension can increase local resolution to better capture topography or the important physical features of atmospheric circulation and cloud dynamics. The underlying mathematics and numerical implementation of unstructured adaptive grid techniques have been evolving rapidly, and in many fields of application there is recognition that these methods are more efficient and accurate than the structured logical grid approach used in more traditional codes (Baum and Löhner, 1993; Schnack, *et al.*, 1993). To date, however unstructured grids and grid adaptivity have not been used in the atmospheric science community (Skamarock and Klemp, 1992). Atmospheric model problems characterized by large model domains, long time integration, and operational time constraints have not been viewed as viable candidates for the emerging CFD grid technologies. OMEGA represents the first attempt to use this advanced CFD technique for atmospheric simulation.

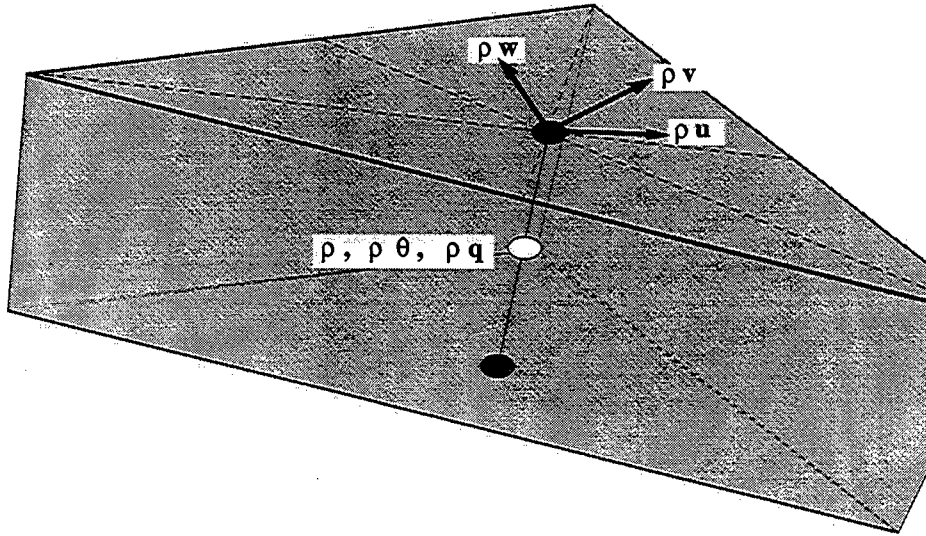


Figure 1. OMEGA grid element.

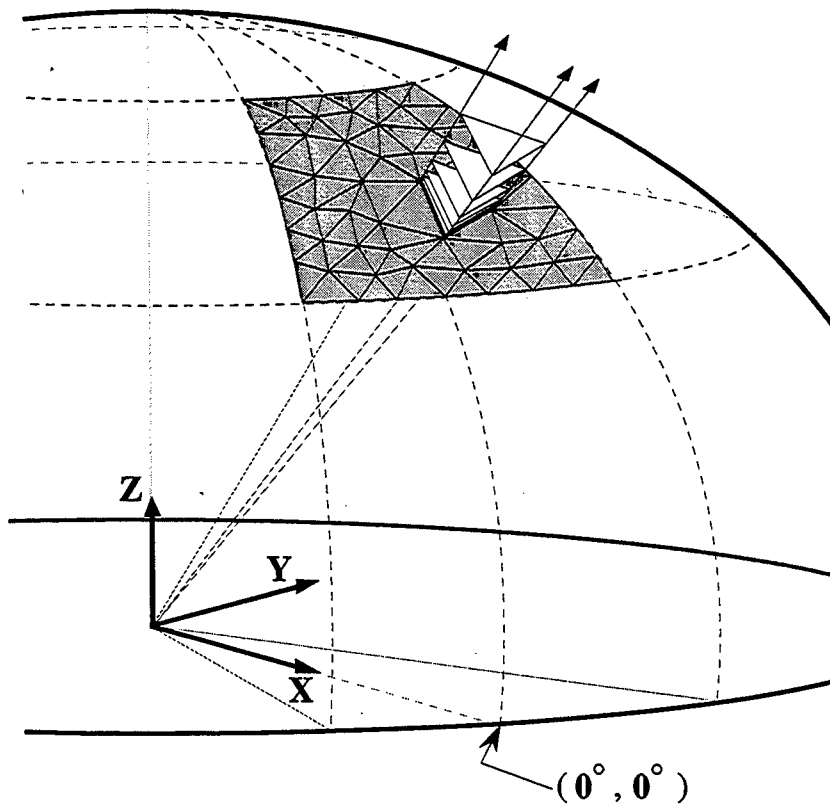


Figure 2. OMEGA coordinate system and vertical alignment of OMEGA grid.

OMEGA is based on an unstructured, triangular prism (Figure 1) computational mesh. This mesh is unstructured in the horizontal dimension and structured in the vertical dimension (Figure 2). The rationale for this mesh is the physical reality that the atmosphere is highly variable horizontally, but always stratified vertically. While completely unstructured three-dimensional meshes have been used for other purposes (Baum, *et al.*, 1993; Luo, *et al.*, 1994), the benefit of having a structured vertical dimension is a significant reduction in the computational requirements of the model.

In discussing unstructured grids, it is necessary to define the elemental objects that describe the properties of a volumetric mesh. The lowest order object of a grid is the *vertex*, which is specified by its position  $(x,y,z)$ . An *edge* conveys the connectivity of the mesh and is defined by the indices of its starting and terminating vertices. The *face* represents the interface area between adjacent volumetric cells and can be described from the list of edges that bound it, or by the sequence of vertices that form its extremities. The *cell* or *control volume* is in turn specified by the list of faces that contain it.

On an unstructured grid, the number of edges that meet at a vertex is arbitrary. Consequently there is no longer a simple algebraic construct that can be used to deduce the relationship of indices for the various elemental objects, as in the case of structured grids that have been used to date as the basic structure for atmospheric and ocean circulation models. The formation of the grid is tied to the actual solution of the model equations and to the topography. This means that the initial grid can be readily adapted to surface features or other fixed terrain features as well as the initial weather.

An important adjunct to the unstructured triangular grid methodology is the requirement that the model has to compute the normal to each face in order to calculate the fluxes across the boundaries. Since these normals must be computed, there is no benefit from orienting the grid in any particular fashion, so long as the numerical resolution of the hardware is sufficient to evaluate the critical fluxes. (We shall discuss this in more detail later in this section.) This leads to a natural separation between the coordinate system for the fundamental equation set and the grid structure. The coordinate system can be as simple as possible (such as Cartesian) while the grid structure, in this coordinate system, is extremely complex. OMEGA uses a rotating Cartesian coordinate system, but the grid structure is terrain following. Figure 2 shows a rotating Cartesian coordinate system in which the origin is the center of the Earth, the  $z$ -axis passes through the North Pole, the  $x$ -axis passes through the intersection of the Equator and the Prime Meridian, and the  $y$ -axis is orthogonal to both.

In this coordinate frame, the equations of motion are in their simplest possible form (without going into a non-rotating frame that would lead to unusual boundary conditions as the surface terrain moved through the grid) with only two terms that are somewhat non-conventional: gravity and the Coriolis acceleration. Gravity in this frame is directed in the  $-\hat{r}$  direction ( $\hat{r}$  representing the unit vector along an outward radial that implies that it potentially has components in all three coordinate directions. The Coriolis force is by definition  $2\rho\Omega \times \bar{v}$  and likewise has components in all three coordinate directions.

An important aspect of the OMEGA grid structure is the fact that all the cells along a radial possess the same footprint. This is accomplished by creating a surface grid and then projecting radials from the center of the Earth through all of the vertices. Each layer is then created by specifying a set of vertices along each radial (Figure 2) (the number of vertices along any radial are the same).

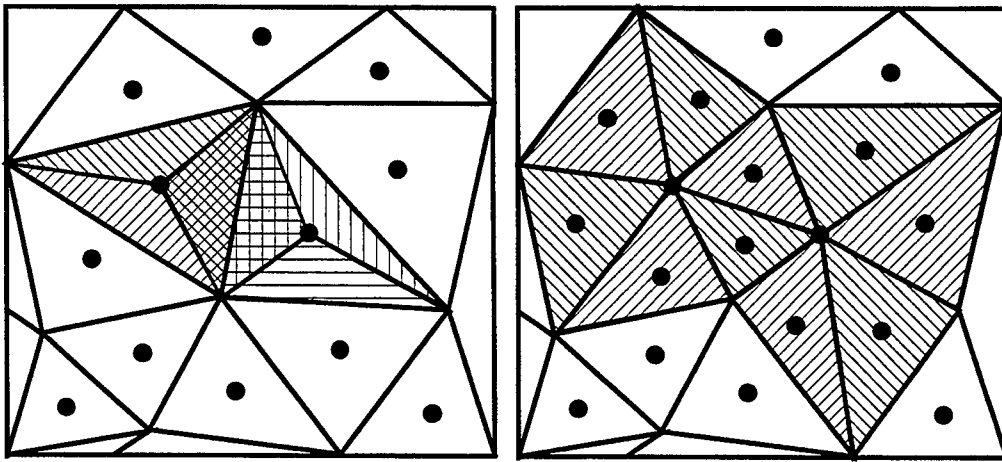


Figure 3. Vertex addition and reconnection.

Because the OMEGA grid structure results in the mixing of the Earth-relative horizontal and vertical components, it is essential that the numerical scheme be able to separate these. Given a grid structure that may be a few meters in vertical resolution and a few kilometers or a few tens of kilometers in horizontal resolution, the numerical resolution must be accurate to better than one (1) part in  $10^5$ .

The adaptation of an unstructured grid takes place through a variety of grid operations. The first is vertex addition and is usually followed by a vertex reconnection step. Figure 3 illustrates these two steps when some activity that would indicate a need for more resolution is noted in two cells. The vertex addition step is accomplished by adding a vertex at the centroid of each affected cell and connecting it to the vertices of the cell. The reconnection step then involves the evaluation of each new cell to see if it is possible to create grid cells with lower aspect ratio by removing an edge and reconnecting the alternative vertices.

Figure 4 shows the reverse process in which the grid is coarsened through the process of vertex deletion. This is also usually followed by a vertex reconnection step. It is important to note that even though the grid adaptation routines may create an apparent motion of the grid, it does not, in fact, move; rather the goal is to refine the grid in advance of any important physical process that could require additional grid

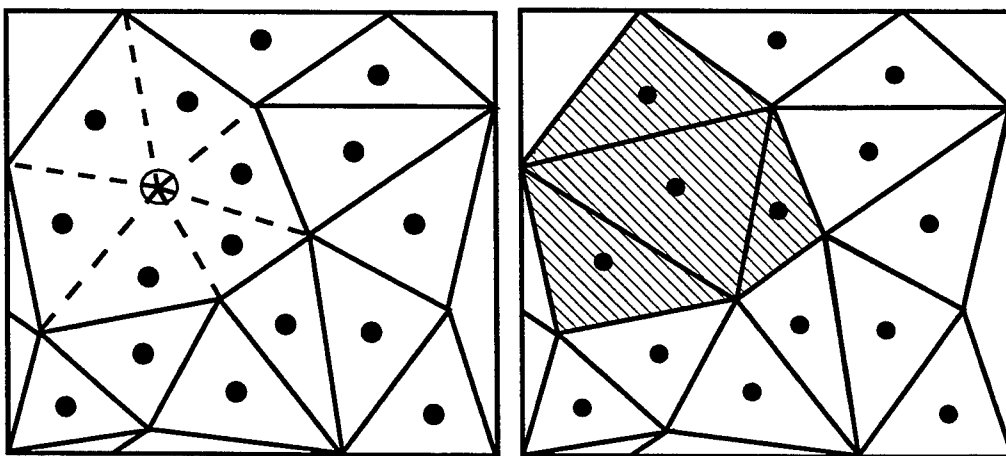


Figure 4. Vertex deletion and reconnection.

resolution, and to coarsen the grid behind the region. This differentiates the method from the adaptation techniques described by Dietachmeyer and Drogemeier (1991) that used vertex movement to adapt to atmospheric features.

A different type of process is shown in Figure 5. In this figure we show vertex relaxation, in which the vertices are allowed to move as a mass-spring system, and edge bifurcation that is equivalent to vertex addition in the special case of a boundary cell.

Currently, the OMEGA grid automatically adapts to static features of the underlying topography and land/water boundary. In addition, other factors (either related to the surface or the atmosphere) can be included through a user-defined field. The code can also be set to adapt the grid during runtime. This enables atmospheric features that require additional grid points for adequate simulation to be resolved by a grid that refines or coarsens based on a given set of adaptation rules. In Section 3 we will describe the procedures for refinement (vertex addition), coarsening (vertex deletion), and reconnection of OMEGA grid system. Each of these procedures is applied to generate the best possible grid based on considerations of resolution and element shape.

The adaptation procedures are the essential features that give unstructured grid algorithms for partial differential equations their great power. This happens on two different levels. First, the total number of grid points necessary to perform a successful numerical computation that recovers the correct physics can be greatly reduced. By this we mean that the recovery of the model physics at the smallest scale length resolved does not require the complete domain to have the same resolution. The resources of the numerical and computational machinery are focused on the regions of importance. This saving is especially true for three dimensional hydrodynamic problems where the resulting economy, in our experience has made the difference between tractability and intractability. The grid can be coarse where the circulation is regular and smooth, but greatly enhanced where there are sharp gradients, where there are discontinuities in the flow, where topographic features are important, or where model physics or dispersion source terms require fine resolution.

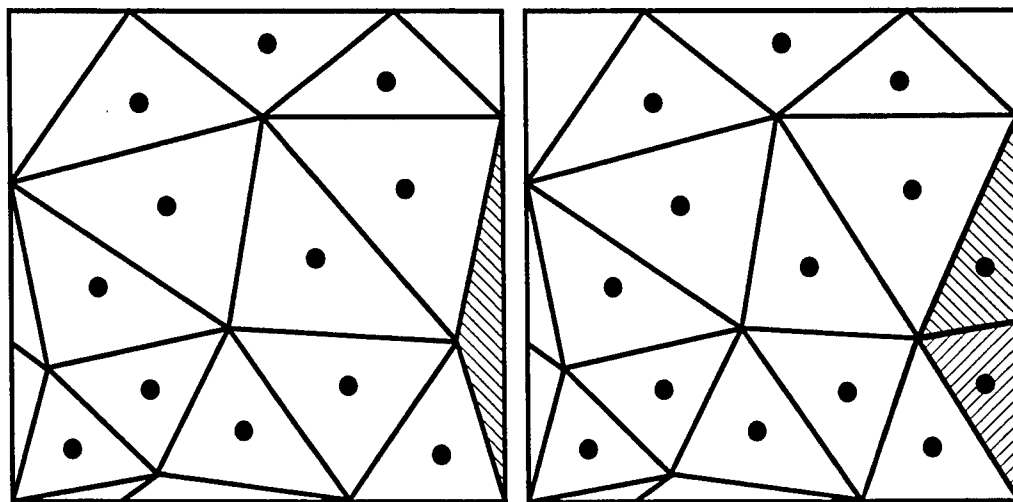


Figure 5. Vertex relaxation and edge bifurcation.



Second, the flexibility of unstructured grids to adapt to the transient physical solution improves the fidelity of the finite difference or finite element numerical schemes, eliminating some of the errors that plague existing models. The improvement comes from aligning the grid structure to the flow and from the local refinement of the grid in the vicinity of rapidly changing horizontal spatial structures in the atmosphere.

## 2.2 Embedded Atmospheric Dispersion Model.

Over the past decade, there has been an increasing interest in using detailed meteorological information in aerosol and gas transport and diffusion models to improve our understanding of atmospheric dispersion. The detailed meteorological information in such models could be obtained either from meteorological observations or from meteorological models. Until recently, the conventional weather observing network has been used to obtain the necessary meteorology for dispersion models (*c.f.*, Pack *et al.*, 1978; Artz, *et al.*, 1985). These and other studies, however, have demonstrated that the weather observing network is too coarse in both time and space to accurately depict local circulations.

An alternative approach to overcome the limitations of the existing weather observation network is to use atmospheric conditions predicted by meteorological models. Therefore, advanced atmospheric dispersion models have involved the coupling of the dispersion model with a meteorological model. One such coupling was accomplished by McNider *et al.* (1988), who studied the influence of diurnal variation and inertial boundary layer oscillations on long-range dispersion. Pitts and Lyons (1992) applied their coupled model to the urban area of Perth, Australia. Still another coupling was performed by Boybeyi *et al.* (1995) with an application to the Bhopal gas accident in India.

Although this coupling approach has been sufficient for these and many other studies up until now, the major problem with this approach is that atmospheric dispersion models can only use the results from the meteorological models at some spatial and temporal resolution. As the grid resolution is increased, the data requirements of this approach grow as the inverse cube of the grid resolution. This can be seen by recognizing that the time between "snapshots" of the wind field must be less than the transit time across a cell. Thus, if the spatial resolution increased by a factor of two, then the data must be provided twice as frequently. An increase in the grid resolution of a factor of two, therefore results in an increase in the data requirements for the model of a factor of eight. Many current aerosol transport and diffusion models use analyzed gridded wind fields with roughly 100 km grid resolution that are output every 12 hours. To improve the aerosol transport capability by increasing the grid resolution to 1 km would increase the data handling requirements of these models by a factor of  $10^6$ .

Models-3, the next generation air quality model of the US Environmental Protection Agency (EPA) (Dennis and Novak, 1991) is an example of the current coupling paradigm carried out to higher resolution. The typical performance characteristics of an EPA study give this approach some merit. The meteorological component of the modeling system is re-used many times over in these studies. A typical study may vary pollutant emissions assumptions and alter the atmospheric chemistry package for fixed atmospheric conditions in order to develop an understanding of the driving factors in that particular air quality situation and to aid in the development of control strategies. Under this paradigm, however, first a meteorological model is used to simulate the atmospheric conditions that are output at selected times, and then a chemistry and transport model evaluates the fate of the pollutants under these atmospheric conditions. The Models-3 program uses the NCAR/Penn State University MM5 model

coupled to the Atmospheric Chemistry Model (a suite of chemistry and transport models); other similar systems include the Colorado State University Regional Atmospheric Modeling System (RAMS) coupled to a particle dispersion model (McNider, *et al.*, 1988; Pielke *et al.*, 1991).

A major drawback to this approach, however, is the large amount of data that must be output by the meteorological model and ingested by the particle dispersion model. As higher and higher resolution is implemented, this method quickly becomes bound by its input/output requirements. OMEGA overcomes this problem by embedding its atmospheric dispersion model (ADM) into the meteorological model. OMEGA/ADM has both Eulerian (grid based) and Lagrangian (grid free) particle and puff transport and diffusion algorithms. These algorithms have the benefit of the full OMEGA simulation fields (temperature, moisture, wind, turbulence, *etc.*) at each timestep. In addition, the flexible grid structure of OMEGA permits the use of high resolution where it is naturally needed (*e.g.*, in regions of complex terrain, near land/water boundaries, near emission sources) without burdening the model with high resolution everywhere. We will discuss the ADM in better detail in Section 8.

### 2.3 Operational Considerations.

The ultimate consideration in the OMEGA design has always been world-wide operational utility. OMEGA has been designed with a delicate balance between physical fidelity, numerical accuracy, and operational constraints (Figure 6). For example, the design point of 1 km for the highest grid resolution was based upon a recognition that although world-wide terrain elevation and land/water boundary information is available at even higher resolution, world-wide albedo, land use, vegetation, soil texture, and soil moisture, as well as the world wide meteorological data observations, are rarely available at even 1 km resolution.

The world-wide real-time operational requirement influenced a number of design decisions. Real-time operational use for a reasonable forecast period dictated a realistic maximum resolution of 1 km. This determined one level of requirements for the physics that had to be contained in OMEGA. (We discuss the OMEGA physics in more detail in Section 4.) World-wide utility required that any physical models that were incorporated into OMEGA would have to have world-wide applicability and could not rely on datasets that were not available with this coverage. This, for example, eliminated the use of a second-order closure turbulence model since the Reynolds stress is not operationally available for either initial or boundary conditions.

As part of the real-time operational requirement, SAIC recognized that a great deal of automation was desirable in the OMEGA system. This resulted in the creation of a highly automated grid generator (discussed in Section 5), an automated meteorological and surface data assimilation system (discussed in Sections 6 and 7), and a user friendly X-windows and Motif™ based (GUI) (Section 11) and graphic post processors (Section 12).

The world-wide requirement forced SAIC to develop a number of world-wide databases including roughly 1 km resolution terrain elevation, standard deviation of terrain elevation (an indicator of surface roughness), and water fraction, coarser 5 arc-minute databases of the same values, and datasets for land use, vegetation, and soil texture at various resolutions. These are discussed in Section 5.

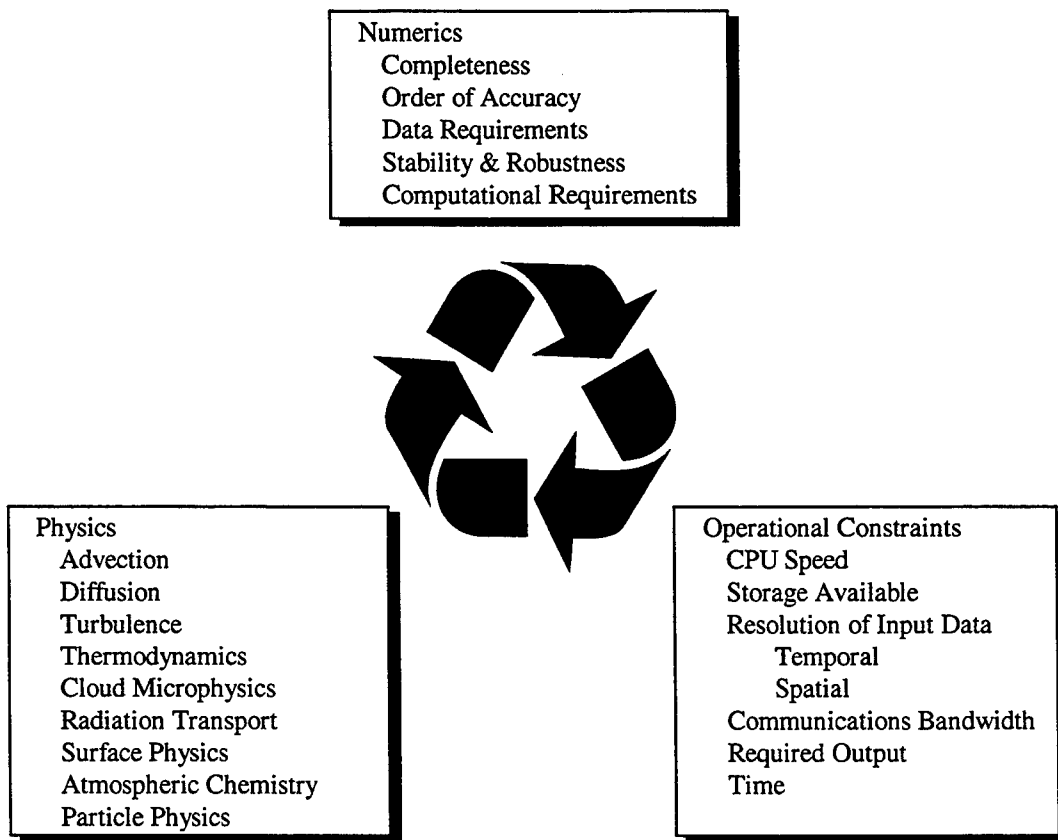


Figure 6. OMEGA represents a balance of physical, numerical and operational considerations.

With this as a basis, the design objective of OMEGA is a tool for real-time hazardous prediction capable of performing a full coupled atmospheric forecast and aerosol or gas dispersion calculation at 10 times real-time. The acceptance level is half of this, or 5 times real-time. As will be seen, the tremendous flexibility of the OMEGA modeling system permits the model to meet these constraints on platforms ranging from CRAY supercomputers to IBM R/S 6000 workstations - albeit by trading of resolution or size of the computational domain. The remainder of this document provides the details of the OMEGA model, its physics, numerics, and the operational design of the system.

## Section 3

### Solution of Governing Equations

#### 3.1 Fundamental Equation Set.

In this section, we document the fully elastic non-hydrostatic equation set used in OMEGA, including the applicable assumptions. For brevity, we classify the five mixing ratios for water substances into two groups: precipitating water substances,  $Q_p$  (where the subscript  $p$  designates either rain, snow, or hail), and nonprecipitating water substances,  $Q_n$  (where  $n$  designates either ice crystals, water vapor, or water droplets). Furthermore, we cast the equations in their conservative form consistent with the fully elastic mass-conservation equation ( $\partial\rho/\partial t = -\bar{\nabla} \cdot \rho\bar{\mathbf{V}}$ ). This form is better suited for the state-of-the-art upwind advection schemes we have used, which have significantly less numerical diffusion (important for the finer resolution we are trying to achieve) than the schemes used in other non-hydrostatic models such as the Terminal Area Simulation System (TASS) (Proctor, 1987).

We begin by decomposing the atmospheric pressure and density into a time-invariant hydrostatic base state and a perturbation upon that state such that

$$p(x, y, z, t) = p_0(x, y, z) + p'(x, y, z, t) \quad (1a)$$

$$\text{and} \quad \rho(x, y, z, t) = \rho_0(x, y, z) + \rho'(x, y, z, t) \quad (1b)$$

with

$$\frac{\partial p_0}{\partial z}(x, y, z) = -g\rho_0(x, y, z). \quad (2)$$

Assuming an Eulerian grid, we then have the following equation set for the conservation of mass, momentum, and energy.

#### Conservation of Mass:

$$\begin{aligned} \frac{\partial \rho}{\partial t} + \bar{\nabla} \cdot (\rho \bar{\mathbf{V}}) + F_\rho &= 0 \\ \frac{\partial \rho Q_n}{\partial t} + \bar{\nabla} \cdot (\rho Q_n \bar{\mathbf{V}}) &= \rho M_n + F_{Q_n} \\ \frac{\partial \rho Q_p}{\partial t} + \bar{\nabla} \cdot (\rho Q_p \bar{\mathbf{V}}) &= \rho M_p + \frac{\partial}{\partial z} (Q_p W_p \rho) + F_{Q_p} \\ \frac{\partial \rho Q_a}{\partial t} + \bar{\nabla} \cdot (\rho Q_a \bar{\mathbf{V}}) &= \rho M_a + \frac{\partial}{\partial z} (Q_a W_a \rho) + F_{Q_a} \end{aligned} \quad (3)$$

In equations 3.3,  $\rho$  represents the dry air density, calculated from the total density as:

$$\rho = \rho_{total} / (1 + Q_{vapor}). \quad (4)$$

### Conservation of Momentum:

$$\frac{\partial \rho \bar{\mathbf{V}}}{\partial t} + \bar{\nabla} \cdot (\rho \bar{\mathbf{V}} \bar{\mathbf{V}}) = -\bar{\nabla} p' - (\rho - \rho_0) g \hat{r} + 2\rho \bar{\boldsymbol{\Omega}} \times \bar{\mathbf{V}} + \bar{\mathbf{F}}_M \quad (5)$$

where the density used in the calculation of momentum is the total density.

### Conservation of Energy:

$$\frac{\partial E}{\partial t} + \bar{\nabla} \cdot (E \bar{\mathbf{V}}) = \frac{E}{c_p T} \sum_j (L_j S_j) + S_R + F_h \quad (6)$$

Terms have been arranged such that the conservative advection terms appear on the left side of each equation. The source terms on the right side of the momentum equation also include buoyancy and gravitational effects,  $-(\rho - \rho_0)g\hat{r}$  (where  $\hat{r}$  is the radial unit vector), and the Coriolis force,  $(2\rho\boldsymbol{\Omega} \times \mathbf{V})$ . Sub-grid scale turbulence contributions,  $F$ , are discussed in detail in Section 4.1. For the remaining equations,  $T$  is the temperature,  $L_i$  and  $S_i$  denote the latent heat and rate of phase conversion of either vaporization, fusion, or sublimation, and  $W_p$  represents the terminal velocity of each of the precipitating water substances.  $S_i$  depends on the microphysics that governs the rate of phase transitions and  $W_a$  depends on the assumed size distribution and mass of the hydrometeors.  $M_n$  and  $M_p$  are the non-precipitating and precipitating microphysics source terms (see Section 4.2). Finally, subscript  $a$  refers to transport of aerosol or gas.

The initial energy density  $E$  is calculated from the total pressure as:

$$E = p^{1-\kappa} \left( \frac{p_{ref}^\kappa}{R_d} \right), \quad (7)$$

and throughout the simulation pressure is diagnosed from energy density using this relationship.

Potential temperature,  $\Theta$ , and temperature,  $T$ , are related by Poisson's equation,

$$T = \Theta \left( \frac{p}{p_{ref}} \right)^\kappa \quad (8)$$

where

$$\begin{aligned} p_{ref} &= 1000 \text{mb}, \\ \kappa &= \frac{R_d}{c_p} = 0.286, \end{aligned} \quad (9)$$

$R_d$  being the gas constant for dry air and  $c_p$  is the specific heat of dry air at constant pressure. Finally,  $S_R$  represents the contribution of radiation flux to heating the atmosphere and will be described in Section 4.4.

### 3.2 Hydrodynamic Solver.

The hydrodynamic elements of the OMEGA model are based on numerical methods of solution of the Navier-Stokes equations on an unstructured grid in the horizontal direction and a structured grid in the vertical. We use a standard split-operator methodology, calculating advection terms explicitly and diffusion terms implicitly. In the calculation of momentum, the pressure gradient, Coriolis, and buoyancy terms are calculated explicitly along with the advection terms. An implicit vertical filter and an explicit horizontal filter are applied to the vertical momentum. The calculation of the new momentum at each time-step thus involves several steps, which are described below. All implicit operations are performed by tri-diagonal matrix inversion.

#### 3.2.1 Advection - Implementation of the Finite Volume Upwind Solver.

In this section we describe the implementation on unstructured grids of the multidimensional positive definite advection transport algorithm (MPDATA) originally developed on regular grids by Smolarkiewicz (1984), Smolarkiewicz and Clark (1986), and Smolarkiewicz and Grabowski (1990). The resulting scheme is second-order-accurate in time and space, conservative, combines the virtues of the MPDATA (e.g., ability to separately ensure monotonicity and positive definiteness) with the flexibility of unstructured grids (Baum and Löhner, 1989, Peraire et al., 1990), is compatible with adaptive mesh algorithms (Fritts, 1988), and can run efficiently on highly parallel computers. Below, we describe the essential methodology and demonstrate the method on two-dimensional passive advection test problems.

In discussing unstructured grids, it is necessary to define the nomenclatures. To reiterate, the basic control volume element in our structured-unstructured computational domain is a truncated triangular prism. Each prism is bounded by five faces. For advection across each face, it is convenient to define a local coordinate system with its origin located at the center of the face. Each face separates the left-hand-side (LHS) from the right-hand-side (RHS) such that the flow from the LHS cell to the RHS cell is considered positive. For simplicity, the advected variable, hereafter denoted as  $\psi$ , is placed at the cell centroid, while the velocity vector is defined on the cell face at the origin of the local coordinate system. Figure 7 shows the basic arrangement of the variables on a two-dimensional grid.

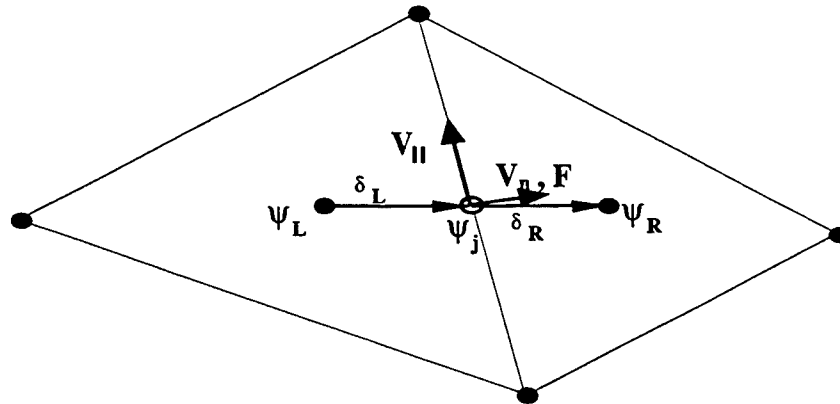


Figure 7. Arrangement of the variables on a 2-dimensional unstructured-grid. The generic advected variable,  $\psi$ , is placed at cell centroids. The subscripts L and R designates their left-hand-side and right-hand-side cell placements. The velocity is decomposed into normal and parallel components (not to scale). The flux  $F$  is co-located with  $V_n$  at the face centers, and points only in the normal direction.

In its explicit form MPDATA adapts naturally to the above construct. As posed by Smolarkiewicz, the algorithm can be generalized to the following steps:

- 1) At each cell face the low-order flux is found in conservative form using the standard first-order-accurate "upwind" scheme;
- 2) The advected variable is integrated using the low-order flux;
- 3) At each cell face, the low-order scheme is expanded in a Taylor series and the truncation error in the flux is explicitly identified;
- 4) The error term is cast in the form of error velocity,  $\mathbf{V}_e$ ;
- 5) The correction velocity,  $\mathbf{V}_c (= -\mathbf{V}_e)$ , is optionally limited to preserve monotonicity of the advected variable (Smolarkiewicz and Gradowski, 1990);
- 6) Replacing  $\mathbf{V}$  with  $\mathbf{V}_c$ , steps (1) through (5) are repeated a chosen number of times ( $=N_c$ ) to achieve greater accuracy.

Although Smolarkiewicz derived  $\mathbf{V}_c$  for a rectangular grid, it can be generalized to a grid with arbitrary control volume shape as long as the bounding faces are flat. Consider the generic advection equation,

$$\frac{\partial \Psi}{\partial t} + \bar{\nabla} \cdot (\bar{\mathbf{V}} \Psi) = 0. \quad (10)$$

To compute the change in  $\psi$  from time  $t = t_0$  to  $t_0 + \Delta t$ , it is necessary to integrate the flux  $\Psi_j \bar{\mathbf{V}}_j$  through each face  $j$  during the period  $\Delta t$ :

$$\Delta \Psi_j = \int_{t=t_0}^{t=t_0+\Delta t} \Psi_j \bar{\mathbf{V}}_j \cdot \bar{\mathbf{a}}_j dt \quad (11)$$

Here  $\bar{\mathbf{a}}_j = a_j \hat{\mathbf{e}}_n$  is the area vector of face  $j$ , where  $\hat{\mathbf{e}}_n$  denotes the unit vector normal to the face and pointing from left to right. For this integral, 2nd-order accuracy in space is achieved automatically by placing  $\bar{\mathbf{F}} = \Psi_j \bar{\mathbf{V}}_j$  at the center of each face (in practice,  $\Psi_j$  at the faces is obtained by interpolation). Similarly, to ensure 2nd-order accuracy in time,  $\Psi_j \bar{\mathbf{V}}_j$  should be evaluated at  $t = t_0 + \Delta t/2$ . Assuming that a leapfrog algorithm is used (i.e.,  $\bar{\mathbf{V}}_j$  is defined at  $t = t_0 + \Delta t/2$ ), we need only expand  $\Psi_j$  in a Taylor's series as

$$\Psi_j = \Psi_j^0 + \frac{\partial \Psi_j}{\partial t} \frac{\Delta t}{2} + O(2), \quad (12)$$

where the superscript 0 denotes an evaluation at  $t = t_0$ . Substituting (3.10) for  $\Psi_j$  in (3.9) and performing the time integral, Equation 3.11 becomes

$$\Delta \Psi_j = \left\{ \Psi_j^0 + \frac{\partial \Psi_j}{\partial t} \frac{\Delta t}{2} \right\} \bar{\mathbf{V}}_j \cdot \bar{\mathbf{a}}_j \Delta t \quad (13)$$

Now substituting (3.10) for  $\frac{\partial \Psi}{\partial t}$  in (3.13) we have

$$\Delta\Psi_j = \left\{ \Psi_j^0 - [\bar{\mathbf{v}}_j \cdot \bar{\nabla}\Psi_j + (\bar{\nabla} \cdot \bar{\mathbf{v}}_j)\Psi_j] \frac{\Delta t}{2} \right\} \bar{\mathbf{v}}_j \cdot \bar{\mathbf{a}}_j \Delta t \quad (14)$$

If we further let  $v_n = \bar{\mathbf{v}}_j \cdot \hat{\mathbf{e}}_n$  denote the component of the velocity normal to the face (and thus  $\bar{\mathbf{V}}_n = v_n \hat{\mathbf{e}}_n$ ), then the first order upwind flux term is given by

$$\Delta\Psi_j^{upwind} = .5\{(\bar{\mathbf{V}}_n + \|v_n\|\hat{\mathbf{e}}_n)\Psi_L + (\bar{\mathbf{V}}_n - \|v_n\|\hat{\mathbf{e}}_n)\Psi_R\} \cdot \bar{\mathbf{a}}_j \Delta t \quad (15)$$

Now letting  $\bar{\delta}_L$  denote the vector pointing from the cell centroid on the left to the face, and  $\bar{\delta}_R$  the vector pointing from the face to the cell centroid on the right, we can write

$$\Psi_L = \Psi_j - \bar{\delta}_L \cdot \nabla\Psi_j, \quad (16a)$$

and

$$\Psi_R = \Psi_j + \bar{\delta}_R \cdot \nabla\Psi_j \quad (16b)$$

Similarly, we will let

$$\delta\Psi_L = \Psi_j - \Psi_L, \quad (17a)$$

and

$$\delta\Psi_R = \Psi_R - \Psi_j \quad (17b)$$

Now we can rewrite (13) as:

$$\Delta\Psi_j^{upwind} = \left\{ \bar{\mathbf{v}}_n \Psi_j^0 - .5\|v_n\|\hat{\mathbf{e}}_n (\delta_L\Psi + \delta_R\Psi) \right\} \cdot \bar{\mathbf{a}}_j \Delta t \quad (18)$$

The correction term is the difference between (14) and (18). After some algebraic manipulation, this correction term can be written as

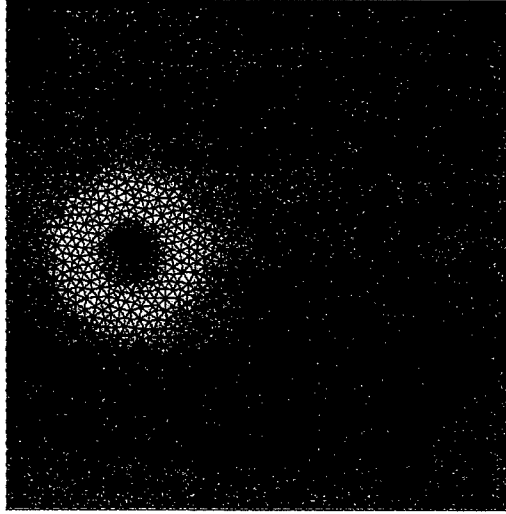
$$\Delta\Psi_c = \left\{ \|v_n\| \left[ \left( \frac{\Psi_R - \Psi_L}{\Psi_R + \Psi_L} \right) - v_n \left[ \bar{\mathbf{v}}_j \cdot \frac{\bar{\nabla}\Psi_j}{\bar{\Psi}} + (\bar{\nabla} \cdot \bar{\mathbf{v}}_j) \right] \right] \frac{\Delta t}{2} \right\} \bar{\Psi} a_j \Delta t, \quad (19)$$

where  $\bar{\Psi} = \frac{\Psi_R + \Psi_L}{2}$ .

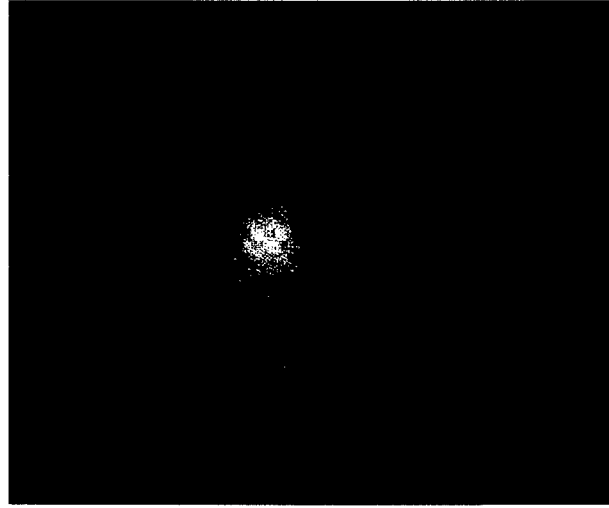
The correction velocity is now:

$$v_c = \|v_n\| \left[ \left( \frac{\Psi_R - \Psi_L}{\Psi_R + \Psi_L} \right) - v_n \left[ \bar{\mathbf{v}}_j \cdot \frac{\bar{\nabla}\Psi_j}{\bar{\Psi}} + (\bar{\nabla} \cdot \bar{\mathbf{v}}_j) \right] \right] \frac{\Delta t}{2} \quad (20)$$





(a) Computational mesh used for the rotating cone advection test.



(b) Initial Conditions.

Figure 8. Rotating cone advection test.

In actual implementation, the correction term becomes

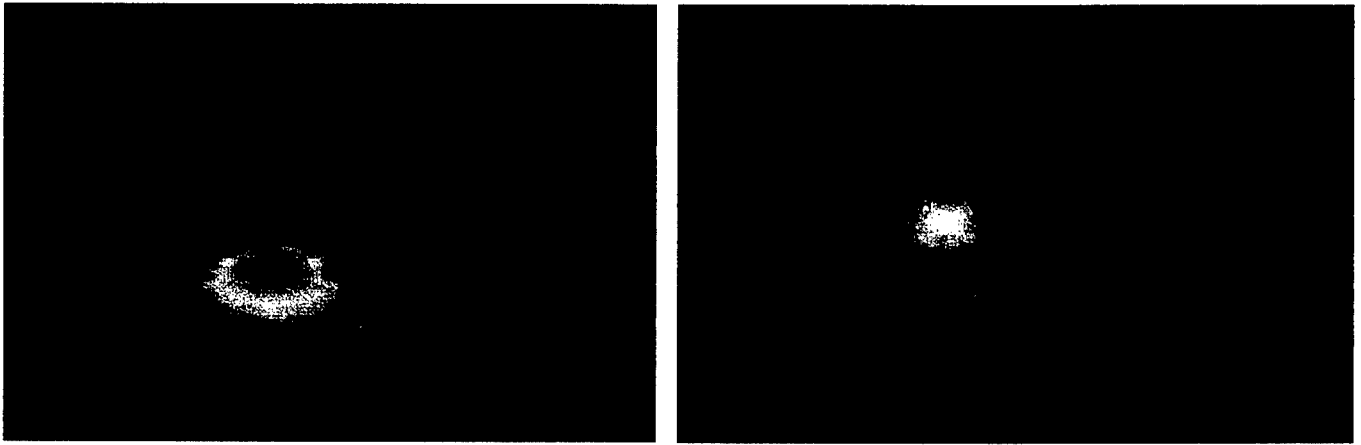
$$\Delta\Psi_c = \left\{ \left\| v_n \right\| \left( \frac{\tilde{\Psi}_R - \tilde{\Psi}_L}{\tilde{\Psi}_R + \tilde{\Psi}_L} \right) - v_n \left[ \frac{\bar{\mathbf{V}}_j \cdot \bar{\nabla} \tilde{\Psi}_j}{\tilde{\Psi}} + \bar{\nabla} \cdot \bar{\mathbf{V}}_j \right] \frac{\Delta t}{2} \right\} \tilde{\Psi}_{L,R} a_j \Delta t, \quad (21)$$

where  $\tilde{\Psi}$  is the value of the advected quantity following the first-order upwind advection step.

We limit the number of correction steps to  $N_c=1$ , since additional correction steps are not cost effective. The effect of additional correction steps is to bring the solution closer to 2nd-order accuracy, which is very nearly achieved with just one correction step; the additional accuracy attainable is limited.

To compare with known results (Smolarkiewicz, 1984, Smolarkiewicz and Clark, 1986, and Smolarkiewicz and Grabowski, 1990), we performed the rotating cone test on triangular grids. Figure 8 shows the mesh and the initial placement of the passive scalar. Figure 9 shows the solutions after six revolutions of the cone. Figure 9 shows the results of the 1st-order "upwind" scheme ( $N_c=0$ ). As shown, the original cone shape is completely smeared out. In Figure 9, we show the case with one correction step. This case has a background value of zero, which when coupled with the positive definiteness aspect of the algorithm, generates extra numerical diffusion which automatically ensures monotonicity (Smolarkiewicz and Grabowski, 1990). Nevertheless, the cone shape has been substantially preserved. In general, all of our results are consistent with previous tests (Smolarkiewicz, 1984, Smolarkiewicz and Clark, 1986, and Smolarkiewicz and Grabowski, 1990).

The claimed near second-order-accuracy of our scheme is demonstrated by testing how the accumulated error in the computation scales with grid size. Three measurements of error are used for the rotating cone test: the root-mean-square error over the whole mesh, the root-mean-square error over an area extended by the original base of the cone, and deviation in the height of the cone. The mesh sizes range



(a) 1<sup>st</sup> order “upwind.”

(b) Correction step.

Figure 9. Rotating cone advection test after five rotations.

from one and a half to one half of those shown in Figure 8, *i.e.*, a factor of three variation. The results are shown in Figure 10. We note that except for the left-most data point, all three measurements of error scale approximately as  $\Delta^2$  (the dotted lines indicate the slopes of both  $\Delta^2$  and  $\Delta$  scaling for comparison). The left-most data points were generated from runs with the largest grid size. By observation, we find that the excess diffusion in these cases had reached the boundary, thus contaminating the runs results.

### 3.2.2 Implicit Acoustic Filtering and Diffusion.

One of the major goals of the OMEGA model development is to achieve a simulation capability that transcends scales through the use of variable resolution. The accurate portrayal of aerosols in the planetary boundary layer will require fine resolution in the structured vertical direction and selective locations of fine horizontal resolution. Accurate, stable numerical solutions require that the time step of integration be determined by the finest grid spacing. This problem is magnified when using the fully-compressible set of nonhydrostatic equations, since fast-moving sound waves are inherent in the solution. Indeed, in the structured direction, the CFL time-step can become too restrictive. To overcome this restriction, the growth and propagation of acoustic waves are controlled through the application of vertical and horizontal filters that act on the vertical component of the momentum.

The momentum equation is integrated using a semi-implicit, fractional time step scheme. After explicit calculation of the advection and source terms, an implicit calculation is performed in which a correction term is added to the vertical component of momentum. This term, which has the effect of slowing the growth and speed of sound waves, is described below. The next partial step consists of the application of a horizontal filter, which is described in the following section. Like the implicit correction, this term is based on and added to the vertical momentum. The implicit calculation of the eddy-diffusion term completes the momentum advance to time step  $m+1$ .

The implicit calculation solves the following equation for  $w^{\hat{n}}$ :

$$w^{\hat{n}} = w^n + c_s v_s \left[ \frac{\partial^2}{\partial z^2} (w^{\hat{n}} - w^n) \right] dt^2, \quad (22)$$

where  $w^n$  is the vertical component of momentum at the beginning of the  $n$ th timestep and  $w^{\hat{n}}$  is the value after the addition of the (explicitly calculated) terms representing advection, the Coriolis force, the pressure gradient contribution, and the buoyancy effect. Here,  $v_s$  is the sound speed, and  $c_s$  is an empirically chosen coefficient. A stability analysis of the above equation shows that  $c_s$  must be greater than 1.0. The default value currently used in OMEGA is 2.5.

Eddy-diffusion is also treated implicitly in the radial direction. The fractional step approach is necessary because the acoustic filter described above effectively increases the inertia at short wavelengths, i.e.,  $\rho_{\text{effective}} \sim \rho(1+k^2)$  where  $k$  is the wave number in the direction of propagation. This can reduce the action of the eddy-diffusion term unless the operations are split into separate fractional steps.

Again, this implementation of the dispersion operator removes the severe time step restriction that can result from diffusion flux along the fine scale radial direction. A separate explicit treatment is used for momentum diffusion in the horizontal direction.

### 3.2.3 Horizontal Acoustic Filtering.

The horizontal filter is based on the horizontal components of the laplacian of the vertical momentum. The coefficient of the horizontal filter is based on vertical height; no horizontal filtering is done at either the top boundary or the surface. The maximum value of the coefficient is self-adjusting, initially having a negligible value and increasing by small increments based on the growth of the laplacian of  $w$ . The Laplacian of the vertical component of the momentum is calculated using Green's formula:

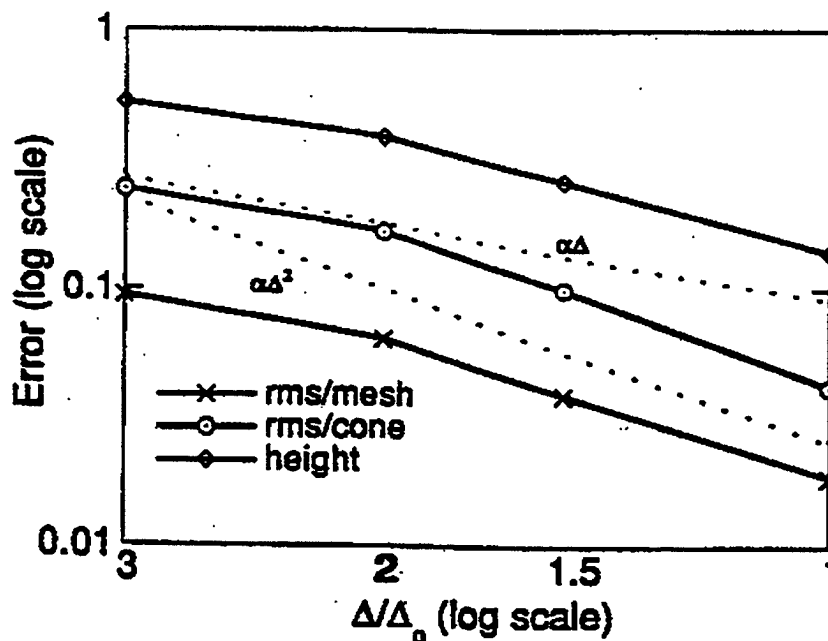


Figure 10. Error scaling with grid resolution. Three measurements of deviation from the original cone are used: root-mean-square error over the whole mesh, root-mean-square error over an area extended by the original cone, and deviation in the height of the cone.

$$\nabla^2 w = \frac{1}{A} \oint \frac{\partial w}{\partial \mathbf{n}}, \quad (23)$$

where  $A$  is the area enclosed by a curve. The discretized form becomes

$$\nabla^2 w = \frac{1}{A} \sum_{i=1}^3 \frac{\partial w}{\partial \mathbf{n}_i} dL_i \quad (24)$$

where  $A$  is now the area of the triangle,  $\mathbf{n}_i$  is the outward normal vector to the  $i^{\text{th}}$  edge, and  $dL_i$  is the length of the  $i^{\text{th}}$  edge. The normal derivative is defined as:

$$\frac{\partial w}{\partial \mathbf{n}_i} = \frac{w_i - w_c}{d_i}, \quad (25)$$

where  $w_i$  is the value of  $w$  at the centroid of the triangle that shares the  $i^{\text{th}}$  edge of the target triangle,  $w_c$  is the value of  $w$  at the centroid of the target triangle, and  $d_i$  is the distance between the two centroids.

This approximation is first-order accurate only if the line segment connecting the centroids is perpendicular to the shared edge; i.e., this line segment coincides with the outward normal vector. To improve the accuracy of the approximation, we define a “ghost” triangle whose edges are the perpendicular bisectors of the line segments connecting the centroid of the target triangle with the centroids of its neighbors. The area and edge lengths of this ghost triangle are used in the formula for  $\nabla^2 w$ . Figure 11 shows the ghost triangle constructed around the centroid of the inner cell.

### 3.2.4 Horizontal Diffusion.

The horizontal diffusion term in the momentum equation can be expanded as:

$$\bar{\nabla} \cdot (\mathbf{K}_d \bar{\nabla} \bar{\mathbf{u}}) = \bar{\nabla} \mathbf{K}_d \cdot \bar{\nabla} \bar{\mathbf{u}} + \mathbf{K}_d \nabla^2 \bar{\mathbf{u}} \quad (26)$$

where  $\mathbf{K}_d$  is the horizontal diffusion coefficient, given by:

$$\mathbf{K}_d = 0.36 D \Delta^2. \quad (27)$$

Here  $D$  is the deformation rate, and  $\Delta$  is the horizontal grid spacing. Assuming local deformation gradients are small, this can be written as:

$$\bar{\nabla} \cdot (\mathbf{K}_d \bar{\nabla} \bar{\mathbf{u}}) \approx \mathbf{K}_d \nabla^2 \bar{\mathbf{u}}. \quad (28)$$

We define orthonormal vectors  $\bar{x}$  and  $\bar{y}$  lying in a plane tangent to the surface of the earth at the centroid of the triangle in which the deformation rate is sought (Figure 12). Projecting the velocity  $\mathbf{u}$  onto this local coordinate system gives  $u$  and  $v$ , the horizontal components of velocity. By assuming the velocity to be locally linear in  $x$  and  $y$ , it is possible to express  $u$  and  $v$  as  $a_u x + b_u y + c_u$  and  $a_v x + b_v y + c_v$ , respectively. For the horizontal deformation rate  $D$  we will use the approximation

Using the values of  $u$  and  $v$  at the vertices of the triangle, it is then possible to solve for  $b_u$  and  $a_v$ , which gives the local deformation rate as  $D = b_u + a_v$ . In this way, actual horizontal deformation is obtained, as opposed to deformation in the plane of the triangle. Since the horizontal grid spacing is squared in the expression for the deformation coefficient, we use the area of the triangle

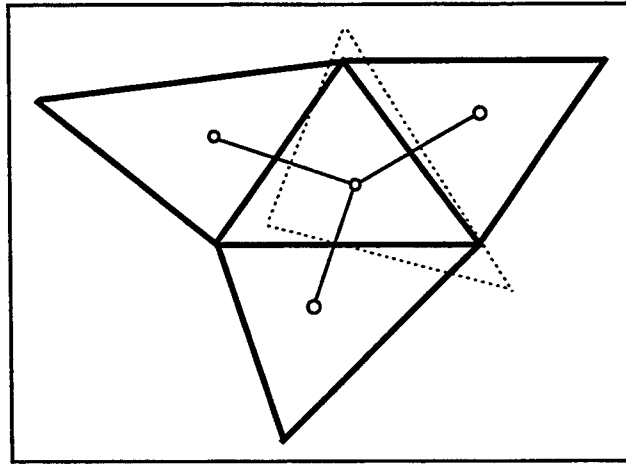


Figure 11. The ghost triangle used in the calculation of the Laplacian.

$$D = \frac{\partial u}{\partial y} + \frac{\partial v}{\partial x}. \quad (29)$$

The Laplacian of each component of the velocity is calculated using the discretization of Green's formula based on the "ghost triangles" described in the previous section.

### 3.2.5 Model Boundary Conditions.

**3.2.5.1 *Surface Boundary Conditions.*** The surface boundary conditions applied in the OMEGA model are based on a diagnostic layer treatment, which is Dirichlet in its implementation but has a Neumann flavor, since new surface values are calculated based on flux estimations. Surface boundary conditions are discussed more fully in the section on planetary boundary layer physics.

**3.2.5.2 *Lateral Boundary Conditions.*** In cloud scale models, in which the time scale is small enough to assume that the environment outside the model domain is unchanged during the simulation, inflow boundaries are usually prescribed from environmental conditions. In mesoscale and larger models this assumption can no longer be made. The environment outside the computational domain has to be

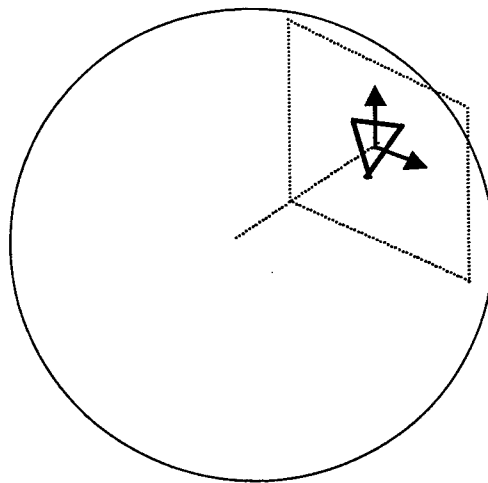


Figure 12. A local coordinate system defines the horizontal plane passing through the centroid of each triangle.

derived from larger scale forecast tools such as the LFM (Limited Fine Mesh model), NGM (Nested Grid Model), ETA model, or MRF (Medium Range Forecast model) run at the National Centers for Environmental Prediction (NCEP). Boundary conditions at user-specified time intervals are calculated based on one of these forecasts, and linear interpolation is used to determine boundary values at intermediate times.

The OMEGA model utilizes “ghost cells” at all boundaries. This single layer of cells holds predicted values of all prognostic variables obtained from the chosen forecast data. Boundary faces are treated in the same way as interior faces throughout the calculation, with one notable exception described below. At the end of each time step, a “nudging” scheme is applied to the new values of all variables in cells immediately inside the boundary to the forecast values in the ghost cells across the boundary.

It is worth noting that linear interpolation of boundary conditions between two forecast times can fail to accurately reflect the diurnal cycle of heating and cooling that affects temperatures and winds near the surface. This is particularly true if data is available only at twelve-hour intervals. If, for example, data is available for a certain locale at 7am and 7pm, the minimum and maximum temperatures obtained in a twenty-four hour period will not appear in the boundary data. This will lead to false temperature and pressure gradients across lateral boundary edges near the surface, which we ignore by assuming zero pressure gradients across lateral boundaries for the purpose of calculating momentum. Thus we avoid the inducement of sea-breeze-like or off-shore-breeze-like winds along lateral boundaries. This is not an ideal solution; nudging of the prognostic variables along lateral boundaries still corrupts temperatures and pressures during certain portions of the diurnal cycle, however, the error is not cumulative, nor does the affect extend far into the domain.

**3.2.5.3 *Top Boundary Conditions.*** At the top of the computational domain, initial values of density and potential temperature are calculated assuming a hydrostatic balance, and these values remain fixed throughout the simulation. A homogeneous Neumann boundary condition is applied to the horizontal components of velocity, while the vertical velocity is assumed to be zero. Thus the upper boundary is a rigid, free-slip surface. To minimize reflection off of this boundary, a diffusive “sponge” is applied to the vertical component of the velocity. The coefficient of the sponge is exponential, and approaches zero rapidly below the top few layers of the grid.

### **3.2.6 Time Splitting.**

The OMEGA user interface and grid generator allow the user to specify selected regions in which the resolution can be as fine as one kilometer or less. The cell size in the outer portion of the domain may be more than two orders of magnitude greater than this. For this reason, it is highly desirable to utilize a time-splitting scheme in which the hydrodynamic solver is sub-cycled over small cells, thus preventing the time step over the entire domain from being limited to that required by the smallest cell.

In OMEGA, we use the term “inner mask” to refer to a collection of cells over which the solution will be sub-cycled. This terminology distinguishes such a collection of cells from a “subdomain,” which is user-specified as part of the grid definition process. An inner mask is selected by the model, which calculates the Courant-limited time step for each cell based on sound speed, and uses this as the criterion for mask definition. Cells in an inner mask need not be contiguous. We impose only one restriction: any cell having two neighbors in an inner mask is added to the inner mask. For stability, no more than two time steps are taken in a cell before the neighboring cell is updated; however, masks can be nested, so that the time-step in the outermost portion of the domain can be many times that of the smallest cells.

The difficulty in implementing a time-splitting scheme lies in the treatment of the mask boundaries. In the OMEGA scheme, a face shared by cells in different masks belongs to the innermost mask. Thus

advection across this face takes place at the smaller timestep associated with the inner mask. Advected quantities are updated in the cell belonging to the inner mask, while the change in the quantity on the cell in the outer mask is stored. Advected quantities in the outer cell are updated when advection across faces belonging to the outer mask occurs. In this way, the accuracy of the advection scheme is formally preserved for both cells, each at their respective time step. This process is aided by the application, at each sub-step, of the horizontal filter to a larger mask consisting of the inner mask and its bounding cells. This filter, which dissipates horizontally traveling acoustic waves, helps to maintain a smooth solution across mask boundaries. In numerous test cases involving as many as five nested masks, this time-splitting scheme has proven to be stable and robust.

### 3.2.7 Model Validation.

In the course of developing the OMEGA model, we have assembled a set of test cases that are used to validate various aspects of the model. We continuously rerun these cases each time a significant change is made. In addition to a number of analytic cases which test specific aspects of the solution, we rely on a collection of real cases for which we have done extensive analysis of the available meteorological and diffusion data.

The simplest analytic test cases consist of pure advection of a passive scalar in either a simple rotational flow field or a more complex flow field consisting of counter-rotating vortices. Figure 13 shows the result of a passive scalar in a steady state flow field composed of six counter rotating vortices. A second order accurate solution of the OMEGA model solution after 1000 time steps (right panel) agrees well with the corresponding analytical solution(center).

The time splitting technique used in the OMEGA model is tested with a rotating cone test case discussed earlier in this section. The domain of integration contains three nested "masks" or (Figure 14) over which the hydrodynamics are subcycled to permit a larger timestep on the outer portion of the domain and smaller time steps in the inner masks. The cone initially located over the southwest region of the domain (Figure 15) rotated clockwise during the model integration and passed over the high resolution

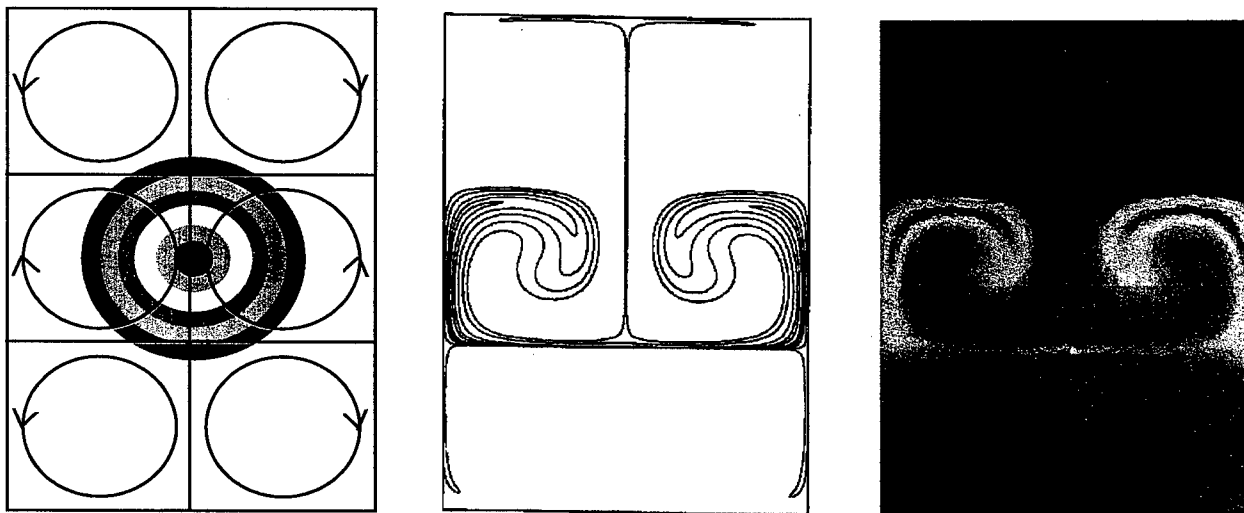


Figure 13. Advection test consisting of a passive scalar in a steady-state flow field composed of six counter-rotating vortices (left). The analytic solution at a given scaled time (from Staniforth) is shown (center); along with the second order solution at the same scaled time (1000 timesteps) for the OMEGA advection solver (right).

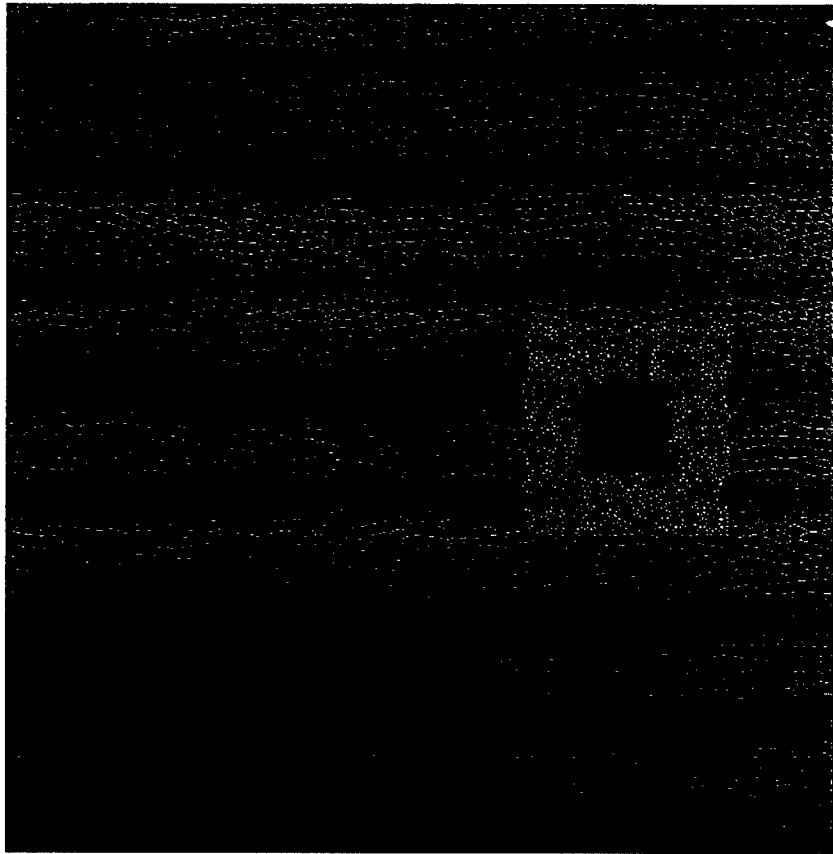
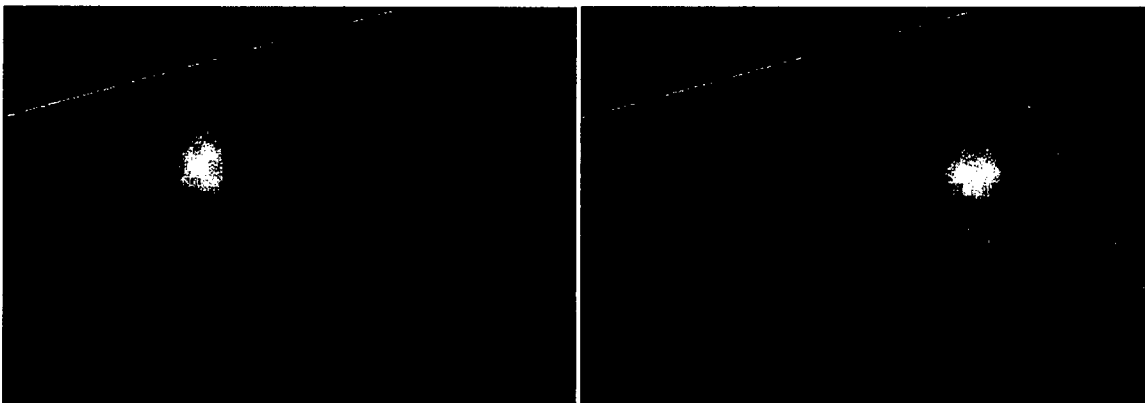


Figure 14. Coarse and two finer subdomains for testing time splitting technique.

region and moved over the southeast region (Figure 15). A comparison of these two figures shows that the cone has not been distorted by the use of time splitting technique. A detail discussion of these runs and validation runs against meteorological and diffusion data sets are given in Volume 2 of this final report.



(a) Initial position of the cone.

(b) Final position of the cone.

Figure 15. Initial and final positions of the cone.



## Section 4

### Model Physics

This section discusses the five most important processes to atmospheric circulation: turbulence, air surface interactions, cloud microphysics, convective parameterization, and radiation transport. Turbulence affects, among other things, the rate at which surface moisture and energy enters the atmosphere. Cloud microphysics and convective parameterization are important in the vertical distribution of this moisture and energy and in the formation of precipitation. And finally, radiation transport is important in determining the solar heating of the Earth's surface and the atmosphere.

#### 4.1 Turbulence and the Planetary Boundary Layer.

Much has been written in recent years concerning modeling and parameterizing atmospheric turbulence. However, little has been resolved in terms of the development of improved parameterizations or the direction and future progress of turbulence parameterization schemes as they relate to numerical weather prediction. The parameterization of turbulence in OMEGA (*i.e.*, the forcing terms,  $F$ , in Equations 3, 4, and 5) are divided into two parts: horizontal and vertical. The horizontal diffusion is a function of the deformation of momentum (Section 3.2.2), while the vertical diffusion is implemented using a multi-level planetary boundary layer (PBL) model.

The effects of the PBL can be incorporated into a mesoscale model in two ways. One way is to parameterize the entire PBL as one layer. This involves identifying and relating unresolved processes in the PBL with resolvable ones. The complexity of this single-layer PBL parameterization lies in the variety and interdependence of atmospheric processes acting on different scales. The second approach is to include several computational levels in the PBL in order to resolve the boundary layer structure effectively and explicitly. Such multi-level PBL formulations require turbulent fluxes of momentum, heat, and moisture at several levels within the PBL. Thus they require some type of closure scheme to relate turbulent fluxes to mean quantities. The atmospheric PBL in OMEGA is treated separately as the viscous sublayer, the surface layer, and the transition layer using a turbulent kinetic energy (TKE) closure scheme.

##### 4.1.1 Viscous Sublayer.

The viscous sublayer is defined as the level near the ground ( $z < z_0$ ) where the transfer of the dependent variables by molecular motion becomes important. Temperature and specific humidity in this layer are related to their ground surface values (Deardorff, 1974):

$$\bar{\theta}_{z_0} = \theta_G + 0.0962 (\theta_* / k) (u_* z_0 / \nu)^{0.45}, \quad (30)$$

and

$$\bar{q}_{z_0} = q_G + 0.0962 (q_* / k) (u_* z_0 / \nu)^{0.45}. \quad (31)$$

By analogy for other gaseous and atmospheric materials ( $\chi$ )

$$\bar{\chi}_{z_0} = \chi_G + 0.0962 (\chi_* / k) (u_* z_0 / \nu)^{0.45}. \quad (32)$$

In these expressions,  $\nu$  is the kinematic viscosity of air,  $k$ , von Karman's constant,  $u_*$ , the friction velocity,  $z_0$ , the surface roughness length,  $\theta_*$ , the subgrid scale temperature flux, and  $q_*$ , the subgrid

scale moisture flux. In this layer, it is assumed that  $\bar{u} = \bar{v} = \bar{w} = 0$ , and the variation of pressure is ignored.

#### 4.1.2 Surface Layer.

There is no precise definition of this layer, (which may contain more than one model layer) but it is that part of the planetary boundary layer immediately above the viscous sublayer where small-scale turbulence dominates the transfer of energy, moisture, and momentum, and the vertical variation of the vertical fluxes is roughly less than 10%. For this reason it is also referred to as the constant flux layer. The depth of this layer usually varies from about 10m to 100m. It has been of considerable interest to micrometeorologists to find a suitable theoretical or semi-empirical framework for a quantitative description of the mean and turbulence structure of this layer. One of the most common formulations used in mesoscale models was reported by Beljaars and Holtslag (1991) and in which

$$u_* = k V_1 / [\ln(z_1/z_0) - \psi_M(z_1/L) + \psi_M(z_0/L)], \quad (33)$$

$$\theta_* = k (\theta_1 - \theta_s) / [\ln(z_1/z_0) - \psi_H(z_1/L) + \psi_H(z_0/L)], \quad (34)$$

$$q_* = k (q_1 - q_s) / [\ln(z_1/z_0) - \psi_H(z_1/L) + \psi_H(z_0/L)], \quad (35)$$

and 
$$\chi_* = k (\chi_1 - \chi_s) / [\ln(z_1/z_0) - \psi_H(z_1/L) + \psi_H(z_0/L)], \quad (36)$$

where the symbols  $V_1$ ,  $\theta_1$ ,  $q_1$ , and  $\chi_1$  are wind speed, potential temperature, specific humidity, and other gaseous concentrations at the first model level in the atmosphere,  $\theta_s$ ,  $q_s$ , and  $\chi_s$  are the corresponding surface values,  $u_*$  is the friction velocity,  $\theta_*$  is the temperature scale,  $q_*$  is the humidity scale,  $\chi_*$  is the other gaseous scale,  $k$  is the von Karman constant ( $k = 0.4$ ),  $z_1$  is the height of the first model level, and  $L$  is the Monin Obukhov length,  $\psi_M$  and  $\psi_H$  are dimensionless stability functions of height divided by the Monin Obukhov length.

These integral functions for unstable surface layer are given by

$$\psi_M = 2 \ln[(1+x)/2] + \ln[(1+x^2)/2] - 2 \tan^{-1}(x) + \pi/2, \quad (37)$$

$$\psi_H = 2 \ln[(1+x^2)/2], \quad (38)$$

where

$$x = (1 - 16z/L)^{1/4}. \quad (39)$$

In stable surface layer the following relationships are used

$$-\psi_M = a \frac{z}{L} + b \left( \frac{z}{L} - \frac{c}{d} \right) \exp\left(-d \frac{z}{L}\right) + \frac{bc}{d}, \quad (40)$$

$$-\psi_H = \left(1 + \frac{2az}{3L}\right)^{3/2} + b \left( \frac{z}{L} - \frac{c}{d} \right) \exp\left(-d \frac{z}{L}\right) + \frac{bc}{d} - 1, \quad (41)$$

where  $a=1$ ,  $b=0.667$ ,  $c=5$ ,  $d=0.35$ , and  $z/L$  is a non-dimensional stability parameter. The Monin-Obukhov stability length,  $L$ , is defined as

$$L = \frac{\bar{\theta} u_*^2}{k g \theta_*}, \quad (42)$$

where  $\bar{\theta}$  is the average air temperature near the surface, and  $g$  is the gravity.

### 4.1.3 Transition Layer.

The turbulent region extending above the surface layer up to the top of the planetary boundary layer (i.e. 90% of its depth) is called the transition layer. Its depth is variable since it depends on the strength of turbulence generated at the ground surface. The PBL height often can be considered to be the depth of turbulent activity. Therefore, defining the top of the PBL is not always simple. For example, on a sunny day with light winds thermal convection may push this layer up to 1-2km above the surface. At night with weak winds and little cloud cover it may contract to less than 100m. One of the most important characteristics of this layer is that the effects of roughness in generating forced convection decrease more rapidly with height than effects of heating on thermal convection. Therefore, this layer tends to be well mixed and is generally characterized by free convection involving rather large eddy sizes associated with thermals and heat plumes. Turbulence associated with these large eddies can be parameterized in terms of the mean flow. This leads to the closure problem that is addressed in this section. In OMEGA a turbulent kinetic energy closure scheme is used.

**4.1.3.1 Turbulent Kinetic Energy (TKE) Closure.** The turbulent kinetic energy (TKE) closure scheme is an improvement on the relatively simple first-order closure scheme. TKE closure accounts for more of the physics of the atmosphere in the formulation of the eddy diffusivity,  $K$ . TKE closure begins with the same fundamental assumptions of first-order closure, but in the TKE method the  $K$  coefficient is determined from more physically realistic relationships given by prognostic equation for turbulent kinetic energy. This type of closure is more economical than higher-order closure schemes. For example, second order closure requires the integration of at least 15 partial differential equations when moisture is included. Second-order closure also requires initial and boundary conditions for terms such as the Reynolds Stress that are not operationally available; this, coupled with the computational expense renders second order closure inappropriate for an operational model such as OMEGA.

In contrast with second order closure, TKE closure requires only one additional equation, yet it provides a more physically realistic solution to the closure problem than does first-order closure. The vertical turbulent exchange is parameterized using the "2.5 level" closure technique developed by Mellor and Yamada (1974). The level 2.5 model has been selected from the hierarchy of available TKE closure schemes because it is a good compromise between accuracy and efficiency, and because it has been applied to many atmospheric modeling studies. The level 2.5 turbulence closure is based on the following prognostic equation for the turbulent kinetic energy  $e$ :

$$\frac{\partial(\rho e)}{\partial t} = -\nabla \cdot (\rho e v) + \nabla_r \cdot (K_e \nabla_r \rho e) + \left[ -\overline{u'w'} \frac{\partial u}{\partial z} - \overline{v'w'} \frac{\partial v}{\partial z} + \frac{g}{\theta} \overline{w'\theta'} \right] - \epsilon. \quad (43)$$

The first two terms on the right hand side represent advection and turbulent transport of TKE ( $\nabla_r$  represents the radial gradient), the third term in the bracket represents both shear and buoyancy production of TKE, and the fourth term dissipation of turbulent energy. In this closure scheme, several terms on the right hand side must be parameterized. Following Deardorff (1980), the eddy fluxes are parameterized as

$$\overline{(u'w', v'w')} = -K_m \left( \frac{\partial u}{\partial z}, \frac{\partial v}{\partial z} \right), \quad (44)$$

$$\overline{w'\theta'} = -K_h \frac{\partial \theta_v}{\partial z}, \quad (45)$$

and

$$\overline{w'q'} = -K_q \frac{\partial q}{\partial z}. \quad (46)$$

The parameterization of the final term, energy dissipation  $\varepsilon$ , is achieved diagnostically using Kolmogorov's hypothesis as

$$\varepsilon = c_\varepsilon e^{3/2} / \ell, \quad (47)$$

where  $c_\varepsilon$  is a constant assumed to be 0.17.

In this closure scheme, the prognostic equations of all other second-order moments are reduced to algebraic equations. It therefore allows the expression of eddy diffusivities after considerable algebraic reduction in the following simple form:

$$K_m = \ell(2e)^{1/2} S_M, \quad (48)$$

$$K_h = \ell(2e)^{1/2} S_H, \quad (49)$$

and

$$K_e = \ell(2e)^{1/2} S_e, \quad (50)$$

where non-dimensional eddy diffusivities  $S_M$  and  $S_H$  are obtained from

$$S_M (6A_1 A_2 G_M) + S_H (1 - 3A_2 B_2 G_H - 12A_1 A_2 G_H) = A_2 \quad (51)$$

and

$$S_M (1 + 6A_1^2 G_M - 9A_1 A_2 G_H) - S_H (12A_1^2 G_H + 9A_1 A_2 G_H) = A_1 (1 - 3C_1) \quad (52)$$

with

$$G_M = \frac{\ell^2}{2e} \left[ \left( \frac{\partial u}{\partial z} \right)^2 + \left( \frac{\partial v}{\partial z} \right)^2 \right] \quad (53)$$

and

$$G_H = -\frac{\ell^2 g}{2e \theta} \frac{\partial \theta_v}{\partial z}. \quad (54)$$

In the above equations, empirical constants are assigned values after Mellor and Yamada (1982),  $(A_1, A_2, B_1, B_2, C_1, S_e) = (0.92, 0.74, 16.6, 10.1, 0.08, 0.20)$ . It is also assumed that  $G_H \leq 0.033$  and  $G_M \leq 0.825 - 25G_H$  to reduce the singularities of the level 2.5 closure.

The turbulent length scale  $\ell$  is still unknown and needs to be parameterized in terms of the known variables. After Mellor and Yamada (1982)

$$\ell = \frac{k(z + z_0)}{1 + k(z + z_0)/\ell_\infty} \quad (55)$$

where  $\ell_\infty$  the master (or primary) length scale defined as

$$\ell_\infty = \alpha \frac{\int_0^H \sqrt{e} dz}{\int_0^H \sqrt{e} dz} \quad (56)$$

with  $\alpha$ , a constant coefficient of the order of 0.1. In order to smoothly change the mixing length from the neutral to the slightly stable condition, the stable mixing length is modified with an upper limit as proposed by Andre et al. (1978) such that

$$\ell \leq 0.75 \left[ \frac{2e}{\frac{g}{\theta} \frac{\partial \theta_v}{\partial z}} \right]^{1/2} \quad (57)$$

## 4.2 Air Surface Interactions.

OMEGA requires as boundary conditions the temperature and humidity at the roughness level. These must be calculated prognostically taking the interaction of the atmosphere and the land surface into account. Numerical studies have demonstrated that contrasts in land surface characteristics (*e.g.*, soil texture and moisture, vegetation type) can generate local circulations as strong as sea breezes (McCorcle, 1988; Chang and Wetzel, 1990). In consequence, landscape variations strongly influence atmospheric dispersion patterns.

The land surface module in OMEGA is based on the scheme proposed recently by Noilhan and Planton (1989). Following their approach, only one energy balance is considered for a whole soil-vegetation system. A single surface skin temperature  $T_s$ , and surface air humidity  $q_s$  are computed for both the canopy and the ground. The calculation of two distinct temperatures for the soil surface and the vegetation would significantly increase the complexity of the scheme since it requires an evaluation of radiative and turbulent transfers between the soil, the plant, and the air inside the canopy.

The implemented scheme allows for two layers in soil and a single vegetation canopy. It computes the evolution of four variables: the surface temperature of the soil-vegetation medium  $T_s$ , the soil water contents  $\eta_1$  and  $\eta_2$  in the upper and lower soil layers, and the amount of liquid water retained on the foliage  $W_d$ .

The parameters used to describe the main physical processes in a soil-vegetation system can be divided into two classes: primary parameters to be specified by spatial distribution, and secondary parameters whose values can be associated with the values of the primary parameters. The land-use in the modeling domain is classified into several categories characterized by two numerical indices which are the primary parameters: type of soil texture and type of land. The secondary parameters describing a variety of physical characteristics of soil are listed in Table 1.

### 4.2.1 Surface Temperature.

The most indicative variable of surface variation is ground temperature  $T_s$ . OMEGA calculates ground temperature using the force-restore rate equation of Deardorff (1978)

$$\frac{\partial T_s}{\partial t} = C_T G_0 + \Omega(T_{ds} - T_s), \quad (58)$$

where  $\Omega$  is angular velocity of earth ( $\Omega = 7.27229 \times 10^{-5} s^{-1}$ ), and  $G_0$  is the heat storage rate in the soil-vegetation medium, which is equal to the sum of all the atmospheric fluxes at the surface

$$G_0 = R_0 + H_{anthrop} - (H_0 + L_c E_0), \quad (59)$$

where  $R_0$  is the net radiation at the surface (see next section for detail),  $H_{anthrop}$  is the anthropogenic heat flux,  $H_0$  and  $L_c E_0$  are the sensible and latent heat fluxes from the atmosphere. Surface turbulent fluxes are parameterized using Monin-Obukhov surface-similarity theory. The sensible heat flux to the atmosphere,  $H_0$ , the latent heat flux from evaporation or dew formation,  $L_c E_0$ , are calculated using the turbulent subgrid scale friction velocity,  $u_*$ , temperature scale,  $\theta_*$ , and humidity scale,  $q_*$ ,

$$H_0 = \rho C_p u_* \theta_* \quad (60)$$

and

$$L_c E_0 = \rho L_c u_* q_* \quad (61)$$

The forcing terms in the force-restore equation may be completed by specification of the anthropogenic heat flux  $H_{anthrop}$  if urban or industrial areas are considered.

The first term on the right-hand side of Equation (58) represents the diurnal forcing of  $T_s$  by the heat storage rate in the soil-vegetation medium,  $G_0$ , and the second one tends to restore  $T_s$  to the mean soil temperature  $T_{ds}$ .

The thermal capacity  $C_T$  combines the capacities of both vegetation  $C_{veg}$ , and soil  $C_g$  weighted by vegetation cover ( $veg$ ) and bare soil cover ( $1-veg$ ) (Noilhan and Planton, 1989)

$$\frac{1}{C_T} = \frac{veg}{C_{veg}} + \frac{1-veg}{C_g} \quad (62)$$

$C_{veg}$  has a value ( $10^{-3} K^{-1} m^2 J^{-1}$ ) related to the weak heat storage and transfer ability of vegetation. The thermal capacity of soil

$$C_g = \frac{\sqrt{2\Omega}}{I_s}, \quad (63)$$

is given by its thermal inertia

$$I_s = \sqrt{\rho_s c_s \lambda_s} = \frac{\rho_s c_s d_s}{\sqrt{\tau_1}}, \quad (64)$$

where  $\rho_s$  is the density of soil,  $c_s$  is the specific heat of soil, and  $\lambda_s$  is coefficient of thermal soil conductivity.  $T_{ds}$  is the approximately constant mean deep soil temperature at the diurnal temperature cycle penetrative soil depth

$$d_s = \sqrt{\frac{\tau_1 \lambda_s}{\rho_s c_s}} \quad (65)$$

where  $\tau_1$  is the period of 1 day.

The soil properties in Equation (63) depend upon both the soil texture and the soil moisture. This dependence is deduced from the analytical expression given by (Noilhan and Planton, 1989)

$$C_g = C_{g_{sat}} \left( \frac{\eta_s}{\eta} \right)^{b/2.1 \log 10} \quad (66)$$

where  $C_{g_{sat}}$ ,  $\eta_s$ , and  $b$  are estimated for each soil texture from table (4.1).

#### 4.2.2 Surface Fluxes of Radiation.

At the surface, the net shortwave solar radiation  $R_s$  (radiative contribution) is obtained by using two empirical functions. The first is a Rayleigh transmission function that includes the effects of the molecular scattering and absorption by permanent gases such as oxygen, ozone, and carbon dioxide (Atwater and Brown, 1974) such that

$$G = 0.485 + 0.515 \left[ 1.041 - 0.16 \left( \frac{0.000949 p + 0.051}{\cos Z} \right)^{1/2} \right], \quad (67)$$

where  $p$  is pressure in mb. A second function accounts for the absorptivity of water vapor (McDonald, 1960)

$$a_w = 0.077 \left[ \frac{r(z)}{\cos Z} \right]^{0.3}, \quad (68)$$

where  $r$  is the optical path length of water vapor above the layer  $z$  given by

$$r(z) = \int_z^{top} \rho q dz. \quad (69)$$

The net shortwave solar radiation at the surface is

$$R_s = \begin{cases} (1 - A_g)(a_1 \cos Z + a_2)(G - a_w)(1 - b_1 N_E^{b_2}) & \cos Z > -a_2 / a_1 \\ 0 & \cos Z \leq -a_2 / a_1 \end{cases} \quad (70)$$

where  $A_g$  is the albedo, the empirical coefficients are  $a_1 = 990 W m^{-2}$  and  $a_2 = -30 W m^{-2}$ , and  $Z$  is the zenith angle

$$\cos Z = \cos \psi \cos \delta \cos H + \sin \psi \sin \delta. \quad (71)$$

$\psi$  is the latitude,  $\delta$  the solar declination, which is a function of Julian day, and  $H$  the solar hour angle

$$H = \frac{\pi(t-12)}{12}, \quad (72)$$

where  $t$  is local time in hours.

In the above equation, the cloud effects on the incoming radiation is also parameterized in terms of the effective cloud cover  $N_E$  following Kasten and Czeplak (1980)

$$N_E = (N_T + N_L)/2, \quad (73)$$

where  $N_T$  is the total cloud cover, and  $N_L$  is the cover due to low clouds. The remaining empirical coefficients are  $b_1=0.75$  and  $b_2=3.4$ .

The net longwave radiation has two components: (1) incoming radiation from the atmosphere (atmospheric radiation), and (2) outgoing radiation from the surface (terrestrial radiation)

$$R_L = R_{L\downarrow} - R_{L\uparrow}. \quad (74)$$

The incoming longwave radiation is expressed by

$$R_{L\downarrow} = c_1 T_a^6 + c_2 N_E, \quad (75)$$

where  $c_1 = 5.31 \times 10^{-13} \text{ Wm}^{-2} \text{ K}^{-6}$ ,  $c_2 = 60 \text{ Wm}^{-2}$ , and the reference air temperature  $T_a$  at  $z=50$  m is recommended by Van Ulden and Holtslag (1985). The outgoing longwave radiation from the surface arises from the Stefan-Boltzmann law

$$R_{L\uparrow} = \varepsilon_g \sigma T_s^4, \quad (76)$$

where  $\varepsilon_g$  is the emissivity for the ground surface specified in terms of land-use categories,  $\sigma$  is the Stefan-Boltzmann's constant ( $5.67 \times 10^{-8} \text{ Wm}^{-2} \text{ K}^{-4}$ ).

Finally, the net radiation flux at ground level is defined as

$$R_0 = R_s + R_L. \quad (77)$$

The surface energy budget, (Equation 59), is updated each timestep to provide an updated ground temperature. The ground temperature is then related to the potential temperature in the lowest cell by the following equation:

$$\theta_{sfc} = T_g \left( \frac{p_{ref}}{p} \right)^\kappa \quad (78)$$

where  $p_{ref}$  is the reference pressure, 1000 mb.

### 4.2.3 Soil Hydrology.

The soil wetness influences the energy balance of the surface by changing the surface albedo by affecting the soil heat flux through the thermal diffusivity, and by determining the partitioning of the heat fluxes into latent and sensible heat flux. The 2-layer soil hydrology model developed by Mahrt and Pan (1984) is implemented to represent the soil moisture.



The transport of water in the soil can be described by the prognostic equation

$$\frac{\partial \eta}{\partial t} = \frac{1}{\rho_w} \frac{\partial W_s}{\partial z} + A(z), \quad (79)$$

where  $\eta$  is the volumetric soil moisture content,  $\rho_w$  is the density of liquid water,  $W_s$  is the moisture flux within the soil. The term  $A(z)$  describes extraction of the soil water by roots due to the transpiration  $E_r$  from vegetation canopy.

The soil moisture flux is expressed as

$$W_s = K_\eta \rho_w \frac{\partial(\Psi + z)}{\partial z}, \quad (80)$$

or in alternate form as

$$W_s = D_\eta \rho_w \frac{\partial \eta}{\partial z} + K_\eta \rho_w, \quad (81)$$

where  $K_\eta$  is the hydraulic conductivity,  $\Psi$  is the moisture potential, which represents the potential energy needed to extract water against capillary and adhesive forces in the soil, and the diffusivity,  $D_\eta$ , is defined as

$$D_\eta = K_\eta \frac{\partial \Psi}{\partial \eta}. \quad (82)$$

The parameters  $K_\eta$ ,  $D_\eta$ , and  $\Psi$  are related to  $\eta$  through a set of simple relationships presented by Clapp and Hornberg (1978) and applied in McCumber and Pielke (1981)

$$K_\eta = K_{\eta_s} \left( \frac{\eta}{\eta_s} \right)^{2b+3}, \quad (83)$$

$$D_\eta = -\frac{bK_{\eta_s}\Psi_s}{\eta} \left( \frac{\eta}{\eta_s} \right)^{b+3}, \quad (84)$$

$$\Psi = \Psi_s \left( \frac{\eta_s}{\eta} \right)^b. \quad (85)$$

The exponent  $b$ , saturated hydraulic conductivity  $K_{\eta_s}$ , saturated moisture potential  $\Psi_s$ , and soil moisture at field capacity (soil porosity)  $\eta_s$  are specified as function of the USDA soil textural classes determined by their percentage of clay, silt and sand (Table 1).

Table 1: Soil parameters of the USDA (United States Department of Agriculture) textural classes.

	Type of soil	$\eta_s$	$\eta_{wilt}$	$\eta_{fc}$	$\Psi_s$	$K_{\eta_s}$	$b$	$\rho_i c_i$	$A_0$	$C_{g\text{sar}}$
1	Sand	0.395	0.068	0.135	-0.121	$1.76 \times 10^{-4}$	4.05	$1.463 \times 10^6$	0.26	3.222
2	Loamy sand	0.410	0.075	0.150	-0.090	$1.563 \times 10^{-4}$	4.38	$1.404 \times 10^6$	0.27	3.057
3	Sandy loam	0.435	0.114	0.195	-0.218	$3.41 \times 10^{-3}$	4.90	$1.320 \times 10^6$	0.28	3.560
4	Silt loam	0.485	0.179	0.255	-0.786	$7.2 \times 10^{-6}$	5.30	$1.271 \times 10^6$	0.29	4.418
5	Loam	0.451	0.155	0.240	-0.478	$7.0 \times 10^{-6}$	5.39	$1.212 \times 10^6$	0.30	4.111
6	Sandy clay loam	0.420	0.175	0.255	-0.299	$6.3 \times 10^{-6}$	7.12	$1.175 \times 10^6$	0.28	3.670
7	Silty clay loam	0.477	0.218	0.322	-0.356	$1.7 \times 10^{-6}$	7.75	$1.317 \times 10^6$	0.26	3.593
8	Clay loam	0.476	0.250	0.325	-0.630	$2.5 \times 10^{-6}$	8.52	$1.225 \times 10^6$	0.24	3.995
9	Sandy clay	0.426	0.219	0.310	-0.153	$2.2 \times 10^{-6}$	10.4	$1.175 \times 10^6$	0.22	3.058
10	Silty clay	0.492	0.283	0.370	-0.490	$1.0 \times 10^{-6}$	10.4	$1.115 \times 10^6$	0.21	3.729
11	Clay	0.482	0.286	0.367	-0.405	$1.3 \times 10^{-6}$	11.4	$1.089 \times 10^6$	0.20	3.600
12	Silt	0.485	0.179	0.535	-0.786	$8.0 \times 10^{-6}$	5.30	$0.836 \times 10^6$	0.14	3.970

Following Mahrt and Pan (1984) equation (4.50) is integrated over two slabs of the soil, from  $z=0$  to  $z=-0.05\text{m}$ , and from  $z=-0.05\text{m}$  to  $z=-1.0\text{m}$ . This gives us two prognostic equations for the mean volumetric water content in the upper thin layer,  $\eta_1$ , and in the lower later,  $\eta_2$

$$\frac{\partial \eta_1}{\partial t} z_1 = - \left( D_\eta \frac{\partial \eta}{\partial z} \right)_i - K_{\eta_i} + \frac{P_g - E_g}{\rho_w} - f_{root} E_{ir}, \quad (86)$$

$$\frac{\partial \eta_2}{\partial t} (z_2 - z_1) = - \left( D_\eta \frac{\partial \eta}{\partial z} \right)_i + K_{\eta_i} - K_{\eta_2} - (1 - f_{root}) E_{ir}. \quad (87)$$

The root extraction term  $A(z)$  was integrated under assumption that the upper soil layer contains fraction  $f_{root}$  of root mass while the remaining fraction of roots  $1 - f_{root}$  is within the lower soil layer. Continuity at the soil surface requires that the flux  $W_s$  of water in the soil at  $z = 0$  equals of the sum of the flux  $P_g$  of liquid water reaching the ground surface and the evaporation  $E_g$  from the soil surface

$$- D_{\eta_1} \frac{\partial \eta}{\partial z} - K_{\eta_i} = - \frac{P_g - E_g}{\rho_w}. \quad (88)$$

The gradient of soil water content at the interfacial level,  $-z_1$ , is evaluated as a finite difference assuming that the mean value of  $\eta$  for each layer is represented for the midlevel of the layer

$$\left( D_\eta \frac{\partial \eta}{\partial z} \right)_i = 2 D_{\eta_i} \frac{\eta_1 - \eta_2}{z_2}. \quad (89)$$

This term is taken equal (except sign) for both soil layers to maintain continuity. The diffusivity  $D_{\eta_i}$  and the hydraulic conductivity  $K_{\eta_i}$  are evaluated using the largest value of  $\eta_1$  and  $\eta_2$ . The gradient term in Equation 89 is calculated between the surface and the midlevel of the upper layer using the

surface value of soil water content  $\eta_1$  and  $\eta_2$ . It allows us to calculate diagnostically the near-surface soil water content  $\eta_1$  from Equation 86.

Thermal properties of soil and its albedo vary depending on the amount of water present. The soil heat capacity,  $\rho_s c_s$ , is calculated as

$$\rho_s c_s = (1 - \eta_s) \rho_i c_i + \eta \rho_w c_w, \quad (90)$$

where dry volumetric soil heat capacity,  $\rho_i c_i$ , is tabulated for each soil class in Table 1, and  $\rho_w c_w$  are corresponding values for liquid water. The thermal conductivity of soil is given by McCumber and Pielke (1981)

$$\lambda_s = \max(419 \exp(-P_f - 2.71), 0.172), \quad (91)$$

where  $P_f = \log(-\Psi/100)$ .

The value of the soil albedo is determined taking into account the effect of soil wetness

$$A_g = A_\eta + A_z, \quad (92)$$

$$A_\eta = A_0(1 - \Delta), \quad \Delta = \min(\beta_g, 0.5), \quad (93)$$

and the effect of solar zenith angle

$$A_z = 0.01(\exp(0.003286Z^{1.5}) - 1). \quad (94)$$

Values of the basic soil albedo,  $A_0$ , are listed in Table 1, and the Halstedt parameter  $\beta_g$  is defined by

$$\beta_g = \begin{cases} 0.5[1 - \cos(\pi\eta_0/\eta_{fc})] & \eta_0 \leq \eta_{fc} \\ 1 & \text{otherwise} \end{cases}. \quad (95)$$

This expression takes into account that the surface evaporates at the potential rate when the soil moisture  $\eta_0$  exceeds the field capacity  $\eta_{fc}$  which corresponds to the hydraulic conductivity of 0.1 mm/day (Table 1).

#### 4.2.4 Water Intercepted by Canopy.

The amount of liquid water,  $W_d$ , intercepted by the foliage due to dew formation or rainfall is governed by the prognostic equation (Deardorff, 1978)

$$\frac{\partial W_d}{\partial t} = \text{veg}P - E_r + R_r, \quad (96)$$

where  $P$  is the precipitation rate at the top of the vegetation,  $E_r$  is the direct evaporation from the fraction  $\delta$  of the foliage covered with a film of water when positive and the dew flux when negative.  $R_r$

is the runoff of the interception reservoir which occurs when  $W_d$  exceeds a maximum value  $W_{d\max}$  depending on the density of the canopy (Dickinson et al., 1986)

$$W_{d\max} = h_w \text{veg} \text{LAI}, \quad (97)$$

where  $h_w$  is the maximum storage of water, assumed to be equal 0.0002 m. The wet fraction of the canopy  $\delta$  is calculated following Deardorff (1978)

$$\delta = \begin{cases} (W_d / W_{d\max})^{2/3} & \text{for } E_r > 0 \\ 1 & \text{for } E_r < 0 \end{cases} \quad (98)$$

The flux of liquid water reaching the ground surface

$$P_g = (1 - \text{veg})P + R_r, \quad (99)$$

includes the nonintercepted rainfall and the runoff from the canopy.

#### 4.2.5 Water Areas.

The surface of water bodies such as lakes and oceans is represented in the OMEGA model rather simply. Because of the large heat capacity of water and strong surface mixing, the surface temperature of water bodies  $T_{sea}$  is initially specified based climatological data and then assumed to be constant during the period of the mesoscale simulation. As in most mesoscale models, OMEGA assumes that the air just above the water surface is fully saturated by water vapor

$$q_0 = q_{sat}(T_{sea}) \quad (100)$$

The spatial variation of surface roughness length  $z_0$  is specified based on land-use categories over land surfaces, while it is determined using the Charnock's relationship (Charnock, 1955) over water surfaces

$$z_0 = a_1 \frac{u_*^2}{g}. \quad (101)$$

Although the coefficient  $a_1$  in the above equation has been found to be somewhat variable, a value of 0.018 is included in the model (Arya, 1988). Also, a minimum value of 0.0015cm is imposed on the  $z_0$  based on observations.

#### 4.3 Microphysics.

Cloud microphysics is the general term used to represent the collection of processes that involve water and the different phases of water that occur in clouds. In nature, these processes include condensation / evaporation (vapor  $\leftrightarrow$  liquid), deposition/sublimation (vapor  $\leftrightarrow$  solid), freezing / melting (liquid  $\leftrightarrow$  solid), interparticle collisions and collection, and sedimentation (fall out). Even though these processes *appear* conceptually straight forward, developing a complete mathematical formulation describing them is a very difficult task. Researchers subdivide cloud microphysics into several conceptual processes, and develop parameterizations for them guided by the actual physical processes they represent and with the relevant parameters derived from experimental and field observations.

The OMEGA microphysics package is derived from that contained in the SAIC version of the MASS model (originally designed by scientists at MESO, Inc.) and is a subset of the scheme described in Lin *et al.* (1983). These parameterizations fall under the category of *bulk-water microphysics* in which the production rates are functions of the total mass density of each water species. As in MASS, the water

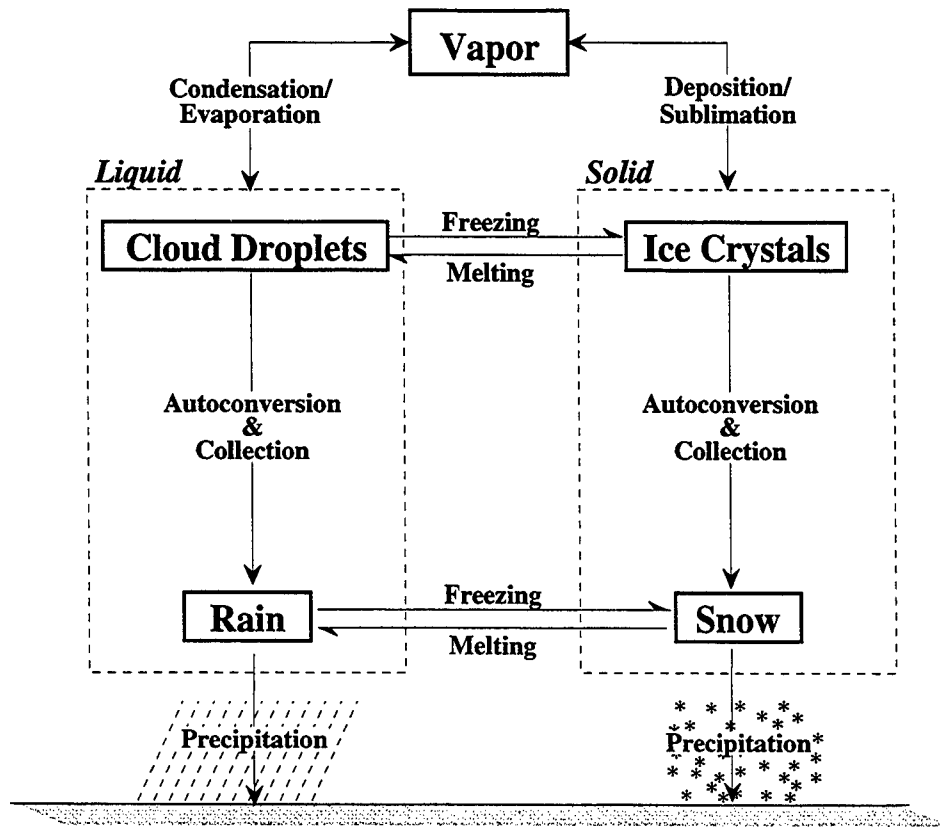


Figure 16. Microphysical processes parameterized in OMEGA.

species in OMEGA are divided into vapor, cloud droplets, ice crystals, rain and snow fields; however liquid and solid phases of water are not allowed to coexist. This implies that neither supercooled liquid nor melting solids (such as wet snow) can exist in the model domain. Because of this simplification, the number of microphysical processes to be dealt with is much smaller than that in the cloud model TASS (Proctor 1987). The microphysical processes included in OMEGA (Figure 16) are:

- 1) Condensation (or evaporation) of cloud water,
- 2) Autoconversion of cloud water to rain,
- 3) Condensation on (or evaporation of) raindrops,
- 4) Accretion of cloud water by rain drops,
- 5) Accretion of cloud water by rain drops,
- 6) Fallout of rain,
- 7) Generation of ice crystals from ice nuclei,
- 8) Deposition (or sublimation) growth of ice crystals,
- 9) Autoconversion of ice crystals to snow,
- 10) Deposition on (or sublimation of) snow,
- 11) Accretion of ice crystals by snow,
- 12) Fallout of snow.

### 4.3.1 Computational Treatment.

In OMEGA the time step used for integration depends on the local Courant number, which is a function of the velocity (advective or acoustic) in the cell and the dimension of the cell. Hence the time step can range from sub-second to tens of seconds depending on the flow characteristics. The microphysical parameterizations, however, only need to be calculated using a time step of at most a few seconds. Hence the microphysical calculations are sub-cycled in time if necessary. The microphysical time step is expected to be at roughly five to ten seconds. In the following discussion all values are assumed to be in SI units unless explicitly specified otherwise. In OMEGA the water substances are categorized into five species: vapor, cloud droplets, ice crystals, rain, and snow (hail and its associated physics could be included in the future). In the following discussion  $Q$  will represent the mixing ratio of a hydrometeor class. Suffixes  $V$ ,  $C$ ,  $I$ ,  $R$ , and  $S$  will refer to water vapor, cloud droplets, ice crystals, rain and snow, respectively.

The cloud droplets and ice crystals are assumed to be monodispersed and non-precipitating. Marshall and Palmer (1948) type relationships are used in describing rainfall droplets and snow crystals with their sizes. These are given as:

and

$$\begin{aligned} N(d_R) &= N_{0R} \exp\left(-\frac{d_R}{\Lambda_R}\right) \\ N(d_S) &= N_{0S} \exp\left(-\frac{d_S}{\Lambda_S}\right) \end{aligned} \quad (102)$$

where  $d_R$  and  $d_S$  are the particle diameters for rain and snow respectively.  $N_{0R}$  and  $N_{0S}$  are the y-intercepts of the distribution of rain and snow and hence represent the limiting number concentration as diameter tends to zero.  $\Lambda_R$  and  $\Lambda_S$  represent the slope of the respective inverse-exponential distribution. The computation of the parameters and variables involved in the microphysical processes can be divided into several levels:

- Parameters that are constants in space and time can be specified at the time of model compilation or at model run time.
- Parameters that are functions of space but are constant in time can be precomputed as part of model initialization.
- Parameters that are functions of space and time need to be evaluated in **MICPHY** (the subroutine in which the microphysical conversion rates are computed) for each time step. Some parameters depend only on a single physical variable which in turn is a function of space and time. For computational efficiency, look-up tables can be created in which these parameters are evaluated over a range of the dependent variable that will sufficiently bracket the ranges that will be encountered in the model domain. This method will be used for variables such as the saturation vapor pressures, latent heats, specific heats etc. These variables are dependent on temperature alone. Their look-up tables will be generated over the temperature range  $-100^\circ\text{C}$  to  $50^\circ\text{C}$  at 0.1 degree intervals. The value of the variable at any given temperature can then be computed by simple linear interpolation between values picked from the table.

The following steps form the computational sequence that will be discussed in detail in the following sections:

- 1) Evaluate local temperature from potential temperature
- 2) Evaluate microphysical parameters
- 3) Evaluate local super-saturation
- 4) Calculate the ice nuclei concentration
- 5) Calculate the particle size distribution parameters for rain and snow
- 6) Calculate the production rates of non-precipitating hydrometeors
- 7) Adjust mixing ratios of non-precipitating hydrometeors
- 8) Calculate the production rates of precipitating hydrometeors
- 9) Adjust mixing ratios of non-precipitating hydrometeors
- 10) Adjust temperature to include the release of latent heat
- 11) Compute the precipitation (rain and snow) fluxes due to their fall velocities.

### 4.3.2 Evaluate Local Temperature from Potential Temperature.

In OMEGA, the prognostic thermodynamic variable is  $\rho\theta$ , where  $\rho$  is the density and  $\theta$  is the potential temperature. ( $\rho\theta$  in effect is the energy density.) The potential temperature of a parcel of air is defined as the temperature that air parcel would have if it is moved adiabatically to a reference pressure level (in meteorology the reference pressure level is assumed to be  $10^5$  Pa, = 1000 mb). The majority of the microphysical processes, however, are driven by temperature and not potential temperature. Hence the temperature has to be calculated from the potential temperature. The temperature and the potential temperature are related via the Poisson equation,

$$T = \theta \left( \frac{P}{P_{ref}} \right)^\kappa; \quad \theta = T \left( \frac{P}{P_{ref}} \right)^{-\kappa} \quad (103)$$

where

$$P_{ref} = 1 \times 10^5 \text{ Pa} \quad \text{and} \quad \kappa = \frac{R_d}{c_p} = 0.286 \quad (104)$$

### 4.3.3 Evaluate Microphysical Parameters.

Several physical parameters are involved in the microphysical calculations. All the microphysical processes involving phase change of any type need the respective latent heats. The phase change processes which involve the vapor phase also depend upon the local saturation condition. Hence the corresponding saturation vapor pressures have to be evaluated. Other processes involving heat transfer need the specific heats of water, ice, vapor, and air, and parameters such as the diffusivity of vapor are required for computing the rate of sublimation or condensation of the precipitating hydrometeors. Once the local temperature is defined, these microphysical parameters can be evaluated.

**4.3.3.1 Latent Heats.** Latent heats of vaporization and fusion are assumed to vary only with temperature,  $T$  such that (These expressions are from Pruppacher and Klett (1978).)

$$L_v(T) = 2.50078 \times 10^6 \left( \frac{T_0}{T} \right)^y \text{ J/Kg} \quad (105)$$

where  $y = 0.167 + 3.67 \times 10^{-4} T$  and  $T_0 = 273.16 \text{ K} (= 0^\circ\text{C})$  and

$$L_f(T) = \begin{cases} \left. \begin{aligned} &3.3369 \times 10^5 + 2030.6(T - T_0) \\ &- 10.467(T - T_0)^2 \end{aligned} \right\} \text{J/Kg} & \text{if } T \leq T_0 \\ 3.3369 \times 10^5 \text{ J/Kg} & \text{if } T > T_0 \end{cases} \quad (106)$$

The latent heat of sublimation is given as

$$L_s(T) = L_v(T) + L_f(T) \quad (107)$$

The latent heat of sublimation varies only very slightly with temperature and can be assumed to be a constant at  $2.83237 \times 10^7 \text{ J/kg}$ . Hence the following scheme is generally used for calculation of latent heats. For temperatures above melting, the latent heat of vaporization is computed using (4.48) and the latent heat of fusion is calculated as

$$L_f = L_s - L_v \quad (108)$$

If temperature is less than melting then the latent heat of fusion is calculated as a function of temperature using (4.49) and then the latent heat of vaporization is calculated as

$$L_v = L_s - L_f \quad (109)$$

**4.3.3.2 Specific Heats and Other Parameters.** The specific heat of water and ice are given by Pruppacher and Klett (1978) (in units of J/Kg-K as

$$C_w(T) = \begin{cases} 5400.0 & \text{if } T < 223.16 \\ 4217.8 + 0.3471(T - T_0)^2 & \text{if } 223.16 < T \leq T_0 \\ \left. \begin{aligned} &4178.0 + 0.01298(T - 308.16)^2 \\ &+ 1.591 \times 10^{-5}(T - 308.16)^4 \end{aligned} \right\} & \text{if } T_0 < T \end{cases} \quad (110)$$

and

$$C_i(T) = \begin{cases} 2106.1 + 7.327(T - T_0) & \text{if } T \leq T_0 \\ 2106.1 & \text{if } T > T_0 \end{cases} \quad (111)$$

The dynamic viscosity of air is given by List (1971) as

$$\begin{aligned} \mu_D(T) &= 1.8325 \times 10^{-5} \frac{416.6}{T + 120.0} \left( \frac{T}{296.16} \right)^{1.5} \\ &= 1.49629 \times 10^{-6} \left( \frac{T^{1.5}}{T + 120.0} \right) \end{aligned} \quad (112)$$

Then the molecular viscosity is simply

$$v_m(P, T) = \frac{\mu_D}{\rho} \quad (113)$$

The thermal conductivity of air is (Wisner *et al.*, 1972)



$$\begin{aligned}
k_T(T) &= 1414.0\mu_D(T) \\
&= 2.11575 \times 10^{-3} \left( \frac{T^{1.5}}{T + 120.0} \right)
\end{aligned} \tag{114}$$

The diffusivity of water vapor in air is (Pruppacher and Klett, 1978)

$$\begin{aligned}
D_v(P, T) &= 2.11 \times 10^{-5} \left( \frac{101325.0}{P} \right) \left( \frac{T}{T_0} \right)^{1.94} \\
&= 4.0119 \times 10^{-5} \frac{T^{1.94}}{P}
\end{aligned} \tag{115}$$

The Schmidt number is defined as the ratio of the molecular viscosity to the diffusivity of water vapor in air or

$$N_{sc}(P, T) = \frac{\nu_m(P, T)}{D_v(P, T)} = 3.72963 \times 10^{-2} R_d \frac{T^{0.56}}{T + 120.0} \tag{116}$$

#### 4.3.4 Evaluate Local Supersaturation.

The processes of condensation/evaporation and deposition/sublimation are very dependent on the amount of water vapor that exists in excess of the saturation limit at that point in space. Hence the local saturation vapor pressures (over water and ice surfaces) are calculated. The saturation vapor pressures are functions of temperature only. Their variation with temperature is given by the Clausius-Clapeyron equation (Hess, 1959). This is somewhat cumbersome to use in a program as it involves other temperature dependent quantities such as the latent heats. We will adopt the method used in TASS (Proctor, 1987) in which the saturation vapor pressures (over water and ice surfaces) are computed using the following polynomial fits to experimental data (Wexler, 1976, 1977):

$$\begin{aligned}
e_{sw}(T) &= \exp(-2991.2729T^{-2} - 6017.0128T^{-1} + 17.87643854 \\
&\quad - 0.028354721T + 0.17838301 \times 10^{-4} T^2 \\
&\quad - 0.84150417 \times 10^{-9} T^3 + 0.44412543 \times 10^{-12} T^4 \\
&\quad + 2.858487 \ln T)
\end{aligned} \tag{117}$$

and

$$\begin{aligned}
e_{si}(T) &= \exp(-5865.3696T^{-1} + 22.241033 + 0.013749042T \\
&\quad - 0.34031775 \times 10^{-4} T^2 + 0.26967687 \times 10^{-7} T^3 \\
&\quad + 0.6918651 \ln T)
\end{aligned} \tag{118}$$

The saturation mixing ratios of water vapor over a water surface  $Q_{vs}$ , and over an ice surface  $Q_{si}$ , can then be calculated from  $e_{sw}$  and  $e_{si}$ , respectively as

$$Q_{vs} = \frac{e_{sw}(Q_v + \varepsilon)}{P} \tag{119}$$

and

$$Q_{si} = \frac{e_{si}(Q_v + \varepsilon)}{P} \tag{120}$$

where  $\varepsilon = R/R_D = 0.622$ .

#### 4.3.5 Calculate the Ice Nuclei Concentration.

Ice nuclei (IN) are aerosols on which water vapor can deposit to form ice crystals. Only a fraction of all the aerosols present in the atmosphere can serve as ice nuclei. This fraction is determined by the surface and crystalline properties of the material. Among all the ice nuclei present only some are active at any given temperature. Observations of the number concentration of active ice nuclei as a function of the local temperature (Fletcher, 1962) yield

$$n_{IN} = \begin{cases} 10^9 & \text{if } T < 230.95 \\ \beta_{IN} \exp\{0.6(T_M - T)\} & \text{if } 230.95 \leq T \leq T_M \\ 0 & \text{if } T_M < T \end{cases} \quad (121)$$

where  $\beta_{IN} = 0.01 m^{-3}$ . The IN concentrations can vary by as much as a factor of 10 at a location and temperature (Pruppacher and Klett, 1978).

#### 4.3.6 Calculate $\Lambda$ 's and Fall Velocities for Rain, and Snow.

The intercepts of the inverse exponential distributions describing rain, and snow are defined as

$$\begin{aligned} \text{and } N_{0R} &= 2.25 \times 10^7 \left( \frac{Q_R}{\rho} \right)^{0.375} \\ N_{0S} &= 5.5 \times 10^6 \exp[-0.088(T - T_M)] \end{aligned} \quad (122)$$

The slopes of the inverse exponential distributions can now be calculated as

$$\Lambda_R = \left( \frac{\rho Q_R}{\pi N_{0R} \delta_w} \right)^{0.25} \quad \text{and} \quad \Lambda_S = \left( \frac{\rho Q_S}{\pi N_{0S} \delta_s} \right)^{0.25} \quad (123)$$

where  $\delta_w$  and  $\delta_s$  are the densities of water, and snow respectively given as.

$$\delta_w = 1000. \text{ Kg/m}^3 \quad \text{and} \quad \delta_s = 100. \text{ Kg/m}^3$$

The precipitating hydrometeors have terminal fall velocities, which are calculated from a single particle fall velocity averaged over the respective distribution in a mass-weighted manner. The mass-weighted fall velocities for rain, and snow are calculated as follows:

$$W_R = \left( -0.267 + 2.06 \times 10^4 \Lambda_R - 2.045 \times 10^7 \Lambda_R^2 + 9.06 \times 10^9 \Lambda_R^3 \right) \left( \frac{1.2}{\rho} \right)^{0.4} \quad (124)$$

$$\text{and } W_S = \begin{cases} 1.1 \left( \frac{1.2}{\rho} \right)^{0.5} & \text{if } T < T_M \\ 2.5 \left( \frac{1.2}{\rho} \right)^{0.5} & \text{if } T \geq T_M \end{cases} \quad (125)$$

#### 4.3.7 Production Rates of Non-Precipitating Hydrometeors.

With the local thermodynamic state and key microphysical parameters computed, it is now possible to evaluate the production/loss of the hydrometeors. Because their smaller size increases the surface area

to volume ratio, the non-precipitating hydrometeors respond most quickly to changes in their surroundings. For this reason we evaluate their changes first. In the following discussion of production terms, we will use the following terminology.  $Q$  will denote the mixing ratios,  $\Delta Q$  the change in  $Q$ , and  $P$  the rate of change of mixing ratios with time. The subscripts of  $\Delta Q$  and  $P$  will indicate the microphysical process involved. The non-precipitating hydrometeors are comprised of the cloud droplets and the ice crystals. Even though they have finite fall velocities, they are small enough to be ignored, and for all practical purposes these particles can be assumed to follow the airstream. For the sake of computational efficiency these calculations are performed in a model layer only if at least one of the participant species is significantly non-zero in some cell in that layer.

**4.3.7.1 Freezing of Cloud Droplets.** Freezing of water is initiated by ice nuclei that are immersed in water, or come into contact with the water surface. Large water drops generally contain enough impurities that they freeze at or near  $0^\circ\text{C}$  ( $T_M$ ). Small droplets, however, can exist in liquid phase at temperatures far below  $0^\circ\text{C}$ , if they do not contain or come into contact with any ice nuclei. Even small droplets however will spontaneously freeze at about  $-40^\circ\text{C}$ . In nature, supercooled liquid is usually found in very vigorous thunderstorms, where the droplets are formed in a rapidly cooling air parcel in the strong updrafts. In this version of OMEGA, however, no supercooled liquid is allowed to exist. (Supercooled liquid and melting solids will be allowed to exist in a future version.) Therefore, if  $T \leq T_M$ , all cloud droplets in that computational cell are frozen to produce ice crystals as shown in the following relation:

$$\left. \begin{aligned} Q_I &= Q_I + Q_C \\ \Delta Q_{CFZN} &= Q_C \\ Q_C &= 0. \end{aligned} \right\} \text{ if } T \leq T_M \quad (126)$$

**4.3.7.2 Melting of Ice Crystals.** If  $T > T_M$  all ice crystals in that cell are melted to form cloud droplets by the following:

$$\left. \begin{aligned} Q_C &= Q_C + Q_I \\ \Delta Q_{IMLT} &= Q_I \\ Q_I &= 0. \end{aligned} \right\} \text{ if } T > T_M \quad (127)$$

**4.3.7.3 If  $T > T_M$  Compute Condensation/Evaporation.** The amount of cloud water vapor condensed into liquid depends on the water vapor excess (over saturation) that is present at a grid point. The excess vapor is assumed to condense into cloud droplets (or undergo deposition to form ice crystals.) This process is assumed to occur instantaneously; thus supersaturated conditions cannot exist in the model domain. (This process will be replaced by a condensation rate equation later, which will then allow for supersaturated conditions to exist.)

The condensation adjustment equation can be derived by considering a closed volume of moist air. If supersaturation exists, the excess water vapor will start to condense. As condensation proceeds, latent heat of vaporization is released, increasing the temperature and hence the saturation vapor pressure of air. Thus the initial water vapor excess  $\Delta Q_V$  is used not only for condensation, but also for the increase in vapor capacity of the air. Let  $\Delta Q_1$ , and  $\Delta Q_2$  denote the amount of water vapor condensed, and the amount of extra vapor the air can hold due to the increase in temperature such that the total  $\Delta Q$  is given by

$$\Delta Q = \Delta Q_1 + \Delta Q_2 \quad (128)$$

The increase in temperature  $\Delta T$  due to the release in latent heat when  $\Delta Q_1$  vapor is condensed is

$$\Delta T = \frac{L_v \Delta Q_1}{c_p} \quad (129)$$

This increase in temperature increases the saturation vapor pressure as given by the Clausius-Clapeyron equation,

$$\frac{de_s}{e_s} = \frac{L_v}{R_v} \frac{dT}{T^2} \quad (130)$$

In an isobaric process (we assume that in each grid cell the pressure does not change during the microphysical adjustments) such that

$$\frac{dQ_{vs}}{Q_{vs}} = \frac{de_s}{e_s} \quad (131)$$

hence,

$$\Delta Q_2 = Q_{sv} \frac{L_v \Delta T}{R_v T^2} = \frac{L_v^2 Q_{sv} \Delta Q_1}{c_p R_v T^2} \quad (132)$$

Define a fraction  $r$  such that  $\Delta Q_2 = r \Delta Q_1$ . Then

$$r = \frac{\Delta Q_2}{\Delta Q_1} = \frac{\Delta Q_2}{\Delta Q_1 + \Delta Q_2} = \Delta Q_1 \left\{ \Delta Q_1 + \frac{L_v^2 Q_{sv} \Delta Q_1}{c_p R_v T^2} \right\}^{-1} = \left\{ 1 + \frac{L_v^2 Q_{sv}}{c_p R_v T^2} \right\}^{-1} \quad (133)$$

Thus the amount of water vapor to be condensed (or the maximum amount of cloud water that can be evaporated) can be written as

$$\Delta Q_{CCND} = r \Delta Q = \frac{Q_v - Q_{sv}}{1 + \frac{L_v^2 Q_{sv}}{c_p R_v T^2}} \quad (134)$$

**4.3.7.4 Initiation of Ice Crystals.** Ice crystals can be produced as vapor deposits directly onto ice nuclei (deposition nucleation). The production rate of ice crystals via this process thus depends on the ice nuclei number concentration, which in turn depends on the local temperature.

In OMEGA cloud ice is initiated at temperatures less than  $-16^\circ\text{C}$ ; at higher temperatures, the rate is near zero. The initiated crystals are assumed to have a maximum diameter of  $12.9 \mu\text{m}$  and a maximum mass of  $10^{-12}$  kg. The amount of ice initiated by this process is limited by the assumed maximum ice crystal mass (and the IN concentration) and by the available supersaturation (with respect to an ice surface). The maximum ice mixing ratio attained by growing all crystals to  $12.9 \mu\text{m}$  is

$$\Delta Q_{I1} = \frac{10^{-12} n_{IN}}{\rho} \quad (135)$$

The maximum ice mixing ratio that can be generated by depositional growth driven by the supersaturation can be derived in a manner analogous to the condensation adjustment (Equation 97) by replacing  $L_v$  by  $L_s$ , and  $Q_{vS}$  by  $Q_{si}$ . Thus,

$$\Delta Q_{I2} = \frac{Q_v - Q_{si}}{1 + \frac{L_s^2 Q_{si}}{c_p R_v T^2}} \quad (136)$$

and 
$$\Delta Q_{ICWV1} = \min(\Delta Q_{I1}, \Delta Q_{I2}) \quad (137)$$

**4.3.7.5 If  $T \leq T_M$  Compute Deposition/Sublimation.** Existing ice crystals grow by deposition if, after ice crystal initiation, excess vapor (over ice saturation) still exists. The depositional growth rate of ice crystals is given by

$$\frac{\partial Q_I}{\partial t} = 65.2 \sqrt{\frac{Q_I \rho}{n_{IN}}} \frac{Q_v - Q_{si}}{Q_{si} A^* + B^*} \quad (138)$$

where

$$A^* = \frac{L_v}{k_T T} \left( \frac{L_s}{R_v T} - 1 \right) \quad (139)$$

and

$$B^* = \frac{1}{\rho D_v} \quad (140)$$

where  $D_v$  is the diffusivity of water vapor given by Equation 115.

This rate has to be limited by the maximum cloud ice that can grow by deposition under the current saturation conditions. This is given by  $\Delta Q_{I2}$ ; hence,

$$P_{IDEP} = \min\left(\frac{\partial Q_I}{\partial t}, \frac{\Delta Q_{I2}}{\Delta t}\right) \quad (141)$$

If  $(Q_v - Q_{si})$  is negative then sublimation occurs. (The sublimation model will need refinement to better define cirrus clouds. Observations suggest that ice crystals from cirrus can fall large distances through sub-saturated air.)

#### 4.3.8 Adjust Mixing Ratios of Non-Precipitating Hydrometeors.

Before proceeding to compute the production/loss of precipitating hydrometeors, the mixing ratios of cloud droplets, ice crystals and water vapor are adjusted.

$$\begin{aligned} Q_C &= Q_C + \Delta Q_{CCND} \\ Q_I &= Q_I + P_{IDEP} \Delta t + \Delta Q_{ICWV1} \\ Q_v &= Q_v - \Delta Q_{CCND} - P_{IDEP} \Delta t - \Delta Q_{ICWV1} \end{aligned} \quad (142)$$

The temperature adjustment is determined from

$$c_p \Delta T = (\Delta Q_{CFZN} - \Delta Q_{IMLT}) L_f + \Delta Q_{CCND} L_v + (\Delta Q_{ICWV1} + P_{IDEP} \Delta t) L_s \quad (143)$$

### 4.3.9 Production Rates of Precipitating Hydrometeors.

Having completed the adjustments of the non-precipitating hydrometeors, we are now able to evaluate the production/loss of the larger precipitating hydrometeors.

**4.3.9.1 Production of Rain by Melting of Snow.** In the current version of OMEGA, all snow melts instantaneously to rain above 0°C ( $T_M$ ) such that

$$\left. \begin{aligned} Q_R &= Q_R + Q_S \\ \Delta Q_{SMLT} &= Q_S \\ Q_S &= 0. \end{aligned} \right\} \text{ if } T > T_M \quad (144)$$

**4.3.9.2 Production of Snow by the Freezing of Raindrops.** This reverse process to the production of rain by melting of snow assumes that all rain freezes instantaneously to snow below 0°C where

$$\left. \begin{aligned} Q_S &= Q_S + Q_R \\ \Delta Q_{RFZN} &= Q_R \\ Q_R &= 0. \end{aligned} \right\} \text{ if } T \leq T_M \quad (145)$$

**4.3.9.3 Autoconversion of Cloud Droplets to Form Rain.** Even though we have assumed the cloud droplets to be monodisperse, in reality they exist in all sizes (small of course). They undergo interparticle collisions and coalesce to form larger droplets or rain drops. This stochastic process of self collection and growth to form rain is termed autoconversion. The rate of production of rain from cloud droplets via autoconversion is given by (Berry and Reinhardt, 1974a and 1974b)

$$P_{RACV} = 7.26 \times 10^{-3} \left[ 10^{20} \left( \frac{\sigma}{0.38} \right) r_c^4 - 0.4 \right] \rho Q_C^2 \left[ \left( \frac{\sigma}{0.38} \right)^{1/3} r_c 10^6 - 7.5 \right] \quad (146)$$

where  $r_c = \left( \frac{3\rho Q_C}{4\pi N_c \delta_w} \right)^{1/3}$  is the mean cloud droplet radius,  $\sigma$  is the dispersion coefficient of the cloud droplet distribution, and,  $N_c$  the cloud condensation nuclei (CCN) concentration.

**4.3.9.4 Collection of Cloud Droplets by Raindrop.** Raindrops collect cloud droplets as the raindrops have a much higher fall speed than the cloud droplets. The collection efficiency is a function of the size of cloud droplets. Large droplets will have a high collection efficiency, whereas the very small droplets will flow around the raindrop and thus have a collection efficiency of zero. The production rate due to this collection mechanism is

$$P_{RAC} = \frac{15\pi}{38} \Lambda_R^3 N_{OR} W_R Q_C E_{RCD} \quad (147)$$

where  $E_{RCD}$  is computed from a polynomial fit to experimental data (Proctor, 1987) given by

$$E_{RCD} = \begin{cases} 0 & \text{if } r_c < 1.2\mu m \\ -0.27544 + 0.26249 \times 10^6 r_c \\ -1.8896 \times 10^{10} r_c^2 + 4.4626 \times 10^{14} r_c^3 \\ 1 \end{cases} \quad \begin{cases} \text{if } 1.2\mu m \leq r_c < 20\mu m \\ \text{if } 20\mu m < r_c \end{cases} \quad (148)$$

**4.3.9.5 Condensation Evaporation of Raindrops.** Raindrops evaporate in sub-saturated conditions, if enough cloud droplets are not present to alleviate the saturation deficit. (The smaller cloud droplets are allowed to evaporate first as the saturation vapor pressure over a curved surface with smaller radius of curvature is higher than over a surface with larger radius of curvature.) Also if the environment is supersaturated, vapor can condense onto the rain drops. The following expression takes into account the ventilation effect of the falling raindrop

$$P_{RCND} = \frac{2\pi(Q_v - Q_{sv})N_{OR}\Lambda_R^2 \left( 1 + 0.3194027N_{sc}^{1/3} \sqrt{\frac{\Lambda_R W_R}{V_m}} \right)}{Q_{sv} \frac{L_v \rho}{k_T T} \left( \frac{L_v}{R_v T} - 1 \right) + \frac{1}{D_v}} \quad (149)$$

**4.3.9.6 Autoconversion of Ice Crystals to Snow.** Cloud ice conversion to snow occurs when the average crystal mass exceeds  $9.4 \times 10^{-10}$  Kg. This assumes that there is a stochastic maximum ice crystal size. The excess ice crystal mass is assumed to contribute to the snow field. This process is analogous to the production of rain by autoconversion of cloud droplets.

$$Q_{imax} \text{ (the maximum cloud ice concentration)} = 9.4 \times 10^{-10} n_{IN} \quad (150)$$

$$P_{SACV} = (Q_I - Q_{imax}) \frac{1}{\Delta t} \quad (151)$$

**4.3.9.7 Collection of Ice Crystals by Snow.** Just as raindrops collect cloud droplets by virtue of their difference in slip velocity, snowflakes collect ice crystals. The production rate of snow due to this collection of ice crystals is given by

$$P_{SACI} = 0.5\pi N_{OS} W_S \Lambda_S^3 Q_I E_{SCI} \quad (152)$$

where  $E_{SCI}$ , the collection of efficiency of snow for ice crystals, is a function of temperature such that

$$E_{SCI} = \exp(0.38(T - T_M)) \quad (153)$$

**4.3.9.8 Deposition/Sublimation of Snow.** The deposition onto (or sublimation of) snow is calculated in a manner similar to condensation on (or evaporation of) raindrops. The following formulation also takes into account the ventilation factor of falling snow:

$$P_{SDEP} = \frac{2\pi(Q_v - Q_{si})N_{OS}\Lambda_S^2 \left( 0.86 + 0.21N_{Sc}^{1/3} \sqrt{\frac{\pi\Lambda_S W_S}{v_m}} \right)}{Q_{si} \frac{L_v \rho}{k_T T} \left( \frac{L_s}{R_v T} - 1 \right) + \frac{1}{D_v}} \quad (154)$$

#### 4.3.10 Adjust Mixing Ratios of Hydrometeors.

With all the production/loss terms evaluated, the mixing ratios of the hydrometeors and water vapor are adjusted by

$$\begin{aligned} Q_R &= Q_R + (P_{RACV} + P_{RCND} + P_{RAC})\Delta t \\ Q_S &= Q_S + (P_{SACV} + P_{SDEP} + P_{SACI})\Delta t \\ Q_C &= Q_C - (P_{RACV} + P_{RAC})\Delta t \\ Q_I &= Q_I - (P_{SACV} + P_{SACI})\Delta t \\ Q_v &= Q_v - (P_{RCND} + P_{SDEP})\Delta t \end{aligned} \quad (155)$$

#### 4.3.11 Adjust Temperature to Include Latent Heat Release.

The final step is to adjust the temperature in the cell to account for the latent heat released or absorbed during condensation/evaporation, deposition/sublimation, and freezing/melting involving the precipitating hydrometeors. The total latent heat released is balanced by the change in sensible heat in the following formulation:

$$c_p \Delta T = (\Delta Q_{RFZN} - \Delta Q_{SMLT})L_f + P_{RCND}\Delta t L_v + P_{SDEP}\Delta t L_s \quad (156)$$

This equation determines the temperature difference due to latent heat release. After the temperature is updated, the new values of potential temperature are calculated using the Poisson equation.

#### 4.3.12 Compute Precipitation Fluxes.

The fluxes due to precipitation are straight up and down, through the top and bottom faces of each cell. Even though the precipitation contribution can be accounted for by adding the fall velocities to the advection velocities, it is computationally more efficient to calculate it separately. The mixing ratio changes to rain and snow can be calculated as follows.

$$\frac{\partial Q_R}{\partial t} = \frac{1}{\rho} \frac{\partial(\rho Q_R)}{\partial z'} W_R \quad \text{and} \quad \frac{\partial Q_S}{\partial t} = \frac{1}{\rho} \frac{\partial(\rho Q_S)}{\partial z'} W_S \quad (157)$$

where  $z'$  denotes the local vertical direction (not to be confused with  $z$  the vertical coordinate of the Cartesian model domain).

#### 4.3.13 Convective Parameterization.

Deep cumulus convection is associated with a deep conditionally unstable layer and the presence of large-scale convergence. The first condition makes it possible for huge cumuli to penetrate into the upper troposphere and the lower stratosphere, while the second condition provides a general lifting mechanism to trigger the convective instability. Therefore, deep cumulus convection always takes place in regions of conditionally unstable stratification and low-level convergence of moisture, and in such regions this process causes the release of latent heat.



The release of latent heat by cumulus convection is one of the most important short term effects on the atmospheric dynamics. In addition, the water droplets within the clouds play a prominent role in the reflection, absorption, and emission of solar and terrestrial radiation. However, due to the large horizontal space scale and time steps of mesoscale models the vertical transport of heat, moisture and momentum by deep cumulus convection may not be adequately resolved. While the goal of OMEGA is to try to explicitly resolve large areas of convection, there will always be regions which are not sufficiently resolved. To circumvent this problem a version of cumulus parameterization that was originally proposed by Kuo (1965, 1974) and later modified by Anthes (1977a) is incorporated to account for the effect of subgrid scale deep cumulus convection on the local environment. This convective parameterization only applies to those regions which are convectively unstable to deep penetrative convection and in which the total horizontal moisture convergence exceeds a critical value. As the cumulus parameterization is a mechanism to account for subgrid convection in large cells, it is usually applied only to cells that large in area ( $O(100 \text{ km}^2)$ ). In OMEGA we are exploring a concept by which we can smoothly transition from regions where no convective parameterization is applied to regions where it is applied. This will be achieved by including a factor in the cumulus adjustment scheme which can vary between 0 and 1 depending on cell area. However, the explicit cloud microphysics is active over the whole domain.

The total rate of moisture accession,  $M_t$ , per unit horizontal area is given by the convergence of moisture in the column of atmosphere above the unit area plus the surface evaporation, thus

$$M_t = - \int_0^{z_t} \rho (\nabla_H \cdot \mathbf{V}q) dz + \delta_c \left[ \rho_0 C_D V_0 (q_s - q_a) \right] \quad (158)$$

where  $z_t$  is the model top,  $q$  the cell averaged mixing ratio,  $q_s$  the saturation value corresponding to sea-surface temperature,  $q_a$  the air value just over the sea,  $C_D$  the drag coefficient,  $\rho$  the density,  $\rho_0$  air density in the surface layer,  $V_0$  wind speed at the surface layer, and  $\delta_c$  is an indicator such that

$$\delta_c = \begin{cases} 0, & \text{over land} \\ 1, & \text{over water} \end{cases} \quad (159)$$

Hence, evaporation within the surface layer is taken into account only over the sea when  $w_0 > 1 \text{ cm s}^{-1}$  and  $\frac{\partial \theta_e}{\partial z} < 0$ , where  $w_0$  is the vertical velocity in the surface layer, and  $\theta_e$  is the equivalent potential temperature. It is assumed that the direct evaporation effects do not contribute to the generation of deep cumulus convection over land. The drag coefficient is determined using the surface layer similarity relationships as follows:

$$C_D = \frac{\beta k^2}{\left[ \ln \left( \frac{z}{z_0} \right) - \Psi_M \left( \frac{z}{L} \right) \right] \left[ \ln \left( \frac{z}{z_0} \right) - \Psi_H \left( \frac{z}{L} \right) \right]}, \quad (160)$$

where  $\beta$  is a constant and set to 1.35,  $k$  von Karman's constant,  $\Psi_M$  and  $\Psi_H$  the integral functions (see PBL parameterization),  $z_0$  the surface roughness height.

The moisture  $M_t$  is then used to make cloud columns  $(T_c, q_c)$  from environmental air  $(T, q)$ . Part of the moisture ( $M_1$ ) will condense and precipitate, raising the temperature from  $T$  to  $T_c$  and the remainder ( $M_2$ ) will increase the mixing ratio of the cloud column from  $q$  to  $q_c$ , that is

$$M_1 = \frac{c_p}{L_c} \int_{z_{cb}}^{z_{ct}} \rho (T_c - T) dz \quad (161)$$

and

$$M_2 = \int_{z_{cb}}^{z_{ct}} \rho (q_c - q) dz \quad (162)$$

where  $c_p$  is the specific heat at constant pressure,  $L_c$  latent heat of condensation,  $z_{cb}$  and  $z_{ct}$  the bottom and top of the cloud, respectively. Hence the total amount of water vapor needed to create the cloud over a unit area is then given by the sum of the two integrals

$$M_c = M_1 + M_2 = \int_{z_{cb}}^{z_{ct}} \rho \left[ \frac{c_p}{L_c} (T_c - T) + (q_c - q) \right] dz. \quad (163)$$

The rate of cloud production per unit time,  $C$  (or fractional area), is assumed to be proportional to the convergence of water vapor plus evaporation for the column divided by the amount of water vapor necessary to produce the model cloud as follows:

$$C = \frac{M_t}{M_c}. \quad (164)$$

Then, the product  $C \Delta t$  gives the total production of cloud air during time  $\Delta t$ .

In 1974, Kuo also introduced a division of the convergence of moisture into a fraction  $bM_t$  of the total which increases the humidity of the air, and a fraction  $(1-b)M_t$ , which is condensed and precipitates as rain or is carried away with the latent heat warming the air (Kuo, 1974). A proper evaluation of the parameter  $b$  is important. Anthes (1977a) proposed that  $b$  depends on the mean relative humidity in the air column in such a way that the moistening associated with cumulus convection is strong when the atmosphere is dry and the moistening is weak when the atmosphere is wet so that

$$b = \begin{cases} \left[ \frac{(1 - \overline{RH})}{(1 - RH_c)} \right]^n & \text{if } \overline{RH} \geq RH_c \\ 1 & \text{if } \overline{RH} < RH_c \end{cases}, \quad (165)$$

where  $\overline{RH}$  is the mean environmental relative humidity in the air column,  $RH_c$  is the critical relative humidity, and  $n$  a positive exponent. Hence, when  $\overline{RH}$  is less than  $RH_c$ , only environmental moistening takes place. Anthes (1977b) chose values of  $n=1$  and  $RH_c=0.5$  for the axisymmetric hurricane model. However, a number of studies have indicated that the  $b$  value computed with  $n=1$  and  $RH_c=0.5$  is too large and consequently convective heating, drying, and rainfall rates are underestimated. In a study on semi-prognostic tests of Kuo-type schemes in an extratropical convective system, Kuo and Anthes (1984) found that the simulated rainfall rate agrees best with observations when  $n$  is between 2 and 3,

and  $RH_c$  is between 0.25 and 0.50. During the Asian summer monsoon periods, Someshwar Das *et al.* (1988) found that the best results are obtained for values of  $n$  between 3 and 5, and  $RH_c$  between 0 and 0.25. In the ECMWF numerical forecasting model, values of  $n=3$  and  $RH_c=0$  are used (Tiedtke 1986). As a compromise between these values, in the OMEGA model  $n$  and  $RH_c$  are specified as 3 and 0.5, respectively.

Now assume that the large-scale forecast is made for a time step  $\Delta t$  giving a temperature  $T_e$  without the effects of cumulus convection. Then, applying the parameterization scheme gives a temperature  $T(t + \Delta t)$  such that

$$T(t + \Delta t) = T_e + (1-b) C \Delta t (T_c - T_e), \quad (166)$$

and the corresponding equation for mixing ratio  $q(t + \Delta t)$  after application of parameterization is

$$q(t + \Delta t) = q_e + b C \Delta t (q_c - q_e). \quad (167)$$

The precipitation from the subgrid cloud scale is that part of the moisture used in warming the air from  $T_e$  to  $T$ . Therefore, the rate of precipitation per unit time per unit volume in the column is given by

$$Pr e_{cl} = \int_t^{t + \Delta t} \int_{z_{cb}}^{z_{ct}} \frac{(1-b) C c_p (T_c - T_e)}{L_c} dz dt. \quad (168)$$

On evaluating the subgrid scale cloud effects, cumulus convective processes are activated when the vertically integrated moisture convergence rate exceeds a critical value of  $10^{-5} \text{ kgm}^{-2}\text{s}^{-1}$  (Anthes 1977b). The cloud base  $z_{cb}$  and cloud top  $z_{ct}$  need to be determined. The cloud base is determined by the lifting condensation level (LCL) of each air parcel. The temperature  $T_c$  and mixing ratio  $q_c$  inside the cloud are considered as those on a moist adiabatic passing through the lifting condensation level. Note that  $q_c$  is the saturation mixing ratio at the temperature  $T_c$ . The cloud top is specified as the height where cloud temperature  $T_c$  becomes less than the environment temperature  $T_e$ .

#### 4.4 Radiation.

The radiative source-sink term in the conservation of energy relation can be written as

$$S_R = \left( \frac{\partial T}{\partial t} \right)_{LW} + \left( \frac{\partial T}{\partial t} \right)_{SW} \quad (169)$$

where the terms on the right hand side represent the temperature change resulting from longwave and shortwave radiative divergence flux in the vertical direction. The divergence of radiative energy in the horizontal direction is neglected, since its variation is much larger in the vertical direction on the mesoscale. The methods of parameterizing this vertical flux takes into account the absorption of shortwave radiation by water vapor and the longwave energy emitted by water vapor and carbon dioxide. It is essentially similar to the one used by (Mahrer and Pielke, 1977). Because of the separation of wavelength in the atmospheric radiation spectra it is convenient to develop separate parameterizations for long and short wavelengths.

#### 4.4.1 Shortwave Radiative Flux.

The diurnal variation of the solar flux on a horizontal surface at the top of the atmosphere is computed from

$$S = S_0 \cos Z, \quad (170)$$

with

$$\cos Z = \cos \psi \cos \delta \cos H + \sin \psi \sin \delta \quad (171)$$

where  $S_0$  is the solar constant,  $Z$  the zenith angle,  $\psi$  the latitude,  $\delta$  the solar declination, a function of Julian day, and  $H$  the solar hour angle. Assuming that shortwave absorption in the atmosphere is only due to water vapor, the heating of the atmosphere by this radiation is then given by

$$\left(\frac{\partial T}{\partial t}\right)_s = \begin{cases} 0.231 \frac{S_0 \cos Z}{\rho C_p} \left[\frac{r(z)}{\cos Z}\right]^{-0.7} \frac{dr}{dz}, & \cos Z > 0 \\ 0, & \cos Z \leq 0 \end{cases} \quad (172)$$

where  $r(z)$  is the optical path length of water vapor above the layer  $z$  and is given by

$$r(z) = \int_z^{\text{top}} \rho q dz. \quad (173)$$

This is the shortwave flux formulation used in the OMEGA model.

#### 4.4.2 Longwave Radiative Flux.

The parameterization of the long wave radiative flux in atmospheric models is typically treated as a function of the normal optical thickness which when integrated over all wavelengths is represented by the broadband emissivity,  $\varepsilon$ . In clear or cloudy air this emissivity is dominated by the water content of the air. Water vapor and carbon dioxide (CO<sub>2</sub>) are considered as emitters of longwave radiation. The path length for water vapor ( $\Delta r_j$ ) expressed in units of g cm<sup>-2</sup> is computed for each vertical layer by

$$\Delta r_j = \rho_j q_j (z_{j+1} - z_j) = -\frac{(P_{j+1} - P_j)}{g} q_j; \quad (174)$$

and the path length for carbon dioxide ( $\Delta c_j$ ) expressed in units of millibars is

$$\Delta c_j = -0.4148239(p_{j+1} - p_j). \quad (175)$$

After these increments are obtained, they are summed up from the first level to the  $i$ th level to give the total path length as follows

$$r_{i+1} = \sum_{j=1}^i \Delta r_j \quad \text{and} \quad c_{i+1} = \sum_{j=1}^i \Delta c_j \quad (176)$$

where  $r_1 = c_1 = 0$  at the surface.

The emissivity for water vapor was derived from data in Kuhn (1963) and is given in Jacobs *et al.* (1974) by

$$\varepsilon_r(i, j) = \begin{cases} 0.113 \log_{10}(1 + 12.63\bar{r}) & \log_{10} \bar{r} \leq -4 \\ 0.104 \log_{10} \bar{r} + 0.440 & -4 < \log_{10} \bar{r} \leq -3 \\ 0.121 \log_{10} \bar{r} + 0.491 & -3 < \log_{10} \bar{r} \leq -1.5 \\ 0.146 \log_{10} \bar{r} + 0.527 & -1.5 < \log_{10} \bar{r} \leq -1.0 \\ 0.161 \log_{10} \bar{r} + 0.542 & -1.0 < \log_{10} \bar{r} \leq 0 \\ 0.136 \log_{10} \bar{r} + 0.542 & \log_{10} \bar{r} > 0 \end{cases} \quad (177)$$

where  $\bar{r} = |r_i - r_j|$  is the optical path length between the  $i$ th and  $j$ th level. The emissivity function for carbon dioxide is given by Kondratyev (1969) as

$$\varepsilon_{CO_2}(i, j) = 0.185 \left[ 1 - \exp(-0.3919 |c_i - c_j|^{0.4}) \right]. \quad (178)$$

Total emissivity for each depth between level  $i$  and level  $j$  is then given by

$$\varepsilon(i, j) = \varepsilon_r(i, j) + \varepsilon_{CO_2}(i, j). \quad (179)$$

The downward and upward radiative fluxes at a level  $N$  can be computed using the above emissivity functions as

$$R \downarrow(N) = \sum_{j=N}^{top-1} \frac{\sigma}{2} (T_{j+1}^4 + T_j^4) [\varepsilon(N, j+1) - \varepsilon(N, j)] + \sigma T_{top}^4 [1 - \varepsilon(N, top)] \quad (180)$$

and

$$R \uparrow(N) = \sum_{j=1}^{n-1} \frac{\sigma}{2} (T_{j+1}^4 + T_j^4) [\varepsilon(N, j) - \varepsilon(N, j+1)] + \sigma T_G^4 [1 - \varepsilon(N, 1)]. \quad (181)$$

where  $T_G$  and  $T_{top}$  are the temperatures at the ground level and model top, respectively and  $\sigma$  is the Stefan-Boltzman constant. Thus the radiative cooling at each level  $N$  except the ground level is computed as

$$\left( \frac{\partial T}{\partial t} \right)_{LW} = \frac{1}{\rho C_p} \frac{[R \uparrow(N+1) - R \uparrow(N) + R \downarrow(N) - R \downarrow(N+1)]}{z(N+1) - z(N)} \quad (182)$$

where LW denotes the longwave radiation and  $z$  is the height.

Without simplification the computation of radiative transfer is computationally expensive. Sasamori's technique (1972) which assumes an isothermal atmosphere for radiative transfer that simplifies the computing procedure. After this simplification, the temperature change resulting from longwave radiative flux divergence at each level  $N$  is computed as

$$\left( \frac{\partial T}{\partial t} \right)_{LW} = \frac{1}{\rho C_p} \frac{(\sigma T_N^4 - \sigma T_G^4) [\varepsilon(N+1, 1) - \varepsilon(N, 1)] + (\sigma T_{top}^4 - \sigma T_N^4) [\varepsilon(N+1, top) - \varepsilon(N, top)]}{z(N+1) - z(N)} \quad (183)$$

This is the method used in OMEGA.

## Section 5

### Grid Generation and Adaptation

#### 5.1 Grid Definition.

As mentioned in Section 2, the OMEGA model uses a structured-unstructured grid consisting of vertical columns of prisms: five-sided polyhedral having triangular tops and bottoms and quadrilateral sides. The grid is unstructured in the horizontal direction (there is no imposed ordering of triangles) and structured in the vertical (indexing in the vertical direction is sequential and is predetermined). The top and bottom faces of the prisms have the same radially projected area, but each triangle is allowed to tilt independently. The surface layer, which is generated first, conforms to the terrain. This layer is then projected radially outward from the earth's surface, resulting in layers of triangular grids that form the tops and bottoms of vertical columns of prisms. The terrain roughness is smoothed over a specified number of layers, resulting in a flat (*i.e.* horizontal) top layer. The complete grid can be described by describing the triangles forming the surface layer and the altitudes of vertices in the upper layers.

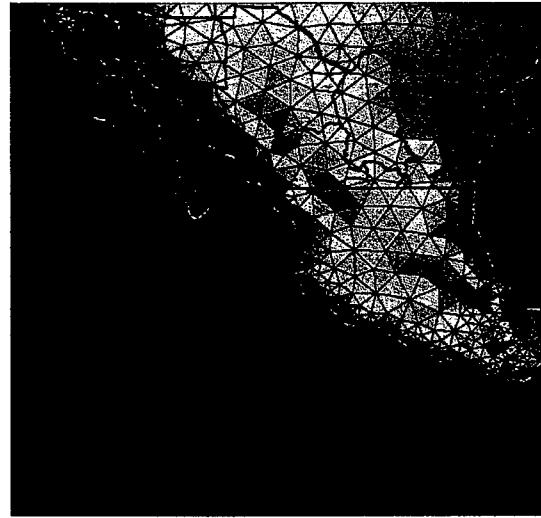
The description of the unstructured grid requires pairs of arrays containing information about each vertex, edge (line segment connecting two vertices), and triangle. Each pair consists of a real array containing spatial information (vertex coordinates, edge lengths, and triangle areas), and an integer array containing connectivity and boundary information. Because the grid is structured in the vertical direction, spatial and connectivity information need only be stored for the surface layer. Within the OMEGA code, adjustments to lengths and areas are made based on radial distance from the earth's surface.

The primary benefit of the unstructured grid over a conventional structured grid lies in the ability of smooth transition from high resolution where needed to low resolution elsewhere. Currently, the OMEGA grid generator automatically adapts a grid to topological features that affect weather, such as terrain roughness and land/water boundaries, producing smaller triangles in these areas. Over oceans, where variations in the horizontal are small, larger triangles are created. By substituting another dataset, the grid can be adapted to any geographical property. For example, by interfacing with a file containing the current meteorological conditions, the grid can be adapted to any field quantity such as pressure or temperature, producing higher resolution in areas of large gradients, thus allowing higher resolution in regions of frontal activity or convection. This latter capability has been developed and tested, but is not interfaced with the current production version of the OMEGA modeling system.

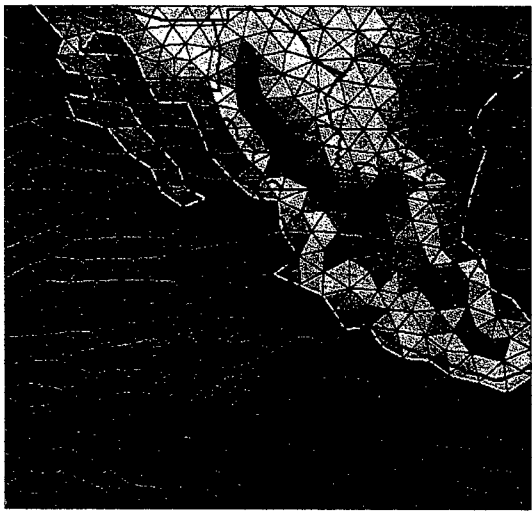
An example of the flexibility of the OMEGA grid is shown in Figure 17. This figure shows a grid generated for Mexico in which the grid was adapted to the underlying topography, the land/water boundary, and to the initial weather conditions. The synoptic situation chosen was Typhoon Linda. In this example, we have broken the grid generation process into different steps for illustration. We have shown a grid generated by adapting to gradients in elevation (refining the grid in mountainous areas), gradients in the land/water index (refining the grid in coastal areas), adapting to typhoon Linda (refining the grid to the initial weather), and, finally, to all of these criteria.



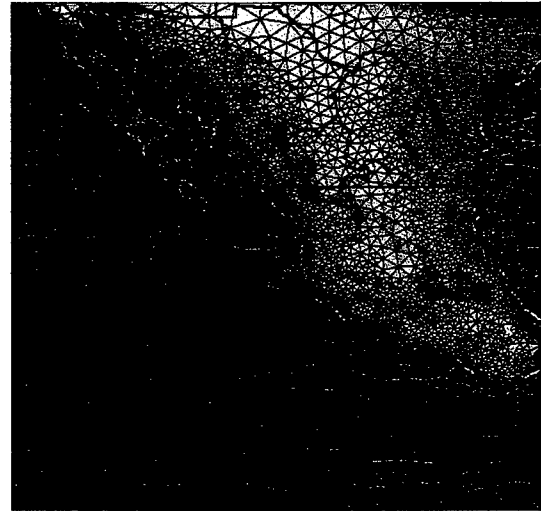
(a) Adapting to topography.



(b) Adapting to land/water boundary.



(c) Adapting to weather (Typhoon Linda).



(d) The resulting grid.

Figure 17. Using an appropriately chosen set of criteria, OMEGA can generate a grid that captures the important physical features.

In addition to the automatic adaptation to geographical features, the grid can be adapted to any user-defined geographical area, such as a theater of operation, by the creation of up to ninety-nine rectangular subdomains on which higher resolution can be specified. Within each subdomain, the adaptation is governed by the user-specified minimum and maximum resolutions. If these limits differ by a factor of two or less, the resulting grid will consist of triangles that appear uniform to the eye. Subdomains can overlap to create a high-resolution region of almost any shape. They can also be layered to produce a high-resolution area within an intermediate-resolution region. In addition to subdomains, the user can also define a point on the grid and a radius of influence around it. The grid will automatically refine within the region of influence. A smoothing process is performed on the resolution specifications to avoid high expansion ratios at the boundaries of subdomains.

## 5.2 Grid Generation.

The OMEGA grid is constructed using several routines that add, subtract, and relocate vertices to satisfy preset specifications. The grid generation methodology consists of the following steps:

1. Create files in the working directory containing the terrain and land/water data, culling information from the global databases.
2. Generate an initial coarse, two-dimensional (terrain following) grid of triangles.
3. Refine the grid through a series of iterations, calculating vertex elevations and cell properties (currently land or water) by interpolation using the database after each iteration.
4. Create the vertical levels, smoothing the roughness gradually in layers above the surface of the earth.
5. Generate the surface characteristics file.

These steps will be discussed in the following paragraphs.

### 5.2.1 Data Files.

Two sets of global terrain and land/water data are currently available for the creation of grids: a fine resolution database and a coarse resolution database. The coarse database currently in use consists of two files. The terrain file contains data for the entire globe at a resolution of five minutes, or about 9.26 km at the equator, while the land/water file contains data at a resolution of ten minutes. The fine resolution databases of both terrain and land/water, are divided into sets of files each of which contains data for a five degrees by five degrees segment of the globe. The resolution of the fine data files is given in Table 2. Any combination of high and low-resolution terrain and land/water databases can be used for the primary domain and subdomains of a grid. While high-resolution databases will almost always result in a grid that captures geographical features more accurately, using a low-resolution database saves on disk space and greatly speeds up the grid generation process.

Table 2: High-resolution OMEGA terrain and land/water databases.

Latitude (N or S)	Resolution (NS x EW)	
80-90°	30 x 180"	0.93 x 0.97 km
75-80°	30 x 120"	0.93 x 0.96 km
70-75°	30 x 90"	0.93 x 0.95 km
50-70°	30 x 60"	0.93 x 1.19 km
0-50°	30 x 30"	0.93 x 0.93 km

The first task of the grid generator is to locate and read the data files. Data that is needed for the case is temporarily stored one degree of latitude at a time, in work arrays. This data is then written to files named `grdnnnlan.dat` and `grdnnnter.dat`, where `nn` is the domain or subdomain number. These files are read repeatedly, and the data used for interpolation, throughout the grid generation process.

The low-resolution databases are the default databases. If the grid generator fails to locate a fine resolution file for any domain, the database for that domain will revert to the coarse database. Since terrain and land/water datasets are created independently, coarse data can be used for terrain definition while fine data is used for land/water definition, and vice-versa.

Because the land/water index for each cell takes the value zero or one, the land/water data is stored as a formatted file using an `f3.0` format, resulting in a significant savings in disk space. The terrain file is written as a binary file, which speeds execution.



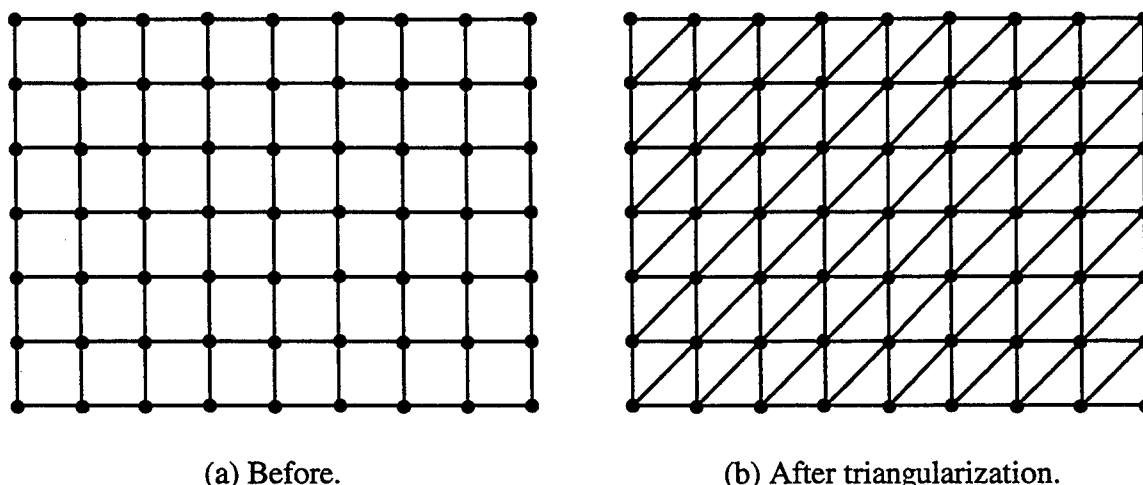


Figure 18. Initial rectangular grid.

### 5.2.2 Initial Grid.

The boundaries of the domain are input as longitude and latitude, while the desired resolution is specified in kilometers. For construction of the initial rectangular mesh, meters per degree of longitude is determined at the center of the domain. Meters per degree of latitude is globally constant. Aside from the variation from north to south, the spacing of the vertices in the initial rectangular grid is equal to the minimum resolution requested for the primary domain (Figure 18). Since the coordinates of each vertex are expressed in longitude and latitude, the grid is rectangular in latitude/longitude space.

Starting with a coarse grid and refining minimizes the work done in generating the grid, since the grid never contains more cells than are necessary. To prevent the final grid from being too “regular”, randomization is produced in the initial grid by randomly selecting a subset of edges and forcing reconnection. The reconnection process is described below.

### 5.2.3 Refinement of the Grid.

After generation of the initial grid, the process of refinement begins. The processes used to refine the grid were described briefly in Section 2; in this section we discuss more fully the mechanics of the grid refinement. The refinement process begins with the calculation of the area of each triangle, which is then compared to the areas of equilateral triangles having edge lengths equal to the minimum and maximum resolutions specified in the input file. A triangle is “flagged” for refinement if trisection will not result in new cells having areas less than or equal to the area of an equilateral triangle with the minimum allowable edge length, and the cell satisfies one or more of the following:

- The area of the triangle exceeds the area of an equilateral triangle with edges equal to the maximum edge length specified for the domain or subdomain in which the centroid is located.
- The elevation gradient between the triangle (the average elevation of the three vertices, since elevation is a vertex-based quantity) and its neighbors exceeds a preset tolerance, currently set to 1.5 percent of the variation in elevation throughout the domain.
- The cell is on a land-water boundary. The land/water index is a cell-centered value, and is set to zero or one; the whole cell is defined as either land or water, depending on the location of the centroid. If the land/water indices of any of the cell's neighbors (the three cells that share

edges with the target cell) differ from that of the target cell, the target cell is on a land-water boundary.

- The area of the cell is greater than four times the area of its smallest neighbor.

Refinement of a triangle is accomplished by adding a vertex at the centroid, if the triangle is in the interior of the grid, or by bisecting the boundary edge, if the triangle is on the boundary. A cell is flagged for recombination (the vertex opposite from the longest edge is will be deleted from the grid) if it satisfies any or all of the following:

- The area of the cell is less than the area of an equilateral triangle with edges equal to the minimum edge length specified by the user for the domain or subdomain in which the centroid is located.
- The cell is water surrounded by water, and combining three cells of the same size into one will not result in a cell whose area exceeds the maximum allowed.
- The cell has aspect ratio less than 0.33. The aspect ratio is defined as the height of the triangle divided by the length of the longest edge.

The criteria for both refinement and recombination are “weighted”, that is, certain criteria will force one or the other action to occur regardless of any other properties of a triangle. These criteria are chosen with the OMEGA solver in mind. Triangles that are too large or too small are forced to trisect or recombine to prevent adverse effects on the time-step, and triangles with poor aspect ratios are forced to recombine to avoid instabilities in the solution. Corner triangles are bisected to avoid triangles having two boundary edges.

Figure 19 shows the grid in Figure 18 after two triangles, one in the interior and one on the boundary, have been refined. Adding and deleting vertices results in a grid with unequal edge lengths and new triangles that are frequently obtuse. These irregularities in the grid may cause instabilities to occur during the simulation; to avoid this the grid is relaxed. Relaxation entails relocating each vertex to a point equidistant from its connecting neighbors. This stage is shown in Figure 19.

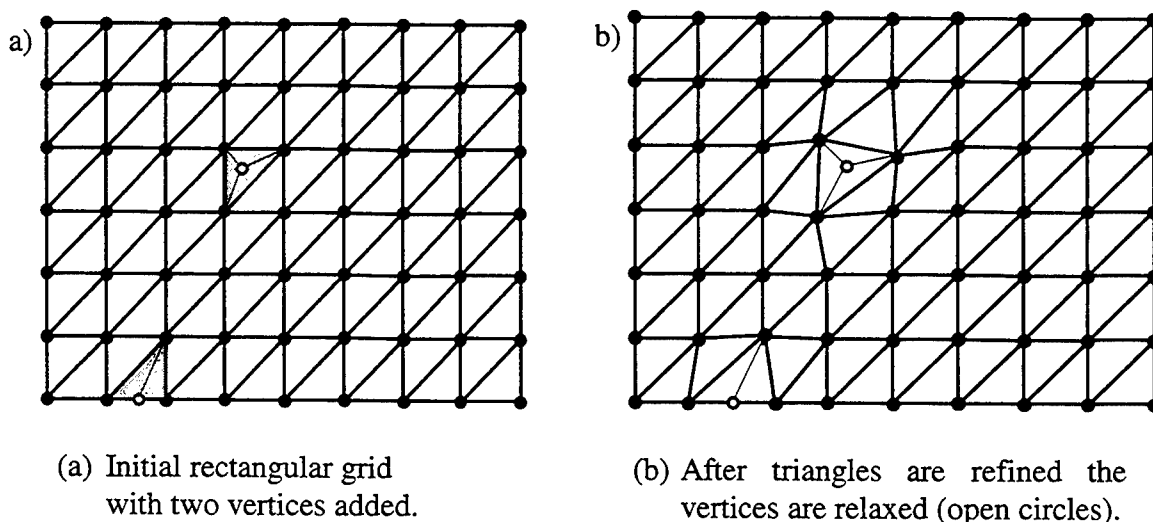


Figure 19. Grid refinement.

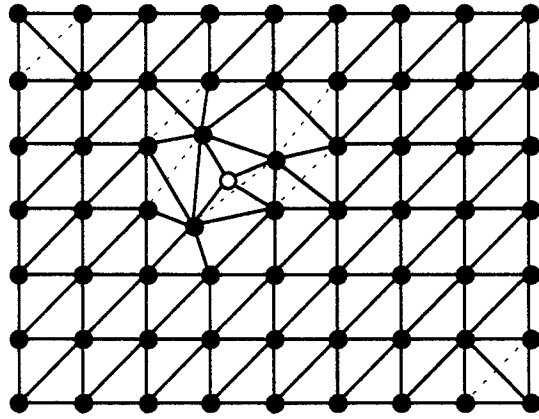


Figure 20. Grid after reconnection. The deleted edges are shown as dashed lines and the new edges are shown as thin lines.

Following relaxation, triangle shape is optimized through the process of reconnection. During reconnection, two neighboring triangles are joined to form a quadrilateral. One diagonal of the quadrilateral is the shared edge. These triangles are compared with the triangles that would result if the other diagonal of the quadrilateral were the shared edge. If the resulting triangles are more nearly equilateral, the original shared edge is deleted from the grid, and the new edge added. Figure 20 shows the grid in Figure 19 after reconnection.

An iteration is complete when all of the flagged cells have been altered. Since grid refinement has resulted in the creation and relocation of both vertices and cell centroids, interpolation to the underlying databases, both terrain and land/water, is repeated. Bilinear interpolation is used to calculate both elevation and the land/water index. A value between zero and one will result for the land/water index, which is then rounded to zero or one.

This process of refinement and interpolation is repeated until the grid is determined to have converged. Convergence is declared when two consecutive iterations result in changes to fewer than 95 and 99 percent of the cells, respectively. The number of iterations required depends largely on the ratio between the minimum and maximum resolution desired, since the initial grid is based on the minimum resolution, and numerous trisections of cells may be required before the maximum resolution is attained. Our experience has shown that four iterations are typical when the minimum and maximum resolutions differ by a factor of two or less, while eight or nine iterations may be required when the resolution ratio is five or more.

A final step prior to the creation of the vertical levels consists of bisecting any corner triangles that have two boundary edges. This process has been found to improve the solution at the corners of the domain (See Figure 20).

#### 5.2.4 Vertical Levels.

The final step in grid generation is the creation of the vertical levels. The OMEGA grid is constructed in two parts in order to provide high resolution near the surface, where it is required, without requiring that same resolution at altitude. The lower levels are considered “stretchable”, while the upper levels represent spherical surfaces. The user is required to specify both the total number of levels,  $N$ , as well as the number of stretchable levels,  $N_s$ .

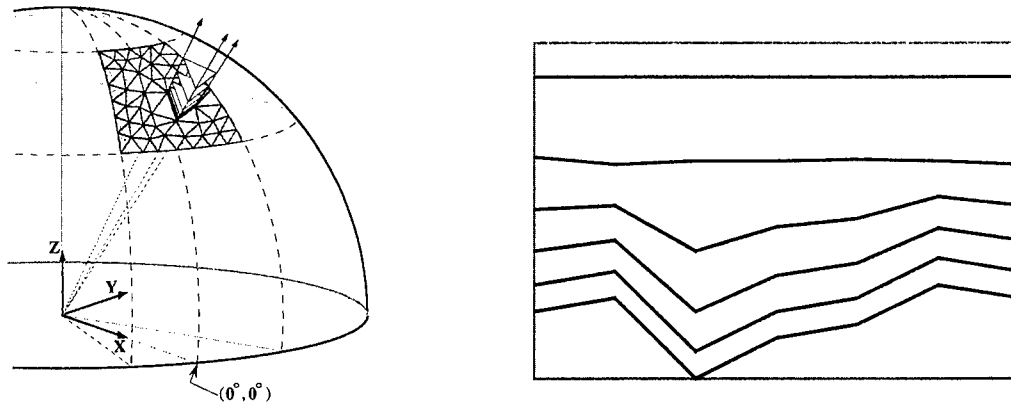


Figure 21. The vertical levels of the OMEGA grid are constructed by extending radials through each of the surface vertices. A set of stretchable layers exists near the surface with constant thickness layers above.

In normal operation, the user specifies the height of the first layer of triangles,  $\Delta z_o$ , above the surface of the earth along with the maximum geometric factor,  $\alpha_{max}$ , by which the heights of the prisms will increase in the radial direction in the stretchable layers. The layers are constructed by taking each surface vertex and constructing an array of vertices along the radial through that vertex. The resulting vertices are then connected to form the OMEGA grid volumes.

The height of each of the vertices in the interior of the OMEGA grid is computed by first evaluating the top of the uppermost stretchable level ( $H_{ts}$ ) above the lowest point in the domain (*c.f.* Figure 21 right). This height is then used as a spherical top for the stretchable levels and the heights of each of the other vertices in the stretchable levels are computed by calculating a local geometric factor  $\alpha_i$  for each radial. Since  $H_{ts}$  was computed using the lowest point in the terrain, these  $\alpha_i$  will always be less than  $\alpha_{max}$ . The resulting grid is terrain following at the surface, but has a constant mean sea level altitude at the top of the uppermost stretchable layer.

An alternative setup method exists in which the user specifies the top of the total domain, and the OMEGA grid generator then calculates the geometric stretching factor. A final means of specification of the vertical grid structure is available to the more sophisticated user by editing the grid generator input file to provide the height of each vertical level above the surface. In this mode, the grid generator uses these heights to construct the radial through the lowest point on the surface grid, and then adjusts the other radials to produce a spherical top to the stretchable layers.

Calculation of the vertical levels completes the construction of the OMEGA model grid. With the grid completed, all vital information is handed over to the model preprocessor. This includes the number of vertices, edges, and faces, and the arrays that contain the vertex locations, their connectivity, the edge connectivity, and the face connectivity.

### 5.3 Surface Characteristics Databases.

The OMEGA Grid Generator accesses some surface datasets during the adaptation process (*e.g.*, terrain elevation and land/water fraction) while others are only interpolated after the grid has been defined (*e.g.*, vegetation, soil moisture, sea surface temperature). Terrain and shoreline datasets have been described in Section 5.2.1. After the grid has been generated, the grid-generator reads the surface characteristics datasets and assigns values of sea surface temperature, landuse, sub-soil temperature, soil moisture, vegetation type and soil type to each grid cell.

The use of an easily configurable adaptive grid requires a set of high-resolution surface databases, built in such a way that they can be efficiently accessed when a new grid is desired. OMEGA has eight major surface characteristic databases: soil type, climatological vegetation index, land use/land cover, climatological sea surface temperature, climatological subsurface temperature and climatological soil moisture. The first two characteristics are determined from global datasets, which have been widely used for numerical modeling. The others rely on newer datasets from various sources. For both vegetation index and land cover, two different datasets are provided. One dataset covers North America only at high resolution, and the other covers the entire globe, but with less resolution. Table 3 lists the surface characteristics databases which are available for OMEGA.

A one-degree (110 km) global soil type database was created from the Global Ecosystems Database (GED) CD-ROM (Webb *et al.*, 1992). The source dataset consists of separate fields containing the amounts of clay, sand and silt in 12 soil types. The twelve types used in the OMEGA preprocessor are sand, loamy sand, silt loam, loam, sandy clay loam, silty clay loam, silt, clay loam, sandy clay, silty clay, and clay.

Vegetation modifies both the thermal and moisture budgets of the Earth's surface and thereby influences atmospheric circulations. In OMEGA, vegetation type is defined for each grid cell based on the Global

Table 3. Datasets used to determine surface characteristics.

Surface Property	U.S. Data	Global Data
Soil Type	Webb Global Soil Texture Class from Global Ecosystems Database (GED) CD-ROM 1 degree resolution	
Climatological Vegetation Index	USGS NDVI Annual Datasets 2 minute resolution	
Land Use/ Land Cover	USGS BATS Land Cover 2 minute resolution	
Climatological Sea Surface Temperature	Bi-weekly USGS SST Climatology 12 minute resolution	Monthly Global Vegetation Index (GVI) from GED 10 minute resolution
Climatological Subsurface Temperature	Average Monthly Air Temperature from GED 30 minute resolution	Olson World Ecosystems BATS Land Cover from GED 30 minute resolution
Climatological Soil Moisture	Budyko Soil Moisture Budget using Average Monthly Temperature and Precipitation from GED 30 minute resolution	

Vegetation index (GVI). The GVI has a resolution of about 13 km. More recently, the USGS has published a 1 km Normalized Difference Vegetation Index (NDVI) over the contiguous U.S. Two climatological NDVI datasets were created for OMEGA: a two minute (4 km) dataset covering the conterminous U.S., and a 30 minute (55 km) dataset covering the globe. A series of high resolution AVHRR datasets (Eidenshink, 1992) over the conterminous U.S. has been published by the Earth Resources Observation System (EROS) Data Center of the U.S. Geological Survey. Datasets beginning in 1990 are available, which contain gridded NDVI values, which have been composited over two weekperiods covering most of each year. The compositing process is an attempt to eliminate the effects of contamination by clouds. The 1990 through 1993 datasets were averaged to produce bi-weekly climatological datasets covering the conterminous U.S. with a resolution of 2 minutes (about 4 km). Global monthly NDVI datasets covering the period 1985-1990 were published on the Global Ecosystems CD-ROM, based on biweekly calibrated GVI data (EDC-NESDIS, 1992).

These monthly datasets were averaged to form a set of monthly climatology files with a resolution of 10 minutes (18 km). Similarly, two separate land use datasets were created. Each set uses the Biosphere-Atmosphere Transfer Scheme (BATS) set of 18 land cover categories, with an additional 19th category added for urban land cover. The categories are: crop/mixed farming, short grass, evergreen needleleaf tree, deciduous needleleaf tree, deciduous broadleaf tree, evergreen broadleaf tree, tall grass, desert, tundra, irrigated crop, semidesert, ice cap/glacier, bog or marsh, inland water, ocean, evergreen shrub, deciduous shrub, mixed woodland and urban. A 2 minute (4 km) land use dataset covering the U.S. was formed from a 1 km BATS dataset and AVHRR data. A 30 minute (55 km) global dataset was formed from the Olson (1992) World Ecosystems dataset on the Global Ecosystems Database CD-ROM. The 73 categories in the original Olson dataset were remapped to the 18+1 BATS categories.

OMEGA uses a global sea surface temperature climatological dataset produced by the USGS (Schweitzer, 1993). The data has been processed into a bi-weekly global, 0.2 degree (about 20 km) dataset. This data does not extend beyond about 70 degrees latitude in either hemisphere. Some areas are not covered resulting in large lakes without data; for example the Caspian Sea in central Asia is completely missed. The original dataset was weekly; every other week was processed for OMEGA.

A monthly global subsurface temperature climatology was built from monthly average surface air temperatures from the Global Ecosystems Database CD-ROM (Legates and Willmott, 1992). This data was built by using monthly average surface air temperature as an estimate of subsurface temperature. The dataset resolution is 30 minutes. Soil moisture is an important variable in numerical weather prediction but is difficult to determine. Budyko's simple soil moisture budget as described by Sellers (1965) was used to generate soil moisture estimates from the temperature and precipitation data (Legates and Willmott, 1992). The monthly budget equation is given by:

$$w_2 = w_1 + r - E - S, \quad (184)$$

where  $w_2$  is the soil moisture value at the end of a month,  $w_1$  is the soil moisture at the beginning of the month,  $r$  is the precipitation,  $E$  is the evapotranspiration, and  $S$  is the moisture surplus term. The key term, evaporation, is based on a potential evaporation, a function of the monthly mean temperature. This simple approach is far from perfect, but seems to give reasonable results for a range of climatic types. An iterative application of the Budyko equations was used to obtain volumetric soil water contents that balanced the annual water cycle. Each of the surface characteristics databases are organized as sets of

latitude-longitude "tiles", which results in complete geographic coverage, efficient searching and logical filenames. The global-scale databases use 30 x 30 degree tiles, while the U.S. databases consist of 5 x 5 degree tiles. FORTRAN logic was devised to allow databases at both resolutions (U.S. and global coverages) to be used simultaneously. The higher resolution data is applied to the OMEGA grid first, then the coarser resolution data is used in any grid cells which have not been filled with values. After all of the available databases have been searched, the database values which have accumulated in each OMEGA grid cell are averaged to obtain the final value. In the case of the discrete fields (soil type and land use), the dominant (most frequent) value in each cell is considered to represent the entire cell. If no database values are found for a grid cell, the cell is flagged and assigned a -99.0 value. The PBL routines later assign values for these cells before the model run starts. Figure 22 shows some of the different data sets that are accessed by the OMEGA Grid Generator.

#### 5.4 Static Grid Adaptation.

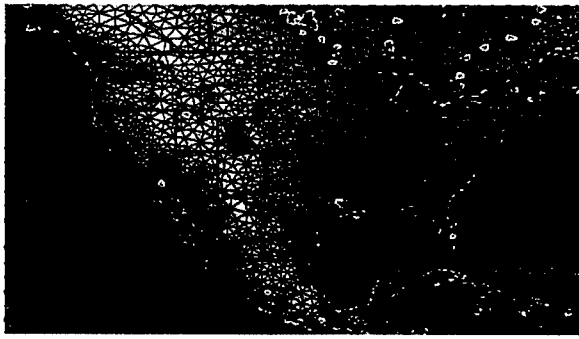
To the extent allowed by the minimum and maximum resolutions requested, the grid generator adapts the grid to features of the geography by creating small triangles in areas where gradients of the underlying data are high, while leaving triangles large in areas of small gradients. In the case of land/water boundaries, a "high" gradient is a non-zero gradient.

The ratio of minimum to maximum resolution (roughly, maximum to minimum edge length) specified must be greater than two to enable adaptation to occur. If the minimum and maximum resolutions are closer than this, the grid generator will be unable to trisect cells without the resulting cells being too small. A minimum to maximum resolution of two results in a grid in which cell size throughout the grid appears uniform to the eye. If the minimum and maximum resolutions specified by the user differ by less than twenty percent, the grid generator will set the maximum resolution to eighty percent of the minimum resolution. This prevents computationally costly "thrashing": repeated trisecting and recombining of cells in an attempt to satisfy resolution criteria that are too restrictive.

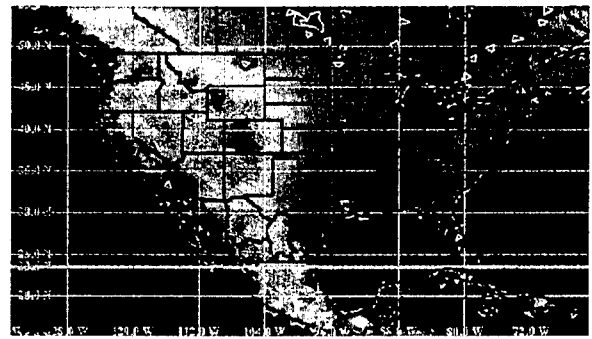
The user can specify through the XOMEGA graphical user interface a point location around which refinement is required (*c.f.*, Figure 23). The resolution and the radius of influence is also required as an input. XOMEGA generates a *grid.ref* file which is read by the grid-generator as an input for point refinement. The OMEGA grid-generator is configured to read in as many as fifty point sources. An example of *grid.ref* is given below:

```
1                ! number of points
10.25 35.25 40.00 1.00 ! longitude latitude radius(km) resolution (km)
```

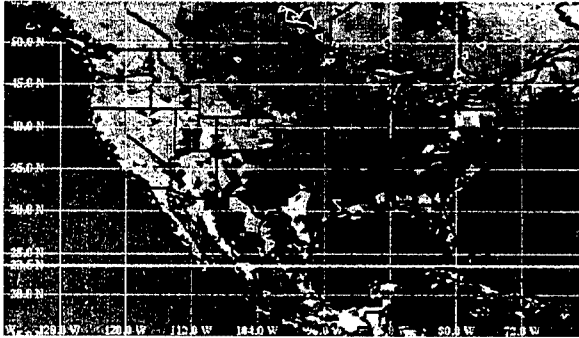
The grid-generator defines a Gaussian function around the point location using the input radius of influence. This function is used to provide weighting to the cell badness function. The cells close to the point source get larger weighting and are therefore tagged for refinement. The major advantage of point refinement is in reducing costly I/O time, while providing resolution exactly where it is needed. For large domains, using the point refinement option can generate high-quality grids relatively quickly. This technique can also be easily employed for refinement around line sources. Figure 23 shows the computational domain for the Middle East. The final grid has 4213 cells with edge lengths varying from 5.33 km to 115.57 km. For this grid a single domain with nine point sources was defined. The *grid.inp* and the *grid.ref* files used to generate the grid are as follows:



(a) OMEGA Grid.



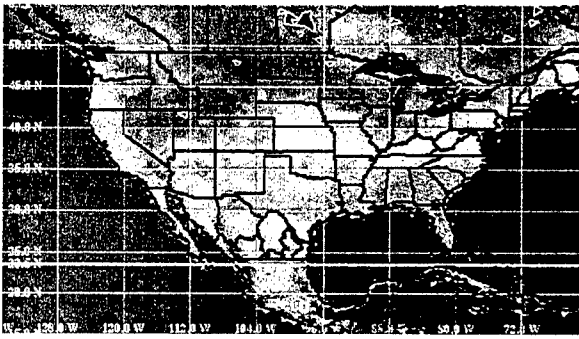
(b) Terrain elevation.



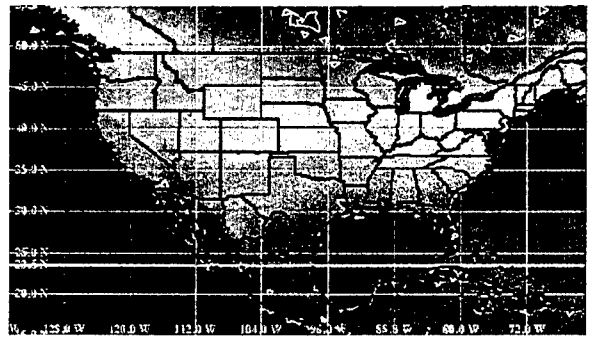
(c) Land use.



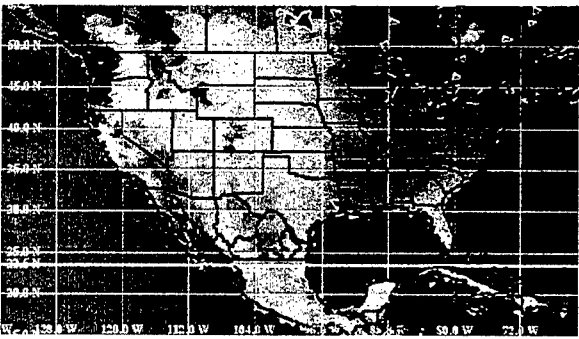
(d) Soil type.



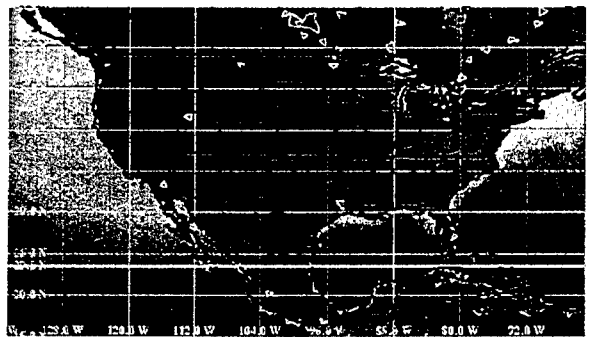
(e) Climatological vegetation



(f) Climatological soil temperature.



(g) Climatological soil moisture.



(h) Climatological sea surface temperature.

Figure 22. Datasets used to initialize OMEGA.



**grid.inp:**

```
new                ! new grid
oldgrid.dat        ! *****
grid.dgn           ! grid diagnostics file name
35.00              ! minimum longitude (degrees);      smoothing = off
55.00              ! maximum longitude (degrees)
22.00              ! minimum latitude (degrees)
40.00              ! maximum latitude (degrees)
40.00              ! minimum resolution (km)
100.00            ! maximum resolution (km)
5min               ! terrain dataset resolution
5min               ! land/water dataset resolution
0                  ! number of sub-domains
30                 ! total number of vertical levels
28                 ! number of stretched levels
1                  ! type of vertical grid
30.00             ! height of the first vertical level (m)
1.15               ! stretch ratio
15                 ! maximum gridgen iterations
0                  ! 0 = no ; 1 = yes      (create .srf file)
```

**grid.ref:**

```
9
46.120  28.330  100.000  7.000  ! Hafr-al-Batin
50.150  26.270  100.000  7.000  ! Dhahran
51.570  25.250  100.000  7.000  ! Doha
43.520  32.380  100.000  7.000  ! Ukhaydir
46.720  24.720  100.000  7.000  ! Riyadh
39.700  24.550  100.000  7.000  ! Medinah
41.680  27.430  100.000  7.000  ! Hail
51.350  35.680  100.000  7.000  ! Tehran
46.380  30.750  100.000  7.000  ! Khamisiyah
```

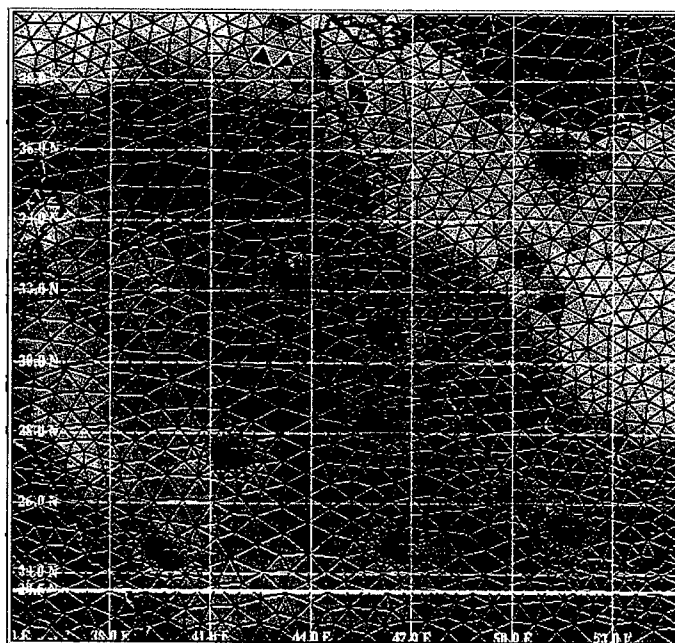


Figure 23. OMEGA grid for the Middle-East region used for gulf war analysis. The grid has been refined around data sources.

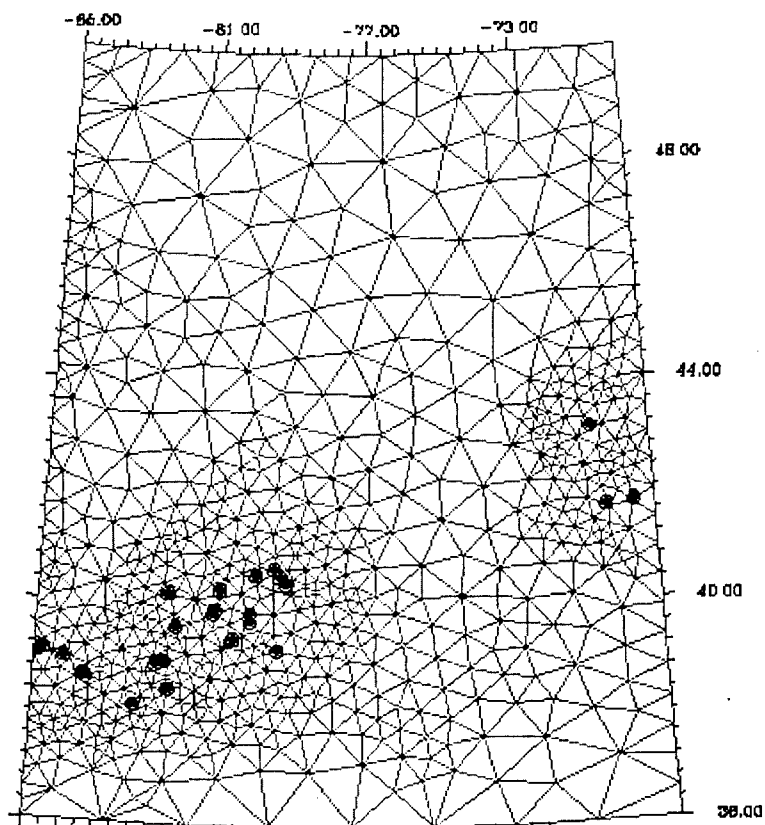


Figure 24. Refinement to regional interim emissions inventory.

Another example of the flexibility of the OMEGA grid is seen in Figure 24. This figure shows an OMEGA grid generated to provide higher resolution in the vicinity of emission sources. In this case, the grid adapted to a subset of the 1990 Regional Interim Emissions Inventory (sources producing more than 25,000 tons per year (TPY) of  $\text{SO}_2$ ). OMEGA, with dynamic adaptation, could be configured to provide high resolution not only in the source region, but also in those regions with high pollutant concentration. This is important in atmospheric chemistry situations where the lack of grid resolution can drastically change the solution due to the strong non-linearity of the physics. This capability is discussed in detail in Section 9.

## 5.5 Grid Editor.

OMEGA Grid Editor has been developed to compliment the grid-generation process. Large amount of CPU time is required to read the terrain and shoreline datasets. To avoid going through the whole process in order to make minor changes to the existing grid, which is an inefficient use of resources, SAIC developed the Grid Editor to perform a variety of functions on an existing grid. Using the Grid Editor, areas can be defined for refinement or coarsening, the entire grid can be regenerated with different resolution without creating the terrain and shoreline datafiles from scratch, and individual cells can be manipulated by deleting vertices or bisecting boundary edges. Bisection of boundary edges is especially useful, since the chances of creating bad cells on the boundary are high. In addition, overall grid-quality can be improved by relaxing the vertices. The Grid Editor is a menu driven program which should be used interactively with XGRID. The main menu of the Grid Editor is shown below:

```

*****
*           OMEGA GRID EDITOR, VERSION 3.5           *
*           *           MAIN           *           *
*****

```

```

r -> Refine Grid.
c -> Coarsen Grid.
b -> Bisect Boundary Edge.
v -> Delete Vertex.
x -> Relax Grid.
s -> Change Resolution.
u -> Undo.
q -> Quit.

```

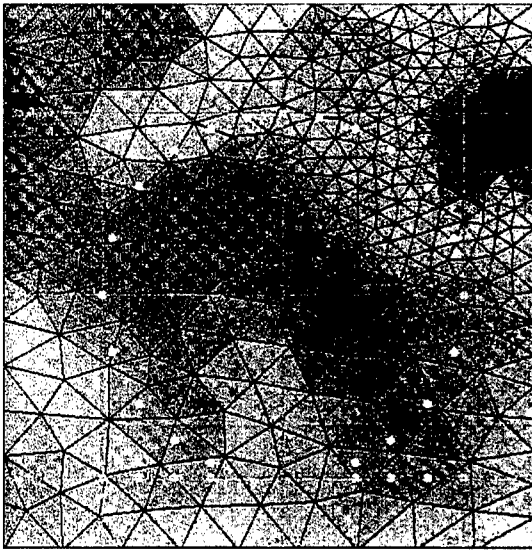
## 5.6 Dynamic Grid Adaptation.

The grid adaptation described so far is “static” adaptation, implemented in the grid generator prior to the beginning of an OMEGA run. The grid in the “static” adaptation case is adapted *a priori* to resolve static features such as terrain gradients and land-water boundaries, or any other feature that the user includes in the adaptation scheme. The grid does not change during the course of the OMEGA run. The latest version of OMEGA also has dynamic adaptation capabilities. This new feature is discussed briefly here (for details see Section 9).

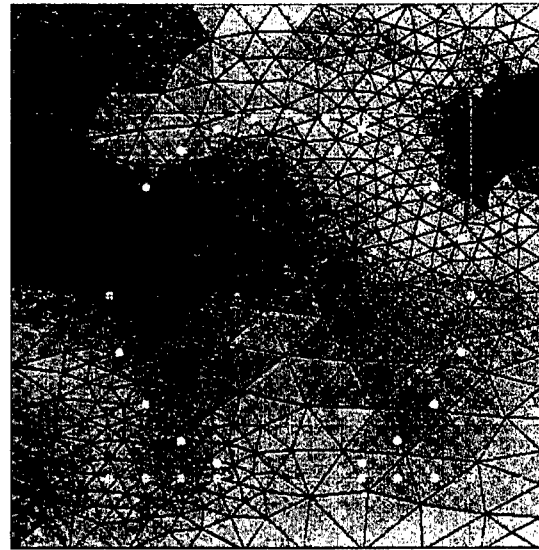
OMEGA has the ability to adapt its grid during a simulation to different criteria, such as, frontal activity and convection or a pollutant plume. The underlying philosophy of dynamic adaptation is to provide a refined grid to resolve important physical events and features as the simulation is in progress. The dynamic adaptation consists of four major steps:

- 1) At a predetermined time step specific variables or their gradients are evaluated to see if they meet the adaptivity criteria.
- 2) The mesh is refined where these criteria are satisfied.
- 3) The physical variables are interpolated to new cell centers, and
- 4) The mesh is coarsened where the criteria are not met.

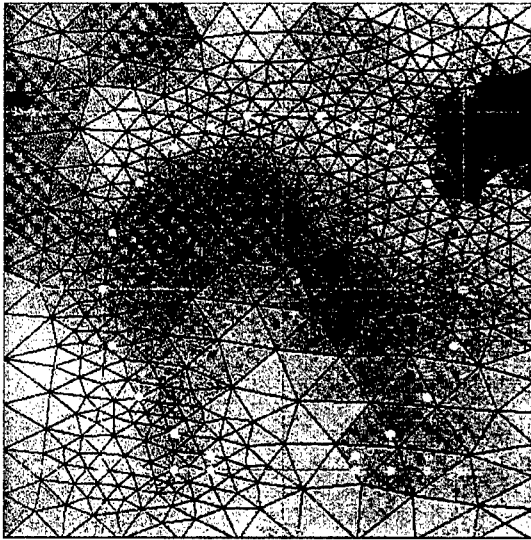
This process can be accomplished in several ways. For example, if there are sharp discontinuities such as propagating fronts the mesh is refined ahead of the front so that a refined mesh already exists when the shock arrives at a specific location. As the front propagates, the refined mesh at the previous location of the front is coarsened to the resolution specific to the background mesh. This type of coarsening and refining is performed at predetermined time-step increments and is useful for tracking frontal or shock activity. The simulation is allowed to advance a number of timesteps defined through an input file without adaptation and then refine-coarsen cycle is performed. However, if we choose to dynamically adapt the mesh to resolve spontaneous events we need to check predetermined physical variables at prescribed time intervals to see if they exceed a threshold or satisfy a criterion. We then perform a refine-coarsen cycle. After the grid has been modified all the physical variables are interpolated to the new mesh and the diagnostic variables are calculated.



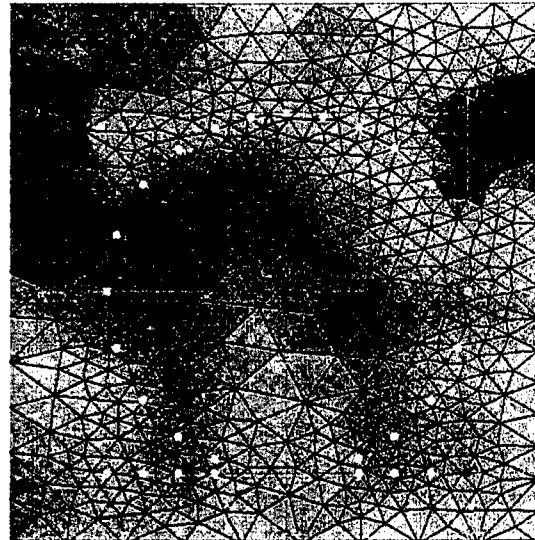
(a) Original grid.



(b) Higher resolution over NW region.



(c) Higher resolution over NE region.



(d) Higher resolution over SE region.

Figure 25. Test of the dynamic adaptation routine. The adaptation was to the presence of test particles (shown in red) initialized in the southwest corner of the grid and traveling on a prescribed trajectory.

Figure 25 shows a simple test of the dynamic adaptation routines. The domain was centered on the Four Corners area. The adaptation criteria were set to point locations. A particle traveling on a prescribed trajectory was initialized in the southwest corner of the domain. Only the refinement cycles were invoked during this run.

## Section 6

### Initial and Boundary Conditions

The function of the data preprocessor is to convert a diverse mixture of real-time atmospheric and surface data for input into an OMEGA simulation. This process produces two datasets. One dataset specifies the initial values of all the model's dependent variables as well as the surface-based model parameters. A second dataset specifies the time dependent behavior of the model's dependent variables along the lateral boundaries of the simulation domain. The general structure of the OMEGA preprocessor is depicted in Figure 26.

The first module is INGEST. Its function is to ingest atmospheric data (e.g. surface or rawinsonde observations) from a real-time data stream and distribute it to a series of files (RTData) organized by type of data and time. INGEST continuously executes on the computer system that is designated for data ingestion and is not part of the model run stream.

Execution of the OMEGA grid generator is the first step in a preprocessor run. The latest version of GRIDGEN also ingests data from the surface characteristics database and generates a specification of all surface properties for each grid cell. This capability is now operational in the latest version of OMEGA.

The DASH module reads real time surface data from both hourly reporting surface stations and daily reporting hydrological stations to maintain an updated global database of snow cover, soil temperature, and soil moisture data. *DASH is not currently being used as part of the operational OMEGA system.*

The PREPDAT module selects data stored by the INGEST and DASH modules based upon the user-specified date and time. PREPDAT then error-checks the data and writes it out to a set of files written in standard OMEGA input format. This includes a "GUESS" file that contains a 3-dimensional first-guess of all dependent atmospheric variables interpolated from forecast model output. Other files include: 1) observational data files ("SFC", "RAOB" and "SST"); and 2) hydrological data files ("TSUB", "WSHL", "WDEP" and "SNGR").

GENINIT assembles the atmospheric, and time varying surface property data into a single initialization file called "INIT". GENINIT also writes a "BC" file for the 3-D atmospheric variables at the initial time.

ANALYSIS accepts processed observational data from PREPDAT files and performs an objective analysis of the data to update values of the dependent atmospheric variables at the centroids of all grid cells. ANALYSIS then outputs a modified "INIT" file.

Finally, the preprocessor ingests forecast data from another atmospheric model and interpolates it to the lateral boundary cells of the OMEGA domain. This function is controlled by RUNPREP and is accomplished by running PREPDAT and GENINIT in Boundary condition mode once for each boundary condition time. GENINIT vertically interpolates the guess generated by PREPDAT to the OMEGA grid. The result is one "BC" file valid at a given forecast time for each time that PREPDAT and GENINIT are executed.

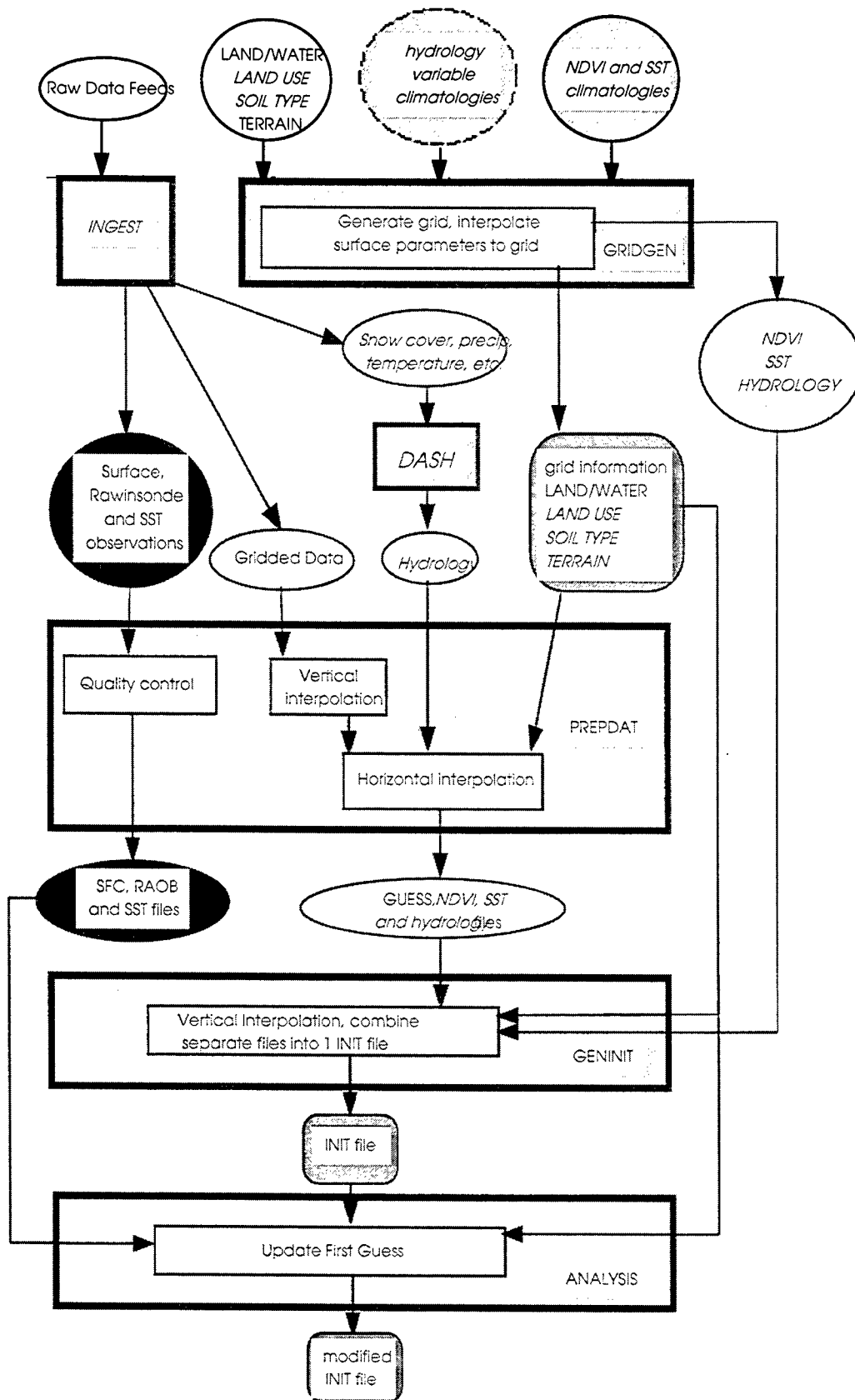


Figure 26. Data flow between the preprocessor and other OMEGA components.

OMEGA receives from the preprocessor initial and boundary values for the latitudinal, longitudinal and vertical components of the wind velocity, pressure, potential temperature, density and mixing ratios of water vapor, cloud water, rain water, cloud ice and snow. In addition, OMEGA receives the initial values of skin and subsoil temperature; shallow and deep soil moisture; snow cover; and vegetation index. The input module of OMEGA converts the latitude-longitude-altitude coordinates into Cartesian coordinates.

The files "BC.tag#" and "INIT.tag" are produced by the preprocessor, where **tag** represents the unique preprocessor run identifier. "BC.tag#" contains boundary condition information at time "#" starting with "0" at the initial time. "INIT.tag" contains the initial conditions at the OMEGA grid cells.

## **6.1 Data Ingestion.**

Real-time gridded and observed atmospheric data is currently acquired from the Fleet Numerical Meteorological and Oceanographic Center (FNMOC). Until recently, gridded and observed data sets were also acquired from the National Centers for Environmental Prediction (NCEP) using their Internet ftp site.

### **6.1.1 NCEP Internet Data Feed.**

NCEP stores their numerical model data in the World Meteorological Organization (WMO) Code FM 92 GRIB format (Ed. 1), and their observational data in the WMO Code Form FM 94 BUFR format (Ed. 2). Observational data that are currently stored in NCEP Office Note formats are gradually being converted to BUFR format. Ultimately, all of the observational data will be stored in BUFR format. The packed binary BUFR format is more efficient in disk space utilization than the internal NCEP formats. This will improve transfer times as well.

The GRIB messages are comprised of packed binary data which is divided into six different sections as follows, some of which are optional:

- Sec. 0 Indicator Section
- Sec. 1 Product Definition Section (PDS)
- Sec. 2 Grid Description Section (GDS) - optional
- Sec. 3 Bit Map Section (BMS) - optional
- Sec. 4 Binary Data Section (BDS)
- Sec. 5 '7777' (ASCII)

The Indicator Section begins with the ASCII string 'GRIB' which defines the beginning of the GRIB message, followed by the total length of the GRIB message and the Edition number of the GRIB message. The next section is the Product Definition Section that is usually 28 octets long, but may be longer. It contains information such as the numerical model that created the data, the center identification, grid identification, and date and time of forecast. It also contains flags specifying whether the next two sections are present. Section 2, the Grid Description Section, is optional and contains a grid description for grids not already defined as NCEP storage grids. Section 3, the Bit Map Section is also optional, and contains either a bit map for the data or a reference to a pre-defined bit map. Section 4 the Binary Data Section, contains the binary scaling information which is used to reconstruct the original model data from the packed binary data in the GRIB file. The last section is four octets long and defines the end of the GRIB message with the ASCII string '7777'. For further information on the GRIB message format, refer to GRIB Ed. 1 (Office Note 388), (Stackpole, 1994).

The BUFR file format is also a packed binary format, but is less structured than the GRIB format, and is more self-defining. Since there is a wide variety of data which may be stored in the BUFR format, from surface observations to aircraft and ship observations to radar and profiler data, each field of data stored in the BUFR format is stored with an accompanying numerical field called a descriptor. The descriptor is matched up against a table (TABLE B) which provides a set of information about that field, including the variable name, units, reference and scaling information and the number of storage bits required for that field. The BUFR decoder uses this information to correctly decode the data.

Decoders were developed for both the GRIB and BUFR data files, using a combination of c-code to read in the binary data, and FORTRAN modules provided by NCEP to decode the binary data records and return arrays filled with the unpacked data, which are then written out to ASCII files. The GRIB decoder uses an option file configured by the user to process the raw data file and save only the model grids and variables requested by the user. Often GRIB files contain data from more than one model and for many different variables. This flexibility to save only the data needed results in smaller files since decoding and saving entire GRIB messages can result in very large files. The BUFR file decoder doesn't use an option file, since these files are usually smaller, and often contain just one data type at one observation time. Table 6.1 contains a list of NCEP files which the GRIB and BUFR decoders can process for input into the preprocessor. For the GRIB files, **MM** refers to the initialization time of the model simulation and is usually either 00 or 12. **NN** and **NNN** are the variable forecast times of the NCEP model runs relative to the model initialization time. **LL** refers to the three-hourly observation time of the data and ranges from 00 to 21 in three-hour increments. **YYMMDDHH** refers to an eight-digit date made up of the year (**YY**), month(**MM**), day (**DD**) and hour (**HH**). A "\*" represents a single character abbreviation for a variable: "R" for relative humidity, "U" for u wind component, "V" for v wind component, "H" for geopotential heights or "T" for temperature.

### **6.1.2 FNMOC Data Feed.**

There are several global and regional model datasets available in real-time from FNMOC. There are two NOGAPS global model grids, which OMEGA is capable of using for initial conditions, and there are also several regional COAMPS model grids available, which will be used in future versions of OMEGA. They also provide rawinsonde data in the standard TTAA/TTBB format and surface observations in the METAR format. Table 4 contains a list of files available from the FNMOC data feed.

For the GRIB files, **X** refers to a single letter that defines the model pressure level, **VV** refers to a two-digit number that defines the variable type, and **MMM** refers to the variable forecast times of the NOGAPS model runs relative to the model initialization time. **YYMMDDHH** refers to an eight-digit date made up of the year (**YY**), month(**MM**), day (**DD**) and hour (**HH**). **YYYYMMDDHH** refers to a similar ten-digit date, but the year includes the century (eg. 1997). A "\*" represents a single character abbreviation for a variable: "R" for relative humidity, "U" for u wind component, "V" for v wind component, "H" for geopotential heights or "T" for temperature.

### **6.1.3 Air Force Weather Agency (AFWA) Data Feed.**

An alternative access to real time atmospheric data for DSWA OMEGA applications is through the databases at the AFWA in Omaha, Nebraska. It is anticipated that most of the data listed in Table 4 will also be able to be obtained through AFWA. The capability to decode and utilize the AFWA data is not included in version 3.2.6 of the OMEGA preprocessor. It will be incorporated into subsequent versions.



Table 4. Summary of NCEP GRIB and BUFR data files ingested by PREPDAT.

GRIB or BUFR	Data Type	Input File Name (stored at NCEP)	Output File Name (read by PREPDAT)
<b>Gridded Data</b>			
GRIB	MRF	CED1.FNN.TMM.MRF	YYMMDDHH*.mrfA
GRIB	NGM 190 km	CED1.RFNN.TMMZ.RGL	YYMMDDHH*.ngmB
GRIB	NGM 90 km	CED1.RFNXP.TMMZ.RGL	YYMMDDHH*.ngmG
GRIB	ETA 190 km	CED1.LFNN.TMMZ.ETA	YYMMDDHH*.etaB
GRIB	ETA 90 km	CED1.LFNN.TMMZ.ETA	YYMMDDHH*.etaG
<b>Rawinsonde Data</b>			
BUFR	Rawinsonde	SNDDATA.BUFR.T00Z.MRF	YYMMDDHH.snd
<b>Surface Data</b>			
BUFR	Ship observations	SFCSH.P.NCBUFR.LATEST(CLLZ)	YYMMDDHH.sfcs
BUFR	SST from ships	SFCSH.P.NCBUFR.LATEST(CLLZ)	YYMMDDHH.sstb

Table 5. Summary of FNMOC data files ingested by PREPDAT.

Data Format	Data Type	Input File Name (from raw FNMOC feed)	Output File Name (read by PREPDAT)
<b>Gridded Data</b>			
GRIB	NOGAPS 2.5 deg	XVV\$MMMGRB	YYMMDDHH*.fncH
GRIB	NOGAPS 1.0 deg	XVV1MMMGRB	YYMMDDHH*.fncX
<b>Rawinsonde Data</b>			
TTAA	Rawinsonde	YYYYMMDDHHZ.wmo	YYMMDDHH.raob
<b>Surface Data</b>			
METAR	Land observations	YYYYMMDDHHZ.sao	YYMMDDHH.sao

#### 6.1.4 Other Data Types.

Gridded and observational data types can be read in several formats that are archived by various government agencies including NCAR and NCEP (detailed in Section 6.4 describing the PREPDAT module); however some data types deserve special mention. The OMEGA preprocessor can read gridded output from previous OMEGA simulations or it can create a first-guess from a single tabular format hand-entered sounding when gridded data is unavailable.

#### 6.2 Processing of Surface Characteristics Databases.

With the exception of the land/water and terrain elevation databases each of the other surface characteristics databases are organized as sets of latitude-longitude "tiles", which results in complete geographic coverage, efficient searching and logical filenames. The global-scale databases use 30 x 30 degree tiles, while the U.S. databases consist of 5 x 5 degree tiles.

FORTTRAN logic was devised to allow databases at both resolutions (U.S. and global coverages) to be used simultaneously. The higher resolution data is applied to the OMEGA grid first, then the coarser resolution data is used in any grid cells which have not been filled with values. After all of the available databases have been searched, the database values which have accumulated in each OMEGA grid cell are averaged to obtain the final value. In the case of the discrete fields (land/water, soil type and land use), the dominant (most frequent) value in each cell is considered to represent the entire cell. If no database values are found for a grid cell, the cell is flagged and assigned a "last resort" default value later in the preprocessor sequence.

### 6.3 Processing of Real-Time Hydrology Data.

The DASH (Daily Analysis of Soil and Hydrology) program can be used to process real-time reports of precipitation, temperature, and snow cover in order to produce analyzed fields of model-ready parameters. Soil moisture at various depths, subsurface temperature and snow cover are output in tiled latitude-longitude files.

DASH reads hydrological data in four specific formats. DASH performs objective analyses of daily hydrological variables from a set of sites and produces a set of gridded latitude-longitude tiles. These primary variables may be processed to obtain soil moisture, snow cover and subsurface temperature, which are needed for input into OMEGA. Error checking is also performed by DASH. A simple inverse-distance weighting scheme is used for the objective analyses.

Daily precipitation is analyzed and then used by the Antecedent Precipitation Index (API) scheme to estimate soil moisture. The retention coefficient used in the API scheme varies as a function of soil depth. The subsurface temperature is estimated by averaging the surface air temperature over a three day period. Snow cover is calculated by analyzing each day's snow cover observations. An API-type algorithm is also applied to gradually deplete the previous day's snow cover.

The primary variables are:

- (1) maximum surface air temperature,
- (2) minimum surface air temperature,
- (3) total daily precipitation,
- (4) maximum soil temperature,
- (5) minimum soil temperature,
- (6) depth of soil temperatures,
- (7) soil moisture,
- (8) depth of soil moisture,
- (9) evaporation,
- (10) solar radiation;
- (11) duration of vegetation wetness,
- (12) total snow on the ground,
- (13) new snowfall, and
- (14) average daily temperature.

The secondary variables are:

- (1) Antecedent Precipitation Index (API) at 5 cm and 30 cm,
- (2) estimated volumetric soil moisture contents,
- (3) average surface air temperature,
- (4) 24-hour precipitation, and
- (5) snow cover.

## 6.4 PREPDAT Module.

The PREPDAT module of the preprocessor serves as the interface between the many forms of atmospheric data which can be utilized by the OMEGA initialization process and the modules which actually use the data to create a three-dimensional initialization dataset for OMEGA. PREPDAT is structured to ingest data from the RTData set of files generated by the INGEST module as well as other archived atmospheric data formats. This permits the OMEGA initialization process to be executed for both research and real-time simulations. After ingesting the data PREPDAT performs a series of simple error-checking procedures. More stringent quality control is performed by ANALYSIS. Once the error-checking is complete each type of data is written to a file in a standard format.

PREPDAT ingests rawinsonde, surface and sea surface temperature observations, first guess gridded data and gridded hydrological data. These data sources are described in Table 6.

### 6.4.1 Gridded First-guess Data.

Currently, OMEGA can ingest the following types of first-guess data:

1. Data from several archive databases maintained by various government agencies including LFM II/Bureau of Reclamation format, NGM data in UNIDATA NetCDF format, Global Optimum Interpolation from NCAR, data on the ETEX experiment grid from ECMWF, and ECMWF 2.5 degree lat/lon global analysis from NCAR;
2. Data decoded from NMC's GRIDded Binary (GRIB) format available in real time by FTP from NMC including MRF output, and NGM and ETA output on several different grids;
3. Data from FNMOC's models also decoded from GRIB format;
4. Data from AFWA including HIRAS and HYSPLIT;
5. Data from a previous OMEGA simulation; and
6. A single hand entered sounding.

The user must choose exactly one gridded data source from the list in the user options file "prepomega.opt". PREPDAT processes the gridded data in the following manner:

1. The data file is read;
2. The data are interpolated horizontally to grid cell centroids and vertically to the pressure levels set by the user in "prepomega.opt";
3. The missing values and levels are filled in; and
4. The data are written to the "GUESS" file.

### 6.4.2 Rawinsonde Data.

Rawinsonde data is optional but recommended for every OMEGA initialization. The types of rawinsonde data that can be ingested by OMEGA are listed in Table 6. The user can choose one or more rawinsonde data source from the list in the user options file "prepomega.opt". PREPDAT processes the rawinsonde data in the following manner:

1. The data file is read;
2. At each rawinsonde site, the mandatory level, significant level and wind level data are merged into a single sounding;
3. Each sounding is checked for errors such as temperature spikes, superadiabatic layers and spikes in the wind hodograph, the errors are corrected, if possible, or the data is eliminated; and
4. The data are written to the "RAOB" file.

Table 6. Summary of data types which can be ingested by PREPDAT.

Data Type	File Name
<b>Gridded Data</b>	
OMEGA output	"<caseid>DHHMMz.out"
LFM II/Bureau of Reclamation format	"GborYYMMDDHH"
NGM (UNIDATA NetCDF format)	"MM_*_DDHH.cdf"
Global Optimum Interpolation	"GgoiYYMMDDHH"
ECMWF 2.5 degree lat/lon global analysis (for validation cases).	"GecmYYMMDDHH"
Decoded GRIB data from NCEP - MRF	"YYMMDDHH*.mrfA"
Decoded GRIB data from NCEP - NGM or ETA 190 km	"YYMMDDHH*.ngmB" "YYMMDDHH*.etaB"
Decoded GRIB data from NCEP - NGM or ETA 90 km	"YYMMDDHH*.ngmG" "YYMMDDHH*.etaG"
Decoded GRIB data from NCEP - ETA 81 km Lambert Conf. (Grid L or 211)	"YYMMDDHH*.etaL"
Decoded GRIB data from FNMOC - NOGAPS 2.5° global grid	"YYMMDDHH.fnIH"
Decoded GRIB data from FNMOC - NOGAPS 1.0° global grid	"YYMMDDHH.fnIX"
ETEX Experiment grid from ECMWF	not implemented
Uniform guess from hand-entered sounding	"RAOBFG"
HIRAS data from AFWA	"GhirYYMMDDHH"
HYSPLIT data from AFWA	user specified in option file
<b>Rawinsonde Data</b>	
Decoded from NCEP Office note 29 real-time format	"RnmcYYMMDDHH"
Decoded from NCEP Office note 29 archive format (for validation cases).	"RnmcYYMMDDHH"
Decoded from NCEP BUFR format	"YYMMDDHH.snd"
TTAA/TTBB/PPBB format from NCEP or FNMOC	"YYMMDDHH.raob"
DSWA historical format	"YYMMDDHH.rhst"
Air force archive format	"RafaYYMMDDHH"
<b>Surface Data</b>	
Decoded From NCEP Archive format (for validation cases).	"SmasYYMMDDHH" and "YYMMDDHH.SEA"
SAO data	"YYMMDDHH.sao"
DSWA historical format	"YYMMDDHH.shst"
Land observations decoded from NCEP BUFR format	"YYMMDDHH.sfcl"
Office note 29 land surface observations (real-time format).	"YYMMDDHH.sfcl"
Office note 29 land surface observations (archive format).	"YYMMDDHH.sfcl"
METAR format	"YYMMDDHH.sao"
Buoys and Ship Reports	"YYMMDDHH.SEA"
Ship observations decoded from NCEP BUFR format	"YYMMDDHH.sfcs"
<b>Sea Surface Temperature Data</b>	
Office note 29 land surface observations (real-time format).	"YYMMDDHH.sfcl"
Weekly OI analysis from NCEP	"oi.mean.bias.YYMMDD"

### **6.4.3 Surface Data.**

Surface data is optional but recommended for every OMEGA initialization. The types of surface data which can be ingested by OMEGA are listed in Table 6. The user can choose one or more surface data source from the list in the user options file "prepomega.opt". PREPDAT processes the surface data in the following manner:

1. The data file is read;
2. Each observation is checked for obvious errors such as out of range values with erroneous data eliminated; and
3. The data are written in a standard tabular format to the "SFC" file.

### **6.4.4 Sea Surface Temperature Data.**

Sea surface temperature (SST) data is optional but recommended for every OMEGA initialization if the domain includes large water bodies. The types of SST data which can be ingested by OMEGA are listed in Table 6. The SST can be initialized using a biweekly climatological database or a new weekly real-time SST analysis which recently became available on the NCEP NIC server. This optimum interpolation (OI) analysis is produced on a one-degree grid using in situ and satellite SST's plus SST's simulated by sea-ice cover. This dataset is usually available by anonymous ftp each Monday for the preceding 7-day period.

The user can choose one or more SST data source from the list in the user options file "prepomega.opt". PREPDAT processes the SST data in the following manner:

1. The data file is read;
2. Each observation is checked for obvious errors such as out of range values with erroneous data eliminated; and
3. The data are written in a standard tabular format to the "SST" file.

### **6.4.5 Hydrological Data.**

Hydrological data is optional but recommended for every OMEGA initialization. Climatological values of subsurface temperature and soil moisture are available in the on-line databases. GENINIT automatically uses the climatological data wherever there is no real-time data available. If no real-time data is available, climatological data is used everywhere. The types of hydrological data which can be ingested by OMEGA are listed in Table 6. The user can choose one or more hydrological data sources from the list in the user options file "prepomega.opt". PREPDAT processes the hydrological data in the following manner:

1. The appropriate real-time data files are read;
2. The data are averaged and/or interpolated to the OMEGA grid - In regions where the OMEGA grid is coarse relative to the data, averaging is performed / if the data is coarse relative to the OMEGA grid, interpolation is performed and
3. The data are written out to the files: TSUB (subsurface temperature), WSHL (shallow soil moisture), WDEP (deep soil moisture) and SNGR (snow cover).

## **6.5 GENINIT Module.**

The GENINIT module of the data preprocessor assembles the atmospheric and surface property data. GENINIT reads the SSTclim, NDVIclim, WSOILclim and TSUBclim files. It then reads the GUESS, TSUB, WSHL, WDEP and SNGR files from PREPDAT. GENINIT writes out an "INIT" file that specifies both atmospheric and surface property variables and a "BC" file that specifies only the atmospheric variables at boundary cells.

### **6.5.1 Surface Property Variables.**

GENINIT assigns the value of the hydrology variables at each grid cell in the following order of preference:

1. Non-flag real-time value from the DASH generated files: TSUB, WSHL, WDEP or SNGR;
2. Climatological values of soil moisture and subsurface temperature are used when the DASH values are unavailable - values from the WSOILclim file are used for both shallow and deep soil moisture; and
3. If neither DASH nor climatological values are available, the default specified by the user in "prepomega.opt" is used.

NDVI and SST are assigned a default value if the climatological values are unavailable. SST can be updated with observations in ANALYSIS, if they are available.

### **6.5.2 Atmospheric Variables.**

The atmospheric variables are vertically interpolated from the constant pressure surfaces provided by PREPDAT to the centroids of the cells specified in the "grid.out" file. The variables are interpolated linearly with respect to height.

## **6.6 ANALYSIS Module.**

Before a numerical simulation can be executed the many forms of raw initialization data must be combined into a single dynamically consistent description of the state of the atmosphere at the time of initialization. This involves: (1) filtering erroneous or inconsistent data from the initialization procedure; (2) obtaining initial values of atmospheric and surface variables at model grid point locations from an array of often irregularly-spaced data from different observing systems (objective analysis); and (3) adjusting the initial state to remove unrealistic relationships among the variables caused by erroneous, unrepresentative or sparse data (initialization). It is the function of the ANALYSIS module of the preprocessor to perform these functions and update a model initialization file "INIT".

The core of the OMEGA analysis and initialization procedure consists of seven steps:

- 1) the ingestion of the available data prepared by the PREPDAT module and the preliminary "INIT" file created by the GENINIT module;
- 2) the objective analysis of sea surface temperature data;
- 3) the processing and quality control of surface and upper air data;
- 4) the objective analysis of surface and upper air data;
- 5) adjustments to insure that the analyzed data meets desired constraints;
- 6) the generation of objective analysis performance statistics; and
- 7) the output of the initialization data to a modified "INIT" file.

### **6.6.1 Setting Up the Grid and Reading the Data.**

The first step in the analysis and initialization procedure is the input of user options from the "prepomega.opt" file. These options permit the user to select many of the attributes of the analysis and initialization procedure: (1) the choice of data that is included in the analysis procedure; (2) the degree of geostrophic coupling between the mass and momentum fields in the multivariate optimal interpolation (OI) scheme; and (3) the e-folding radius of the correlation functions used in the OI scheme. The next step in the procedure is the input of the data from the files that define the grid that will be used for the model simulation. The information that is ingested includes the latitude, longitude and elevation of each cell vertex, the terrain elevation, the land and water designation of each grid point, the land use classification, the climatological NDVI and the climatological sea surface temperature (SST).

After the input of the grid description and user option data, a sequence of subroutines which ingest rawinsonde, surface and sea surface temperature data from PREPDATA are executed. The flags set by the specifications in the "prepomega.opt" file determine which of these subroutines are executed and, as a result, which datasets are ingested into the ANALYSIS module. The preliminary "INIT" file from GENINIT is also read at this time.

### **6.6.2 Sea Surface Temperature Analysis.**

Once all the data has been ingested, the next step is to analyze the SST. The SST first-guess is prepared in the following manner: If a first-guess is available, it is "smeared" onto land grid cells that are within 2 grid cells of a water point. This improves the calculation of differences between the first-guess and the observations. If no SST first-guess is available, the first-guess level one air temperature is used. The SST guess data is a static database of biweekly 30 year average sea surface temperature data interpolated to the model grid. Current SST data is generally considered to be observations that were made up to 7 days prior to the time of initialization. The use of this time period is based on the premise that sea surface temperatures change relatively slowly and that SST reports from many ships are at infrequent intervals. The analysis consists of a two-dimensional version of the OI scheme.

### **6.6.3 Observational data processing and quality control.**

The next step is to process the rawinsonde and surface data. Each rawinsonde sounding is searched for gaps that are larger than 50 mb. These gaps are filled through interpolation. Next, the first-guess is interpolated to the location of each rawinsonde observation. This value is then subtracted from the observation to produce a residual or "observation increment". Finally, the rawinsonde observation increments are interpolated to mandatory pressure levels and the root mean square observation increment is calculated for winds and heights at each level. These values are used by the multivariate OI scheme as well as in the verification of the analysis. This is done by objectively analyzing not only at the model grid points but also at the rawinsonde sites at mandatory levels and at the surface observation sites. The RMS differences between the analysis and the observations is then compared to the RMS differences between the first-guess and the observations.

Surface data are converted to observation increments as are rawinsonde data. A search is then made for duplicate observations which are flagged. Then the surface observation list is consolidated and flagged observations are removed.

At this point quality control is done for both surface and rawinsonde data. The quality control algorithm is essentially equivalent to the horizontal check component of Gandin's (1988) complex quality control algorithm. The 3-D OI scheme is used to analyze the observation increments  $O-B$  (where  $O$  is the observed value and  $B$  is the first-guess interpolated value) from nearby observations not including the observation itself to the location of each observation. The observation increment at each site is then subtracted from the analyzed value to determine how well each observation increment agrees with its neighbors. This difference between the observation increment and the value of nearby observation increments objectively analyzed to the observation location is called  $D$ . If the value of  $D$  for a given observation is larger than a threshold, the observation is thrown out. The current error-thresholds are shown in Table 7. Up to 8 observations are allowed in each matrix for the rawinsonde QC algorithm and 6 for the surface QC algorithm. QC for rawinsondes includes height, relative humidity and horizontal wind. In addition, the level 1 height correction is checked against height corrections for the complete set of surface and rawinsonde observations. If the level 1 height corrections differ from the

Table 7. Observation Increment Error Thresholds.

Variable	Surface	Rawinsonde
Height (m)	20.0	20.0 at surface, increasing linearly to 50.0 at top of model domain.
Relative humidity (fraction)	0.3	0.3
Horizontal wind vector (% of wind speed)	50.0 % or 5 ms <sup>-1</sup> , whichever is greater	22.0%
Temperature (K)	4.0	4.0

analyzed value by more than the threshold, all height reports from the sounding are tossed. If the disagreement is greater than 200 m, the entire sounding is tossed. For surface data, horizontal wind vector, height, temperature and relative humidity corrections are subject to quality control.

After the quality control is performed, the last step before the multivariate OI is the combination of surface observations into "superobservations" to help improve the conditioning of the correlation matrices which are solved by the 3D-OI scheme. The number of surface observations within 45 km of each observation are counted. Those with the most nearby observations are processed first. A simplified version of the OI scheme is used to interpolate the observation increment for each surface variable to the site of the central observation. This value is taken as the superobservation and the others are eliminated. This procedure is iterated until no two surface observations are within 45 km of each other.

#### 6.6.4 Three Dimensional Multivariate Optimal Interpolation Scheme.

The basic principle in the OI scheme is that an estimate of the value of a variable  $A_i$  at a set of grid points ( $i = 1, 2, \dots, I$ ) can be created from a set of "J" meteorological observations  $O_j$  (where  $j=1, 2, \dots, J$ ) distributed irregularly throughout the analysis domain by forming an "optimal" linear combination of the "K" observations closest to the grid point. Following Daley (1991), this approach yields the following equation for the analyzed value of  $A_i$  at the grid point:

$$A_i = B_i + \sum_{k=1}^K w_k \frac{rms_i}{rms_k} [O_k - B_k] \quad (186)$$

where  $A_i$  = analyzed value at model grid points

$B_i$  = first guess or background value at model grid points

$O_k$  = meteorological observations

$K$  = total number of observations allowed to influence grid point  $i$ ,

$w_k$  = weight associated with observation  $k$

$rms_i$  = root mean square first-guess error for variables of the same type as the analysis variable

$rms_k$  = root mean square observational error for variables of same type as observation  $k$ ,

$B_k$  = first-guess or background value at observation locations

$O_k$  = observed value.

The rms errors are computed by averaging horizontally over many events. In the OMEGA preprocessor, both of the rms errors are approximated by the rms difference between the observation and the first-guess at a given pressure level. In the univariate case, they cancel each other, since the analysis variable is always the same as the observation variables. The method to obtain the "optimal" linear weighting coefficients for each of the observations is based on Gandin's (1963) theory of optimum interpolation.



The weighting coefficients are determined by attempting to minimize the root mean square error  $(\bar{T}_k - A_k)^2$  of the interpolated values (i.e. the analyzed values) where T represents the true value not including signals at scales that cannot be resolved by the observing network and the overbar denotes an ensemble average of many cases. The minimum of the root mean square error of the analyzed values can be found by taking a partial derivative of Equation 6.2 with respect to the weighting coefficients, and setting it to 0 to form the set of equations:

$$\frac{\partial \left\{ O_i - \left[ B_i + \sum_{k=1}^K w_k (O_k - B_k) \right] \right\}}{\partial w_j} = 0 \quad \text{for } k=1, \dots, K \quad (187)$$

This procedure results in a system of n linear equations:

$$\begin{pmatrix} \rho_{(B-T)_{11}} + \epsilon \rho_{(O-T)_{11}} & \rho_{(B-T)_{21}} + \epsilon \rho_{(O-T)_{21}} & \dots & \rho_{(B-T)_{K1}} + \epsilon \rho_{(O-T)_{K1}} \\ \rho_{(B-T)_{12}} + \epsilon \rho_{(O-T)_{12}} & \rho_{(B-T)_{22}} + \epsilon \rho_{(O-T)_{22}} & \dots & \rho_{(B-T)_{K2}} + \epsilon \rho_{(O-T)_{K2}} \\ \vdots & \vdots & \ddots & \vdots \\ \rho_{(B-T)_{1K}} + \epsilon \rho_{(O-T)_{1K}} & \rho_{(B-T)_{2K}} + \epsilon \rho_{(O-T)_{2K}} & \dots & \rho_{(B-T)_{KK}} + \epsilon \rho_{(O-T)_{KK}} \end{pmatrix} \begin{pmatrix} w_1 \\ w_2 \\ \vdots \\ w_K \end{pmatrix} = \begin{pmatrix} \rho_{(B-T)_{1i}} \\ \rho_{(B-T)_{2i}} \\ \vdots \\ \rho_{(B-T)_{Ki}} \end{pmatrix} \quad (188)$$

- where K = total number of observations allowed to influence grid point i;  
T = true value not including signals at scales that cannot be resolved by the observing network;  
B-T = first-guess error;  
O-T = observational error;  
 $\rho_{(B-T)_{KL}}$  = correlation between the first-guess errors at observing locations K and L;  
 $\rho_{(O-T)_{KL}}$  = correlation between the observational errors at observing locations K and L;  
 $\rho_{(B-T)_{Ki}}$  = correlation between the first-guess errors at observing location K and grid point i;  
 $\epsilon$  = ratio of the mean observational error to the mean first-guess error, assumed to be invariant in space.

The observational error includes two parts, the instrument error and the error of representativeness produced when information at very small wavelengths is aliased to the larger wavelengths due to the coarseness of the observing network. Essentially the analyzed value is the sum of the first-guess and the sum of the weights multiplied by the difference between the observation and the first-guess at each observation location. The weights are determined by solving the system of equations represented by the matrix problem in Equation 188. OI is superior to successive correction schemes such as the Barnes (1964) scheme since it takes into account the locations of observations relative to each other and effectively reduces the weight given two nearly collocated observations. It also takes into account the relative reliability of the observations relative to the first-guess.

The two dimensional matrix in Equation 188 can be simplified in several ways. First, notice that it is symmetric about the diagonal since  $\rho_{(B-T)_{kl}} + \epsilon \rho_{(O-T)_{kl}} = \rho_{(B-T)_{lk}} + \epsilon \rho_{(O-T)_{lk}}$ . Also, with a few exceptions,  $\rho_{(O-T)_{lk}} = 0$  when  $l \neq k$  and  $\rho_{(O-T)_{lk}} = 1$  when  $l=k$ , since most observations are independent of each other. The two most notable exceptions are observations at different levels in the same rawinsonde sounding and observations from the same satellite-based sensor. Since  $\rho_{(B-T)_{kl}} = 1$  when  $l=k$ , the diagonal terms in the matrix simplify to  $1+\epsilon$ .

The true value,  $T$ , is unknown. The explicit calculation of statistically significant correlations from raw data requires the processing of large datasets and Fourier or power spectrum analysis to extract the dominant wavelengths. In order to avoid this computational burden and improve the flexibility of the analysis scheme, the OMEGA OI scheme represents the covariances by an idealized autocorrelation function. One common correlation function, used by DiMego (1988) among others is:

$$\rho_{lk} = \frac{C_{lw} \exp\left(-\left(\frac{D_{lk}}{L}\right)^2\right)}{1 + k_p \ln^2\left(\frac{p_l}{p_k}\right)} \quad (189)$$

where  $D_{lk}$  = distance between points  $l$  and  $k$ ;

$L$  = a characteristic length scale;

$k_p$  = constant which determines the sharpness of the vertical correlation function;

$p_l$  and  $p_k$  = pressures at points  $l$  and  $k$ .

In a 2-dimensional OI scheme,  $k_p$  would be set to zero. The factor  $C_{lw}$  serves to reduce the correlation between points when one is located over land and the other is located over water.  $C_{lw}$  is set to one for grid cells that are not within 100 mb of the surface, when the two points are both located over the same surface type, and for the SST analysis. Otherwise it is set to 0.33 for grid cells at the surface and increases linearly to 1.0 for cells 100 mb above the surface.

Since most operational forecast systems derive their first-guess from the same source and are integrated on the same grid each day, some reasonable estimate can be made of  $\epsilon$ , the ratio of the observational error to the first-guess error. OMEGA derives its first-guess from any number of sources and is run on grids located anywhere on the globe with grid point distributions that can vary from run to run. For this reason, the estimation of  $\epsilon$  is considerably more difficult. Currently  $\epsilon$  is assumed to be 0.3 (0.37) for rawinsonde (surface) height errors, 0.45 (0.9) for rawinsonde (surface) wind errors, 0.45 (0.75) for rawinsonde (surface) relative humidity errors, 0.3 (0.75) for rawinsonde (surface) temperature errors, and 0.3 for SST errors.

The multivariate algorithm in the OMEGA data preprocessor is based on that described by DiMego (1988). The multivariate problem is similar to the univariate problem with the exception that correlation functions between different variables (geopotential,  $u$  and  $v$ ) are multiplied by an additional factor. The factor is based on the assumption that the geostrophic relation applies in the coupling of the wind and mass fields. Of course, in the tropics, within the PBL, in the presence of strongly curved and/or unbalanced flow, this may not be entirely true. But the approximation works fairly well in most cases with the addition of a coupling factor  $G$  that reduces the coupling near the surface, near the top of the model domain and at low latitudes. The user has the option of performing a univariate analysis if a high resolution analysis in regions of highly unbalanced flow. The additional factors as described in DiMego (1988) are:

$$\rho_{uz} = G \frac{\text{abs}(lat_u)}{lat_u} \sqrt{2} \left( \frac{r_z}{D} \right) (lat_u - lat_z) \quad (190)$$

$$\rho_{vz} = G \frac{\text{abs}(lat_v)}{lat_v} \sqrt{2} \left( \frac{r_z}{D} \right) (lon_z - lon_v) \cos(lat_i) \quad (191)$$

$$\rho_{u_1 u_2} = \frac{abs(lat_{u_1})abs(lat_{u_2})}{lat_{u_1} lat_{u_2}} \left[ 1 - 2 \left( \frac{r_e}{D} \right)^2 (lat_{u_1} - lat_{u_2})^2 \right] \quad (192)$$

$$\rho_{v_1 v_2} = \frac{abs(lat_{v_1})abs(lat_{v_2})}{lat_{v_1} lat_{v_2}} \left[ 1 - 2 \left( \frac{r_e}{D} \right)^2 (lon_{v_1} - lon_{v_2})^2 \cos^2(lat_i) \right] \quad (193)$$

$$\rho_{uv} = G \frac{abs(lat_u)abs(lat_v)}{lat_u lat_v} 2 \left( \frac{r_e}{D} \right)^2 (lon_u - lon_v)(lat_u - lat_v) \cos(lat_i) \quad (194)$$

where:

subscripts u, v and z represent u wind component, v wind component and geopotential observations;

$\rho_{uz}$ ,  $\rho_{vz}$ ,  $\rho_{u_1 u_2}$ ,  $\rho_{v_1 v_2}$ , and  $\rho_{uv}$  represent the correlation factors between variables of different types; lat and lon = latitudes and longitudes (in radians) at the location of the observation or gridded value represented by the subscript;

i = the analysis grid point location;

G = degree of geostrophic coupling between the mass and wind fields; and

$r_e$  = radius of the Earth.

As an example, consider the correlation between a height observation's deviation from the first-guess and a u-wind component observation's deviation. If the two observations are at the same latitude, one would expect no correlation, since a change in the height field at one location does not contain any information about a change in the north-south height gradient at that location or any location at the same latitude. A positive height perturbation, however, would be correlated with a positive (negative) change in the height gradient immediately to its north (south). For this reason, one would expect a positive (negative) correlation between height perturbations and u-wind perturbations at locations to the north (south) of the height perturbations.

The geostrophic coupling factor G is set at its maximum user specified value  $G_{ml}$  only at mid and high latitudes (more than  $25^\circ$  from the equator) in the mid-troposphere. At mid-latitudes, G increases linearly from  $0.5G_{ml}$  at the surface to  $G_{ml}$  175 mb above the surface. Above 250 mb, it begins to decrease linearly and reaches a value of about  $0.80G_{ml}$  at 100 mb. It varies latitudinally as in Dey and Morone (1985). Points greater than  $25^\circ$  latitude from the equator retain their full coupling. The coupling is set to zero for points within  $10^\circ$  latitude of the equator. The coupling for points that are between  $10^\circ$  and  $25^\circ$  from the equator is determined by the following relationship:

$$G = \frac{G_{ml} \{ \cos[(|\phi| - 10)12 - 180] + 1 \}}{2} \quad (195)$$

Recommended values for  $G_{ml}$  are specified in Table 8.

Table 8. Recommended values for user specified OI variables.

Variable	Description	Value
$G_{ml}$	Maximum geostrophic coupling	0.85
$L_s$	Correlation weighting radius at surface	450 km
$L_T$	Correlation weighting radius in free atmosphere	700 km

The wind-wind correlations on the diagonal of equation (6.4) are multiplied by an additional factor, H. H increases linearly from 0.5 at the surface to 1.0 at 175 mb above the surface. It is then constant up to 175 mb. Above 175 mb, it begins to increase linearly again and reaches 1.2 at 100 mb. The net effect is to decrease the weight of wind observations relative to geopotential observations in the PBL and increase their weight relative to geopotential observations in the stratosphere where geopotential errors are accumulated from the entire sounding.

The correlation weighting radius, the length scale in Equation (189), is

$$L = \begin{cases} L_s & \Delta p \leq 0 \\ L_s + \left[ \frac{\Delta p}{\Delta p_{\max}} (L_r - L_s) \right] & 0 < \Delta p \leq \Delta p_{\max} \\ L_r & \Delta p_{\max} < \Delta p \end{cases} \quad (196)$$

where  $L_s$  ( $L_r$ ) is a length scale selected by the user for surface (rawinsonde) observations and  $\Delta p$  is the pressure difference between the surface and the grid point. This allows for a smooth transition between the relatively high resolution surface data and the coarser rawinsonde data. The weights are entered into the system of equations and the matrix is inverted to calculate the correction at each grid point.

Recommended values of  $L_s$  and  $L_r$  are listed in Table 8.

The correlation matrix size is set to 27 at the surface. It decreases approximately linearly to 15 at 200 mb above the surface. Above this level it is set to 12. The matrix size is always set to a value that is divisible by 3 so that a height, a zonal (E-W) wind and a meridional (N-S) wind observation from each location can be used. Twelve spots in the matrix are reserved for rawinsonde observations from the 4 nearest soundings to the grid point. One u wind component, one v wind component and one geopotential observation are included from each sounding. These observations are interpolated to the pressure level of the analysis grid point, unless the analysis pressure is within a data void region for a given sounding. In this case, the nearest observation in the sounding is chosen. For the purposes of Equation (189), the observation pressure is assumed to be that of the nearest actual observation in the sounding. The remaining spots in the matrix are reserved for observations from the nearest surface stations. Surface pressure observation increment hydrostatically converted to a height increment and wind competence are selected from each station. At the surface, this leaves room for the five nearest surface stations, while there is only room for one 200 mb above the surface and none above that. In the univariate case, the matrix is filled with observations of the same type, so that 3 times as many observing stations can be used.

The analysis proceeds horizontally, layer by layer, cell by cell. The analysis is performed at the top center of each OMEGA grid cell as well as at the bottom of the lowest layer of cells. Corrections to the first-guess field for height and wind are computed using the multivariate algorithm while those for relative humidity are computed using the simpler univariate algorithm. If the user sets  $G_{ml}$  to zero, all corrections are computed with the univariate algorithm. Corrections are computed for an entire layer and smoothed with a 4 point smoother before being added to the first-guess. The smoother sets the value at a given cell to 50% of the original value plus 1/6 the value at each of the 3 adjacent cells. The height corrections are converted to pressure corrections since OMEGA defines grid locations at constant heights. The variables are then vertically interpolated to cell centroids. Temperature is analyzed only at the surface. At cell centroids, it is derived hydrostatically from the pressure at the top and bottom of the cell. If a level is less than 10 mb from the last analyzed level, the analysis at this level is skipped. The corrections to the first-guess are then interpolated from the corrections at the nearest analyzed layers above and below. This reduces the problem of noisy temperature fields due to small differences in the height correction at closely spaced analysis layers.

The surface temperature data is used to hydrostatically adjust the surface height increment in the lowest levels as in DiMego (1988). At the ground, the surface height increment will be used directly. In the first few model levels above the ground (up to about 40 mb above the surface), the surface height increment is hydrostatically corrected by assuming that the surface temperature perturbation is valid over this layer. The corrected height increment is considered to be valid at the model level. In effect, a mini-sounding is created from each surface observation. The profile extends about 40 mb above the ground. Only the nearest height increment to a given level is included in the analysis matrix at any given grid point. This has the effect of influencing the thickness field near the ground so that the hydrostatically derived temperature field closely resembles a direct surface temperature analysis. In summary, the procedure to obtain an estimate of the analysis variable  $A_j$  with the OI scheme is:

- (1) determine the matrix size and the observations which go into it as described above;
- (2) calculate the autocorrelation function value for each pair of observations and for each of grid point location-observation pair using Equations 189 through 195;
- (3) solve equation set 6.4 using a standard matrix inversion technique (Gaussian elimination), to obtain a weighting coefficient ( $w_k$ ) for each observation; and
- (4) substitute the  $w_k$  values into Equation 186 to obtain an estimate of  $A_i$  at the grid point.

#### **6.6.5 Adjustment of Analyzed Values.**

The final process in the preparation of the initialization file is the adjustment of the vertical temperature profile. Since height rather than temperatures are analyzed by the 3-D OI scheme, temperature profiles will sometimes include regions of superadiabatic lapse rates or temperature spikes. This is particularly true near the surface where closely spaced analysis layers mean that a small error in the height analysis at one level can produce large temperature anomalies in the layers above and below. Spikes are removed, one at a time, starting with the most significant spike. The spike is removed by adjusting the height of the layer interface which lies between the grid point that contains the spike and the adjacent grid point which most resembles a spike of the opposite sign. This method is based on the assumption that a small error in the height analysis at one layer interface relative to the interfaces above and below will introduce a warm-cold dipole in the temperature field at the layers immediately above and below. Once all significant spikes are removed, superadiabatic layers are removed in a similar manner. Often, the removal of temperature spikes also removes superadiabatic layers so that this final step is not needed. The adjustment of the intermediate height is done so that temperature lapse rate between the grid point above and below is set to the mean lapse rate of a layer which extends one level above and below any contiguous layers which contain a spike or superadiabatic lapse rate.

The lapse rate adjustment is an iterative process in which the largest temperature spikes and the most superadiabatic lapse rates are removed first. The process continues until no superadiabatic layers remain and the largest temperature spike is below a threshold magnitude. Layers near the surface with a moderate superadiabatic lapse rate are allowed to remain. The interpolation of variables from cell tops and bottoms to centroids as well as the hydrostatic calculation of temperatures from the pressure field and the interpolation of temperature to the new pressures at the cell centroids which result from the surface pressure analysis are all an integral part of the lapse rate adjustment process.

#### **6.6.6 Generation of Analysis Performance Statistics.**

At this point, temperature, humidity, winds and heights are analyzed to the mandatory pressure levels at rawinsonde sites and to the locations of surface observations for verification purposes. A summary of the RMS differences between the 3-D dataset both before and after the update by the 3-D OI scheme are written to the "ANainfo" file.

### **6.6.7 Final Processing and Writing the "INIT" File.**

Next, the values in all of the arrays that contain variables which define the properties of the earth's surface are checked. If any of these arrays contain "flag" values because no actual data was available, a default value is assigned to that variable. The default values for each variable are determined by the values specified by the user in the "prepomega.opt" file.

The output from subroutine ANALYSIS consists of an "INIT" file in which the 3-dimensional variables and the skin temperature have been updated with the observations.

## **6.7 Preparation of Lateral Boundary Conditions.**

The lateral boundary condition data for the OMEGA model is orchestrated by the RUNPREP script. It takes advantage of the capabilities of PREPDAT and GENINIT to be run in both the Initialization mode described above and Boundary condition mode. A separate BC file is created for each boundary condition time. The initial file "BC.tag0" is created when PREPDAT and GENINIT are run in Initialization mode. RUNPREP then runs the two modules once for each subsequent boundary condition time to create the files "BC.tag1", "BC.tag2" and so on.

### **6.7.1 Execution of PREPDAT in Boundary Condition Mode.**

When PREPDAT is run in Boundary condition mode, no observational or surface property data is processed. A gridded data file is read in from one of the gridded data sources listed in Table 7. The data is processed in the usual way, but it is interpolated horizontally only to the boundary points that are created by reflecting each cell that borders on the edge of the domain across the domain boundary. The processed data is then written to the "GUESS" file.

### **6.7.2 The Execution of GENINIT in Boundary Condition Mode.**

When GENINIT is run in Boundary condition mode, it reads in the "GUESS" file written by PREPDAT's Boundary condition mode execution. It then interpolates this data vertically from pressure surfaces to the cell centroids of the boundary cells. It then writes out a "BC" file identical in format to the "BC.tag0" file without writing an "INIT" file. RUNPREP renames this file to "BC.tag#" where number represents the sequence of the file in the list of boundary condition times.

## Section 7

### Model Boundary Conditions

#### 7.1 Lower Boundary Conditions.

The OMEGA model prognostic variables ( $\rho u, \rho v, \rho w, \rho \theta, \text{ and } \rho q$ ) at the lower boundary are treated in the following form

$$\Delta \rho \zeta = \rho_{ave} \Delta \zeta + \zeta_{ave} \Delta \rho, \quad (197)$$

where  $\zeta$  represents  $u, v, w, \theta, \text{ and } q$ .

The lower boundary conditions for  $\zeta$  and  $\rho$  (represented as  $\varsigma$ ) are formulated with the aid of Monin-Obukhov similarity theory for the atmospheric surface layer. This theory allows one to derive relationships between the values of ground level prognostic variables at the first ( $\varsigma_s$ ), and second computational level ( $\varsigma_2$ ), and a diagnostic level ( $\varsigma_1$ )

$$\varsigma_1 = \varsigma_2 P_\alpha + (1 - P_\alpha) \varsigma_s, \quad (198)$$

where

$$P_\alpha = \frac{\ln(z_1/z_0) - \psi_\alpha(\xi_1) + \psi_\alpha(\xi_0)}{\ln(z_2/z_0) - \psi_\alpha(\xi_2) + \psi_\alpha(\xi_0)}, \quad \alpha = m, h, \quad (199)$$

and  $\psi_m$  and  $\psi_h$  are universal functions of nondimensional height  $\xi = z/L$ . The revised formulas for  $\psi_m$  and  $\psi_h$  proposed by Beljaars and Holtslag (1991) are used. The two lowest computational levels of the model are assumed to be placed within the atmospheric surface layer.

At the ground surface, a no-slip condition is imposed for the wind so that

$$u(z_0) = v(z_0) = w(z_0) = 0. \quad (200)$$

The hydrostatic equation is used to obtain the surface pressure at level  $z_0$  (the sub-terrain "ghost" cell layer) from level 2 (the lowest atmospheric layer) OMEGA pressure, while a zero gradient boundary condition is imposed on density,  $\rho$ . For all Eulerian tracers ( $Q_t$ ) zero flux boundary condition (i.e., complete reflection)

$$K \frac{\partial Q_t}{\partial z} = 0 \quad (201)$$

are assumed at the ground, as the surface absorption rates are not well known. Lower boundary conditions for turbulent kinetic energy,  $e$ , is taken to be

$$\frac{\partial e}{\partial z} = 0. \quad (202)$$

## 7.2 Lateral Boundary Conditions.

While OMEGA simulates processes that occur over all of the atmospheric system, usually only a portion of the atmosphere is chosen for simulation. This requires certain assumptions to be made regarding the portion of the physical domain that is outside the computational domain. These assumptions are applied as boundary conditions to the edge of the computational domain. In OMEGA, the bottom boundary is the surface of the earth, either land (with varying surface properties) or water. The lateral and top boundaries are continuations of the atmosphere itself. Each of these boundaries have to be treated in an appropriate manner.

The lateral boundaries are open and should allow the unimpeded flow of air (and associated properties) through them. Outflow boundaries are deterministic, while the inflow boundaries are not. In cloud scale models, in which the time scale is small enough to assume that the environment outside the model domain is unchanged during the simulation, the inflow boundaries are usually prescribed from environmental conditions. In mesoscale and larger models this assumption can no longer be made. The environment outside the computational domain has to be derived from larger scale forecast tools such as the NCEP ETP, Nested Grid Model (NGM), Medium Range Forecast model, (MRF), or the FNMOC NOGAPS model.

The key requirement in connecting the solution within the computational domain with the outside environment is that acoustic disturbances be allowed to propagate out with minimal reflection. To ensure this we use a radiative boundary condition based on the method of characteristics (Hedstrom, 1979). Presently, a 1-D formulation is used, although it can be upgraded to multidimensional treatments in the future. Consider the linearized 1-D gas dynamics equation in matrix form:

$$\frac{\partial \mathbf{U}}{\partial t} + \mathbf{A} \cdot \frac{\partial \mathbf{U}}{\partial x} = 0 \quad (203)$$

where

$$\mathbf{U} = \begin{bmatrix} \rho \\ V_b \\ P \end{bmatrix}, \quad \mathbf{A} = \begin{bmatrix} V_b & \rho & 0 \\ 0 & V_b & \frac{1}{\rho} \\ 0 & \rho c^2 & V_b \end{bmatrix} \quad (204)$$

and a local coordinate system is used such that the boundary flow,  $V_b$ , is positive when directed outward. There are three characteristic speeds,  $\lambda_i$ , derived from the eigenvalues of  $\mathbf{A}$ :

$$\lambda_0 = V_b, \lambda_+ = V_b + c, \text{ and } \lambda_- = V_b - c. \quad (205)$$

where  $c$  is the local sound speed. The characteristic equations along  $dx/dt = \lambda_i$  are

$$\mathbf{l}_i \cdot \frac{d\mathbf{U}}{dt} = 0. \quad (206)$$

where  $\mathbf{l}_i$  are eigenvectors of  $\mathbf{A}$ :

$$\mathbf{l}_0 = \begin{bmatrix} 1 \\ 0 \\ -\frac{1}{c^2} \end{bmatrix}, \quad \mathbf{l}_{\pm} = \begin{bmatrix} 0 \\ \pm \rho c \\ 1 \end{bmatrix} \quad (207)$$



From (204), we get:

$$dp = dp/c^2 \text{ along } dx/dt = V_b, \quad (208)$$

and

$$\pm \rho c dV_b + dp = 0 \text{ along } dx/dt = V_b \pm c, \quad (209)$$

To minimize reflection, signals along the incoming characteristics should be “quiescent,” *i.e.*,  $I_i \cdot \partial U / \partial t = 0$  for  $\lambda_- = V_b - c$ , and for  $\lambda_0 = V_b$  when  $V_b < 0$  (inflow). We can now write the boundary condition in the form of initial value equations for the boundary variables  $V_b$ ,  $\rho$ , and  $p$ . For an inflow boundary,  $V_b < 0$ , we get

$$\begin{aligned} \Delta V_b &= -\frac{1}{2\rho c} \frac{\partial P}{\partial x} \Big|_{-} (V_b + c)\Delta t - \frac{1}{2} \frac{\partial V_b}{\partial x} \Big|_{-} (V_b + c)\Delta t, \\ \Delta P &= -\frac{1}{2} \frac{\partial P}{\partial x} \Big|_{-} (V_b + c)\Delta t - \frac{1}{2\rho c} \frac{\partial V_b}{\partial x} \Big|_{-} (V_b + c)\Delta t, \text{ and} \\ \Delta \rho &= \frac{\Delta P}{c^2} \end{aligned} \quad (210)$$

where  $\frac{\partial}{\partial x} \Big|_{-}$  indicates that the gradient should be evaluated inside the computational domain. For the outflow boundary, we get

$$\begin{aligned} \Delta V_b &= -\frac{1}{2\rho c} \frac{\partial P}{\partial x} \Big|_{-} (V_b + c)\Delta t - \frac{1}{2} \frac{\partial V_b}{\partial x} \Big|_{-} (V_b + c)\Delta t, \\ \Delta P &= -\frac{1}{2} \frac{\partial P}{\partial x} \Big|_{-} (V_b + c)\Delta t - \frac{1}{2\rho c} \frac{\partial V_b}{\partial x} \Big|_{-} (V_b + c)\Delta t, \text{ and} \\ \Delta \rho &= \frac{1}{c^2} \left( \Delta P + \frac{\partial P}{\partial x} \Big|_{-} U\Delta t \right) - \frac{\partial \rho}{\partial x} \Big|_{-} U\Delta t \end{aligned} \quad (211)$$

The three boundary variables are advanced in time explicitly. Finally, at the lateral boundaries, zero gradient boundary condition is applied for turbulent kinetic energy.

### 7.3 Upper Boundary Conditions.

Since the top boundary is also assumed to be open, an appropriate radiative boundary condition should be imposed on it, which will allow vertically propagating gravity waves to escape the model domain without being reflected back into it. This is more complicated than for sound waves. Klemp and Durran (1983) show that when the gravity wave phase speed is larger than the mean horizontal wind, the vertical phase speed and group velocity are in opposite directions, *i.e.*, a simple characteristic treatment will not work. They formulated a top boundary condition scheme that can radiate gravity waves but is both difficult and computationally expensive to implement on an unstructured grid. Hence in OMEGA we are using a Perkey-Kreitzberg (1976) type sponge defined over the top few layers. This is in addition to the acoustic radiative boundary condition described in the previous section. Since the phase speeds for sound and for the gravity waves differ by an order of magnitude, the acoustic boundary condition should have no influence on gravity waves.

The sponge treatment should be adequate in most cases especially if the sponge layers are placed well above the tropopause. According to this scheme the prediction of a dependent variable  $\phi$  can be written as

$$\phi^{t_0+\Delta t}(r) = \phi^{t_0}(r) + \left\{ w(r) \frac{\partial \phi}{\partial t} \Big|_{t_0, m} + [1 - w(r)] \frac{\partial \phi}{\partial t} \Big|_{t_0, ls} \right\} \Delta t \quad (212)$$

where subscripts  $m$  and  $ls$  refer to the model predicted tendency and a large scale tendency which is derived from a larger scale forecast model (LFM or NGM models), and  $w(r)$  is a weighting function defined as follows:

$$w(r) = \begin{cases} \left[ \frac{(r_{top} - r)}{(r_{top} - r_{sp})} \right]^\alpha & \text{for } r > r_{sp} \\ 1 & \text{for } r \leq r_{sp} \end{cases} \quad (213)$$

where  $r_{sp}$  specifies the start of the sponge layer, and  $\alpha$  is usually set at 0.5. Thus the value at the boundary is completely prescribed by the large-scale flow and the values at the bottom of the sponge layer are the model calculated values. If the large-scale tendency is not used this scheme becomes a porous sponge in which the boundary is not tied down to any specific value but allowed to float in response to the interior flow.

Finally, turbulent kinetic energy,  $e$ , vanishes at the top boundary (i.e.,  $e=0$ ).

## Section 8

### Atmospheric Dispersion Model Structure

#### 8.1 Overview.

The Atmospheric Dispersion Model (ADM) is embedded within OMEGA. The model is composed of Eulerian and Lagrangian transport algorithms that advect massless tracers, gases, and/or solid and liquid particles using the OMEGA-resolved wind field while simultaneously solving a diffusion model that simulates the effect of unresolved physics including turbulence. Massless tracers and gases are in thermodynamic and dynamic equilibrium with the ambient atmosphere whereas solid and liquid particles are allowed to settle out with a size and density-dependent vertical slip velocity due to gravity. The Lagrangian routines provide a means of modeling point releases. The Eulerian tracer capability provides a means to track releases of gaseous species originating from OMEGA grid cells where it is assumed that the released gas instantaneously and uniformly fills the OMEGA cell containing the source. The Eulerian tracer capability also provides a first order comparison against the Lagrangian particle transport.

#### 8.2 Eulerian Model.

An Eulerian tracer methodology is applicable to large area releases. It is assumed that the released gas instantaneously and uniformly fills the OMEGA cell containing the source and that the source strength (release rate), remains constant through the OMEGA run. The OMEGA Eulerian tracers are currently assumed to be massless and hence are advected and diffused with the ambient air. The conservation equation for the tracer field can be written as

$$\frac{\partial Q_t}{\partial t} = -\nabla \cdot (QV) + S_t \quad (214)$$

where  $Q_t$  is the tracer concentration,  $S$  is the subgrid, and  $S_t$  represents the tracer sources/sinks including subgrid transport fluxes.

Sources can be specified via their source strength, latitude, longitude, and altitude locations. The source specification can be allocated through the OMEGA graphical user interface or by editing the OMEGA configuration file. An example of an Eulerian release is shown in Figure 27.

#### 8.3 Lagrangian Particle Model.

The ADM Lagrangian particle transport provides a comprehensive injection and dispersion capability for puffs or discrete mass elements. The user can choose to initialize multiple release locations for either massless or settling particles. In addition, these particles can represent individual masses or the centroids of diffusing puffs. The user also has the ability to predetermine the altitude of release, the injection time interval, the start and stop time of the injection, the number of particles (or puff centroids) initialized per injection time interval, and a number of particle physical parameters. The resulting particle output can be post-processed to produce concentration fields for comparison to observed data or simply as a means to visualize OMEGA flowfields.

### 8.3.1 Particle Transport.

The ADM Lagrangian model uses a particle-in-cell technique to simulate the transport of particles in the OMEGA wind field. Particles are advected using the OMEGA-wind components. In addition, particle velocity is adjusted so that particles are allowed to fall out with a vertical slip velocity due to gravity.

In order to transport a particle horizontally and vertically in response to the OMEGA-generated wind field, ADM first averages the domain cell-centered spherical (u, v, w) components of velocity to the domain cell vertices. Next, the velocity components are interpolated to the projection of the particle position in the model layers both above and below the actual vertical location of the particle. Finally, a bilinear interpolation is performed between the model layers above and below the vertical location of the particle to get the components of velocity at the particle location.

Massless particles and the centroids of vapor puffs are advected with the components of velocity generated in this manner. Since they are in thermodynamic and dynamic equilibrium with the ambient atmosphere, they follow an average of the local wind flow exactly. Massive particles on the other hand, must be adjusted for particle slip velocity due to gravity. The slip velocity is determined by calculating the terminal velocity,  $V_t$ , using modified Stokes drag. The terminal velocity calculation starts with the particle momentum equation

$$M_p \frac{\partial w}{\partial t} = -M_p g - \frac{\alpha}{2} \left( 0.4 + \frac{24}{R_e} \right) A_p \rho_a w \|V_p\| \quad (215)$$

where

$w \equiv$  the component of particle velocity perpendicular to the ground,

$\alpha \equiv$  drag coefficient multiplier for rough spheres,

$g \equiv$  acceleration due to gravity,

$R_e \equiv$  Reynold's number,

$A_p \equiv$  cross-sectional area of the spherical particle, and

$\rho_a \equiv$  ambient air density.

Setting  $\frac{\partial w}{\partial t} = 0$  gives

$$V_t = \left( \frac{30\mu}{\rho_a D} \right) \left( -1 + \sqrt{1 + \frac{D^3 g \rho_a \rho_p}{405\mu^2}} \right) \quad (216)$$

where  $\mu \equiv$  dynamic viscosity of air.

Particles crossing the top and side boundaries are removed and the resulting particle arrays compressed. Those particles impacting the surface can either deposit or perfectly reflect.

### 8.3.2 Particle Tracing Methodology.

Once particles or puff centroids are initialized, their origin and subsequent locations on the OMEGA unstructured grid are updated in the vertical using a simple comparative search on particle and layer altitudes. Horizontal locations are updated using a successive nearest-neighbor search routine based on the use of vector cross products (Lottati, 1993).

The basic steps of this routine are illustrated in Figures 27 and 28. In Figure 27, a particle,  $X1$ , the relative horizontal location of one element of the unstructured grid, is evaluated with respect to each vertex location of the element. The search routine computes the cross product between the vector formed from the first vertex location to the current particle location,  $\vec{A}$ , and the vector formed from the first vertex location to the second vertex location,  $\vec{B}$ . A positive value of  $A \times B$  (positive area with respect to  $\vec{B}$ ), indicates that the particle is located in the element with respect to the first vertex location. Additional cross products are computed with respect to the other two vertices with the result that three positive returns indicate that the particle is located in the element.

In Figure 28, the particle, now at location  $X2$ , has advected some distance from its original location to a point out of the original element. The search routine again evaluates the cross products using the old vertex locations and the new particle location. Evaluation of the cross product returns a negative  $\vec{A} \times \vec{B}$  (negative area with respect to  $\vec{B}$ ), for the first vertex indicating that the particle has crossed the element boundary and now possibly resides in the adjacent element. Stored grid information updates the element identifier on the right hand side of the original element boundary, and the search routine moves on to the adjacent element for testing. If the particle had advected several elements away, the scheme would continue to advance through neighboring elements in a directional sequence dictated by which vector cross products return negative values. The search would continue until three positive cross products are returned for one element, thus indicating that the particle has been located and its new cell id determined.

### 8.3.3 Particle Dispersion.

ADM has the capability to simulate the dispersion of non-buoyant particles using either a Lagrangian particle model or a formulation for puff diffusion. The particle model treats each particle as a discrete element of mass. This differs from the puff model which treats each particle as the centroid of an expanding puff. The Lagrangian particle model simulates the dispersion of pollutants or by tracking a large set of Lagrangian particles moving, at each time step, with pseudo-velocities. These pseudo-velocities simulate the effects of the two basic dispersion components: (1) transport due to the mean wind, and (2) diffusion due to turbulent velocity fluctuations. Subsequent positions of each particle ( $x$ ,  $y$ ,  $z$ ) representing a discrete element of pollutant mass are computed from the following

$$x(t + \Delta t) = x(t) + [\bar{u}(t) + u'(t)]\Delta t, \quad (217)$$

$$y(t + \Delta t) = y(t) + [\bar{v}(t) + v'(t)]\Delta t, \quad (218)$$

and

$$z(t + \Delta t) = z(t) + [\bar{w}(t) + w'(t)]\Delta t \quad (219)$$

where  $\bar{u}$ ,  $\bar{v}$  and  $\bar{w}$  are the mean wind components obtained directly from OMEGA model, and  $u'$ ,  $v'$  and  $w'$  are the corresponding subgrid scale turbulent velocity fluctuations whose statistics are derived from the boundary layer formulations used in the OMEGA model.

The particle turbulent velocity fluctuations are calculated using a Markov chain scheme

$$u'(t + \Delta t) = R_{u'}(\Delta t) u'(t) + u''(t + \Delta t) \quad (220)$$

$$v'(t + \Delta t) = R_{v'}(\Delta t) v'(t) + v''(t + \Delta t) \quad (221)$$

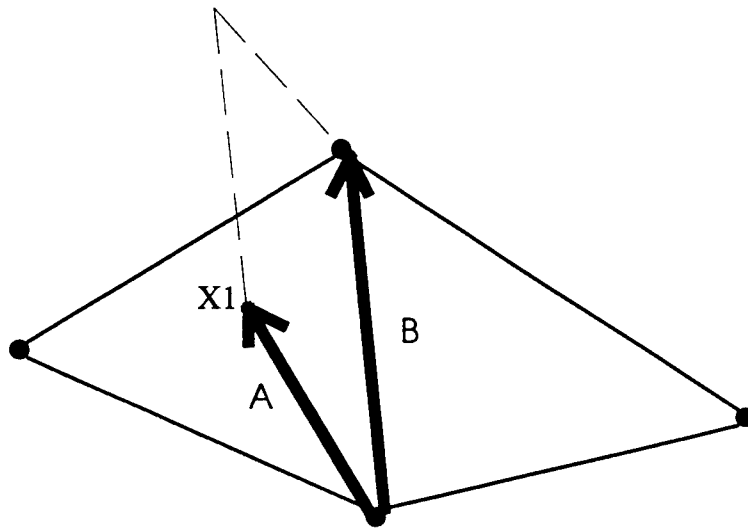


Figure 27. A particle,  $X_1$ , located in one element of the OMEGA unstructured grid, is evaluated using  $A \times B$ . The cross product between the vector formed from the first vertex location to the current particle location,  $\vec{A}$ , and the vector formed from the first vertex location to the second vertex location,  $\vec{B}$  indicates a positive value of area with respect to  $\vec{B}$ .

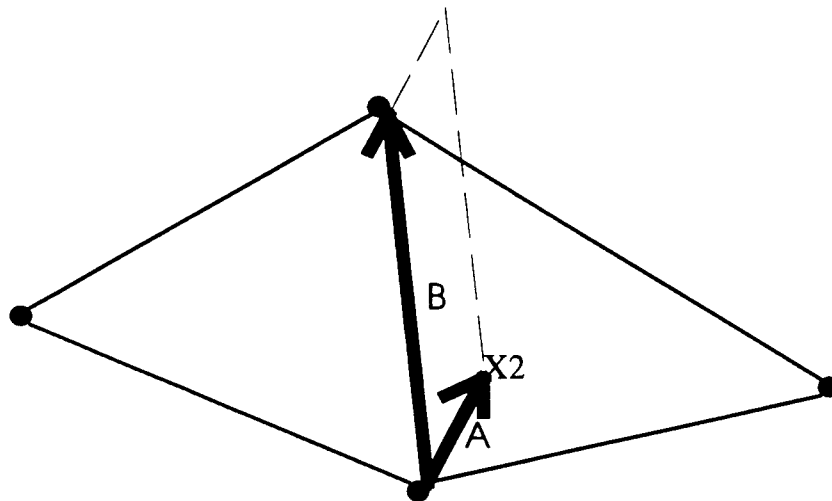


Figure 28. A particle,  $X_2$ , located in one element of the OMEGA unstructured grid, is evaluated using  $A \times B$ . The cross product between the vector formed from the first vertex location to the current particle location,  $\vec{A}$ , and the vector formed from the first vertex location to the second vertex location,  $\vec{B}$  indicates a negative value of area with respect to  $\vec{B}$ .

$$w'(t + \Delta t) = R_w(\Delta t) w'(t) + w''(t + \Delta t) \tag{222}$$

where  $u''$ ,  $v''$ , and  $w''$  are purely random uncorrelated turbulent velocity components. Distributions of these random turbulent velocity components are Gaussian with zero mean values, *i.e.*, they are completely characterized by the following variances

$$\sigma_{r_u}^2 = \sigma_{u'}^2 (1 - R_u^2) \quad (223)$$

$$\sigma_{r_v}^2 = \sigma_{v'}^2 (1 - R_v^2) \quad (224)$$

$$\sigma_{r_w}^2 = \sigma_{w'}^2 (1 - R_w^2) \quad (225)$$

where  $R_u$ ,  $R_v$ , and  $R_w$  are auto-correlation coefficients for each velocity component and assumed to be exponential

$$R_u(\Delta t) = \frac{\overline{u'(t)u'(t-\Delta t)}}{\sigma_{u'}^2} = \exp\left(-\frac{\Delta t}{T_L^u}\right), \quad (226)$$

$$R_v(\Delta t) = \frac{\overline{v'(t)v'(t-\Delta t)}}{\sigma_{v'}^2} = \exp\left(-\frac{\Delta t}{T_L^v}\right), \quad (227)$$

and

$$R_w(\Delta t) = \frac{\overline{w'(t)w'(t-\Delta t)}}{\sigma_{w'}^2} = \exp\left(-\frac{\Delta t}{T_L^w}\right) \quad (228)$$

where  $T_L^u$ ,  $T_L^v$  and  $T_L^w$  are the Lagrangian integral time scales of the sub-grid scale turbulence.

The Lagrangian turbulent statistics ( $\sigma_u$ ,  $\sigma_v$ ,  $\sigma_w$ ,  $T_L^u$ ,  $T_L^v$ , and  $T_L^w$ ), in each of the three component directions must be determined. An important advantage of Turbulent Kinetic Energy (TKE) closure is that it allows one to determine a variety of turbulent variables including the Lagrangian turbulent statistics (Uliasz, 1990). The variances of wind velocity components used in the Lagrangian particle model can be written in the following form

$$\sigma_u^2 = 2e \left\{ \frac{1}{3} - 2A_1(S_M G_M + S_H G_H) + 6A_1 S_M \frac{\ell^2}{2e} \left( \frac{\partial u}{\partial z} \right)^2 \right\} \quad (229)$$

$$\sigma_v^2 = 2e \left\{ \frac{1}{3} - 2A_1(S_M G_M + S_H G_H) + 6A_1 S_M \frac{\ell^2}{2e} \left( \frac{\partial v}{\partial z} \right)^2 \right\} \quad (230)$$

$$\sigma_w^2 = 2e \left\{ \frac{1}{3} - 2A_1(S_M G_M + S_H G_H) + 6A_1 S_H G_H \right\} \quad (231)$$

In addition, the Lagrangian integral time scales are related to the diagonal elements of the diffusivity tensor,  $K_{xx}$ ,  $K_{yy}$ ,  $K_{zz}$ ,

$$T_L^u = \frac{K_{xx}}{\sigma_u^2}, \quad T_L^v = \frac{K_{yy}}{\sigma_v^2}, \quad T_L^w = \frac{K_{zz}}{\sigma_w^2} \quad (232)$$

where 
$$K_{xx} = \ell\sqrt{2e}S_{xx}, \quad K_{yy} = \ell\sqrt{2e}S_{yy}, \quad K_{zz} = \ell\sqrt{2e}S_{zz} \quad (233)$$

with the functions  $S_{ij}$  expressed by the following parameter.

$$S_{xx} = 3A_2 \left\{ 6A_1 S_M + \frac{3A_2}{1 - 1.5A_2 B_2 G_H} [S_M + 1.5A_2 B_2 (S_M + S_H) G_H] \right\} \frac{\ell^2}{2e} \left( \frac{\partial u}{\partial z} \right)^2 \quad (234)$$

$$\dots + A_2 [1 - 6A_1 (S_M G_M + S_H G_H)]$$

$$S_{yy} = 3A_2 \left\{ 6A_1 S_M + \frac{3A_2}{1 - 1.5A_2 B_2 G_H} [S_M + 1.5A_2 B_2 (S_M + S_H) G_H] \right\} \frac{\ell^2}{2e} \left( \frac{\partial v}{\partial z} \right)^2 \quad (235)$$

$$\dots + A_2 [1 - 6A_1 (S_M G_M + S_H G_H)]$$

$$S_{zz} = S_H \quad (236)$$

## 8.4 Probabilistic Puff Model.

Continuous plumes are commonly represented by subdividing them into discrete, overlapping volumes, often called “puffs”. The major components of the probabilistic puff model are discussed in detail below.

### 8.4.1 Generation of Puffs.

The model generates a new group of Lagrangian puffs (N) at a user’s defined time interval ( $\Delta t$ ). The number of puffs released, N, depends on local wind speed and turbulent diffusion at the source. N is chosen in a such way that the distance between 2 puffs should be approximately equal to  $\sigma_h / 2$ . Each puff generated represents a discrete element of the total material released into atmosphere. The amount of the material, Q, is the same in each puff so that

$$Q = \frac{q\Delta t}{N} \quad (237)$$

where q is the source strength (kg/s).

### 8.4.2 Motion and Modification of Puffs.

All motions and changes in size are determined by conditions at the puff center by the following three operations: (a) the transport of puff centroid by the mean wind, (b) the distribution of material within each puff (around the puff centroid) in space according to a Gaussian function whose  $\sigma_x$ ,  $\sigma_y$ , and  $\sigma_z$  values increase with travel time or distance, and (c) plume rise.

Large scale air modification of each puff is discussed in detail in Section 8.3.1 (particle transport by the mean wind). For puff diffusion, the standard deviations of the Gaussian distribution are estimated based on Taylor’s homogeneous diffusion theory which use turbulence characteristics from the turbulence closure scheme used in PBL model

and 
$$\sigma_x(t + \Delta t) = \sigma_x(t) + \sigma_u \Delta t \quad \text{for } t \leq 2T_L^u \quad (238)$$

$$\sigma_x^2(t + \Delta t) = \sigma_x^2(t) + 2T_L^u \sigma_u^2 \Delta t \quad \text{for } t > 2T_L^u$$



where the variance of wind velocity component,  $\sigma_u$ , and the Lagrangian integral time scale,  $T_L^u$ , are discussed in Section 8.3 (Lagrangian Particle Model). In a similar way  $\sigma_y$  and  $\sigma_z$  are determined (Uliasz, 1990).

For the plume rise treatment, the work of Briggs (1969,1979) provides the basis. The following plume rise equations are applied separately to each puff centroid, using the wind and stability values at the point. This allows spatial and temporal variations of atmospheric stability to be treated. For plume rise, the governing parameter is the buoyancy flux  $F(m^4 s^{-3})$ , given by

$$F = \frac{g v_e d_e^2 (T_e - T)}{4 T_e} \quad (239)$$

where  $g$  gravitational acceleration,  $v_e$  stack gas exit speed,  $d_e$  stack exit diameter,  $T_e$  stack gas exit temperature, and  $T$  ambient temperature. Then, four different equations (depending on wind speed and stability) are used to determine plume rise. For purpose of determining plume rise, stability is needed and defined by

$$S = \frac{g \Delta \theta}{\theta \Delta z} \quad (240)$$

The equations for plume rise  $w_p$  when  $S > 4.2 \times 10^{-2} V^2 / H^2$  (stable conditions) are

$$w_p = \frac{2.6}{\Delta t} \left( \frac{F}{100 S H_s^2 V} \right)^{1/3} \left[ (x_i + V \Delta t)^{2/3} - x_i^{2/3} \right] \quad \text{when } V > V_s \quad (241)$$

or

$$w_p = \frac{5.3}{\Delta t} \left( \frac{10 H_s}{V_s} \right)^{-2/3} \left( \frac{F}{S^{3/2}} \right)^{1/4} \left[ (t + \Delta t)^{2/3} - t^{2/3} \right] \quad \text{when } V \leq V_s \quad (242)$$

where  $H_s$  is stack height,  $V$  is horizontal wind speed, and  $V_s$  is critical wind speed separating 'calm' from 'not calm' conditions for stable conditions and is defined by

$$V_s = 0.14 F^{1/4} S^{1/8} \quad (243)$$

Note that at low wind speeds, travel time is used to determine plume rise instead of travel distance. Maximum plume rise under stable conditions is achieved when

$$t = 10 \frac{H_s}{V_s} \quad (244)$$

A similar approach is used in the following equations when  $S > 4.2 \times 10^{-2} V^2 / H^2$  (neutral and unstable conditions)

$$w_p = \frac{1.6 F^{1/3}}{V \Delta t} \left[ (x_i + V \Delta t)^{2/3} - x_i^{2/3} \right] \quad \text{when } V > V_n \quad (245)$$

or

$$w_p = \frac{1.6 F^{1/3}}{V_n \Delta t} \left[ (x_i + V \Delta t)^{2/3} - x_i^{2/3} \right] \quad \text{when } V \leq V_n \quad (246)$$

where  $V_n$  is critical wind speed separating 'calm' from 'not calm' conditions for neutral or unstable conditions and is defined by

$$V_n = \frac{1.6F^{1/3}}{Z_{\max}} (10H_s)^{2/3} \quad (247)$$

where  $Z_{\max}$  is the maximum plume rise allowed during light winds and neutral or unstable conditions. It is set to 3000 m to ensure that all parameters remain finite, but that the plume does not impinge at ground level.

### 8.4.3 Puff Splitting Scheme.

As the puffs grows, the local representation of the turbulence and velocity fields using puff centroid location becomes increasingly inaccurate. When the meteorological fields are inhomogeneous, the accuracy of the calculation can only be maintained by splitting puffs into smaller components which can sample the variations in the meteorology explicitly. Puff splitting scheme is implemented in such a way that when the growth of a puff extends either vertically or horizontally over one cell area of OMEGA model, then the puff is divided into two or more puffs in which the sum of their masses equals the mass of the initial puff.

The horizontal growth of a puff continues until ratio of the puff radius,  $R$ , to the grid spacing,  $G$ , is greater than 1. At this point the puff is divided into four new puffs, each with 0.25 of the initial mass. The new positions are orthogonal and equidistant from the old position by  $0.5 R$ , with a  $\sigma_h$  value of 0.5 of the initial value but with the same  $\sigma_z$  values.

In the vertical dimension this process can be described as follows. When the growth of the puff is large enough to fully encompass at least two vertical layers, then the puff is divided into two puffs of mass. The new puff centroids have the same horizontal position but have an elevation equal to the layer midpoint. The  $\sigma_h$  value remains the same but the new  $\sigma_z$  value is proportional exactly the same way as the mass.

### 8.4.4 Puff Merging and Purging Scheme.

The key element to the practical application is the elimination of duplicate puffs. The generation of new puffs, especially due to vertical diffusion can quickly overwhelm even the fastest and largest computers.

Therefore, overlapping puffs with Gaussian concentration distributions is merged when they are separated by about  $\sigma_h$  or less. This reduces the number of puffs used in probabilistic puff model. Every ten minutes all adjacent puffs are checked to see if puff centroids are within  $\sigma_h$  of each other. If so, the material from both is merged into a single puff. The centroid of the merged puff is assigned new coordinates and  $\sigma_h$  values that are averages of those in the original puffs.

Puffs are also removed from further considerations when the puff centroid point is outside of the modeling domain. This approach should cause no problems within the area of interest, except when a wind reversal brings puffs back into the modeling domain.

#### 8.4.5 Concentration Calculation.

The concentration within each puff is distributed in space according to a Gaussian function whose  $\sigma_x$ ,  $\sigma_y$ , and  $\sigma_z$  values increase with travel time or distance. Knowledge of puff location, the material in it, and its geometrical dimensions allows concentration to be determined anywhere by summing contributions from each puff. Local concentration values are receptor oriented and based on summing contributions from each puff using generalized Gaussian distribution with reflection terms from the ground and the mixing layer height

$$C(x, y, z, t) = \frac{Q}{(2\pi)^{2/3} \sigma_x \sigma_y \sigma_z} \exp\left[-\frac{(x-x_c)^2}{2\sigma_x^2}\right] \exp\left[-\frac{(y-y_c)^2}{2\sigma_y^2}\right] \times \left\{ \exp\left[-\frac{(z-z_c)^2}{2\sigma_z^2}\right] + f_g \exp\left[-\frac{(z+z_c)^2}{2\sigma_z^2}\right] + f_m \exp\left[-\frac{(2z_m - z - z_c)^2}{2\sigma_z^2}\right] \right\} \quad (248)$$

where  $C$  is the concentration,  $Q$  is the mass of puff,  $x, y, z$  are the position of receptor,  $x_c, y_c, z_c$  are the position of the puff center point,  $f_g$  is the fraction of cloud mass reaching the ground reflected back into cloud mass,  $f_m$  is the fraction of cloud mass reaching the mixing layer reflected back into the cloud,  $z_m$  is the mixed layer height.

#### 8.4.6 Surface Dosage.

The integrated surface dosage can then be defined as

$$\chi(x, y, t) = \int_0^t C(x, y, 0, t') dt' \quad (249)$$

This quantity is accumulated on a stationary receptor network.

#### 8.4.7 Calculation of Concentration Fluctuation.

Time series of all atmospheric boundary layer variables exhibit turbulent fluctuations and air pollutant concentrations are no exception. Observations have shown that concentration fluctuations are sometimes at least as large as the mean. Therefore, there is a growing need for methods of predicting fluctuations of concentration. For example, accidentally released some gases are toxic and their flammability is determined by short term concentration levels (e.g., the accidental release of MIC gas during Bhopal gas accident). In this emergency case, the concentration fluctuations are crucial to predict. On the other hand, the magnitude of turbulent fluctuations of concentration determines the uncertainty in air quality models. Uncertainty calculation is also important in most emergency hazard predictions.

Wilson et al. (1982a, b) were concerned with simulating concentration fluctuations from a continuous source observed in a wind tunnel and proposed a simplified empirical model based on the standard Gaussian formula. This model is used in probabilistic puff model for concentration fluctuations

$$\sigma_c^2 = \left( \frac{q}{bUd_y d_z} \right)^2 G \left( \frac{y}{d_y} \right) F \left( \frac{z}{d_z} \right) \quad (250)$$

where  $q$  is the effective variance source strength,  $b$  is a constant determined by the form of the vertical distribution,  $U$  is the effective transport speed,  $d_y$  and  $d_z$  are lateral and vertical plume half-widths, and  $G$  and  $F$  are dimensionless functions

$$G\left(\frac{y}{d_y}\right) = \frac{1}{2} \exp\left[-A\left(\frac{y}{d_y} - \beta\right)^2\right] + \frac{1}{2} \exp\left[-A\left(\frac{y}{d_y} + \beta\right)^2\right] \quad (251)$$

$$F\left(\frac{z}{d_z}\right) = \exp\left[-A\left(\frac{z}{d_z} - \beta\right)^2\right] - \alpha \exp\left[-A\left(\frac{z}{d_z} + \beta\right)^2\right] \quad (252)$$

where the source location parameter,  $\beta$ , and the sink strength,  $\alpha$ , are both assumed to equal 0.6 based on analyses of the wind tunnel data, and the constant  $A = 0.693$ .

## 8.5 Lagrangian Model Modes of Operation.

### 8.5.1 Tracer Mode.

Operating in tracer mode, the ADM Lagrangian model allows the user to inject non-buoyant, passive particles into the evolving OMEGA wind field. The user has the option to select the number of injection points, their locations and altitudes, and the frequency of particle injection. Additional input fields exist for particle diameter, density, and mass which allows the user to physically-characterize massive particles.

Tracer mode particles are assumed to represent discrete mass elements or the centroids of diffusing puffs. Particles are removed from the computational domain when they cross the top or lateral boundaries. If they impact the surface, massless particles are allowed to perfectly reflect (*i.e.* no surface deposition); massive particles remain on the surface.

### 8.5.2 Monitor Mode.

Monitor mode is designed to provide a monitoring capability over time at multiple locations within the OMEGA domain when an accidental release or spill is expected but the precise release location and/or time and/or altitude is not known *a priori*. The particle output from these monitor station locations can then be postprocessed to determine a quick, first-order estimate of the expected atmospheric hazard. When combined with air sampling data, monitor mode can also be used to determine the most probable geographic source area from which particles have advected. In either application, the user has the option to select the number, location, and particle injection interval of the monitor stations. The characteristics of the particles (particle type, diameter, and release altitude, etc.) that monitor mode injects into the wind field can also be specified.

## Section 9

### Dynamic Grid Adaptation

#### 9.1 Introduction.

The accurate solution of any complex computational problem depends on fine spatial discretization of the computational domain. The degree of grid refinement is usually constrained by CPU restrictions and by run-time expectations. In atmospheric flow simulations, a large amount of CPU time is required by planetary boundary layer physics, cloud microphysics and radiation transfer calculations. For real-time flow predictions, optimizing the degree of grid refinement, given the CPU constraint becomes crucial. Use of unstructured grids simplifies this problem by adapting to regions where a high degree of resolution is required, such as shorelines and areas of large terrain gradients (see Section 5). Adapting the grid dynamically can make further improvement in solution accuracy and run-time. Solution-adaptive grid generation schemes have been widely used in aerospace applications with successful results, e.g. Lottati and Eidelman [1994] and Baum and Lohner [1989] and Baum et. al. [1993] have applied dynamic grid-generation for simulating flows over aircraft, tracking shock waves, and in simulating fluid-structure interactions. Dietachmayer and Droegemeier [1992] and Fiedler et. al. [1998], have approached the use of dynamic grid adaptation for atmospheric flows using structured grids. Their methodologies have been restricted to idealized problems so far and are not suitable for real atmospheric flow simulations, which can include complicated terrain features.

Structured grids are not suitable for dynamic adaptation, because the grid-generation requires a high degree of user-interaction and user-expertise. It is unrealistic to have a completely automated grid-generation code for real-time predictions. Some atmospheric models such as the Regional Atmospheric Modeling System (RAMS) have employed a different approach to overcome the shortcomings of structured grids. In RAMS, for example, there is an option of a finer moving grid within a larger coarser domain. One disadvantage of this methodology lies in the fact that the trajectory of the moving grid has to be pre-defined and therefore cannot be used for prediction. The other disadvantage of moving grids is in errors introduced due to interactions between the coarse and finer nested grids. Using unstructured grids eliminates these disadvantages. The main advantage of unstructured grids is the ease with which dynamic/solution adaptation can be implemented. There is no longer a need for involved user-expertise/interaction for creating topologies of complicated terrain features. The whole procedure can be fully automated. Automation of the process is not only highly desirable but can also be required in operational settings. The unstructured grid has a smooth and continuous transition from coarse to fine regions within the whole domain, thus eliminating interpolation errors, which occur due to interactions of different nests in structured grids.

OMEGA is the only operational atmospheric flow model based on an unstructured grid, and fully exploits the advantages and flexibility of unstructured grids. It can adapt dynamically to different criteria such as particle location and velocity deformation, etc. This capability is crucial in responding to emergency scenarios such as release of hazardous materials. OMEGA with its dynamic adaptation capability has a unique advantage over other atmospheric flow models in providing accurate solutions quickly in an operational setting.

## 9.2 Methodology.

If OMEGA is run with dynamic grid adaptation option, then additional memory needs to be allocated for all the arrays. The user needs to define the upper bounds of the size of arrays for memory allocation. The user also specifies the adaptation criteria (e.g. particle locations or velocity deformation, etc.) and time for invoking adaptation cycle (e.g., every one or two hours). At the time of adaptation OMEGA checks if the specified criteria is met. The cells are tagged for refinement or coarsening accordingly. The processes of grid refinement and coarsening are discussed in Section 5. Physical variables, which are cell-centered, are interpolated to vertices before each adaptation cycle using the pseudo-Laplacian weighted averaging scheme. As new cells are created or removed locally a simple linear interpolation is done to assign values to new vertices and cell centers. All the diagnostic variables are calculated for new cells, the particle locations array is updated, underlying terrain is updated, and the mesh is re-masked to calculate new time steps for the time-splitting scheme. At the beginning of a simulation the minimum elevation is saved. As the grid is refined or coarsened, no cell is allowed to have an elevation lower than the initial minimum elevation value. This is to insure that no extrapolation is done. The original base state variables are also saved and as new cells are created, base state profiles are generated for these cells using the initial base state. The whole procedure requires only a few user inputs at the beginning of the simulation and after the initial inputs, it is completely automated.

## 9.3 Adaptation Criteria.

Setting the right criteria for adaptation is very important. If the adaptation criteria are particle locations, then it becomes a simple step of locating the particles in terms of cell id's and then tagging those cells for refinement. This method can become costly if there are multiple release sources and the frequency of particle release in time is very high. The alternative method is adapting to the flow itself. This is not as straightforward as tagging the cells for particle locations. Atmospheric flows are almost always turbulent and highly stratified in the vertical. The gradients are weaker (as compared to problems arising in aerodynamics, e.g., tracking shock waves) and harder to detect. One advantage in simulating atmospheric flows, however, is the large temporal scale of the simulation (usually 12 hours to 48 hours). Therefore, even if an event is missed at first, the chances of capturing it at a later time are higher. Different adaptation criteria used by OMEGA are discussed below:

### 9.3.1 Particles.

OMEGA was conceived primarily as a hazard prediction model. It already has the unique feature of an embedded atmospheric dispersion model. The latest version of OMEGA also has the capability of adapting its grid to particle locations. OMEGA can provide high fidelity solutions in the regions of a particle plume by refining the grid around the particle locations. Coarsening the grid where high resolution is not required (e.g., areas from which the plume has already passed), further optimizes the problem. The criteria for adaptation is set by defining a Gaussian function around each particle. The region close to particles therefore gets higher weighting and is tagged for refinement. Areas, which do not have particles and consist of relatively flat terrain are tagged for coarsening. Considerable reduction in CPU time is achieved by providing higher resolution only when and where it is needed.

### 9.3.2 Velocity Deformation.

Deformation is an important factor in the processes of frontogenesis and frontolysis. Deformation is defined as:

$$DEF = \sqrt{\left(\frac{\partial u}{\partial x} - \frac{\partial v}{\partial y}\right)^2 + \left(\frac{\partial u}{\partial y} + \frac{\partial v}{\partial x}\right)^2} \quad (253)$$

Where,

$\left(\frac{\partial u}{\partial x} - \frac{\partial v}{\partial y}\right)$  is the *stretching deformation*

and,

$\left(\frac{\partial u}{\partial y} + \frac{\partial v}{\partial x}\right)$  is the *shearing deformation*.

OMEGA has the capability to adapt its grid in regions of highly deforming flows. Averaging the values of deformation in each cell over the first ten levels sets the criteria for adaptation. The maximum value of these averages is calculated which is used to normalize all the average values. In this way regions of critical flow development are tagged for refinement.

### 9.3.3 Adaptation to Other Physical Quantities.

OMEGA can also adapt its grid to other physical quantities such as absolute vorticity and the potential temperature gradient. Work is in progress to define criteria, which is a weighted set of different meteorological variables. An important step in this direction would be to create a database of responses for different scenarios and use neural networks/artificial intelligence to identify and set adaptation criteria.

### 9.4 Pseudo-Laplacian Interpolation.

During the dynamic adaptation, as new cells are generated, all the physical variables are interpolated using a pseudo-Laplacian weighted averaging scheme suggested by Holmes and Connell [1989].

Rausch[1992] compared the pseudo-Laplacian averaging scheme with area-weighted and reciprocal distance schemes and found that the pseudo-Laplacian scheme, although more expensive, computationally, yields more accurate results.

The pseudo-Laplacian for a vertex can be defined as,

$$L(\varphi)_o = \sum_{i=1}^n w_i (\varphi_i - \varphi_o) , \quad (254)$$

stability requires the weights,  $w_i$  to be as close to unity as possible,

$$w_i = 1 + \Delta w_i, \quad (255)$$

Since, linear functions have zero Laplacians, we can write,

$$L(x)_o = \sum_{i=1}^n w_i (x_i - x_o) = 0, \quad (256)$$

and

$$L(y)_o = \sum_{i=1}^n w_i (y_i - y_o) = 0, \quad (257)$$

Defining the cost function, C as

$$C = \sum_{i=1}^n (\Delta w_i)^2. \quad (258)$$

We now have an optimization problem of minimizing the cost function given the constraints in Equations (256) and (257).

Using Lagrange multipliers we can write,

$$\Delta w_i = \lambda_x (x_i - x_o) + \lambda_y (y_i - y_o), \quad (259)$$

where,

$$\lambda_x = \frac{(I_{xy}R_y - I_{yy}R_x)}{(I_{xx}I_{yy} - I_{xy}^2)}; \quad \lambda_y = \frac{(I_{xy}R_x - I_{xx}R_y)}{(I_{xx}I_{yy} - I_{xy}^2)};$$

and

$$\begin{aligned} R_x &= \sum_{i=1}^n (x_i - x_o); & R_y &= \sum_{i=1}^n (y_i - y_o); \\ I_{xx} &= \sum_{i=1}^n (x_i - x_o)^2; & I_{yy} &= \sum_{i=1}^n (y_i - y_o)^2; \\ I_{xy} &= \sum_{i=1}^n (x_i - x_o)(y_i - y_o). \end{aligned}$$

## 9.5 Adaptation to Atmospheric Dispersion.

Two simulations are compared to illustrate the advantage of dynamic grid adaptation vs. global refinement.

### Case A: Global Refinement

Simulation domain extended from -98.65 degrees to -95.65 degrees in the west-east direction and from 41.0 degrees to 45.0 degrees in the north-south direction, covering parts of Nebraska, South Dakota, Iowa and Minnesota. A variable grid resolution of 5 km to 15 km was specified. Thirty (30) second resolution terrain and 5 minute resolution shoreline data was used. The final grid had 2335 cells and 30 vertical levels, for a total of 70,050 cells (Figure 29, left). In the vertical a stretched grid was used. The first level near earth's surface had a thickness of 15 meters and further levels were generated using a stretch ratio of 1.15. A particle source was defined in the southwest corner of the domain with an emission rate of 5 particles per minute. The simulation was initialized using the U.S. Navy's NOGAPS gridded data. The simulation was run for a real-time prediction at 15 hours after initialization.



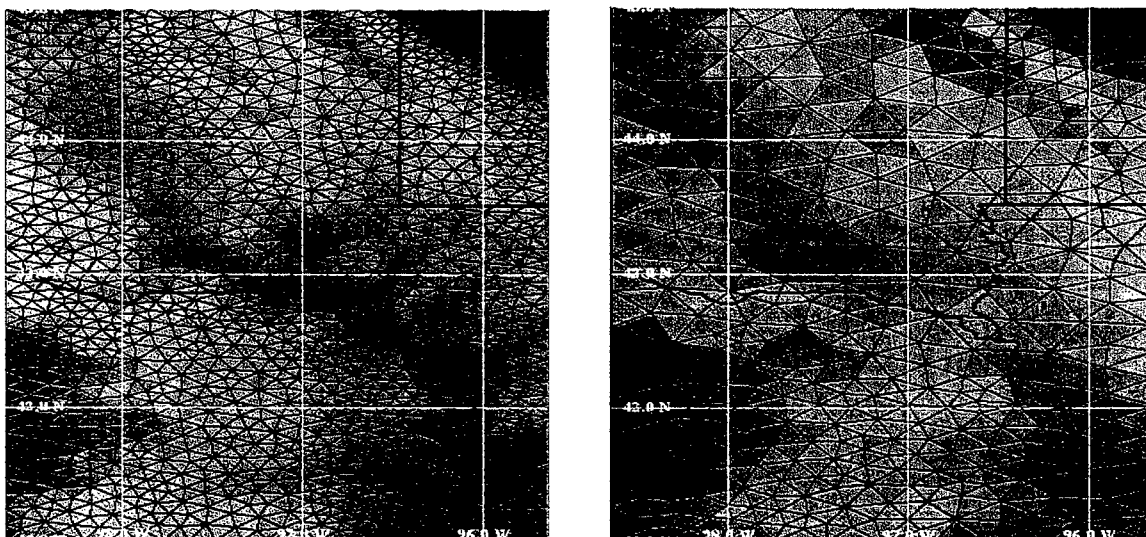


Figure 29. Computational grid for Case A simulation (left) and Case B simulation (right).

### Case B: Dynamic Adaptation

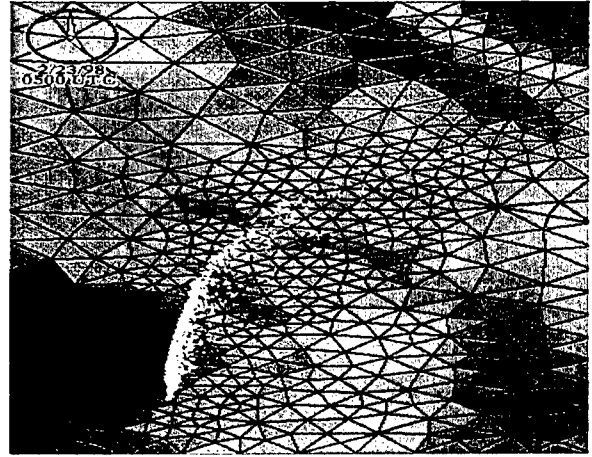
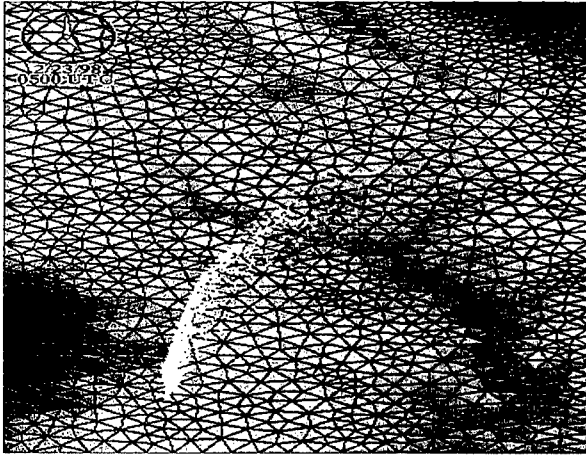
All the parameters in this run were identical to Case A simulation, except the initial grid size. The starting grid had 582 cells in the horizontal (Figure 29, right). In this case a variable resolution of 10 km to 36 km was prescribed in the initial grid generated. The adaptation criteria was set to particle locations.

A refinement cycle was invoked after every hour of simulation time. Cells were tagged by defining a Gaussian function around the particles. Tagged cells were refined and all physical fields were interpolated at each adaptation cycle. A coarsening cycle was invoked after every three hours to remove triangles from areas where higher resolution was not needed. This was done by identifying the cells, which did not contain particles and were in the regions which were relatively flat and then deleting them (Figures 29 and 30). The final grid after 15 hours (Figure 30) into the simulation had 1162 cells. The edge lengths varied from 6.3 to 36.7 km.

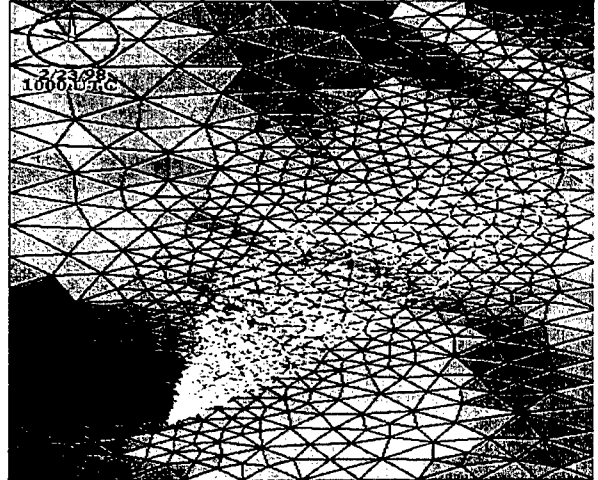
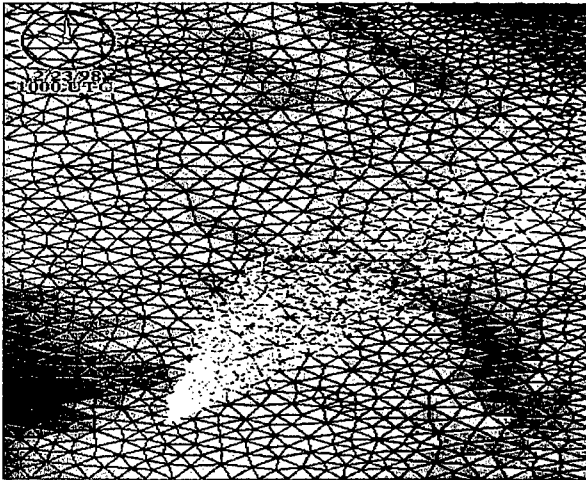
Use of dynamic grid-adaptation resulted in more than 40 percent reduction in CPU time and produced similar results compared to global refinement. This example clearly demonstrates the inherent advantages in using unstructured grids. The simulation required only the initial user inputs (adaptation criteria: particle locations, time of refinement: every 1 hour, time of coarsening: every three hours, maximum bounds for arrays: 2.5 times the initial grid), after which the whole process was seamless and automated.

### 9.6 Effects of Improving the Underlying Terrain.

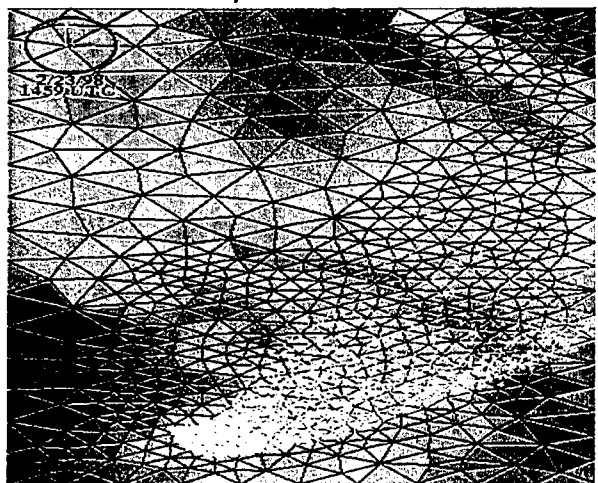
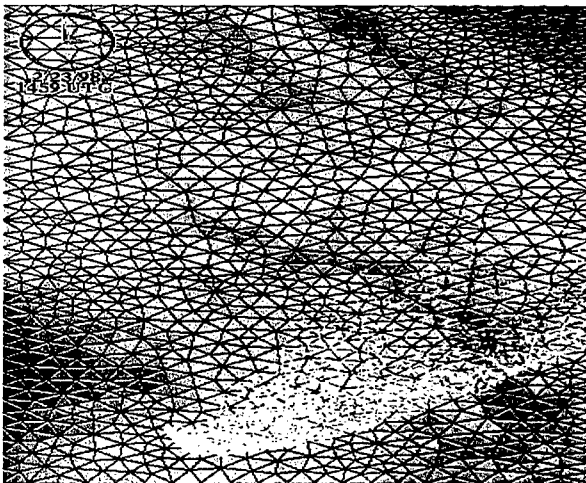
In each adaptation cycle OMEGA has the option of updating the underlying terrain. The refinement cycle resolves finer topographic features, which can drastically improve the solution. In the following section three simulations of an idealized case are discussed to examine the effect of growing terrain. By introducing an obstacle in uniform cross flow, dynamic pressure builds up around the obstacle and is deflected by the obstacle. The perturbation introduced eventually dissipates and the flow reaches steady state. Figure 31 shows the time evolution of pressure perturbation field, as the height of the mountain is



(a) 5 hours



(b) 10 hours



(c) 15 hours.

Figure 30. Particle locations for Case A simulation (left) and Case B simulation (right).

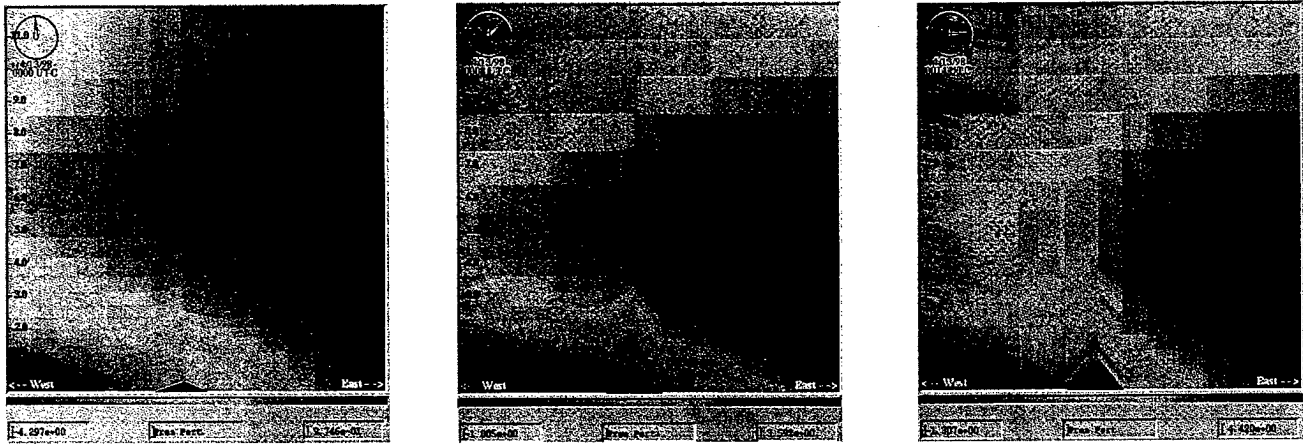


Figure 31. Time evolution of pressure perturbation field for the growing mountain case. Vertical cross sections at initialization (left), 8 minutes (center), and 15 minutes (right).

increased from 350m to 1000m. Although this is a physical phenomenon, it *can* create noise in the solution. Our results so far have shown that these perturbations do not effect the solution in any adverse manner, or they dissipate quickly (on the order of 15-30 minutes).

Figure 32 (left) shows the pressure perturbation field for the static case. In this case the mountain was at a constant height of 1000m AGL through out the simulation. Figure 32 (right) shows the pressure perturbation field for the dynamic case. In this simulation, the mountain was initially 300m high and was raised to 1000m AGL after +8 minutes into the simulation.

The effect of improving the resolution of underlying terrain, on the other hand, can be drastic. A simple scenario is shown in Figure 33. A single mountain lies in the middle of the domain. All the cells surrounding it are flat. There is a uniform southeasterly flow. Particle locations shown in the figures correspond to +3 hours into the simulation. The only difference in the three simulations is the height of

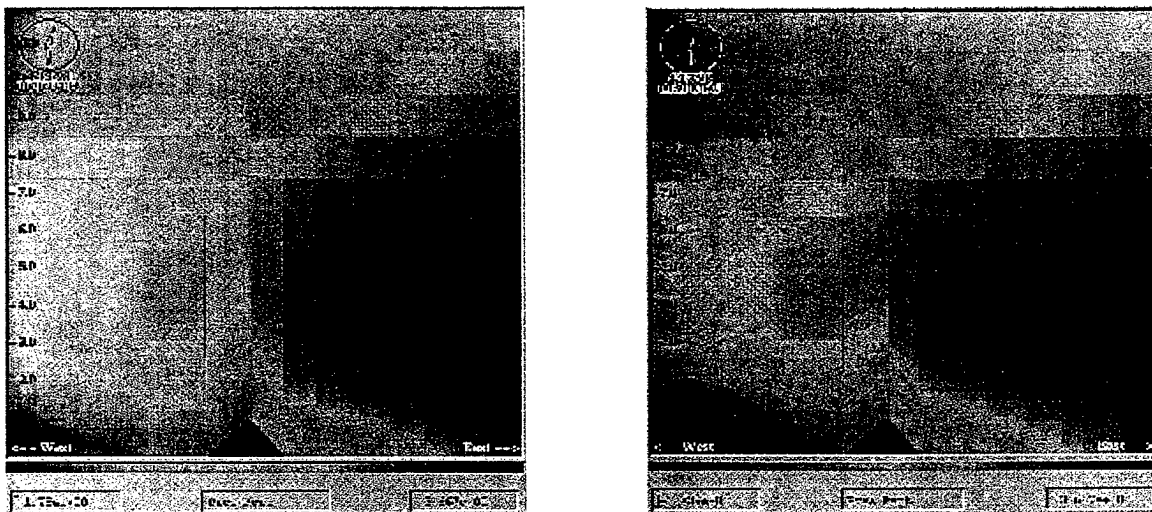


Figure 32. Pressure perturbation fields for 1000m static mountain case (left) and 350m-1000m growing mountain case (right) after 30 minutes into the simulation.

the mountain. In Figure 33 (left), the height of the mountain was held constant at 350m AGL. In Figure 33 (center), the height of the mountain was held constant at 1000m AGL. In Figure 33 (right), the height of the mountain was initially 350m AGL and was raised to 1000m AGL after +8 minutes into the simulation.

When applied to a full-scale operational run, dynamic adaptation can yield more accurate results by providing resolution when and where it is needed. The following figures are for two simulations run for the Four Corners area, which is characterized by complex terrain features. The domain and the initial conditions for both simulations were identical. The domain extends from -110.55 to -107.61 degrees in the west-east direction and 35.61 to 38.61 degrees in the north-south direction. The initial grid had 437 cells in the first horizontal layer and thirty vertical layers for a total of 13,110 cells. The edge lengths vary from 6.81 km to 42.18 km. In the first simulation (Case A), the grid was not refined during the simulation. Figure 34 (left) shows the particle locations after +12 hours into the simulation. In the second simulation (Case B), the grid was adapted dynamically during the simulation. The adaptation criteria was set to particle locations. Figure 34 (right) shows the particle locations for Case B simulation after +12 hours. An adaptation cycle was invoked after every two hours for this simulation. The final grid had 891 cells in the horizontal layer with 30 vertical layers for a total of 26,730 cells. By resolving finer terrain features as the plume evolved, a more accurate representation of the flow field was achieved.

### 9.7 Adaptation to Velocity Deformation.

OMEGA is primarily a hazard prediction model and using particle locations as the adaptation criteria meets the mission goal. It is desirable, however, to use other physical variables (depending on different situations) as adaptation criteria. OMEGA has been configured to adapt to a series of physical variables such as velocity deformation and potential temperature gradient, etc.

A simulation was run with velocity deformation as the adaptation criteria for southwest U.S. The computational domain extended from -112.0 degrees to -96.0 degrees in the west-east direction and 30.0 degrees to 41.0 degrees in the north-south direction. Terrain data with 30 second resolution and land/water data with 5 minutes resolution was used. The initial grid had 2283 cells in the horizontal and



Figure 33. Particle locations for 350m static mountain simulation (left); 1000m static simulation (center); and 350-1000m growing mountain simulation (right).

thirty vertical levels (Figure 35 left). The vertical grid was stretched. The first vertical level was 15 meters high and the remaining levels were generated using a stretch ratio of 1.15. The edge lengths varied from 20.8 km to 68.9 km. The domain covered parts of Texas, Arizona, New Mexico, Oklahoma, Utah, Colorado and Kansas. The simulation was initialized using U.S. Navy's gridded NOGAPS data for 00Z on June 8, 1998. The date was chosen for high frontal activity over parts of Texas, Colorado and Kansas. Figure 35 (right) shows the initial sea level pressure in mb. Color scale is from 995.5 mb to 1017.0 mb, with blue color representing low values and red color representing high values.

This simulation was run for 12 hours. An adaptation cycle was invoked after every two hours. Cells with relatively large values of total deformation were tagged for refinement. Figure 36 (left) shows the final grid at 12 hours into the simulation. The final grid had 3257 cells in the horizontal. As the front moved towards the east over Texas and Oklahoma, the grid dynamically adapted to regions of high activity. The simulation was able to capture the low pressure system developing over northern Texas and Colorado (Figure 36, right).

Work is in progress to develop new adaptation criteria, as generic weighted functions of different physical variables. This way the different complex physical processes occurring in the Earth's atmosphere would be taken into account. Implementation of dynamic adaptation into OMEGA model is a major advancement in numerical modeling of the atmosphere. It is the first step, however, and there is need for further improvements and optimization of the techniques described in this section.

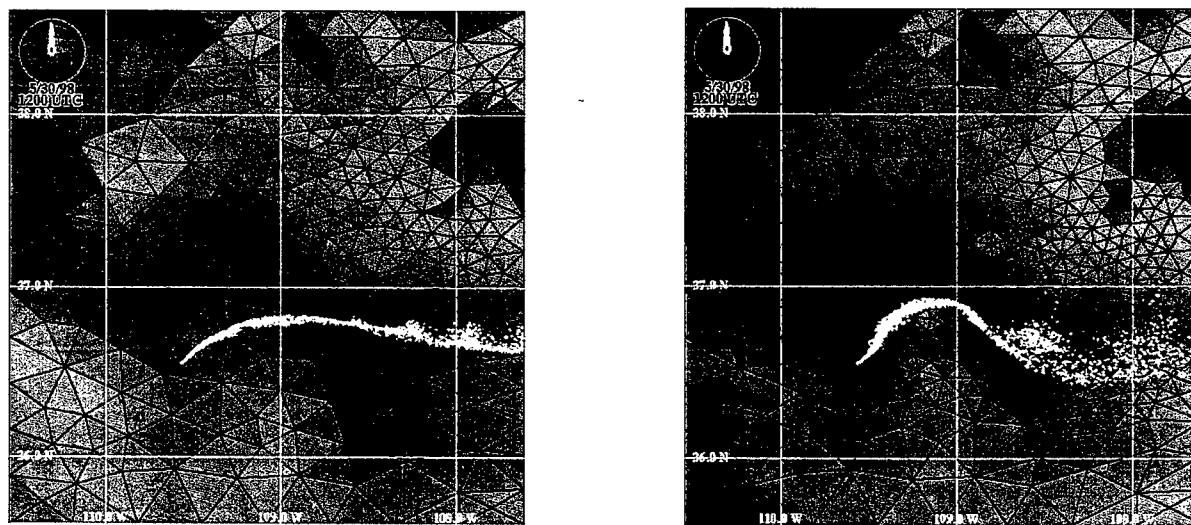


Figure 34. Simulations for the Four Corners, USA. Static (Case A) simulation results after 12 hours into the simulation are shown in the left panel and dynamically adapting simulation (Case B) results after 12 hours into the simulation are shown in the right panel.

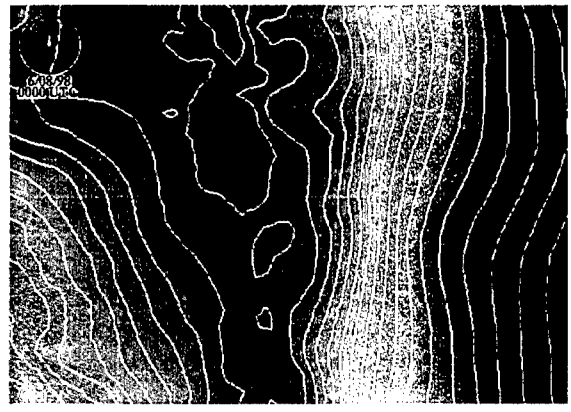
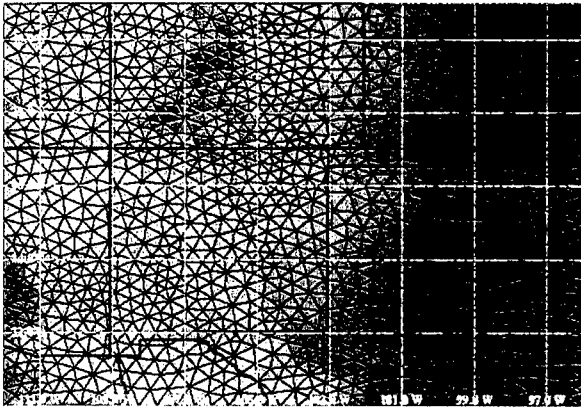


Figure 35. Adaptation to velocity deformation. Initial grid (left) and sea level pressure (right) at the start of the simulation.

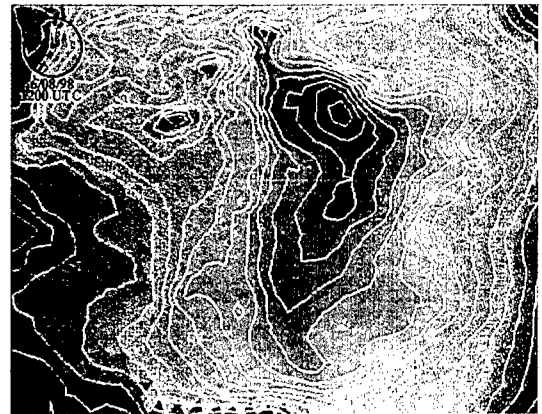
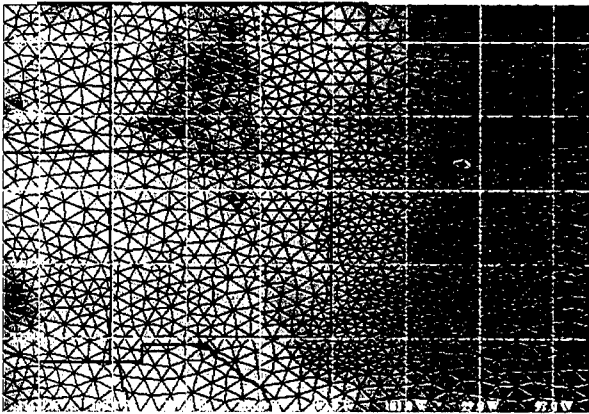


Figure 36. Adaptation to velocity deformation. Final grid (left) and sea level pressure (right) after 12 hours into the simulation.

## Section 10

### Parallelization

OMEGA is CPU bound. Normally less than 1% of the CPU is used for I/O and memory management. The computational intensity of OMEGA has been evaluated by the Jumpview profiling system. Jumpview determined that OMEGA is dominated by vector operations, which are inherently faster than scalar operations; thus, good execution speeds are being achieved. OMEGA exhibits good, but not outstanding, vectorization for memory references, primarily due to the indirect addressing inherent in an unstructured grid model. OMEGA also showed a computational intensity ratio of flops to memory references of 0.99.

The optimization level used in OMEGA is good. It maximizes inlining and vectorization. Inlining is a technique to reduce CPU associated with subroutine/function calls. It can cost up to 150 clock cycles to call a single argument subprogram. Vectorization allows a single operation to be performed on "vectors" of operands instead of sequentially for each operand. With the optimization level used in OMEGA, the overall computational speed achieved is slightly over 40 Mflops.

Parallelization is a state-of-the-art technique to boost computational speedup by multiprocessing. However, unstructured grid models tend to demand significantly more synchronization and geometry mapping overheads in their parallelization algorithm. Figure 37 shows a speedup projection of OMEGA by a power Fortran automatic code-parallelization compiler in terms of factor speedup versus processors. The two major reasons for the rather fast diminishing return: (1) many non-contiguous parallelized segments, and (2) large idle time.

The execution chronology histogram on top of Figure 37 shows that the OMEGA code is translated by the power Fortran into many parallelized segments (checkered) and unparallelized segments (striped) intermittently interrupting each other. The unparallelized segments represents synchronization bottle necks. Another major overhead incurred is inter-processor communication as shown in the short checkered bars where the gain in parallelization have been defeated by the expensive cost of message passing.

To overcome (1) and (2) simultaneously, manual parallelization with a standard message passing interface (MPI) is a promising approach. The functionality of MPI's allows:

- (a) Parallelization in an overarching manner in the OMEGA time advancement loop, making message passing minimal
- (b) Pin pointed solutions to the idle time, or the imbalance load problem, such as techniques for accounting the time-masked subcycling and dynamic domain-decomposition, can be incorporated.
- (c) Transportability.

Figure 38 shows the file structure being implemented.

Parallelization by domain decomposition of the model domain into contiguous sub-domains is currently under development and testing. The decomposition routine is called after dynamic adaptation. Figure 39 shows an example of the technique applied to the k10m (the Kamisayah fine mesh about observation

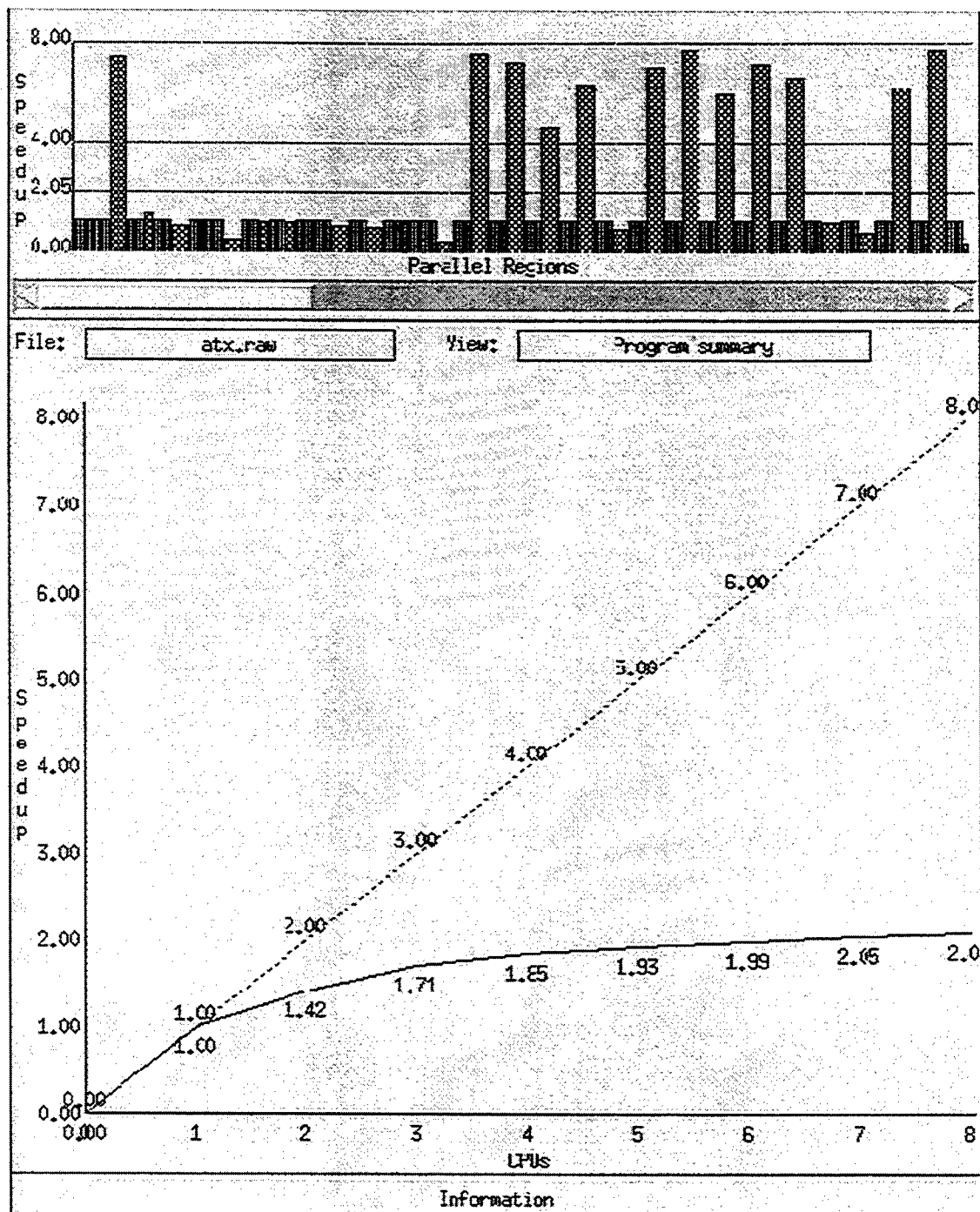


Figure 37. Speedup projection of the OMEGA code by a power Fortran compiler.

points) model domain which is consisted of 4331 cells. It shows how the k10m domain with several regions of fine resolution areas is decomposed into 9 and 16 sub-domains resulting in roughly the same number of cells in each of the sub-domains. For application on massively parallelized machines the scheme is designed to utilize over a hundred processors.

MPI command call facilitates the parallelization of the time advancement loop of the model. The test case of parallelizing the advancement loop with only the microphysics module turn on has been tested on



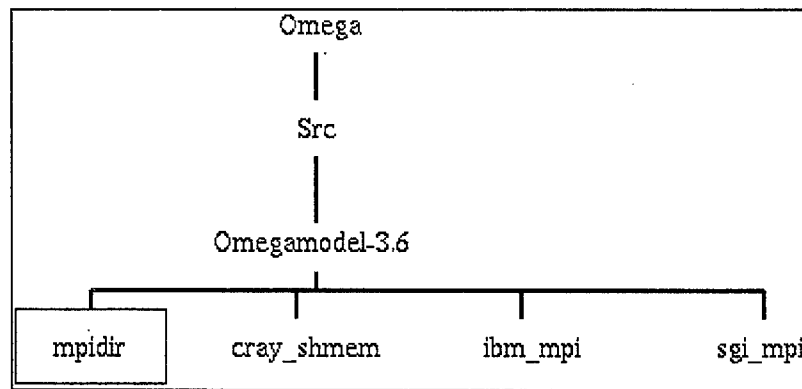
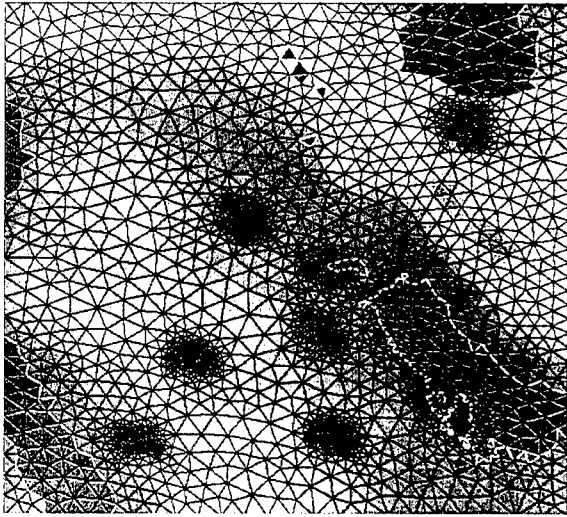


Figure 38. File structure for the parallelized OMEGA code.

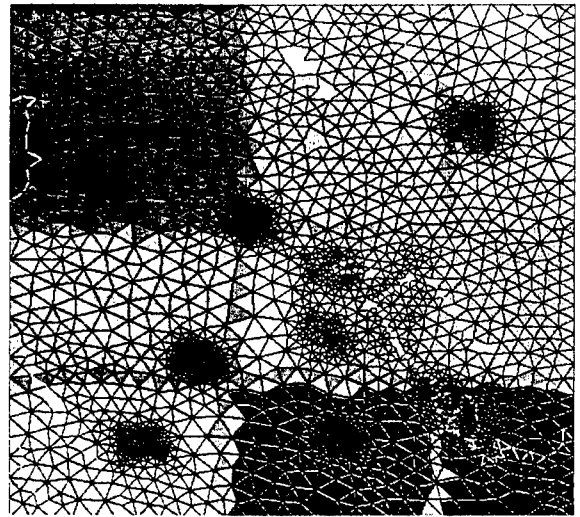
an IBM-SP2 and an Origin 2000 platforms. Figure 40 shows linear speedups are obtained on both platforms for up to 6 processors.

Sub-linear speedup however is expected for the totality of the parallelized OMEGA code. Interprocessor communication is about 10 times more intensive for many of the other modules than that of microphysics. For instance, the advection and diffusion modules are among the major interprocessor communication overhead consumers due to the evaluations of Laplacian and kinetic energy dissipation calculations which require updated neighboring cell information.

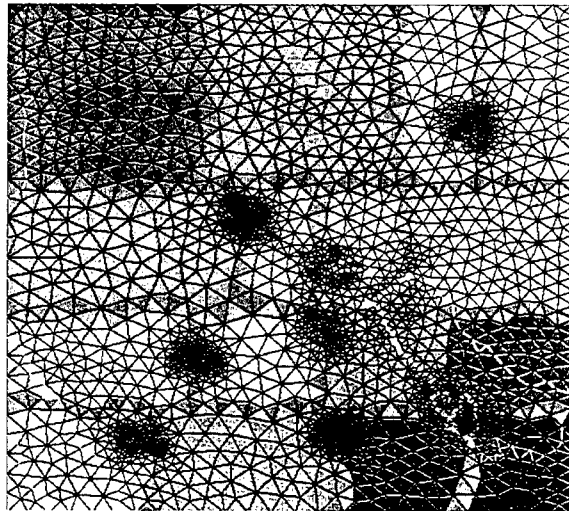
On top of the communication overheads, stacking and unstacking arrays for lumped message passing is an inherent overhead for unstructured grid models. These extra CPU costs are both related to message passing. However by far the majority of the total overhead is due to uneven load balancing among the processors. Figure 41 shows timings of 2 series of runs of a preliminary version of the parallelized OMEGA code for a test case of 1369 cells and 31 variable levels on an IBM SP2 (RS/6000) machine. The figure shows timings for the 1-time-mask and the 2-time-masks series. The 1-time-mask series means that subcycling of fine mesh cells is not accounted for, hence small time steps of 2.23 s are required. The 2-time-mask series does subcycling of the smaller cells and in so doing allows the time steps to be relaxed to 4.46 s. The latter is faster than the former for small pools of processors. However, for bigger pools of processors, the CPU time gained through the using of larger time step size is superseded by the subcycling-induced load imbalance among the processors, *i.e.*, subcycling introduces one more level of uneven threadlength across the processors.



(a) The k10m model domain topography and grid configuration.



(b) Domain decomposition of 9 sub-domains with roughly equal number of cells in each sub-domain. Also visible are the boundary cells.



(c) As in figure (b) except for 16 sub-domains.

Figure 39. The k10m model with one domain, 9 sub-domains and 16 sub-domains.

In light of the important contribution of even load balancing to overall parallelization efficiency, there exist various techniques to optimize even load balancing. Inverse cell-area weighted domain decomposition can be a good way to improve even load balancing, hence, improve the speedup performance of the 2-time-mask series of Figure 41. This is an important area of future work of the parallelized OMEGA code. For the purpose of illustration, Figure 41 shows the corresponding parallelization efficiencies of the runs in Figure 41.

Another subject of interest is the speedup performance and parallelization efficiency of the OMEGA code across different platforms. Workstations are usually more cache limited than mainframe

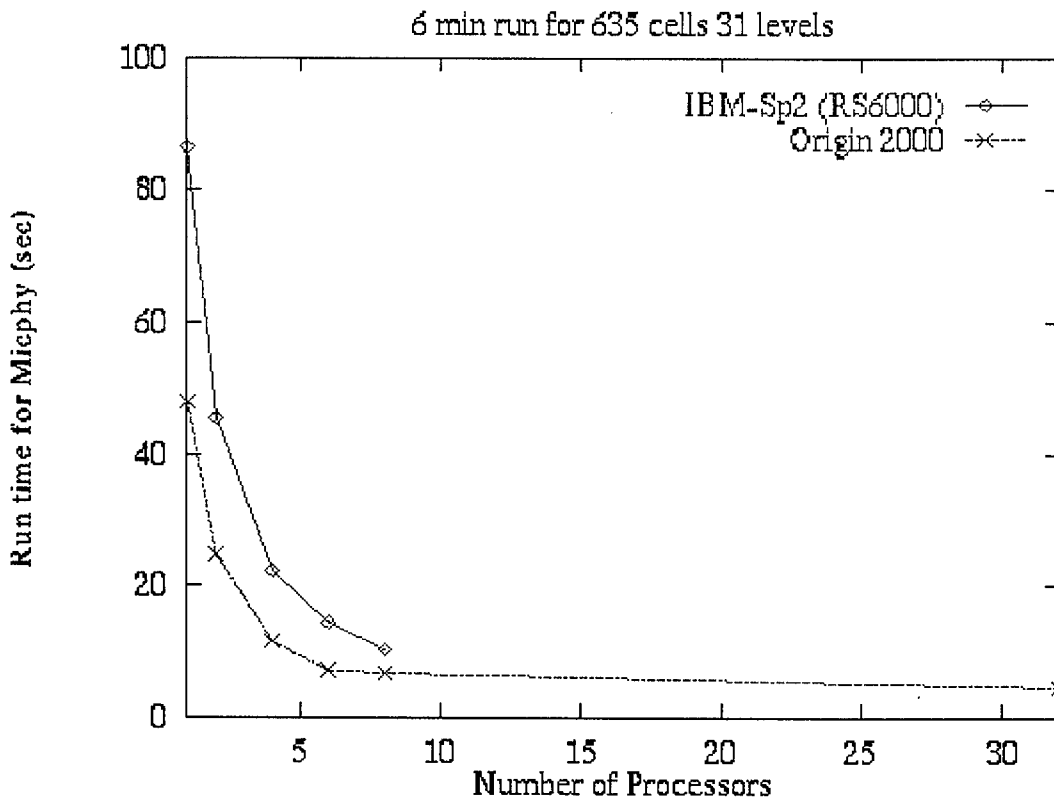


Figure 40. Run time plotted as a function of processor allocation.

computers. This affects the message passing bandwidth. An investigation of how these are dependent on the hardware has been carried out on a cluster of IBM SP2 (RS/6000) machine with 120 MHz clock speed and a cluster of SGI Origin 2000 machines with 195 MHz speed. The two platforms are not exactly comparable as their Fortran compilers are different. Figure 42, from the same run used in Figure 41, do show the evolution of speedups and parallelization efficiencies between a mainframe architecture and a workstation architecture

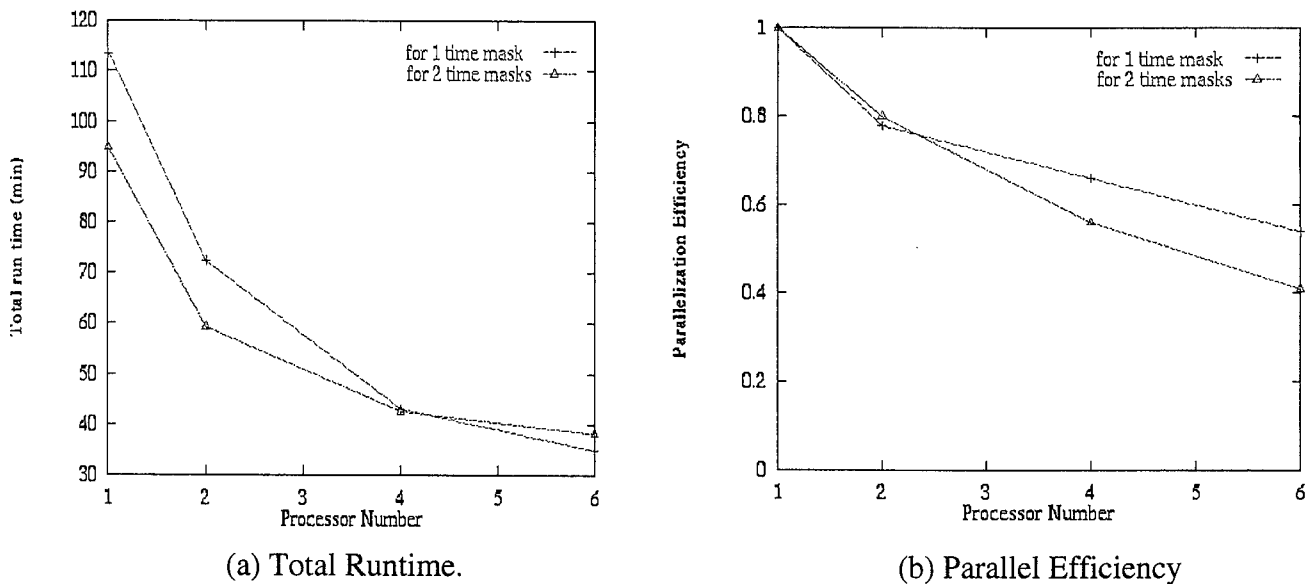
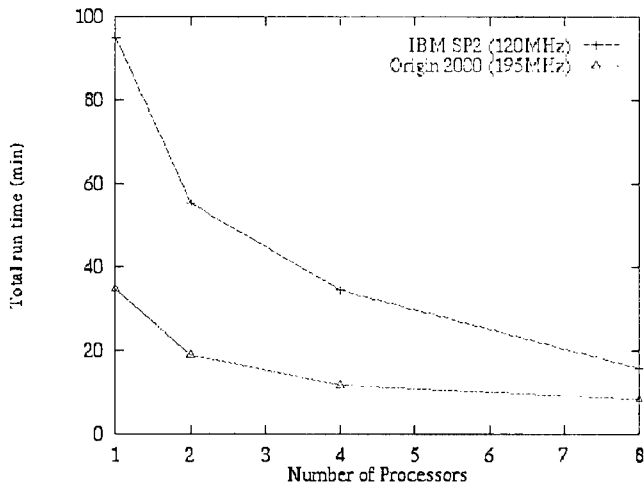
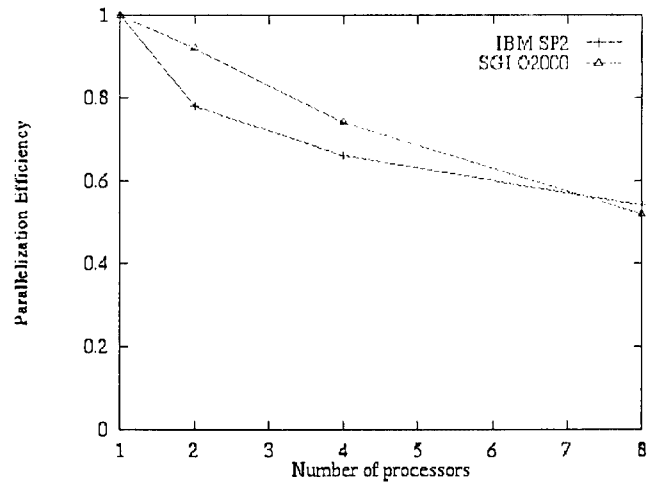


Figure 41. Run time and parallel efficiency plotted as a function of processor allocation.



(a) Total Runtime.



(b) Parallel Efficiency.

Figure 42. Runtime and parallel efficiency plotted as a function of processor allocation for a mainframe and a workstation cluster.

## Section 11

### XOMEGA Graphical User Interface

#### 11.1 Overview.

The OMEGA user interface system is designed around a "case". An OMEGA case is an encapsulation that holds all the information relevant to the simulation. A case name is four (4) characters long and serves as the name of the directory holding all the associated configuration, input, and output files. An interactive text-based shell script is used to create and name a case. The shell script can also be used to examine the status of existing cases.

The OMEGA System is composed of several distinct modules that are activated in sequence one after the another. They are linked together by the interface so that each module gets its specific input and is able to direct its output to the next module in line. When creating an OMEGA simulation the user makes choices about the geography and meteorology to be simulated. The X Window interface (XOMEGA) is the mechanism that translates those choices into input for the other modules.

After the case has been established, XOMEGA starts. It is used to control parameter settings for the other modules of OMEGA. At this stage the cursor and keyboard are used to make selections and input data. First, a domain is chosen by using the cursor to define regions on a map. The OMEGA computational grid is then generated. The specific meteorology input is chosen for use in creating the initial and boundary conditions for the simulation. The meteorological data are fit to the grid by the OMEGA preprocessor. Then the simulation is started in a background window.

#### 11.1.1 X Window Basics.

XOMEGA is an X windows client. An X widows client is an application program that issues requests to an X Display Server (user machine) to show text, buttons, and pictures in windows. These are the elements with which the user interacts to make choices about the OMEGA simulation. The mouse is used to enclose regions on a map, press buttons, and toggle switches; the keyboard is used to input text. Several additional windows will "pop up" and "pop down" during the session. These are called dialog boxes and serve to divide the input process according to the modules in OMEGA. Some warnings and errors may also appear in dialog boxes. There are a few standard X Windows conventions used in XOMEGA listed below.

These key strokes are used when dialog boxes. The current control is generally outlined in black.

TAB-	Shifts the current control down (or right) one unit.
Shift-TAB-	Shifts the current control up (or left) one unit.
Return-	Activates the current control. (button press, text input)
OK, Yes, Done-	Close the current window with affirmative status.
Cancel, No -	Close the current window with negative status.
	Cancel will clear any text data input in that window.
Help-	Invokes the OMEGA Online Reference System.
	Currently most Help buttons are insensitive.
Clear Form-	Blanks out text input boxes.
Default-	Sets all controls to the system defaults.

Menus are activated by holding down the left mouse button, moving the mouse over the menu, and dragging down. The menu items will appear below the title; releasing the mouse button on the desired item selects that item.

The menus may also be accessed via keyboard strokes. By holding down the ALT key and pressing the underlined letter in the menu name the menu will "pull down". For example, pressing ALT-f the *File* menu will come down. Once a menu is brought down in this manner, the up and down arrow keys are used to cycle through the menu's items. Pressing RETURN will activate the highlighted item. The left and right keys may be used to skip to other menus and "pull down" on them. Once the menu is down the user may release the ALT key. Each of the items on the menu also has an underlined letter. Pressing the underlined letter will activate that item.

At the top of each of the pull down portions of the menus is a thin dashed line. If the mouse button is released on this line the menu will "tear off" from the menu bar and become a separate window. This allows for semi-permanent access to the menu items. The tear off window may be closed by using the window manager's built-in means. Typically this is done by double clicking with the middle mouse button on the title of the tear off window.

Please refer to the operating system manual and window manager manual pages for more information on your particular X Window Server.

## **11.2 OMEGA Shell Script Interface.**

To invoke OMEGA, the user types "omega" at a UNIX prompt. This starts a shell script that asks a series of questions. At any time prior to launching the XOMEGA interface CTRL-C may be used to abort the program. There are several sections of the script outlined below.

### **11.2.1 Copyright Notice.**

Legal and security notices are given in this section. OMEGA is government funded therefore is freely distributable to U.S. government agencies and their contractors.

### **11.2.2 Case Selection.**

The current directory is searched and a listing of all valid OMEGA cases is displayed in tabular form (Figure 43). At this stage the user may create a new case by typing in a unique four letter case ID, or may view the details of an existing case by typing its case ID.

The resulting table gives an idea of how much of the case has been worked on. In the left column are the names of some key files OMEGA uses as the run progresses. The right column shows the status of these files, and what they indicate about this case. Figure 44 shows an example of viewing a case.

The user may continue with the current case by typing its case id. A warning message will alert him that some files will be overwritten. The user may view other cases by typing their case ID's, or the user may get a listing of the cases by simply hitting return.

```

1997-11-18 11:30:58 EST Case Selection

The following are the OMEGA cases found in:

/scratch/turner

(NOTE: Some older OMEGA cases may not appear in the list below.)

  Case   Creation Date
+-----+-----+
| aaaa | 1997-11-18 11:26:46 EST |
+-----+-----+
| zzzz | 1997-11-17 12:16:49 EST |
+-----+-----+

You may specify a four (4) character case id to create a new case,
Or
You may type one of the above case id's to examine its status.

  Select case id: █

```

Figure 43. Select case.

```

You have selected to view case: zzzz

Partial listing of /scratch/turner/zzzz :
-----
case.info      Found;  The case directory has been created.
grid.inp      Found;  The domain has been defined.
zzzz.adm      Missing; The domain has no ADM sources.
zzzz.grd      Found;  The grid has been created.
time.inp      Found;  The case has time domain defined.
met.inp       Found;  The case has some met data defined.
prep/seg1     Found;  The case has some met data.
zzzz.ini      Found;  The case has an Initialization file.
zzzz.bc00     Found;  The case has a BC 0 file.
zzzz.bc01     Found;  The case has a BC 1 file.
zzzz.i        Found;  The case has a model control file.
zzzz10000z.out Missing; The case has no analysis output file.
zzzz10000z.adm Missing; The case has no ADM output file.
zzzz10000z.bc Missing; The case has no BC output file.
-----

You may continue with this case by typing its case id (zzzz),
Or
You may specify a new four character case id to create a new case,
Or
You may type another existing case id to examine its status,
Or
You may simply hit <ENTER> to get a listing of the OMEGA cases.

  Select case id or hit <ENTER>: █

```

Figure 44. View case.

### 11.2.3 Case Creation.

After choosing a case name, a sequence of directories are created that will hold all the files associated with the case. First, the case directory itself is created, then two sub-directories are created below that. The "grid/" directory will hold input and output files used in generating the case grid. The "prep/" directory will hold files used in processing meteorology into initial and boundary conditions. In addition, some system configuration files are copied into the case directory, and a few specific environment variables are set. All of the creation in this section is automatic. However, there may be warnings about trying to re-make existing directories if the user is overwriting a case.

### 11.2.4 Launch OMEGA.

Once the initial case is set up the graphic interface to the OMEGA System begins. XOMEGA launches, and now the cursor and keyboard are used to control the system. If the user is not at the machine where OMEGA is running, the "DISPLAY" environment variable must be set to the current screen.

## 11.3 XOMEGA.

The XOMEGA application window has four main sections: the Menu Bar, the Operations Column, the Status Message Area, and the Drawing Area. Each section has a different purpose and features. The Menu Bar spans the top of XOMEGA window and allows for intermediate and advanced use. The Operations Column is the group of buttons at left and is for basic use. Status Messages are displayed in a large text box at the bottom. The Drawing Area displays graphics and user selections. Each section of the interface is described below. Figure 45 shows XOMEGA as it appears when first opened.

### 11.3.1 File Menu.

The file menu is used to open and close files, set preferences, and exit XOMEGA.

Choosing any of the "Open ..." items pops up a file selection dialog box that allows the user to navigate among the directories and files, searching for the desired file to open. The default location is within the current case directory. The filter line is set to only show files with the proper name and/or extension for the type of file the user is trying to open.

Once the file opens, the information reads into the appropriate data structure. If the data contains errors, an error dialog and the corresponding parameters dialog box pops up. If there are no errors the corresponding button in the Operations Column colors gold, to indicate completion of that operation. The chart below shows the correspondence between File Menu choice, file type, and Operation button:

File Menu Choice	File Type	Operations Button
Open a Time Input File	time.inp	Set Time Domain
Open a Grid Input File	grid.inp	Set Spatial Domain
Open a ADM Input File	adm.inp	Set ADM Sources
Open a Met Input File	met.inp	Set Meteorology

Choosing "Preferences" pops up a dialog box (Figure 46) with text entries for the user configurable parameters for the Grid Generator and Model. The options and their default values are explained below.



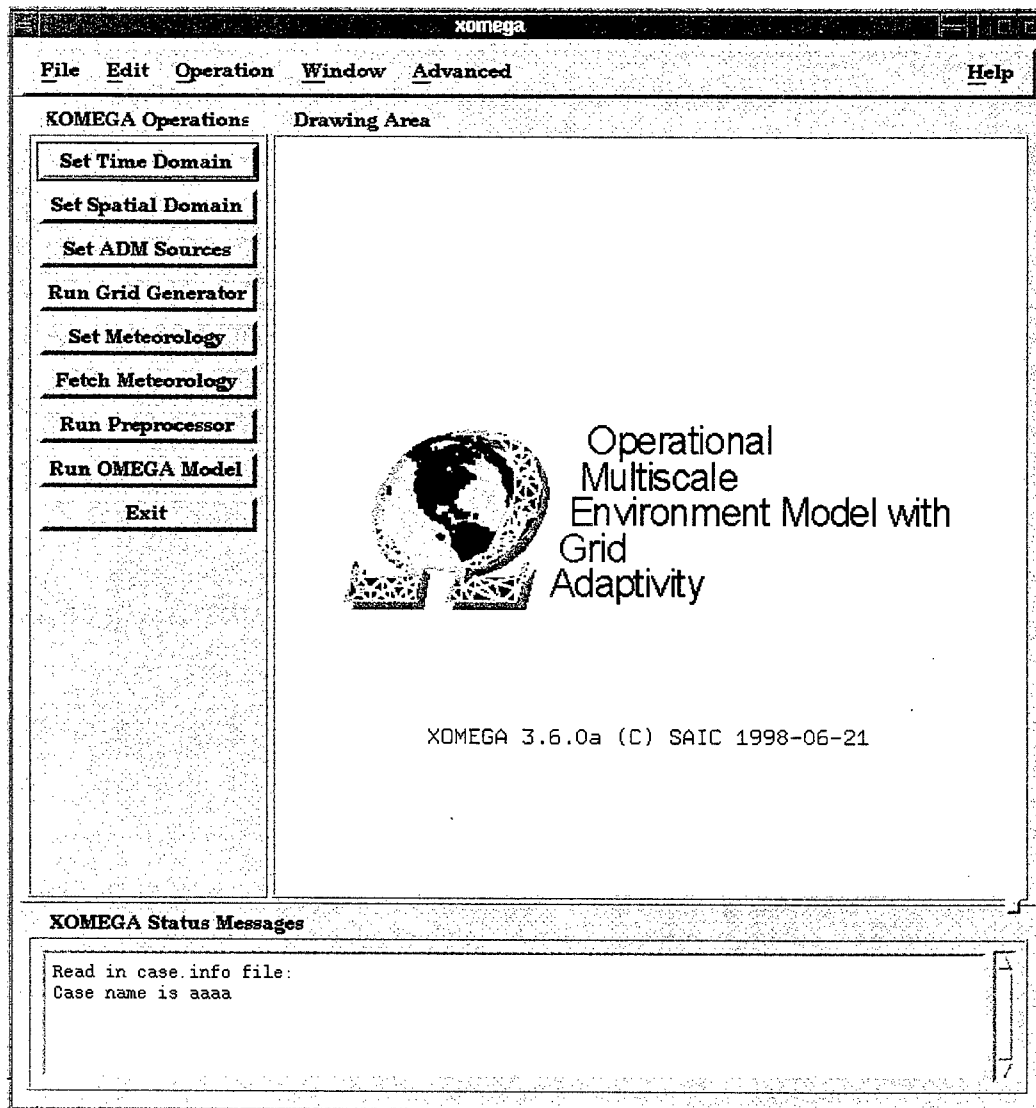


Figure 45. XOMEGA.

**Grid Preferences:**

Number of Stretchable Levels (28) - this is the number of levels that are created during the grid generation process.

Vertical Stretching Factor (1.2) - this number determines the spacing of layers in the grid.

Grid Iterations (10) - this is the maximum number of iterations that the grid generator will process before finishing.

Please see Section 5 for more information on the OMEGA Grid Generator.

**Model Preferences:**

Field Variable Output Interval (1800 seconds) - the number of seconds between each output file.

Diagnostic Output Interval (50 steps) - the number of timesteps between each diagnostic report.

Please see Sections 4,6,7 for more information on the OMEGA Model.

Choosing "Quit" exits XOMEGA.

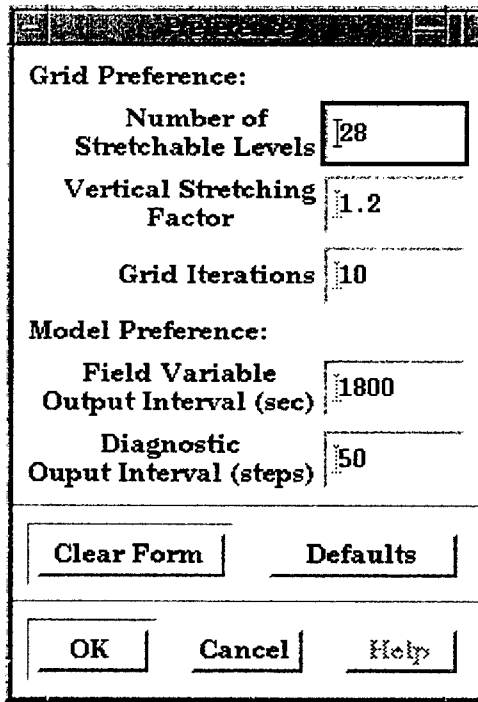


Figure 46. Set preferences dialog box.

### 11.3.2 Edit Menu.

The Edit Menu choices offer alternative ways to pop up the various "Set ..." dialog boxes. The main method uses one of the buttons in the Operations Column. This menu is included for completeness.

### 11.3.3 Operation Menu.

The Operation Menu choices offer alternative ways to execute the external programs of OMEGA (Grid Generator, Fetch, Preprocessor, and OMEGA Model). The main method uses one of the buttons in the Operations Column. This menu is included for completeness.

### 11.3.4 Window Menu.

The only choice on the Window Menu is "XGRID". Choosing this option starts a copy of the XGRID program. Section 12 contains more information on XGRID.

### 11.3.5 Advanced Menu.

The only choice on the Advanced Menu is "Set Refinement Disks". This option pops up the Set Refinement Disks dialog box. This box is used in combination with the Drawing Area and Map dialog to define circular zones within the OMEGA domain. The use of the Refinement Dialog box is discussed in Section 11.5.6.

### 11.3.6 Help Menu.

All the choices on this menu activate the Help dialog box and fill the text window with the appropriate help file. The help topics available are:

XOMEGA in General  
 Setting Time Domain  
 Setting Spatial Domain  
 Setting ADM sources  
 Grid Generation  
 Fetching Meteorology  
 Preprocessing  
 OMEGA Model Execution

When a topic is selected the appropriate help file is loaded into the dialog's text window. The text will scroll to the top of the section. As the user needs more help sections, they will be appended to the text window. The text always scrolls to the top of the most recent section. All Help text remains in the window even when it is closed and reopened. The user may refer back to prior help messages at any time by simply selecting Open Help from the Help menu.

### 11.3.7 Operations Column.

This group of controls is presented in order of use (top to bottom). Each button opens either a dialog box for detailed input to a module, or a dialog for output from running an external module. The buttons are listed below with their basic function. The details of each dialog and action, including user guidelines for input, are presented in then next few sections (11.4 - 11.11).

Set Time Domain	Time Domain dialog box	Input
Set Spatial Domain	Spatial Domain and Map Operations dialogs	Input
Set ADM Sources	ADM Sources and Map Operations dialogs.	Input
Run Grid Generator	Run Grid Generator dialog.	Output
Set Meteorology	Meteorology Parameters dialog.	Input
Fetch Meteorology	Fetch Meteorology dialog.	Output
Run Preprocessor	Run Preprocessor dialog.	Output
Run OMEGA	Run OMEGA dialog.	Output

For each button there is an associated dialog box and process. The dialog box pops up when the button is pressed. Once the dialog is finished and the process is complete without errors the button turns gold colored. If there are errors, or the process is not completed or canceled the button turns gray.

### 11.3.8 Status Messages.

As the user builds the OMEGA simulation messages are received in the text block at the bottom of the interface. Errors, warnings, and other status messages are printed in this window. Using the scroll bar the user is able to see previous messages. The mouse can be used to increase the size of the Status Message window by grabbing the small square on the right hand side above the scroll bar. Be sure to drag the window back when using the Drawing Area.

### 11.3.9 Drawing Area.

The Drawing Area is the largest part of the interface and is used to display images, maps, and user input. When setting the Spatial Domain, Setting ADM Sources, or Setting Refinement Disks, the mouse is positioned in the Drawing Area to "point and click" the input. The behavior of the mouse is controlled

by toggle buttons on the Map Operations dialog box. While XOMEGA is drawing, the cursor changes from an arrow to a watch. No other activity may take place in the XOMEGA windows while drawing.

### 11.3.10 Map Operations Dialog Box.

The Map Operations dialog box (Figure 47) is the main control for the function of the cursor when it is inside the Drawing Area window. This dialog pops up automatically as needed. There are four drawing modes: Zoom Box, Domain Region, Refinement Disk, and ADM Point. The four modes represent the geometric shape drawn by the cursor and the input to the interface.

The mode is changed by clicking one of the diamond shaped buttons on the dialog. The coordinates of the cursor are displayed as the user tracks over the map. The cursor will change image for each mode of map control. Before drawing in the window make sure that the cursor is the correct image. Use the following visual cues to prevent mistakes.

Mode	Cursor Image	Drawing Geometry
Zoom Box	four pointed arrow	Rectangle
Domain Region	simple cross-hair	Rectangle
Refinement Disk	circle	Circle
ADM Point	solid dot	Point

The Zoom Box mode is for enlarging sections of the map. The user holds down the left mouse button while dragging the cursor into a rectangle shape enclosing the area of the map the user would like to zoom in on. This new portion of the world fills the activity window.

The Domain Region mode is used to enclose specific regions of the map that will become part of the OMEGA domain. While holding down the left mouse button, drag the cursor into a rectangle shape enclosing the area of the map that is the outer-most, or largest, region in the domain. Note that all subsequent regions must be within this first region, so make sure it completely encloses the intended domain. A total of ten (10) regions may be selected.

The Refinement Disk mode is used to enclose circular areas in the domain that will undergo a refinement process in during grid generation.

The ADM Point mode is used to select points in the domain that will act as sources for the Atmospheric Dispersion Model within the OMEGA System. Place the cursor over the desired location and press the left mouse button. Up to one-hundred (100) points may be defined.

There are four buttons on the bottom row of the Map Operations dialog box. The "Close" button closes the dialog, leaving, the cursor in the current mode, the map in the current state, and with no loss of data.

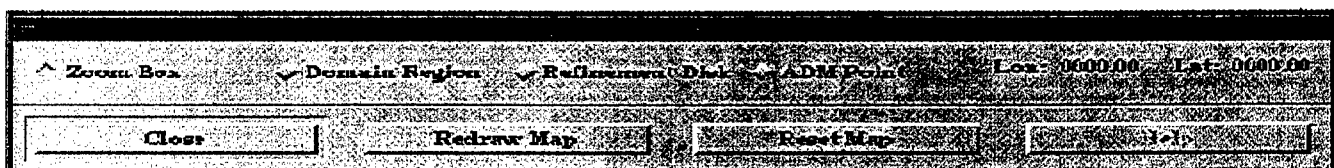


Figure 47. Map operations dialog box.

"Redraw Map" refreshes the activity window. The map view may be un-zoomed back to the entire world by pressing "Reset Map", keeping the same mode and with no loss of data.

### 11.3.11 Drawing Area Window Features.

When the Map Operations dialog box pops up, a world map will be drawn in the Drawing Area Window. The map has several static features. The user should use these to aid his choice of domain parameters such as size and terrain data set. Lines are used for cartographic features. Coverage areas are shown as square panels and indicate what resolution of data is available for a given portion of the world. The dynamic features of the map are objects drawn by the user. These are features used to represent data input and other selections. This chart is a key to the map's features. An example with most of the features is presented in Figure 48.

#### Static Features

Shape	Style	Weight	Color	Feature
Line	Solid	Thick	Black	Equator
Line	Solid	Thick	Black	Prime Meridian
Line	Solid	Thin	Black	Tropics
Line	Dash	Thin	Black/Gray	10deg Latitude
Line	Dash	Thin	Black/Gray	10deg Longitude
Space	---	---	White	Areas of 5 minute Resolution Coverage
Sqaure	Filled	Thin	Yellow	Areas of 30 second Resolution Coverage

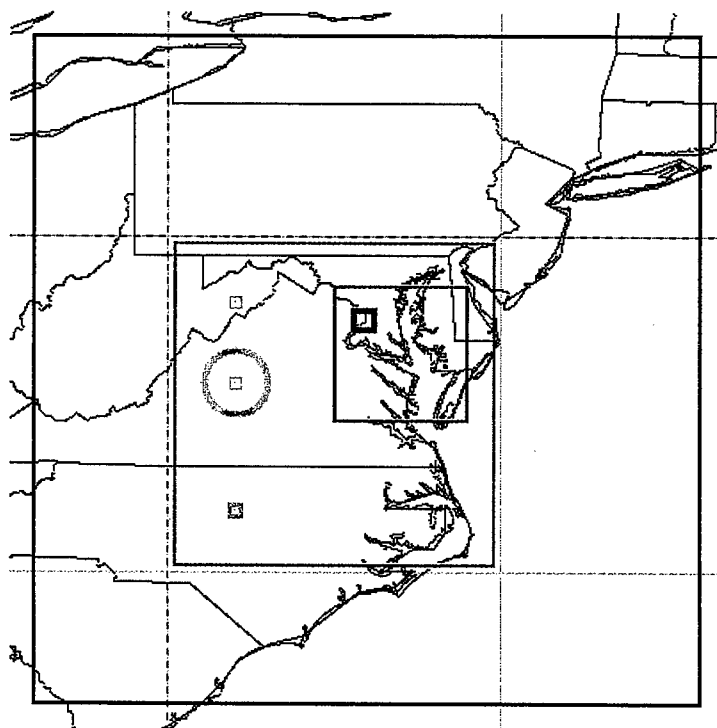


Figure 48. Draw area features.

Dynamic Features				
Shape	Style	Weight	Color	Feature
Rectangle	Outline	Variable	Black	Region using 5 minute Resolution Data
Rectangle	Outline	Variable	Blue	Region using 30 second Resolution Data
Circle	Outline	Variable	Plum	Refinement Disk
Dot	Solid	Variable	Orange	ADM Source Location

## 11.4 Set Time Domain.

When performing a simulation of the atmosphere the user creates a weather forecast. Even if the user simulates an historic event, the user still starts with the atmosphere in some state and evolves it in time to an end state. The Set Time Domain dialog box is the mechanism used to set the temporal bounds on the simulation.

The first operation in the Operations Column is "Set Time Domain". This placement reflects the idea that the time bounds of an OMEGA simulation are the most fundamental part. The user first decides the time period of the simulation before setting other parameters. When the button is pressed the Set Time Domain dialog box (Figure 49) pops up.

This dialog box is one of the easiest dialogs to use. The dialog consists of three sections: Forecast Time Settings and two rows of Action Buttons. How to use each section is described, followed by exact specifications of each control's actions, valid data range, and default value.

The data for each region is stored internally as both the times you input and the total length of time for the simulation.

### 11.4.1 Forecast Time Settings.

This section has eight text entry boxes. By clicking the first mouse button within the box the user enters his choices. The cursor location is a blinking bar. The user may now type as usual in the box to enter the desired Start and End Times in broken-down form for the simulation.

On most systems both backspace and delete will work to remove digits. Be sure to abide by the digit conventions listed in parenthesis beside the box when entering data.

Start Year - Year of Start Time in four digit form.  
Valid Range: 1900 to 2100  
Default Value: current year

Start Month - Month of Start Time in two digit form.  
Valid Range: 1 to 12  
Default Value: current month

Start Day - Day of Start Time in two digit form.  
Valid Range: 1 to 31  
Default Value: current day

**Forecast Time Settings:**

Start Year (YYYY) [1997]

Start Month (MM) [11]

Start Day (DD) [18]

Start Hour (HH) [00]

End Year (YYYY) [1997]

End Month (MM) [11]

End Day (DD) [19]

End Hour (HH) [00]

Clear Form Defaults

OK Cancel Help

Figure 49. Set time domain dialog box.

- Start Hour - Hour of Start Time in four digit form.  
Valid Range: 00 to 23  
Default Value: 00
- End Year - Year of Start Time in four digit form.  
Valid Range: 1900 to 2100  
Default Value: current year + 24 hours
- End Month - Month of Start Time in two digit form.  
Valid Range: 1 to 12  
Default Value: current month + 24 hours
- End Day - Day of Start Time in two digit form.  
Valid Range: 1 to 31  
Default Value: current day + 24 hours
- End Hour - Hour of Start Time in four digit form.  
Valid Range: 00 to 23  
Default Value: 00

## 11.4.2 Action Buttons.

Clear Form - This button resets the text entries to blanks.

Default - This button resets all text entries to their default values.

OK - This button checks the Time data, cause XOMEGA to write out a "time.inp" file in the case directory, and close the dialog box. If any values are in error, a Set Time Domain Error dialog box will pop up alerting the user of the specific errors and suggestions on how to correct them. See Section 11.4.3 for information on the Error dialog box. No "time.inp" file will be written if there are errors in the data.

Cancel - This button declines the Time data, reset the values to default, and close the dialog box. There is no confirmation process.

Help - This button opens the Help dialog and load this section.

## 11.4.3 Set Time Domain Error.

If an error is made while entering values into the text entries, a dialog box pops up alerting the user of the errors and suggesting ways to correct them. The top part of the dialog box contains the error message and the suggestions. The bottom part has a row with two action buttons:

OK - This button dismisses the Error dialog.

Help - This button will open the Help dialog and load this section.

## 11.5 Set Spatial Domain.

The domain selection process is one of the most critical steps in creating an OMEGA simulation. If the domain parameters are not set correctly the model quickly produces errors and may stop altogether. When "Set Spatial Domain" is pressed two dialog boxes, Set Spatial Domain and Map Operations, pops up and a world map is displayed in the Drawing Area window. The dialog boxes are used to input spatial domain information, which then displays on the map.

The Set Spatial Domain dialog box (Figure 50) is the main control for the OMEGA domain. It is used to define the horizontal regions of the domain and to define the vertical spacing of the grid levels. The dialog has five sections: Current Region Controls, Region Parameters, Vertical Parameters, and two rows of Action Buttons. Each section is described below, followed by exact specifications of each control's actions, valid data range, and default value.

The data for each region is stored internally as a list of regions. The Current Region's information is displayed in the Set Spatial Domain dialog. To view data from the other regions the Current Region Controls are used.

Please see Chapter 5 for more information on the OMEGA Grid Generator.

### 11.5.1 Current Region Controls.

When using the cursor to enclose a region on the map, the numbers located at the top of the Set Spatial Domain dialog change accordingly. By clicking on the arrow buttons the user may cycle through the regions. On the map the current region is outlined by a thick rectangle. Any other regions the user may



have defined will be drawn with thin rectangles. Any region may be deleted by clicking on "Delete"  
(Note: there is NO confirmation process).

Current Region - A dynamic label showing the current region and the total number of regions. The current region's values appear in the Region Parameters' text entry boxes and radio buttons.

Left Arrow - Decrement the Current Region filling the Region Parameters' information and drawing the Current Region with a thick rectangle Cyclic action going down: 1 <- 2 <- 3 <- 1 <- 2

Right Arrow - Increment the Current Region filling the Region Parameters' information and drawing the Current Region with a thick rectangle. Cyclic action going up: 1 -> 2 -> 3 -> 1 -> 2 ...

The image shows a dialog box titled "Current Region 1 of 1". At the top, there are navigation arrows and a "Delete" button. Below this is the "Region Parameters" section, which includes text entry boxes for "Minimum Longitude" (-77.20), "Maximum Longitude" (-76.90), "Minimum Latitude" (38.60), and "Maximum Latitude" (38.90). There are also text entry boxes for "Min. Resolution (km)" (3.00) and "Max. Resolution (km)" (11.00). Below these are two sections for "Terrain Data Resolution" and "Shoreline Data Resolution", each with radio buttons for "05 min" and "30 sec". The "Vertical Parameters" section includes text entry boxes for "Total Number of Levels in Domain" (30) and "Level Thickness (m)" (30.00). A "Total Spatial Height (km)" label shows a value of 11.91. At the bottom, there are buttons for "Clear Form", "Default", "OK", "Cancel", and "Help".

Figure 50. Set spatial domain dialog box.

Delete - Remove the Current Region and shift up any subsequent Regions. For example: four regions are defined, the current region number 3, and Delete is clicked. Region 3 is removed from the list, and Region 4 becomes Region 3.

### 11.5.2 Region Parameters.

The Region Parameters section displays the bounding coordinates of the region in latitude and longitude, the desired resolution range in kilometers, and the data set used for that region. Each region will be displayed on the map by a colored rectangle. The color is determined by the terrain data set chosen. The user must ensure that the requested data set is available for the part of the world being simulated (*e.g.*, a simulation of the mid-Pacific may only use the 5 minute (white area on the map) data set; simulations of the United States may use 30 second (yellow panels on the map) data).

When making an OMEGA domain it is best to choose the outer-most region with 5-minute data and then make smaller sub-regions with the 30-second data. These regions must be nested together, and must have resolution ranges that slightly overlap, so that the final grid has a smooth transition from coarse to fine resolution. Note that no subsequent region may be drawn outside Region 1, so the first region must enclose the entire intended domain.

As an example, consider a simulation for Washington DC. A total domain (Region 1) covering the Mid-Atlantic part of the US might be specified, using the 5-minute data set with a resolution range of 50-70km. Then, Region 2 covering Maryland and Virginia using the 30-second data set with a resolution range of 35-55km and Region 3 covering the Chesapeake Bay area using the 30-second data set with a resolution range of 10-36km could be defined. Finally, Region 4 consisting of the city itself with 30-second data set with a resolution range of 3-11km could be specified. The final grid will be smooth with a reasonable spatial resolution gradient.

- Minimum Longitude - Western edge of Current Region. Negative values are West Longitude.  
Valid Range: -180.00 to 180.00  
Default Value: 0.00
- Maximum Longitude - Eastern edge of Current Region. Negative values are West Longitude.  
Valid Range: -180.00 to 180.00  
Default Value: 0.00
- Minimum Latitude - Southern edge of Current Region. Negative values are South Latitude.  
Valid Range: -90.00 to 90.00  
Default Value: 0.00
- Maximum Latitude - Northern edge of Current Region. Negative values are South Latitude.  
Valid Range: -90.00 to 90.00  
Default Value: 0.00
- Min. Resolution - Minimum acceptable resolution for Current Region in km.  
Valid Range: 1 to 200 km  
Default Value: 30 km
- Max. Resolution - Maximum acceptable resolution for Current Region in km.  
Valid Range: 1 to 200 km  
Default Value: 60 km

**Terrain Data Resolution** - Radio button pair: only one button may be active. This button controls the terrain data source to build the part of the grid defined by this region. Regions using 5-minute data will be drawn in black. Regions using 30-second data will be drawn in blue. Default Value: 5 minute

**Shoreline Data Resolution** - Radio button pair: only one button may be active. This button controls the shoreline data source used to build the part of the grid defined by this region.  
Default Value: 5-minute

### 11.5.3 Vertical Parameters.

The Vertical Parameters section allows the user to change how many total levels to use in the model, and the base thickness of Level 1. From these numbers the total height of the domain is calculated and displayed on the dialog in kilometers. For most applications the default values should be used.

**Total Number of Levels in Domain** - This is the total number of levels of the computational domain.  
Valid Range: 5 to 100  
Default Value: 30

**Level 1 Thickness** - This is the thickness in meters of the first level.  
Valid Range: 5.0 to 250.0 meters  
Default Value: 30

### 11.5.4 Action Buttons.

**Clear Form** - This button resets the text entries to zeros, de-select terrain and shoreline data sets, and reset the Vertical Parameters to default values. It does not modify the Region Data in any way. The user must modify the values before continuing.

**Default** - This button resets all text entries and radio buttons to their default values. It does not modify the Region Data in any way. The user must modify the values before continuing.

**OK** - This button checks the Region data, cause XOMEGA to write out a "grid.inp" file in the grid directory and close the dialog box. If any values are in error, a Set Spatial Domain Error dialog box will pop up alerting the user of the specific errors and suggestions on how to correct them. See Section 11.5.5 for information on the Error dialog box. No "grid.inp" file will be written if there are errors in the data.

**Cancel** - This button declines the Region data, remove all regions, reset the values to default, and close the dialog box. There is no confirmation process.

**Help** - This button opens the Help dialog and load this section.

### 11.5.5 Set Spatial Domain Error.

While entering values into the text entries if the user makes errors a dialog box pops up alerting him of the errors and suggesting ways to correct them. The top part of the dialog box contains the error message and the suggestions. The bottom part has a row with three action buttons:

**Delete Current Region** - This button will remove the Current Region from the list similar to Delete on the Set Spatial Domain dialog. Be sure that the Current Region is the one

containing the error before clicking this button. Use the arrow buttons if needed to change to the Current Region. This button will dismiss the Error dialog.

**Modify Regions -** This button will return control to the Set Spatial Domain dialog box and dismiss the Error dialog box. You may now modify the regions as usual.

**Help -** This button opens the Help dialog and load this section.

### 11.5.6 Set Refinement Dialog.

XOMEGA allows for an advanced feature call Point Refinement. This is activated using the “Advanced” menu and “Set Refinement Disks”, or the “Map Operations” dialog and “Refinement Disk”. The cursor is then used to draw circles. These circles represent regions of the domain whose resolution will be fixed to the specified value. The Grid Generator makes sure that the cells produced within the disk are of a fixed resolution.

Selecting a refinement disk enables the user to have increased resolution about a specific point, without defining another region. This saves on I/O process time, allowing the user to pinpoint a specific resolution instead of a range.

The effect of point refinement is Gaussian in nature: cells produced close to the center point of the disk are as close to the prescribed resolution as possible, while those farther out will vary in resolution to match the bounding region's resolution.

The Valid Range for the resolution of a Refinement Disk is determined by the bounding Region. The resolution must be no smaller than 0.5 times the Minimum Resolution of the bounding region, and no greater than the Maximum Resolution of the bounding region. For example if the user has defined a region with 10-20km resolution and wants to put a refinement disk within this region, he must make sure the resolution of the disk is between 5-20km. This ensures a smooth transition from the refinement disk to the bounding region.

The Set Refinement Disks dialog (Figure 51) has four sections: Current Disk Controls, Disk Parameters, and two rows of Action Buttons.

**Current Disk -** A dynamic label showing the current disk and the total number of disks. The current disk's values appear in the Disk Parameters' text entry boxes.

**Left Arrow -** Decrement the Current Disk filling the Disk Parameters' information and drawing the Current Disk in thick circle.

Cyclic action going down: 1 <- 2 <- 3 <- 4 <- 1 ...

**Right Arrow -** Increment the Current Disk filling the Disk Parameters' information and drawing the Current Disk in thick circle.

Cyclic action going up: 1 -> 2 -> 3 -> 4 -> 1 ...

**Delete -** Remove the Current Disk and shift up any subsequent Disks.

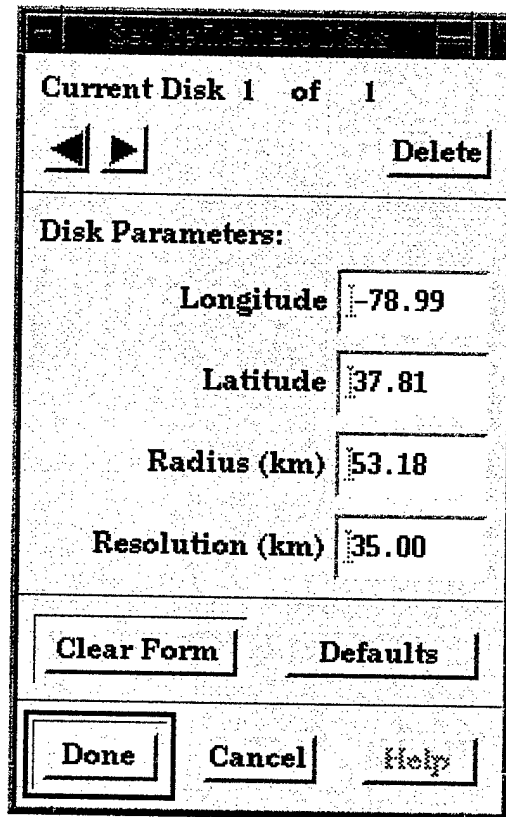


Figure 51. Set refinement disks dialog box.

- Longitude - Longitude value of the Current Disk's center point.  
Valid Range: -180.00 to 180.00  
Default Value: 0.00
- Latitude - Latitude value of the Current Disk's center point.  
Valid Range: -90.00 to 90.00  
Default Value: 0.00
- Radius - The radius of the Current Disk in kilometers.  
Valid Range: 0.5 km to 100 km  
Default Value: 0.00
- Resolution - The desired resolution for the Current Disk.  
Valid Range: See discussion above  
Default: 10.00
- Clear Form - This button resets the text entries to zeros. It does not modify the Disk Data in any way. The user must modify the values before continuing.
- Default - This button resets all text entries and radio buttons to their default values. It does not modify the Region Data in any way. The user must modify the values before continuing.
- OK - This button checks the Disk data, cause XOMEGA to write out a "grid.ref" file in the grid directory and close the dialog box. If any values are in error, a Set Refinement Disk Error dialog box will pop up alerting the user of the specific errors and suggestions on how to correct them. No "refine.lst" file is written if there are errors in the data.

- Cancel - This button declines the Disk data, remove all disks, reset the values to default, and close the dialog box. There is no confirmation process.
- Help - This button opens the Help dialog and load this section.

## 11.6 Set ADM Sources.

OMEGA has a built-in Atmospheric Dispersion Model (ADM) and XOMEGA allows the user to select source locations for this model. All these locations must be within the model domain. When "Set ADM Sources" is clicked two dialog boxes, Set ADM Sources and Map Operations, pops up and a world map is displayed in the Drawing Area window. The dialog boxes are used to input ADM source information that will then be displayed on the map.

The Set ADM Sources dialog box (Figure 52) is the main control for the ADM program. It is used to define the source locations and strengths. The dialog has five sections: Atmospheric Dispersion Model Options, Current Source Controls, Source Parameters, and two rows of Action Buttons. Each section will be described below, followed by exact specifications of each control's actions, valid data range, and default value.

The data for each source is stored internally as a list of sources. The Current Source's information is displayed in the Set ADM Sources dialog. Data from the other sources is viewed using the Current Source Controls dialog.

Note that several of the controls are only used with advanced ADM modes. The general user is encouraged to leave the default values as is, and specify only Location, Altitude, and Time values.

Please see Chapter 8 for more information on the Atmospheric Dispersion Model.

### 11.6.1 Atmospheric Dispersion Model Options.

This group of option menus is responsible for setting the most general features of the ADM module. These options will apply to all sources selected. The options control which ADM program is run, and how it behaves.

- Mode - Currently this option menu has two choices: Off and Tracer. Off will cause the ADM program to be skipped when running the OMEGA Model. Tracer activates tracer type particles in the ADM model.  
Default: Tracer
- Diffusion - This option menu has two choices: Puff and LPDM. Puff causes the ADM program to use puff computations when it runs. LPDM causes the ADM program to use Lagrangian Particle Diffusion when it runs.  
Default: Puff
- Eulerian - This option menu has two choices: Off and On. If On is selected, The ADM takes the first three sources defined and duplicates them as Eulerian Sources.  
Default: Off

**Atmospheric Dispersion Model Options:**

Mode

Diffusion

Eulerian

---

Current Source: 2 of 3

---

**Source Parameters:**

Longitude	<input type="text" value="-79.00"/>	Mass (kg)	<input type="text" value="0.00"/>
Latitude	<input type="text" value="35.94"/>	Density (kg/m3)	<input type="text" value="0.00"/>
Altitude (m AGL)	<input type="text" value="0.00"/>	Vapor (kg/m3) Concentration	<input type="text" value="0.00"/>
Start Time (s)	<input type="text" value="0.00"/>	Sigma in x (m)	<input type="text" value="0.00"/>
End Time (s)	<input type="text" value="0.00"/>	Sigma in y (m)	<input type="text" value="0.00"/>
Injection Interval (s)	<input type="text" value="0.00"/>	Sigma in z (m)	<input type="text" value="0.00"/>
Diameter (m)	<input type="text" value="0.00"/>	Particle Multiplier	<input type="text" value="0"/>

Figure 52. Set ADM sources dialog box.

### 11.6.2 Current Source Controls.

When using the cursor to click on an ADM Point on the map, the numbers located in this section increments. Clicking on the arrow buttons allows the user to cycle through the sources. On the map the current sources are shown as an open orange dot. Any other sources the user may have defined are drawn with solid orange dots. The user may delete any source by clicking on "Delete" (Note: there is NO confirmation process).

**Current Source** - A dynamic label showing the current source and the total number of sources. The current source's values appear in the Source Parameters' text entry boxes.

**Left Arrow** - Decrement the Current Source filling the Source Parameters' information and drawing the Current Source as an open orange dot.  
 Cyclic action going down: 1 <- 2 <- 3 <- 4 <- 1 ...

- Right Arrow - Increment the Current Source filling the Source Parameters' information and drawing the Current Sources an open orange dot.  
Cyclic action going up: 1 -> 2 -> 3 -> 4 -> 1 ...
- Delete - Remove the Current Source and shift up any subsequent sources. For example: four sources are defined, the current source is number 3, and Delete is clicked. Source 3 is removed from the list, and source 4 becomes source 3.

### 11.6.3 Source Parameters.

The Source Parameters section displays all the information about a source, including its location, time bounds, and strength. Typical values for some parameters are listed for 1000-micron diameter dust particle. Other types of particles will have different typical values.

- Longitude - Longitude of current source location.  
Valid Range: -180.00 to 180.00  
Default Value: 0.00
- Longitude - Latitude of current source location.  
Valid Range: -180.00 to 180.00  
Default Value: 0.00
- Altitude - Altitude of current source location in meters above ground level.  
Valid Range: 1.00 to 100.00m  
Default Value: 20.00
- Start Time - Number of seconds after start of simulation to begin release of particles from current source.  
Valid Range: 0.00 to maximum number of seconds in simulation  
Default Value: 0.00
- End Time - Number of seconds start of simulation to halt release of particles from current source.  
Valid Range: 0.00 to maximum number of seconds in simulation  
Default Value: maximum number of seconds in simulation, if defined.
- Injection Interval - Number of seconds between release of particle from current source.  
Valid Range: 1.00 to 10800.00 seconds (30 hours)  
Default Value: 1800.00s (1/2 hour)
- Diameter - Diameter of particle in meters released from current source.  
Default Value: 0.00 m  
Typical Value: 0.001 m
- Mass - Mass of particle in kilograms released from current source.  
Default Value: 0.00 kg  
Typical Value: 1.05e-6 kg
- Density - Density of particle in kilograms per cubic meter for current source. Note this number must be consistent with the Mass and Diameter.  
Default Value: 0.00 kg/m<sup>3</sup>  
Typical Value: 2000.00 kg/m<sup>3</sup>
- Vapor Concentration - Vapor Concentration of puff in kilograms per cubic meter for current source. Note this number must be consistent with the Mass and Diameter.  
Default Value: 0.00 kg/m<sup>3</sup>  
Typical Value: 1.00 kg/m<sup>3</sup>



- Sigma in x - Initial sigma x-value of the puff in meters for the current source.  
Default Value: 0.00 m  
Typical Value: 5.00 m
- Sigma in y - Initial sigma-y value of the puff in meters for the current source.  
Default Value: 0.00 m  
Typical Value: 5.00 m
- Sigma in z - Initial sigma-z value of the puff in meters for the current source.  
Default Value: 0.00 m  
Typical Value: 5.00 m
- Particle Multiplier - Number of actual particles to release from current source. If this value is not one, it is used to modify the source term in the ADM so that multiple particles are released at each interval from the same source. For example if this value is three, then the source releases three particles every interval, not just one.  
Valid Range: 1 to 10  
Default Value: 1

#### 11.6.4 Action Buttons.

- Clear Form - This button resets the text entries to zeros, and re-set the option menus to the default values. It does not modify the Source Data in any way. The user must modify the values before continuing.
- Default - This button resets all text entries and option menus to their default values. It does not modify the Source Data in any way. The user must modify the values before continuing.
- OK - This button checks the Source data, causes XOMEGA to write out a "adm.inp" file in the case directory and close the dialog box. If any values are in error, a Set ADM Sources Error dialog box will pop up alerting the user of the specific errors and suggestions on how to correct them. See Section 11.6.5 for information on the Error dialog box. No "adm.inp" file is written if there are errors in the data.
- Cancel - This button declines the Source data, remove all sources, reset the values to default, and close the dialog box. There is no confirmation process.
- Help - This button opens the Help dialog and load this section.

#### 11.6.5 Set ADM Sources Error.

If an error is made while entering values into the text entries, a dialog box pops up alerting the user of the errors and suggesting ways to correct them. The top part of the dialog box contains the error message and the suggestions. The bottom part has a row with three action buttons:

- Delete Current Source - This button removes the Current Source from the list similar to Delete on the Set ADM Sources dialog. Be sure that the Current Source is the one containing the error before clicking this button. Use the arrow buttons if needed to change to the Current Source. This button dismisses the Error dialog.
- Modify Regions - This button returns control to the Set ADM Sources dialog box and dismiss the Error dialog box. You may now modify the sources as usual.
- Help - This button opens the Help dialog and load this section.

## 11.7 Run Grid Generator.

When the user is satisfied with the arrangement of Spatial Domain Regions, the ADM Source locations (and possible Refinement Disks), the next step is to create the OMEGA grid. The program that translates the 2-D domain region information into a full 3-D computational mesh is called the OMEGA Grid Generator.

Since this program is independent of XOMEGA it needs to be called with a controlled process. The mechanism for doing this is to use a UNIX pipe to send the text output of the Grid Generator back to XOMEGA into a read-only text window. While the Grid Generator is running all of its text output is captured and displayed so that the user may watch the progress.

The Grid Generator first reads the file "grid.inp" to get information about the domain regions and levels. The grid is then made by first gathering the requested data and "stitching" together the individual data sets into a seamless block of terrain and shoreline data. Next, a series of triangles is interpolated to the underlying data. The interpolation process adds and deletes triangle vertices until all triangles are within the resolution range requested. The grid is now a single entity with varying resolution, but no distinct regions. The regions are temporary boundaries used to specify desired resolution ranges and data set usage. Please see Chapter 5 for more information on the OMEGA Grid Generator.

When the user clicks on "Run Grid Generator" a large dialog box pops up. This dialog consists of two sections: Text Output Window and a row of Action Buttons. Figure 53 shows the dialog after the Grid Generator has started.

Note that if the Spatial Domain has not been specified the Run Grid Generator dialog will not pop up. Instead an error message will pop up informing the user of the error. When acknowledging the error by clicking the "OK" button the Set Spatial Domain dialog will pop up. Please see Section 11.5 for information on setting the Spatial Domain.

### 11.7.1 Text Output Window.

When initially popped up the Text Output Window is blank. As the grid generation progresses the window becomes filled with text. The output is saved as it scrolls off the window, and even saved when the dialog is popped down. The scroll bar on the right hand side of the window may be used to view text beyond the window. On subsequent pop-ups the previous information is still in the Text Output Window. Any new text will be appended in the window.

### 11.7.2 Action Buttons.

Close - This button dismisses the dialog box. XOMEGA will read the report file created by the Grid Generator, "grid/grid.rep", and pop up a dialog with this information

Compression Ratio: Ratio of simulated time to cpu time for the grid 24-Hours Run Time: Real time to simulate 24 hours with this grid. Note that this information is machine dependent.

If the Grid Generator is unable to make these estimations, the dialog box contains the values "-99.0" for the numbers. Please see Chapter 5 for more information on the OMEGA Grid Generator.

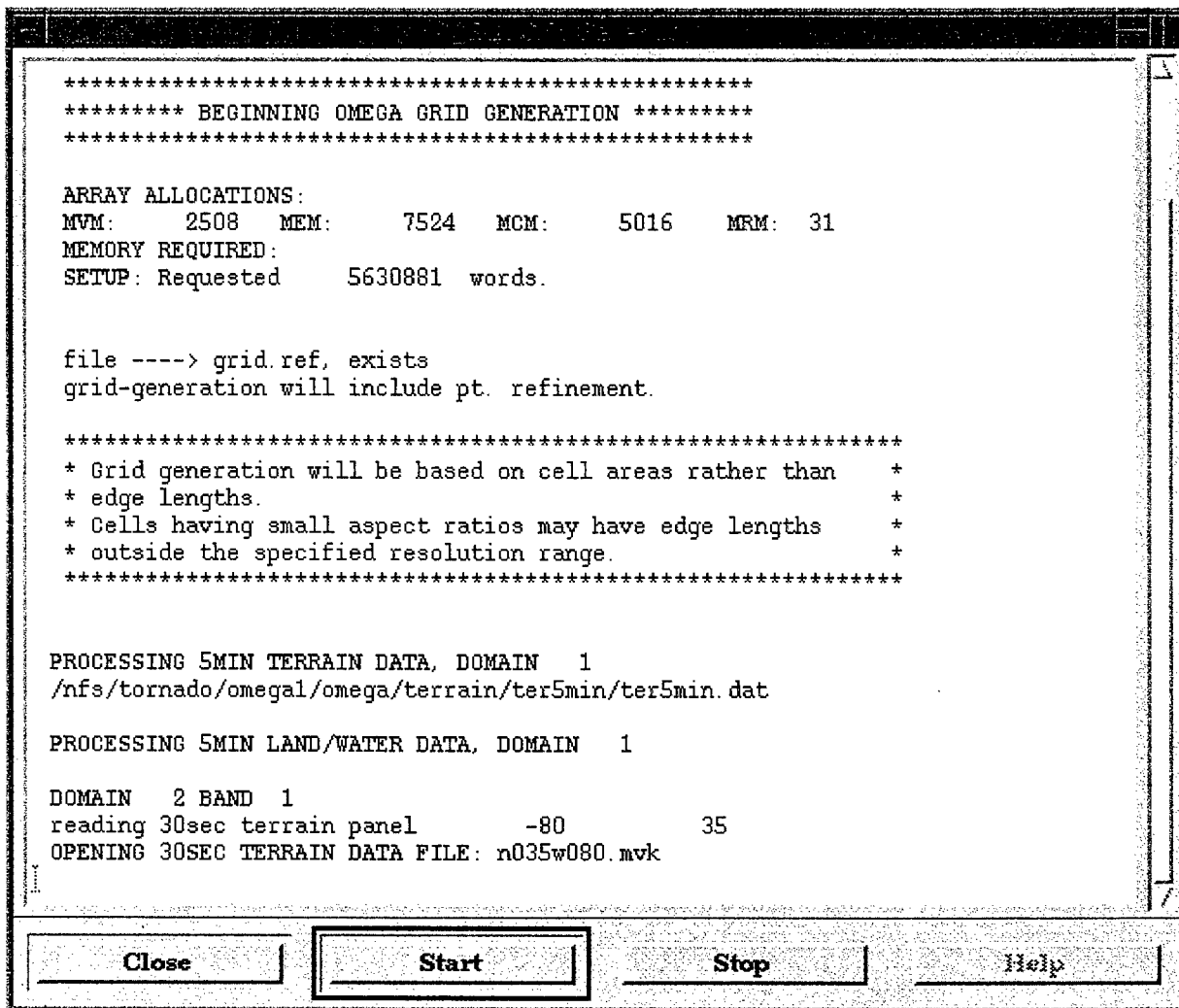


Figure 53. Run grid generator dialog box.

**Start -** When this button is pressed a check is made to determine if a grid file already exists. If a valid grid already exists the Grid Generation warning dialog box pops up. See Section 11.7.3 for information on the Warning dialog box.

If no grid exists then the Grid Generator is started. While the Grid Generator is running only the Stop button will accept input. All other controls on this dialog, and XOMEGA are locked out.

**Stop -** If the Grid Generator is not running this button has no effect. If the Grid Generator is running this button will stop it.

Note that when this button is pressed its effects may not be immediately apparent. It may take a few seconds for the "Stop" command to propagate to the Grid Generator program, and for XOMEGA to reset its windows and controls.

Since the external program is run through a UNIX pipe its output is sent back down the pipe to the dialog box. When the dialog is waiting for output from the program XOMEGA is unable to update its windows or process a "Stop" button press. If windows are covered and uncovered, parts of XOMEGA

may become gray. When the next line of output from the external program is piped to the dialog the windows are redrawn and the button press processed. XOMEGA resets itself.

Help - This button will open the Help dialog and load this section.

### 11.7.3 Grid Generation Warning .

This dialog box is popped up when the user tries to run the Grid Generator and a valid grid file already exists. The top part of the dialog contains the warning message. The bottom part has a row of three action buttons:

Overwrite - This button starts the grid generation process. All existing information in the "grid/" sub-directory will be overwritten as the new grid is made. The output from the Grid Generator appears in the Text Output Window normally. If the program has no errors the Run Grid Generator operation is completed. The Grid Generation Warning dialog is dismissed. The Run Grid Generator dialog remains.

Proceed - This button accepts the existing grid. All existing grid information is left untouched and the Run Grid Generator operation is completed. The Grid Generation Warning dialog is dismissed. The Run Grid Generator dialog is dismissed.

Cancel - This button declines the existing grid. All existing grid information is left untouched and the Run Grid Generator operation is NOT completed. The Grid Generation Warning dialog is dismissed. The Run Grid Generator dialog is dismissed.

## 11.8 Set Meteorology.

An OMEGA simulation requires weather data to build initial conditions and boundary conditions. Common weather data sources are models whose domains are global or hemispheric, and whose forecast times are days. Observational data may also be used. Both surface and upper air observations may be used in an OMEGA run.

When constructing an OMEGA simulation the user must be sure that the meteorology data is valid for the time and space of your simulation. Not all models have global coverage and some model's forecast times may not match the user's times.

XOMEGA uses the concept of meteorology segments to allow for maximum flexibility when specifying the input meteorology. Essentially, a meteorology segment is a subdivision of the time domain coupled with the sources of data used for that time period. A meteorology segment is defined by parameters that allow the specification of different sources of meteorology data be used for different times.

As an example, consider modeling the weather for the city of Washington DC. The user might want to produce a 3-day forecast for the Metro region. Initial conditions for 00Z on the first day will have to be generated as well as boundary conditions for all days of the simulation.

This city is within the domain of nearly all major atmospheric models, so grid model data should be available for the user's domain. Suppose the user is interested in small-scale effects and thus wants to use the highest resolution data possible to generate the boundary conditions. Most high-resolution models do not forecast for total forecast period (3-days) so the same model cannot be used for all of the boundary conditions.

This is where meteorology segments become very useful. The user can define a series of meteorology segments that specify which data sources to use for different periods of his forecast. Meteorology data can be mixed and matched to use the highest resolution possible at each analysis time.

Assuming he has both a NWS feed and a FNMOC feed, his forecast period may be split into these three segments:

- Segment 1 covers the first 24-hour period and use ETAXP data.
- Segment 2 covers the next 24-hour period and use NORAPSN data.
- Segment 3 covers the last 24-hour period and use NOGAPS data.

Using meteorology segments gives the user the flexibility to generate boundary conditions from different data sources at different times. This allows the use of the best data available in OMEGA simulations. The Set Meteorology dialog box (Figure 59) is the control for defining meteorology segments. The dialog has five sections: Time Domain label, Current Segment Controls, Segment Parameters, and two rows of Action Buttons. How to use each section will be described, followed by exact specifications of each control's actions, valid data range, and default value.

Note that if the Time Domain data has not been filled the Set Meteorology dialog does not pop up. Instead an error message will pop up informing you of the error. When acknowledging the error by clicking the "OK" button the Set Time Domain dialog will pop up. Please see Section 11.4 for information on setting the Time Domain.

### 11.8.1 Time Domain Label.

This section of the dialog is a simple reminder of the Time Domain. It is presented so that the user has the total time span of your simulation available as you define meteorology segments. If the Time Domain is changed, the labels are updated.

### 11.8.2 Current Segment Controls.

Initially the dialog has only one segment defined spanning the entire time domain. The controls in this section are used to add, delete and cycle through all defined regions.

- Current Segment - A dynamic label showing the current segment and the total number of segments. The current segment has its Segment Number Label non-shaded. All other Segment Numbers are shaded.
- Left Arrow - Decrement the Current Segment.  
Cyclic action going down: 1 <- 2 <- 3 <- 4 <- 1 ...
- Right Arrow - Increment the Current Segment.  
Cyclic action going up: 1 -> 2 -> 3 -> 4 -> 1 ...
- Add - Add a segment to the end of the list. The text entry and option menus will be set to default values. It is the user's responsibility to adjust the Time entries to fit within the bounds. Up to five meteorology segments may be defined.
- Delete - Remove the Current Segment and shift up any subsequent Segments. If four segments are defined, and Segment 3 is current, Delete removes Segment 3 from the list, and Segment 4 becomes Segment 3.

Time Domain: Start: 1997 11 18 00 End: 1997 11 19 00

Current Segment 1 of 1

◀ Add ▶ Delete

Segment Number	Start Time YYYY MM DD HH	End Time YYYY MM DD HH	Gridded Weather Model	Surface Observations	Rawinsonde Observations
<b>1</b>	1997 11 18 00	1997 11 19 00	7_NOGAPS ▾	0_None ▾	0_None ▾
2			0_None ▾	0_None ▾	0_None ▾
3			0_None ▾	0_None ▾	0_None ▾
4			0_None ▾	0_None ▾	0_None ▾
5			0_None ▾	0_None ▾	0_None ▾

Clear Form Default

OK Cancel Help

Figure 54. Set meteorology dialog box.

### 11.8.3 Segment Parameters.

- Segment Number - Dynamic label used to highlight which segment is the current segment. The current segment will have its number in bold print. All other segments will have shaded gray numbers.  
Valid Range: 1 to 5, in fixed sequence  
Default Value: 1
- Start Time - Start Time of Segment in full digit form: four digits for year, two digits for month, day and hour, single space between numbers.  
Valid Range: 1900 01 01 00 to 2100 12 31 23  
Default Value: value copied from Start Time of Time Domain
- End Time - End Time of Segment in full digit form: four digits for year, two digits for month, day and hour, single space between numbers.  
Valid Range: 1900 01 01 00 to 2100 12 31 23  
Default Value: value copied from End Time of Time Domain
- Gridded Weather Model - Source model to use for Segment.  
Valid Range: Installation dependent  
Default: Installation dependent
- Surface Observations - Source of observations to use for Segment.  
Valid Range: Installation dependent  
Default: None
- Rawinsonde Observations - Source of upper air observations for Segment.  
Valid Range: Installation dependent  
Default: None

#### **11.8.4 Action Buttons.**

- Clear Form - This button deletes all segments, reset the text entries to blank and de-select all option menus.
- Default - This button deletes all segments, except the first. It will set the first segment to default values.
- OK - This button checks the Segment data, cause XOMEGA to write out a "met.inp" file in the prep directory and close the dialog box. If any values are in error, a Set Meteorology Error dialog box will pop up alerting the user of the specific errors and suggestions on how to correct them. See Section 11.8.4 for information on the Error dialog box. No "met.inp" file will be written if there are errors in the data.
- Cancel - This button declines the Segment data, remove all segments, clear all values, and close the dialog box. There is no confirmation process.
- Help - This button opens the Help dialog and load this section.

#### **11.8.5 Set Meteorology Error.**

If an error is made while entering values into the text entries, a dialog box pops up alerting the user of the errors and suggesting ways to correct them. The top part of the dialog box contains the error message and the suggestions. The bottom part has a row with two action buttons:

- OK - This button acknowledges the error and dismiss the Error dialog.
- Help - This button opens the Help dialog and load this section.

#### **11.9 Fetch Meteorology.**

When the user is satisfied with the subdivision of his time domain into one or more meteorology segments, the next step is to gather together the raw data. The program that searches the file system for the appropriate meteorology data files is called Fetch.

Since this program is independent of XOMEGA it needs to be called with a controlled process. The mechanism for doing this is to use a UNIX pipe to send the text output of Fetch back to XOMEGA into a read-only text window. While the Fetch program is running all of its text output is captured and displayed so that the user may watch the progress.

To keep the individual meteorology segments separate each segment is processed in its own subdirectory. These directories are below the prep directory. For example "case/prep/seg1" will hold all the raw data specified in Segment 1. XOMEGA writes a simple shell script that creates the sub-directory and calls Fetch from there for each segment. Fetch is called by the script with command line arguments specifying the time span to use and what source of data to gather. Fetch scans the file system for the files. If the files are found a temporary copy is placed in the segment directory. If a file is missing, Fetch will look for another file that satisfies the time of the missing file.

When the user clicks on "Fetch Meteorology" a large dialog box pops up. This dialog consists of two sections: Text Output Window and a row of Action Buttons. Figure 55 shows the dialog after Fetch has started.

Time Domain: Start: 1997 11 13 00 End: 1997 11 19 00

Current Segment 1 of 1

◀ Add ▶ Delete

Segment Number	Start Time YYYY MM DD HH	End Time YYYY MM DD HH	Gridded Weather Model	Surface Observations	Rawinsonde Observations
1	1997 11 18 00	1997 11 19 00	1_NDCAPS ▾	1_Name ▾	1_Name ▾
2			2_Name ▾	2_Name ▾	2_Name ▾
3			3_Name ▾	3_Name ▾	3_Name ▾
4			4_Name ▾	4_Name ▾	4_Name ▾
5			5_Name ▾	5_Name ▾	5_Name ▾

Clear Form Default

OK Cancel Help

Figure 55. Fetch meteorology dialog box.

Note that if the Meteorology Segments data has not been filled the Fetch Meteorology dialog will not pop up. Instead an error message will pop up informing the user of the error. When acknowledging the error by clicking the "OK" button the Set Meteorology dialog will pop up. Please see Section 11.8 for information on setting the Meteorology.

### 11.9.1 Text Output Window.

When initially popped up the Text Output Window will be blank. As the gathering of meteorology data progresses the window will become filled with text. The output is saved as it scrolls off the window, and even saved when the dialog is popped down. The scroll bar on the right hand side of the window can be used to view text beyond the window. On subsequent pop ups the previous information will still be in the Text Output Window. Any new text will be appended in the window.

### 11.9.2 Action Buttons.

Close - This button dismisses the dialog box.

Start - When this button is pressed a check is made to determine if a set of meteorology data already exists for the case. If a valid set already exists the Fetch Meteorology Warning dialog box pops up.

See Section 11.9.3 for information on the Warning dialog box.

If no meteorology exists for the case then Fetch is started. While Fetch is running only the Stop button will accept input. All other controls on this dialog, and XOMEGA are locked out.

Stop - If Fetch is not running this button has no effect.  
If Fetch is running this button stops it.



Note that when you press this button its effects may not be immediately apparent. It may take a few seconds for the "Stop" command to propagate to Fetch program, and for XOMEGA to reset its windows and controls.

Since the external program is run through a UNIX pipe its output is sent back down the pipe to the dialog box. When the dialog is waiting for output from the program XOMEGA is unable to update its windows or process a "Stop" button press. If the windows are moved (or covered and uncovered) parts of XOMEGA become gray. When the next line of output from the external program is piped to the dialog the windows will be redrawn and the button press processed. XOMEGA will reset itself.

Help - This button opens the Help dialog and load this section.

### **11.9.3 Fetch Meteorology Warning .**

This dialog box is popped up when the user tries to run Fetch and a valid set of meteorology data already exists for the case. The top part of the dialog contains the warning message. The bottom part has a row of three action buttons:

- Overwrite - This button starts the Fetch process. All existing information in the "prep/seg\*" sub-directories will be overwritten as the new set of data is gathered. The output from Fetch appears in the Text Output Window normally. If the program has no errors the Fetch Meteorology operation is completed. The Fetch Meteorology Warning dialog is dismissed. The Fetch Meteorology dialog will remain.
- Proceed - This button accepts the existing set of meteorology data. All existing meteorology data is left untouched and the Fetch Meteorology operation is completed. The Fetch Meteorology Warning dialog is dismissed. The Fetch Meteorology dialog remains.
- Cancel - This button declines the existing set of meteorology data. All existing meteorology data is left untouched and the Fetch Meteorology operation is NOT completed. The Fetch Meteorology Warning dialog is dismissed. The Fetch Meteorology dialog remains.

### **11.10 Run Preprocessor.**

After all raw meteorology data has been gathered for the meteorology segments, the next step is to process this data into initial conditions and boundary conditions. There are several programs that work on the data and collectively they are known as the OMEGA Preprocessor. A parent script program has been written that binds the other programs together. Since all processing is performed by the programs the parent script calls it will be referred to as the Preprocessor.

Please see Chapters 6 and 7 for more information on the OMEGA Preprocessor.

Since this program is independent of XOMEGA it needs to be called with a controlled process. The mechanism for doing this is to use a UNIX pipe to send the text output of the Preprocessor back to XOMEGA into a read-only text window. While the Preprocessor is running all of its text output is captured and displayed so that the user may watch the progress.

XOMEGA writes a simple script ("prep/prep.csh") to manage the processing of the meteorology segments and to keep the boundary conditions produced in time sequence. This script calls the Preprocessor once for each meteorology segment. Within each segment boundary conditions are made.

After all the segments are processed the script will rename the boundary files to form a sequence and copy them up to the case directory.

When the user clicks on "Run Preprocessor" a large dialog box pops up. This dialog consists of two sections: Text Output Window and a row of Action Buttons. Figure 56 shows the dialog after the Preprocessor has started.

Note that if the Fetch Meteorology operation has not been completed (i.e. no meteorology data was gathered) the Run Preprocessor dialog will not pop up. Instead an error message will pop up informing the user of the error. When acknowledging the error by clicking the "OK" button the Fetch Meteorology dialog will pop up. Please see Section 11.9 for information on Fetch Meteorology.

### 11.10.1 Text Output Window.

When initially popped up the Text Output Window will be blank. As the preprocessing progresses the window will become filled with text. The output is saved as it scrolls off the window, and even saved when the dialog is popped down. The scroll bar on the right hand side of the window may be used to view text beyond the window. On subsequent pop ups the previous information will still be in the Text Output Window. Any new text will be appended in the window.

### 11.10.2 Action Buttons.

Close - This button dismisses the dialog box.

Start - When this button is pressed a check is made to determine if valid set of initial and boundary conditions already exist. If a valid set already exists the Run Preprocessor Warning dialog box pops up. See Section 11.10.3 for information on the Warning dialog box.

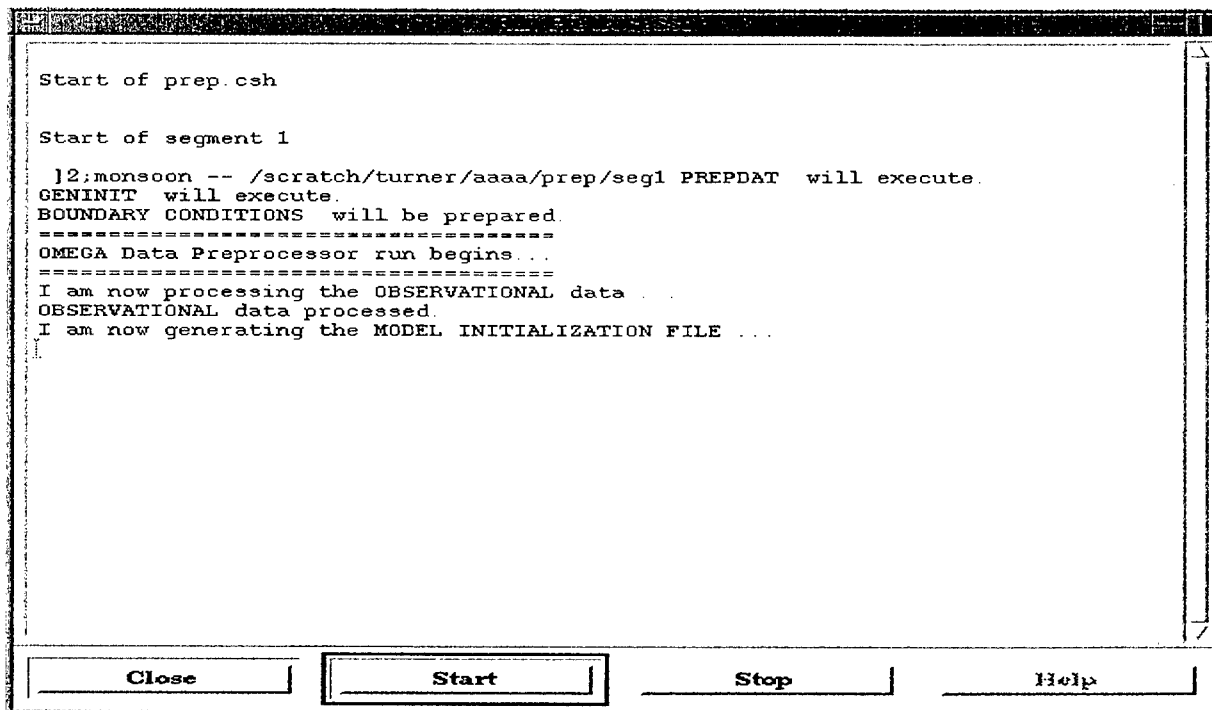


Figure 56. Run preprocessor dialog box.

If no set exists then the Preprocessor is started. While the Preprocessor is running only the Stop button will accept input. All other controls on this dialog, and XOMEGA are locked out.

Stop - If the Preprocessor is not running this button has no effect. If the Preprocessor is running this button stops it.

Note that when this button is pressed its effects may not be immediately apparent. It may take a few seconds for the "Stop" command to propagate to the Preprocessor program, and for XOMEGA to reset its windows and controls.

Since the external program is run through a UNIX pipe its output is sent back down the pipe to the dialog box. When the dialog is waiting for output from the program XOMEGA is unable to update its windows or process a "Stop" button press. If the user moves windows (or covers and uncovers them) parts of XOMEGA become gray. When the next line of output from the external program is piped to the dialog the windows will be redrawn and the button press processed. XOMEGA will reset itself.

Help - This button opens the Help dialog and load this section.

### **11.10.3 Run Preprocessor Warning.**

This dialog box is popped up when the user tries to run the Preprocessor and a valid set of initial and boundary conditions already exists. The top part of the dialog contains the warning message. The bottom part has a row of three action buttons:

- Overwrite - This button starts the Preprocessor. All existing information in the "prep/seg\*" sub-directories will be overwritten as the new files are made. The output from the Preprocessor appears in the Text Output Window normally. If the program has no errors the Run Preprocessor operation is completed.  
The Run Preprocessor Warning dialog is dismissed.  
The Run Preprocessor dialog remains.
- Proceed - This button accepts the existing files. The Run Preprocessor operation is completed.  
The Run Preprocessor Warning dialog is dismissed.
- Cancel - This button declines the existing files. The Run Preprocessor operation is NOT completed.  
The Run Preprocessor Warning dialog is dismissed.  
The Run Preprocessor dialog is dismissed

### **11.11 Run OMEGA Model.**

Once all preliminary setup steps are complete the user is ready to run the OMEGA Model. The Model is a single program that will use the grid the user has created and the preprocessed meteorology data gathered to simulate the atmosphere.

Please see Chapters 4,7,8 for more information on the OMEGA Model.

Since this program is independent of XOMEGA it needs to be called with a controlled process. Also since the Model may take a long time to run the process should be placed in the background. The mechanism for doing both these things is to use a small script program that will run the Model in the background and send status messages back to XOMEGA. As with the other external programs, a UNIX

pipe is used to send the text output of the script (status messages) back to XOMEGA into a read-only text window. The Model output (iteration information) is sent to a file called "model.log" in the case directory.

When clicking on "Run Model" a small dialog box pops up. This dialog consists of two sections: Text Output Window and a row of Action Buttons. Figure 57 shows the dialog after the Model has started.

Note that if the Run Grid Generator or Run Preprocessor operations have not been completed (i.e. no grid was made or data processed) then the Run Model dialog do not pop up. Instead an error message will pop up informing the user of the error. When acknowledging the error by clicking the "OK" button the appropriate dialogs pop up.

### 11.11.1 Text Output Window.

When initially popped up the Text Output Window will be blank. As the Model starts up the window will become filled with text. The output is saved as it scrolls off the window, and even saved when the dialog is popped down. The scroll bar on the right hand side of the window may be used to view text beyond the window. On subsequent pop-ups the previous information will still be in the Text Output Window. When the Model is fully running the window will show the current status of the run. About every 5 seconds the information will be updated.

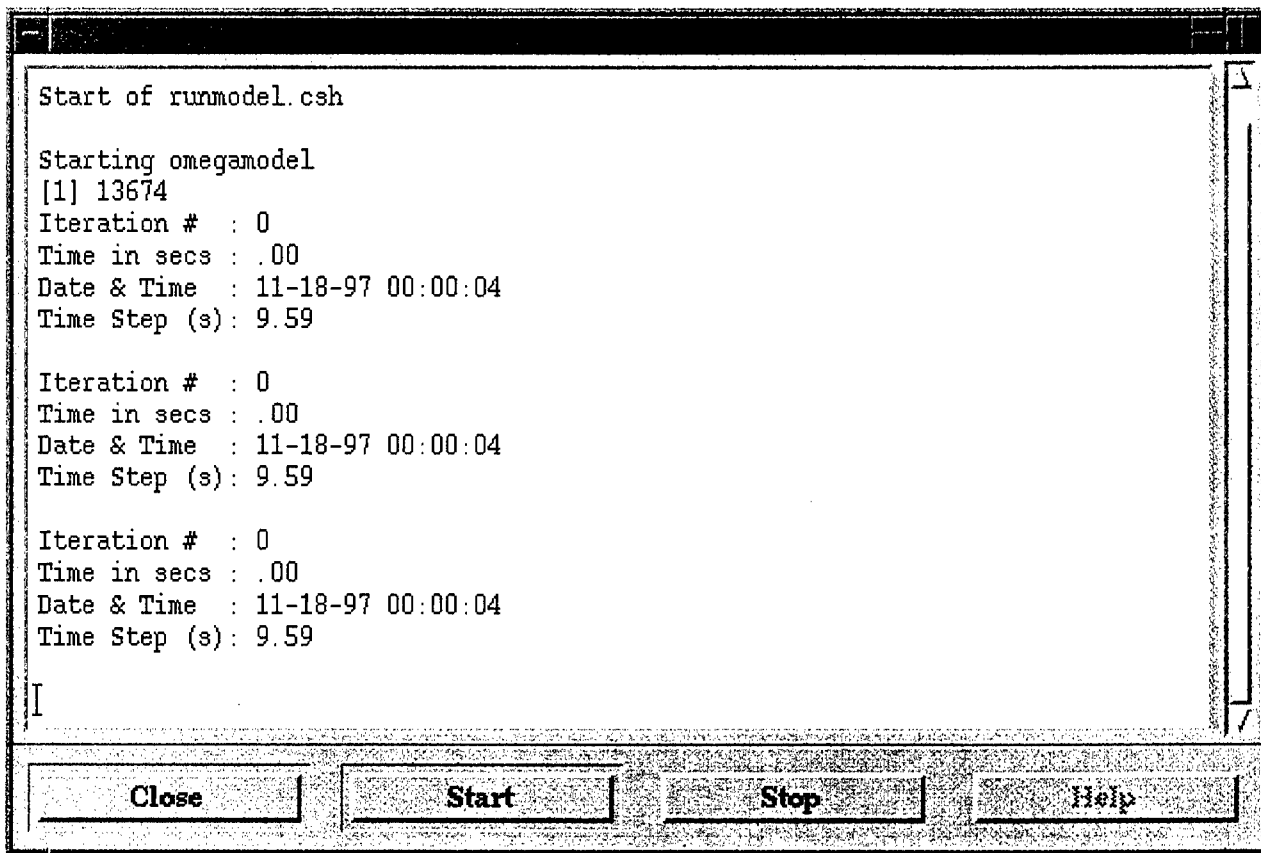


Figure 57. Run model dialog box.

### **11.11.2 Action Buttons.**

Close - This button dismisses the dialog box.

Start - When this button is pressed a check is made to determine if valid output already exist. If a valid set of output files already exists the Run Model Warning dialog box pops up.

See Section 11.11.3 for information on the Warning dialog box.

If no set exists then the Model is started. While the Model is running only the Stop button will accept input. All other controls on this dialog, and XOMEGA are locked out.

Stop - If the Model is not running this button has no effect. If the Model is running this button will stop the status reporting process. The Model itself will continue to run in the background and must be stopped from a terminal with the kill command.

Note that when you press this button its effects may not be immediately apparent. It may take a few seconds for the "Stop" command to propagate to the Model program, and for XOMEGA to reset its windows and controls.

Since the external program is run through a UNIX pipe its output is sent back down the pipe to the dialog box. When the dialog is waiting for output from the program XOMEGA is unable to update its windows or process a "Stop" button press. If the windows are moved (or covered and uncovered) parts of XOMEGA become gray. When the next line of output from the external program is piped to the dialog the windows will be redrawn and the button press processed. XOMEGA will reset itself.

Help - This button opens the Help dialog and load this section.

### **11.11.3 Run OMEGA Model Warning.**

This dialog box is popped up when you try to run the Model and a valid set of output files already exists. The top part of the dialog contains the warning message. The bottom part has a row of three action buttons:

Overwrite - This button starts the Model. All existing output files will be overwritten as the new files are made. The output from the Model will appear in the Text Output Window normally. The Run Model Warning dialog is dismissed. The Run Model dialog remains.

Proceed - This button accepts the existing files. The Run Model operation is completed. The Run Model Warning dialog is dismissed. The Run Model dialog is dismissed.

Cancel - This button declines the existing files. The Run Model operation is NOT completed. The Run Model Warning dialog is dismissed. The Run Model dialog is dismissed.

## Section 12

### OMEGA Output and Visualization

#### 12.1 OMEGA Output.

The OMEGA Model produces a variety of output files depending on the mode of operation. The frequency of output is controlled by the user and generally occurs for each hour of simulation time. The standard meteorological files are suffixed with ".pkb", which stands for "packed binary". Similar files which contain the same data but at full computer accuracy are generated at user defined intervals and used for restarting the model. These files are suffixed with ".out". If the user is running the ADM, a suite of other files may be generated as well. These files are currently written in ASCII.

Binary format files are smaller and more efficient to read. Thus, it is our aim to convert the ASCII format files to a binary format in the future. However, there is a cross-platform issue that has meant frequent post-processing of these binary files when porting to different platforms. We have resolved this problem by implementing a new type of format called "packed binary".

The packed binary format is a form of compression which results in files which are written and read on the byte level by routines written in the C programming language. These files are now completely portable and may be cross ported to any machine, including PCs. There is a small penalty in runtime, which is far made up for by savings in post-processing.

There is an additional cost in accuracy which is irrelevant for visualization. In the past, data has been written using eight bytes to represent one number. With packed binary, this same number may be represented by as little as one byte. Accuracy diminishes as fewer bytes are used. In practice we use two bytes, which results in accuracy to five significant digits, which is sufficient for most purposes. This will require one quarter the amount of disk space used in the past.

There is a requirement for files with full accuracy in order to restart the model. These files will continue to be produced as in the past in platform dependent binary, but less frequently than the routine files.

In the future we will be converting the remainder of OMEGA generated files to packed binary format which will result in a much smaller database and less time required for post-processing.

#### 12.2 XGRID - OMEGA Visualization Tool.

Due to the unstructured nature of the OMEGA grid, it is not easy to generate graphics with many of the common visualization packages. Hence SAIC designed and built a visualization tool for OMEGA to handle it's unique characteristics. This has also allowed us to make continuous improvements and add new features to the display system with relative ease.

XGRID is comprised of a graphical user interface (GUI), a viewing area for displaying the requested graphics, and a diagnostic text window. The first step in viewing OMEGA data is to open a .pkb file. This is done using a file selection browser launched from the File menu. XGRID will then search for and load its corresponding grid file and load the omega data into memory. At this point XGRID displays the grid terrain in the first of four possible modes: Layer - a horizontal section of the domain.

Additionally, the Field menu now becomes visible, allowing the user to select any of the meteorological fields, which have been generated from the model. A number of additional fields may be available, including some which are automatically calculated by XGRID upon loading the data; wind speed and direction, and mean sea level pressure. Surface characteristics will be available if the corresponding .srf file exists (Figure 58).

In layer mode the user may select a variety of different options: using the mouse and clicking the cursor on different cells in the viewing area will display all information for that cell in the diagnostic window. Clicking on the vertical scale bar to the right of the viewing area will change the horizontal level which is displayed. The user may use the View menu to have the data contoured, overlay map information, or overlay wind barbs or arrows. The viewing area may be zoomed in or out, and text, boxes, title or clock can be displayed, some of which can be user controlled through separate files (Figures 59, 60).

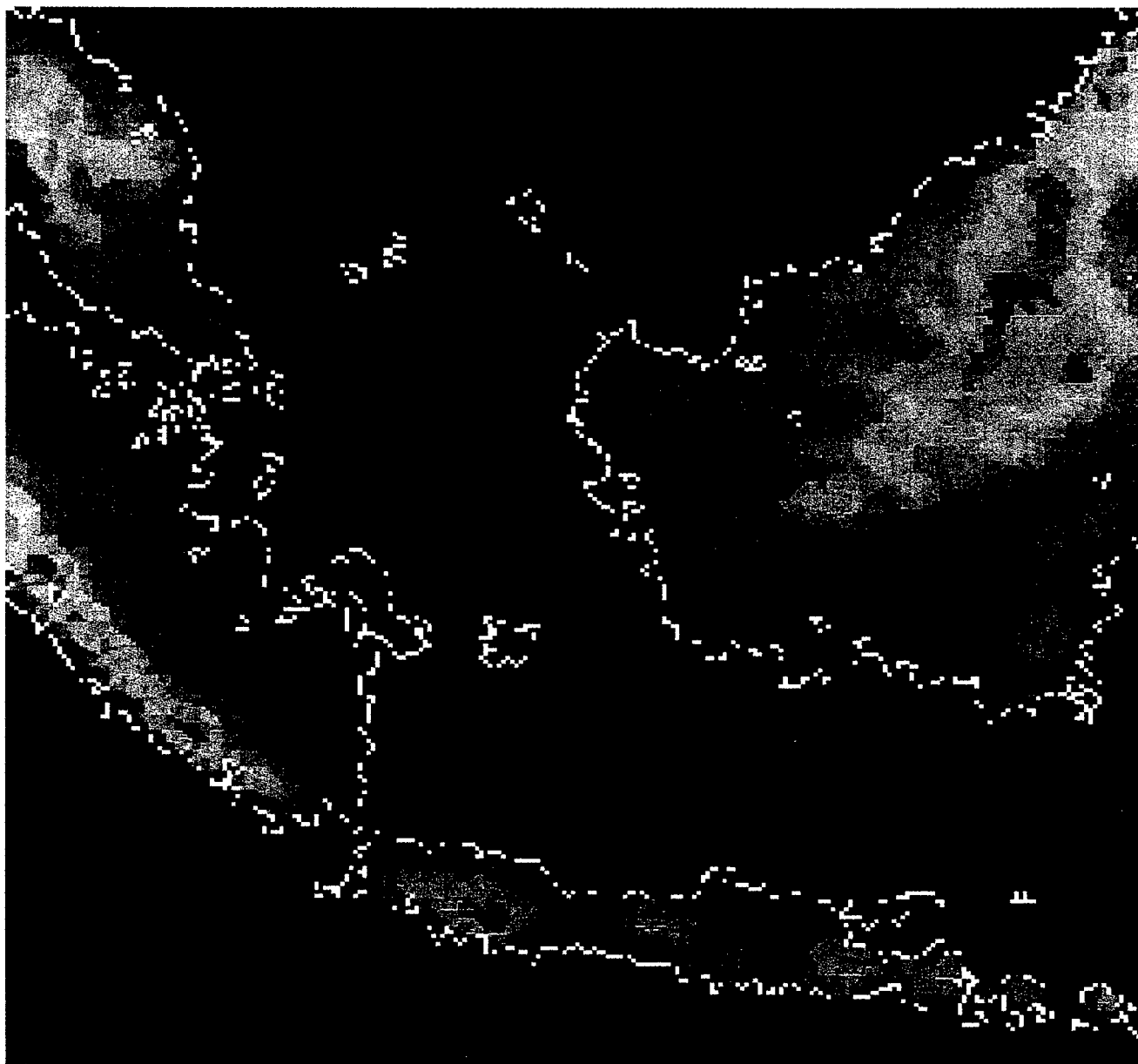


Figure 58. XGRID terrain view upon initial data load.

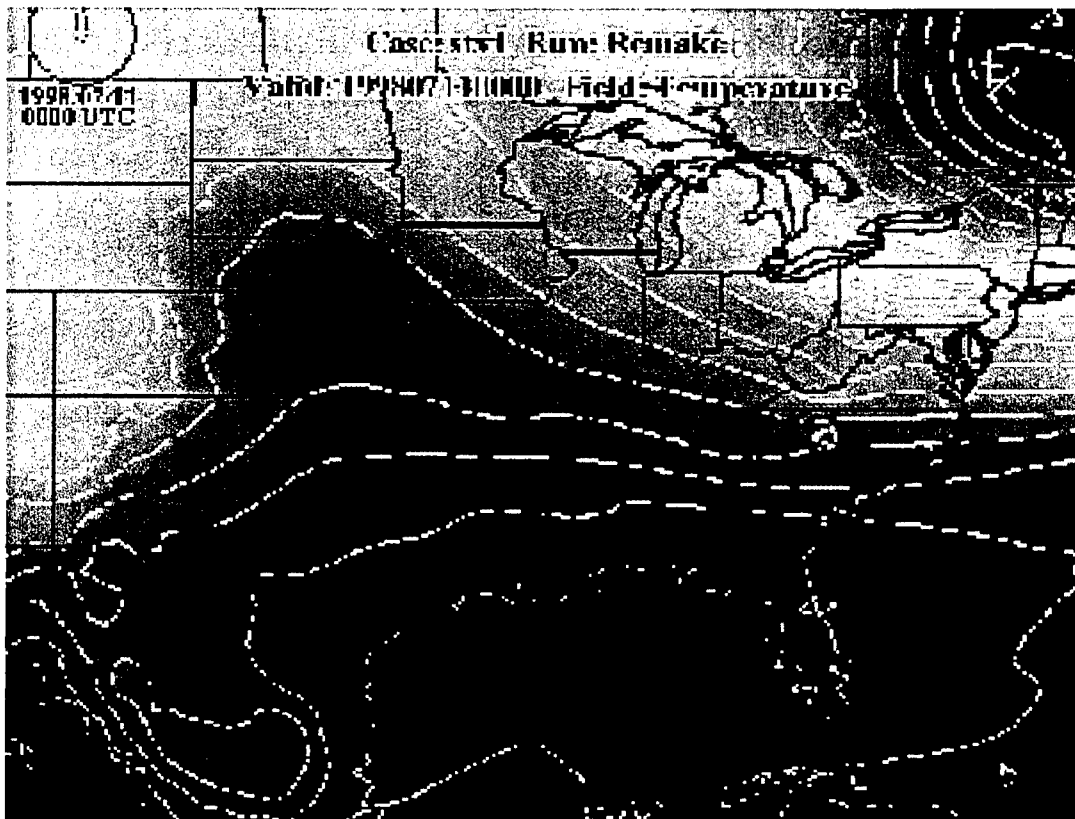


Figure 59. Display of map and contour options.

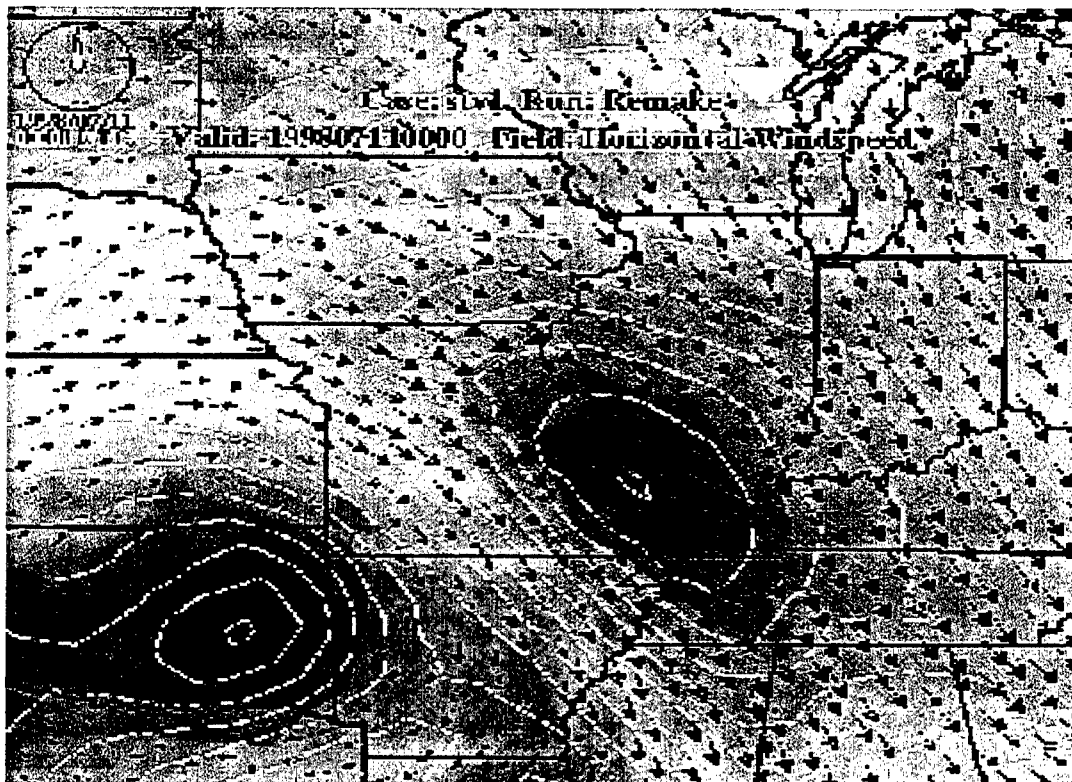


Figure 60. Zoomed in, with wind arrows.



The user may view data as a vertical cross section. When this mode is selected, the user may click on the display and drag a line across the area of interest. When the button is released, XGRID will display a vertical cross section of the current field corresponding to this line (Figure 61).

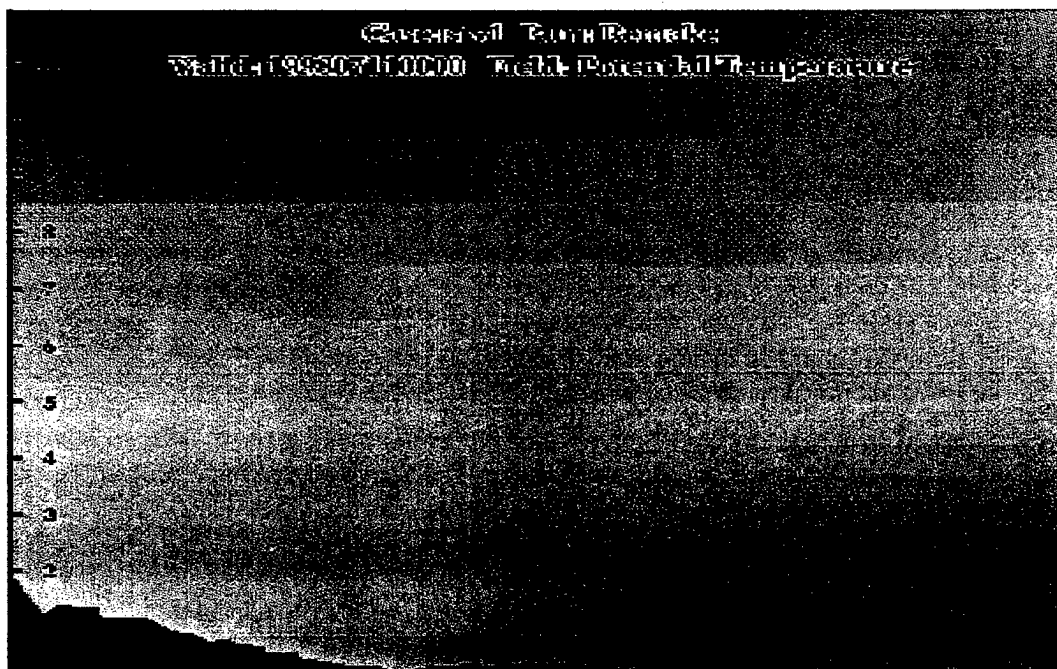


Figure 61. XGRID vertical cross section.

Vertical point profiles may be generated for any field with vertical extent (Figure 62).

Lastly, one may view a thermodynamic diagram called a SkewT-logP, which depicts a vertical profile of temperature and dewpoint (Figure 63).

OMEGA ADM files may be displayed on XGRID showing the location of each particle, in layer or cross section mode (see section 10). Particle trajectories and field of regard may also be displayed (Figure 64). When the model is run in Puff mode, concentrations of Lagrangian tracers may be viewed (Figure 65).

The new version of XGRID has undergone extensive internal change. Most memory allocation is now done dynamically, which negates the requirement for recompilation when viewing larger grids. This and the removal of all FORTRAN code have reduced the program memory requirements from 135 MB to about 2 MB. Extensive streamlining of the code will make it much easier to adapt in the future. Planned capabilities include reading structured grids from other models, animation on the fly, a new GUI with multiple display windows, and grid editing. Additionally, the new packed binary files will allow us to have only currently required data in memory. This will allow even greater speed and memory savings.

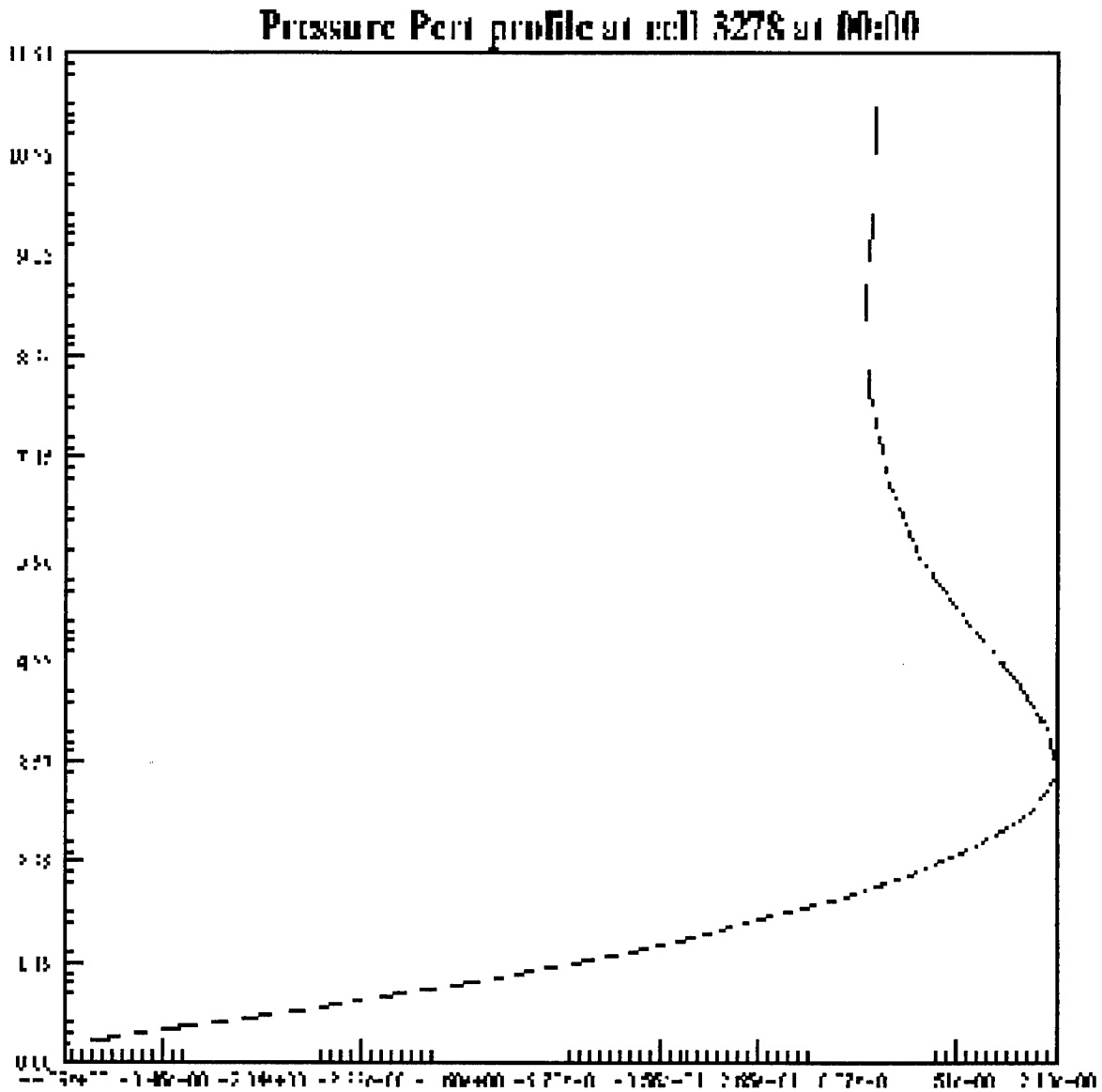


Figure 62. XGRID profile.

### 12.3 OMEGA Simulation Image Maker (OSIM).

While XGRID has the ability to create graphics guided by the user, there is a requirement for system generated graphics. XGRID has the capability of reading and executing a script file, but must do so under an actively running XGRID process with the GUI displayed. A new command line version of XGRID has been created which reads a script file for its instructions. SAIC has created a web page on a remote system using this program which will substantially reduce the required bandwidth for viewing desired data.

The first step in the process is to access the OSIM web page (Figure 66). This page displays the runs and valid times available in the database, which the user must select from.

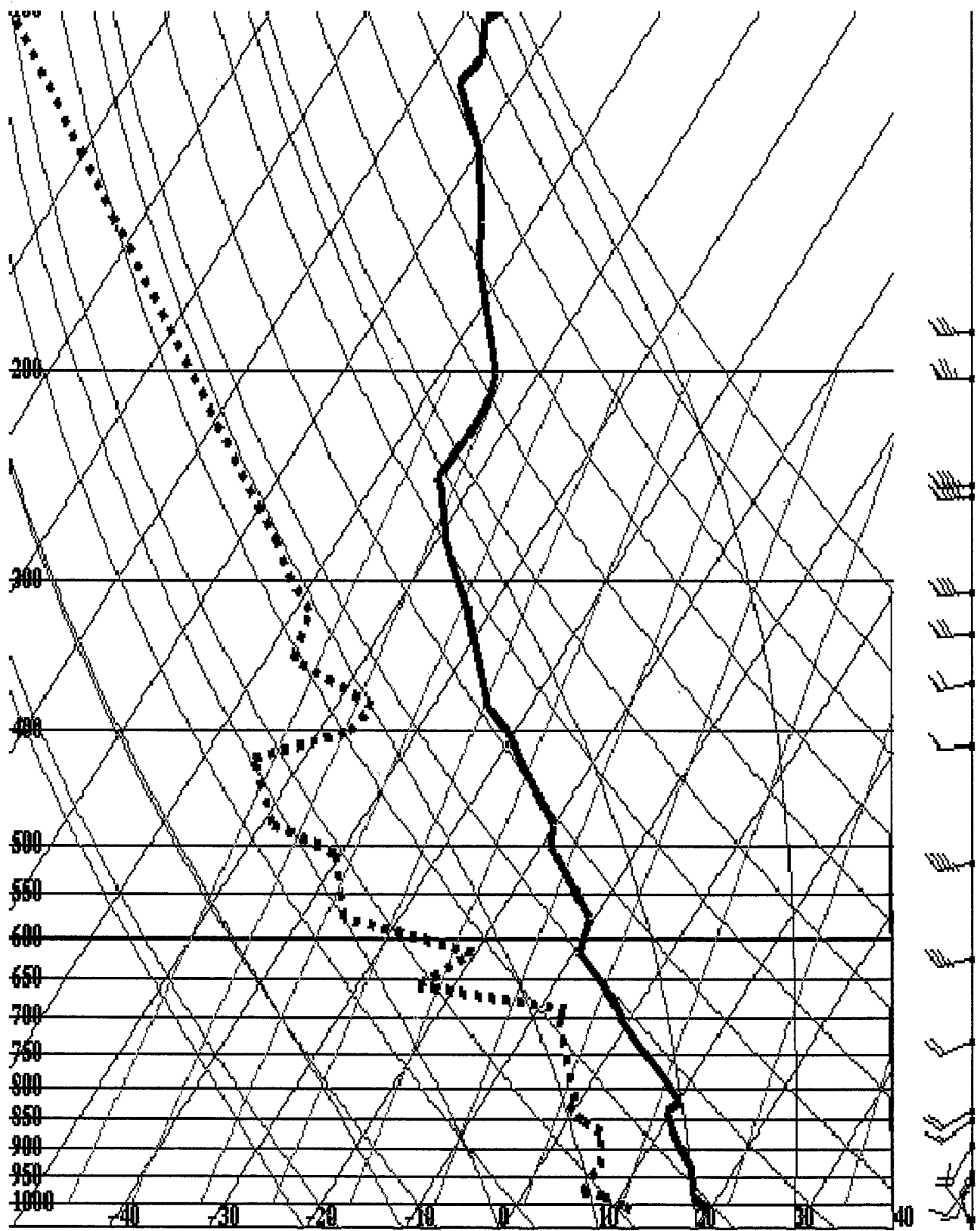


Figure 63. XGRID skewT-logP diagram.

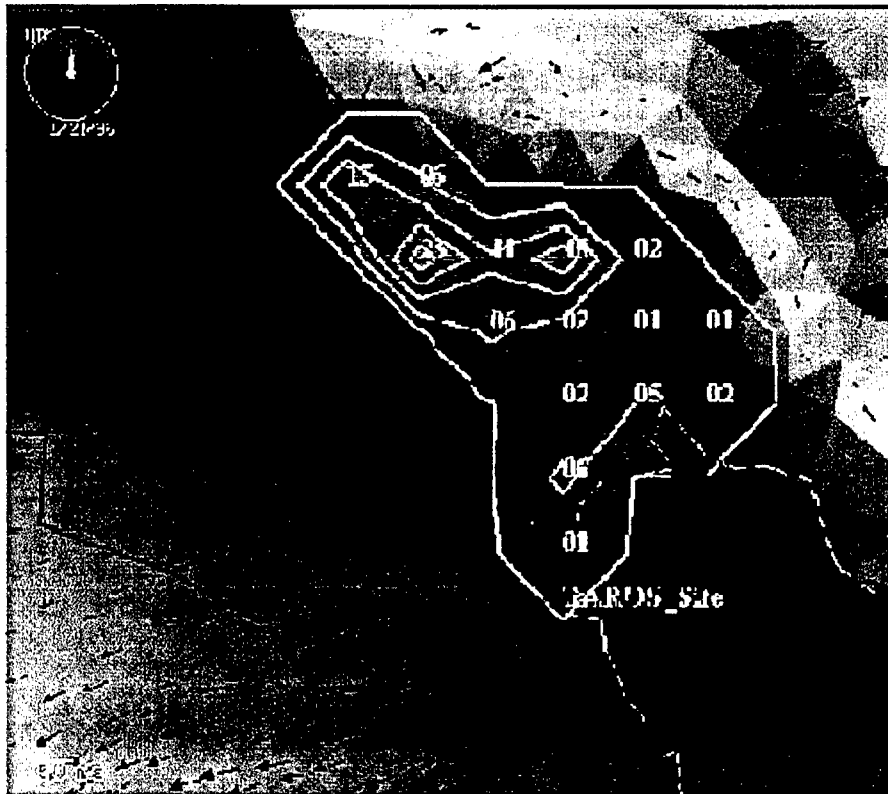


Figure 64. Field of regard and particle trajectories.

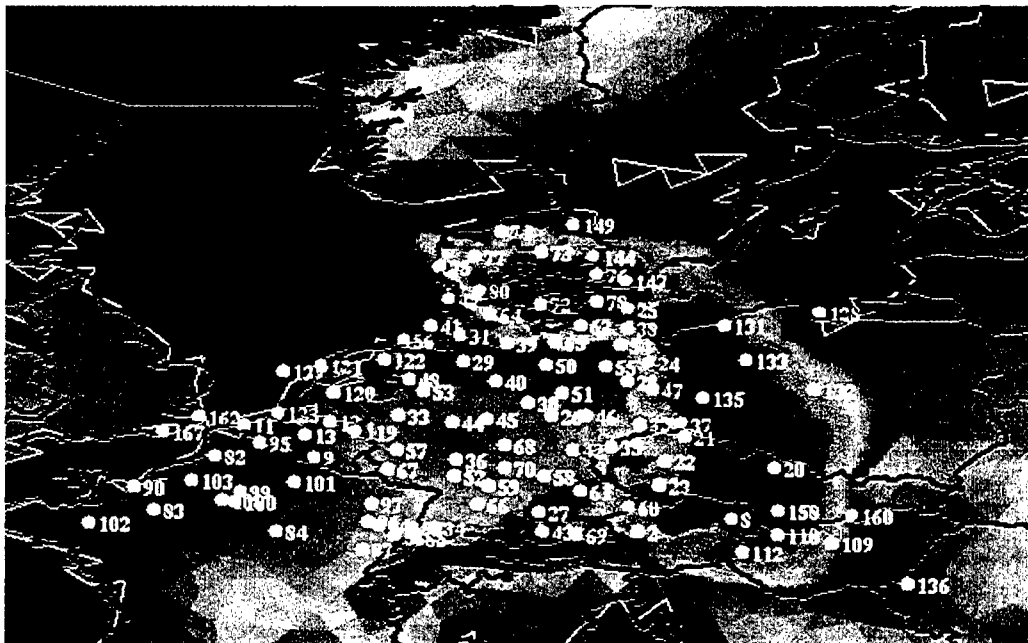


Figure 65. Concentration values computed from the ADM Lagrangian tracers.



# OMEGA Simulation Image Maker (OSIM)

## 1. Select a Single Valid Forecast Time

Cases	Runs	00h Analysis	12h Forecast	24h Forecast	36h Forecast	48h Forecast
dj4b	1998060700	◇	◇	◇	◇	◇
ind1	1998051100	◇	◇	◇	◇	unavailable
jsb2	1998031700	◇	◇	◇	◇	◇
jsb2	1998031800	◇	◇	◇	◇	unavailable

OSIM

OMEGA

APO

SAIC

© 1998 SAIC

1998-08-31 12:42:11 UTC

[turner@apo.saic.com](mailto:turner@apo.saic.com)

Figure 66. OSIM stage one.



# OMEGA Simulation Image Maker (OSIM)

## Current Active Simulation:

Case: ind1

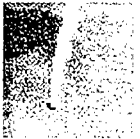
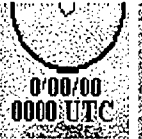

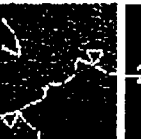

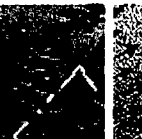
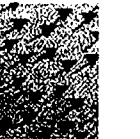
Run: 1998051100

Valid Time: 199805111200

## 2. Select Fields and Options

Please select one or more **Fields** to plot.  
For each field selected choose zero or more **Plot Options**.

*ADM particles available only for some runs.*

Fields	Plot Options						
	ADM Particles	Clock	Contours	Grid	Lat/Lon Lines	Map	Wind Vectors
							
<input type="checkbox"/> Pressure	<input type="checkbox"/>	<input type="checkbox"/>	<input type="checkbox"/>	<input type="checkbox"/>	<input type="checkbox"/>	<input type="checkbox"/>	<input type="checkbox"/>
<input type="checkbox"/> Wind Speed	<input type="checkbox"/>	<input type="checkbox"/>	<input type="checkbox"/>	<input type="checkbox"/>	<input type="checkbox"/>	<input type="checkbox"/>	<input type="checkbox"/>
<input type="checkbox"/> Temperature	<input type="checkbox"/>	<input type="checkbox"/>	<input type="checkbox"/>	<input type="checkbox"/>	<input type="checkbox"/>	<input type="checkbox"/>	<input type="checkbox"/>
<input type="checkbox"/> Terrain	<input type="checkbox"/>	<input type="checkbox"/>	<input type="checkbox"/>	<input type="checkbox"/>	<input checked="" type="checkbox"/>	<input type="checkbox"/>	<input type="checkbox"/>

OSIM

OMEGA

APO

SAIC

© 1998 SAIC

1998-08-31 12:43:26 UTC

[tuner@apo.saic.com](mailto:tuner@apo.saic.com)

Figure 67. OSIM stage two.

The second step is the selection of desired fields and display options (Figure 67). When this step is completed, the web server calls a program which generates an XGRID script, then calls the command line version of XGRID. The requested graphics are then linked back to the web server, which displays them on the page (Figure 68).

This new capability will drastically reduce the bandwidth required to get model results to users in the field. It is no longer necessary to transport large data files across the Internet in order to view a relatively small portion of that data.

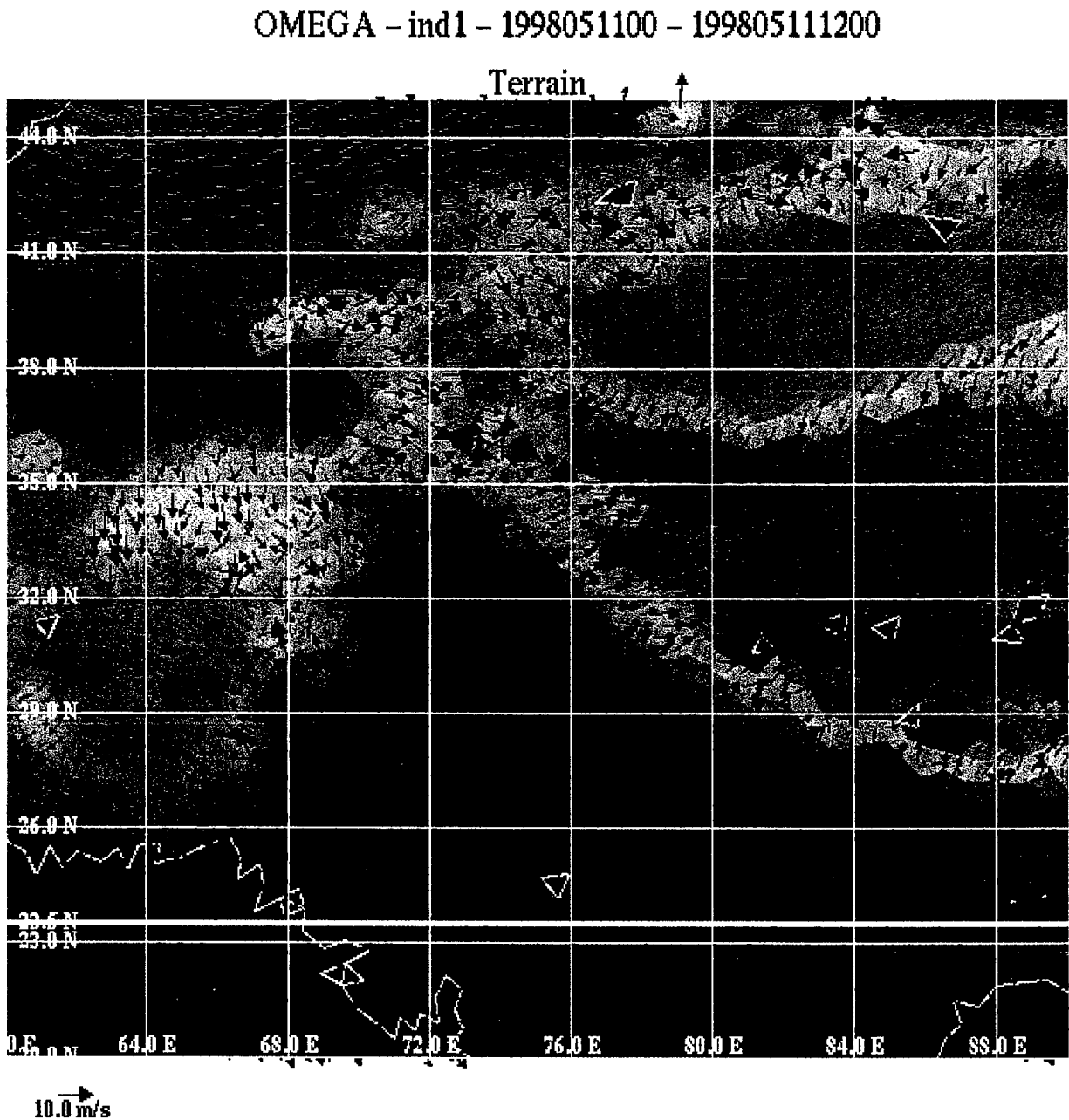


Figure 68. OSIM stage three.

## Section 13

### Conclusions

OMEGA has grown tremendously over the last three years. Major changes have been made throughout the OMEGA modeling system, from the GUI to the Post-processors. The OMEGA GUI, XOMEGA, has been made more powerful, while maintaining its user-friendliness. We have added case management, greatly expanded the options and capabilities for specifying the meteorological data to be used for initial and boundary conditions, increased the possibilities for grid refinement through the interface, and added additional controls on the ADM model. The grid generator was made more capable, adding point refinement routines and automating the generation of surface description fields (*e.g.*, land use, soil type, vegetation). The OMEGA data pre-processor was improved adding more sources of data that can be accepted and adding options for mixing and matching data sources to create the initial and lateral boundary conditions.

The OMEGA model itself was greatly improved. A new time-split solver was implemented so that the entire model would not be restricted by the smallest cell. This has greatly reduced run-time and improved performance. Dynamic grid adaptation was implemented so that the resolution can be maintained in a limited region of intense interest. And a first prototype parallel version using MPI has been tested. In addition, major changes were made in the model physics including the PBL model and the inclusion of inhomogeneous surface properties, explicit cloud microphysics, statistical output routines to support the HPAC model with direct values of the variance of the OMEGA wind parameters over an extended (*e.g.*, 1 hour) sample period, and updating the re-start capability to include all of these changes. The Atmospheric Dispersion Model (ADM) was also upgraded to include a probabilistic transport model based on the concentration variance.

The model output format was changed to a machine independent, packed binary data format that is both more efficient in its storage requirement and considerably speeds up the post-processing of OMEGA output. The post-processing now includes quantitative verification routines (see Volume II) and a new, Web-based graphics visualization system was prototyped, the OMEGA Web Links (OWL) and the OMEGA Simulation Image Maker (OSIM). These systems permit custom product generation and display over the World Wide Web with very modest hardware; the prototype system used a 233 MHz Pentium II PC.

OMEGA has again re-defined the state-of-the art in numerical weather prediction and atmospheric dispersion. It has been subjected to a suite of operational and field tests, which is the subject of Volume II of this report.



## Section 14

### References

- AGARD (Advisory Group for Aerospace Research and Development), 1992: Special course on unstructured grid methods for advection dominated flows. AGARD-R-787, NATO, Neuilly sur Seine, France. (UNCLASSIFIED)
- Andre J. C., G., De Moor, P. Lacarrere, G. Therry, and R. du Vachat, 1978: Modeling the 24-hour evolution of the mean and turbulent structures of the planetary boundary layer. *J. Atmos. Sci.*, **35**, 1861-1883. (UNCLASSIFIED)
- Anthes R. A., 1977a: A cumulus parameterization scheme utilizing a one-dimensional cloud model. *Mon. Wea. Rev.*, **105**, 270-286. (UNCLASSIFIED)
- Anthes R. A., 1977b: Hurricane model experiments with a new cumulus parameterization scheme. *Mon. Wea. Rev.*, **105**, 287-300. (UNCLASSIFIED)
- Artz, R., R. A. Pielke, and J. Galloway, 1985: Comparison of the ARL/ATAD constant level and the NCAR isentropic trajectory analyses for selected case studies. *Atmos. Env.*, **19**, 47-63. (UNCLASSIFIED)
- Arya S. P. S., 1988: *Introduction to Micrometeorology*. Academic Press, New York. (UNCLASSIFIED)
- Atwater M. A., and P. S. Brown Jr., 1974. Numerical; calculation of the latitudinal variation of solar radiation for an atmosphere of varying opacity. *J. Appl. Meteor.*, **13**, 289-297. (UNCLASSIFIED)
- Barnes, S. L., 1964: A technique for maximizing details in numerical weather map analysis. *J. Appl. Meteor.*, **3**, 396-409. (UNCLASSIFIED)
- Baum, J. D., and R. Lohner, 1989: Numerical simulation of shock-elevated box interaction using an adaptive finite element shock capturing scheme. *Proc. of the 27th Aerospace Science Meeting, AIAA-89-0653*. (UNCLASSIFIED)
- Baum, J. D., H. Luo, and R. Lohner, 1993: Numerical simulation of a blast inside a Boeing 747. *AIAA 93-3091, 24th Fluid Dynamics Conference*. (UNCLASSIFIED)
- Bennet, C. R., M. K. Patel, J. Zhao, and L. Hu, 1998: Grid Adaption Strategies using Neural Networks. *Proceedings of the 6th International Conference on Numerical Grid Generation in Computational Field Simulations*. Greenwich, England. 869-878. (UNCLASSIFIED)
- Berry, E. X., and R. L. Reinhardt, 1974a: An analysis of cloud drop growth by collection: Part I. Double distributions. *J. Atmos. Sci.*, **31**, 1814-1824. (UNCLASSIFIED)
- Berry, E. X., 1974b: An analysis of cloud drop growth by collection: Part II. Single initial distributions. *J. Atmos. Sci.*, **31**, 1825-1831. (UNCLASSIFIED)
- Boussinesq J., 1877. Essai sur la theorie des courantes. *Mem. Pres. Divers Svant Acad. Sci., Paris*, **23**, 46. (UNCLASSIFIED)
- Boybeyi, Z., and S. Raman, 1992: A three-dimensional numerical sensitivity study of convection over the Florida peninsula. *Boundary-Layer Meteorology*. **60**, 325-359. (UNCLASSIFIED)

- Boybeyi, Z., S. Raman, and P. Zannetti, 1995: Numerical investigation of possible role of local meteorology in Bhopal gas accident. *Atmos. Env.*, **28** (in press). (UNCLASSIFIED)
- Businger J. A., J. C. Wyngaard, Y. Izumi, and E. F. Bradley , 1971: Flux-profile relationships in the atmospheric surface layer. *J. Atmos. Sci.*, **28**, 181-189. (UNCLASSIFIED)
- Byers, H. R., and H. R. Rodebush, 1948: Causes of thunderstorms of the Florida peninsula. *J. Meteorol.*, **5**, 275-280. (UNCLASSIFIED)
- Chang, J. T., and P. J. Wetzel, 1990: Effects of spatial variations of soil moisture and vegetation on the evolution of a prestorm environment: A numerical case study. *Mon. Wea. Rev.*, **119**, 1368-1390. (UNCLASSIFIED)
- Charnock H., 1955: Wind stress on a water surface. *Quart. Jl. R. Met. Soc.*, **81**, 639-640. (UNCLASSIFIED)
- Daley, R., 1991: *Atmospheric Data Analysis*. Cambridge University Press, 457 pp. (UNCLASSIFIED)
- Deardoff J. W., 1974: Three-dimensional study of the height and mean structure of a heated planetary boundary layer. *Boundary Layer Met.*, **7**, 81-106. (UNCLASSIFIED)
- Deardoff J. W., 1978: Efficient prediction of ground surface temperature and moisture with inclusion of a layer of vegetation. *J. Geophys. Research.* **83**(C4), 1889-1903. (UNCLASSIFIED)
- Deardoff J. W., 1980: Stratocumulus-capped mixed layer derived from a three-dimensional model. *Boundary-Layer Meteor.*, **18**, 495-527. (UNCLASSIFIED)
- Dennis, R. L., and J. H. Novak, 1991: "EPA's third generation modeling system (Models-3): An overview." Proceedings, *Tropospheric Ozone and the Environment II: Effects, Modeling and Control*, TR-20, Atlanta, GA, Air & Waste Management Association, 137-147 (1991). (UNCLASSIFIED)
- Dessert, S. (Jaycor), R. Gibbs (NSWC), R. E. McNally (SAIC), M. G. B. Pace (MITRE), and S. White (LANL), 1991: *Programmer's Guide to the Chemical/Biological Simulation System for ANBACIS II, An Improved Chem/Bio Downwind Hazard Prediction Support System for Operation Desert Storm*. Jaycor, Dayton, OH; NSWC, Dahlgren, VA; Science Applications International Corporation, Joppa, MD; MITRE, McLean, VA; and LANL, Los Alamos, NM. (UNCLASSIFIED)
- Dey, C. H., and L. L. Morone., 1985: Evolution of the National Meteorological Center Global Data Assimilation System: January 1982 - December 1983. *Mon. Wea. Rev.*, **113**, 304-318. (UNCLASSIFIED)
- Dietachmeyer, S. G., and K. K. Droegemeier, 1991: Application of continuous dynamic grid adaptation techniques to meteorological modeling, Part I: Basic formulation and accuracy. *Mon. Wea. Rev.*, **120**, 1675-1706. (UNCLASSIFIED)
- Dietachmeyer, G. S., and K. K. Droegemeier, 1992: Application of Continuous Dynamic Grid Adaptation Techniques to Meteorological Modeling. Part I: Basic Formulation and Accuracy. *Mon. Wea. Rev.*, **120**, 1675-1706. (UNCLASSIFIED)
- DiMego, G. J., 1988: The National Meteorological Center regional analysis system. *Mon. Wea. Rev.*, **116**, 977-1000. (UNCLASSIFIED)
- Dudia, J., 1993: A nonhydrostatic version of the Penn State/NCAR mesoscale model: Validation tests and simulation of an Atlantic cyclone and cold front. *Mon. Wea. Rev.*, **121**, 1493-1513. (UNCLASSIFIED)

- Dunn, T. J., D. P. Bacon, S. E. Peckham, and R. A. Sarma, 1995: Single Burst Nuclear Cloud Database Volume 5 - Sensitivity Studies, Defense Nuclear Agency, DNA-TR-94-34-V5 (UNCLASSIFIED).
- Duynkerke P. G. and A. G. Driedonks, 1987: A model for the turbulent structure of the stratocumulus-topped atmospheric boundary layer. *J. Atmos. Sci.*, **44**, 43-64. (UNCLASSIFIED)
- EDC-NESDIS, 1992: Monthly Global Vegetation Index from Gallo Bi-Weekly Experimental Calibrated GVI (April 1985-December 1990). Digital raster data on a 10-minute Geographic (lat/long) 1080x2160 grid. In: *Global Ecosystems Database Version 1.0: Disc A*. Boulder, CO: NOAA National Geophysical Data Center. 69 independent single-attribute data layers on CD-ROM, 161 MB. [first published in 1991]. (UNCLASSIFIED)
- Eidenshink, J. E., 1992: The conterminous United States AVHRR data set. *Photogrammetric Engineering & Remote Sensing.*, **58**, 809-813. (UNCLASSIFIED)
- Fiedler, B., Z. Huo, and P. Zhang, 1998: Dynamic Grid Adaption for Atmospheric Boundary Layers. *Proc. of the 12th Conf. on Num. Wea. Prediction*. AMS. 253-254. (UNCLASSIFIED)
- Fletcher, N. H., 1962: *The Physics of Rainclouds*. Cambridge University Press, 386 pp. (UNCLASSIFIED)
- Foote, B., 1991: *Scientific Overview and Operations Plan for the Convection and Precipitation/Electrification Experiment (CaPE)*. A cooperative program sponsored by the National Science Foundation, Federal Aviation Administration, National Oceanic and Atmospheric Administration, and Air Force. (UNCLASSIFIED)
- Frank, N. L., P. L. Moore, and G. E. Fisher, 1967: Summer shower distribution over the Florida peninsula as deduced from digitized radar data'. *J. Appl. Meteorol.*, **6**, 309-316. (UNCLASSIFIED)
- Fritts M. H., 1988: Adaptive gridding strategies for Lagrangian calculations. *Comput. Phys. Comm.*, **48**, 75 (1988). (UNCLASSIFIED)
- Gandin, L., 1963: Objective analysis of meteorological fields, (English translation, 1965): Program for Scientific Translations. Jerusalem, Israel, 242 pp. (UNCLASSIFIED)
- Gandin, L. S., 1988: Complex quality control of meteorological observations. *Mon. Wea. Rev.*, **116**, 1137-1156. (UNCLASSIFIED)
- Gerald, C. F., and P. O. Wheatley, 1983: Applied Numerical Analysis. 3rd edition. Addison-Wesley. (UNCLASSIFIED)
- Hedstrom, G. W., 1979: Nonreflecting boundary condition for nonlinear hyperbolic systems. *J. Comp. Phys.*, **30**, 222-237. (UNCLASSIFIED)
- Hess, S. L., 1959: *Introduction to Theoretical Meteorology*. Holt, Rinehart, and Winston, New York. (UNCLASSIFIED)
- Hoke, J. E., N. A. Phillips, G. J. DiMego, J. J. Tuccillo, and J. G. Sela, 1989: The regional analysis and forecast system of the National Meteorological Center. *Wea. Forecasting*. **4**, 323-334. (UNCLASSIFIED)
- Holmes, D. G., and S. D. Connell, 1989: Solution of the 2D Navier-Stokes Equations on Unstructured Adaptive Grids. AIAA. Paper AIAA-89-1932. (UNCLASSIFIED)

- Jacobs C. A., Pandolfo J. B., and Atwater M. A., 1974: A description of a general three dimensional numerical simulation model of a coupled air-water and/or air-land boundary layer. IFYGL final report, CEM Report No. 5131-509a. (UNCLASSIFIED)
- Janjic, Z. I., 1990: The step-mountain coordinate: physical package. *Mon. Wea. Rev.*, **118**, 1429-1443. (UNCLASSIFIED)
- Kasten F., and G. Czeplak , 1980: Solar and terrestrial radiation dependent on the amount and type of cloud. *Solar Energy*. **24**, 177-189. (UNCLASSIFIED)
- Klemp, J. B., and D. R. Durran, 1983: An Upper Boundary Condition Permitting Internal Gravity Wave Radiation in Numerical Mesoscale Models. *Mon. Wea. Rev.*, **111**, 430-444. (UNCLASSIFIED)
- Klemp, J. B., and D. K. Lilly, 1978: Numerical simulation of hydrostatic mountain waves. *J. Atmos. Sci.*, **32**, 78-107. (UNCLASSIFIED)
- Kondratyev J., 1969: *Radiation in the Atmosphere*. Academic Press, New York, 912 pp. (UNCLASSIFIED)
- Kuhn P. M., 1963: Radiometeorsonde observations of infrared flux emissivity of water vapor. *J. Appl. Meteor.*, **2**, 368-378. (UNCLASSIFIED)
- Kuo H. L., 1965: On formation and intensification of tropical cyclones through latent heat release by cumulus convection. *J. Atmos. Sci.*, **22**, 40-63. (UNCLASSIFIED)
- Kuo H. L., 1974: Further studies of the parameterization of the influence of cumulus on large scale flow. *J. Atmos. Sci.*, **31**, 1232-1240. (UNCLASSIFIED)
- Kuo Y.-H., and R. A. Anthes, 1984: Semiprognostic tests of Kuo-type cumulus parameterization schemes in an extratropical convective system. *Mon Wea. Rev.*, **112**, 1498-1509. (UNCLASSIFIED)
- Legates, D. R., and C. J. Willmott, 1992: Monthly Average Surface Air Temperature and Precipitation. Digital raster data on a 30 minute geographic (lat/long) 360x720 grid. In: *Global Ecosystems Database Version 1.0: Disc A*. Boulder, CO: NOAA National Geophysical Data Center. 48 independent and 4 derived single-attribute spatial layers on CD-ROM, 47.2 MB. [first published in 1989]. (UNCLASSIFIED)
- List, R. J., 1971: *Smithsonian Meteorological Tables*. Smithsonian Institution Press, Washington, D. C. (UNCLASSIFIED)
- Lottati, I., and S. Eidelman, 1994: A second-order Godunov scheme on a spatial adapted triangular grid. *Applied Numerical Mathematics*. **14**, 353-365. (UNCLASSIFIED)
- Luo, H., J. D. Baum, R. Lohner, and J. Cabello, 1994: Implicit schemes and boundary conditions for compressible flows on unstructured meshes. *AIAA 94-0816*, 32nd Aerospace Sciences Meeting and Exhibit, Reno, NV. (UNCLASSIFIED)
- Mahrer Y., and R. A. Pielke, 1977: The effects of topography on the sea and land breezes in a two-dimensional numerical model. *Mon. Wea. Rev.*, **105**, 1151-1162. (UNCLASSIFIED)
- Marshall, J. S., and Palmer, W. M., 1948: The distribution of raindrops with size. *J. Meteor.*, **5**, 165-166. (UNCLASSIFIED)
- Mailhot J., and Benoit R., 1982: A finite-element model of the atmospheric boundary layer suitable for use with numerical weather prediction. *J. Atmos. Sci.*, **39**, 2249-2266. (UNCLASSIFIED)

- McCorcle, M. D., 1988. Simulation of soil moisture effects on the Great Plains low-level jet. *Mon. Wea. Rev.*, **116**, 1705-1720. (UNCLASSIFIED)
- McDonald J. E., 1960: Direct absorption of solar radiation by atmospheric water vapor. *J. Meteor.*, **17**, 319-328. (UNCLASSIFIED)
- McNally, R. E., 1991: *Support to Desert Shield/Storm: Activities and Observations*. Science Applications International Corporation, Joppa, MD. (UNCLASSIFIED)
- McNider, R. T., M. D. Moran and R. A. Pielke, 1988: Influence of diurnal and inertial boundary layer oscillations on long-range dispersion. *Atmos. Env.*, **22**, 2445-2462. (UNCLASSIFIED)
- McPherson, R. D., 1970: A numerical study of the effect of a coastal irregularity on sea breeze. *J. Appl. Meteorol.*, **9**, 767-777. (UNCLASSIFIED)
- McPherson, R., 1991: 2001 - An NMC Odyssey. *Ninth Conf. on Num. Wea. Prediction*. AMS, Boston, MA. (UNCLASSIFIED)
- Mellor G. L., and T. Yamada, 1974: A hierarchy of turbulence closure models for planetary boundary layers. *J. Atmos. Sci.*, **31**, 1791-1806. (UNCLASSIFIED)
- Mellor G. L. and T. Yamada, 1982: Development of a turbulence closure model for geophysical fluid problems. *Rev. Geophys. Space Phys.*, **20**, 851-875. (UNCLASSIFIED)
- Mesinger, F., Z. I. Janjic, S. Nickovic, D. Gavrilov, and D. G. Deaven, 1988: The step-mountain coordinate: Model description and performance for cases of Alpine lee cyclogenesis and for a case of an Appalachian redevelopment. *Mon. Wea. Rev.*, **116**, 1494-1518. (UNCLASSIFIED)
- O'Brien J. J., 1970: A note on the vertical structure of the eddy exchange coefficient in the planetary boundary layer. *J. Atmos. Sci.*, **27**, 1213-1215. (UNCLASSIFIED)
- Olson, J. S., 1992: World Ecosystems (WE1.4). Digital Raster Data on a 10-minute Geographic 1080x2160 grid. In: *Global Ecosystems Database Version 1.0: Disc A*. Boulder, CO: NOAA National Geophysical Data Center. Three independent single-attribute spatial layers on CD-ROM, 5 MB. [first published in 1991]. (UNCLASSIFIED)
- Pack, D. H., G. J. Ferber, J. L. Heffter, K. Telegadas, J. K. Angell, W. H. Hoecker, and L. Machta, 1978: Meteorology of long range transport. *Atmos. Env.*, **12**, 425-444. (UNCLASSIFIED)
- Paegle, J., J. N. Paegle, M. McCorcle, and E. Miller, 1984: Diagnoses and numerical simulation of a low-level jet during ALPEX. *Beitr. Phys. Atmos.*, **57**, 419-430. (UNCLASSIFIED)
- Pearson, R. A., 1973: Properties of the sea breeze front as shown by a numerical model. *J. Atmos. Sci.*, **30**, 1050-1060. (UNCLASSIFIED)
- Pennsyle, R. O., 1991: NUSSE4: Improvements and Extensions of the NUSSE3 Model. U.S. Army Chemical Research, Development and Engineering Center CRDEC-TR-xxxx, 290 pp. (UNCLASSIFIED)
- Peraire, J., K. Morgan, and J. Peiro, 1990: Unstructured mesh methods for CFD. In *Numerical Grid Generation*, Von Karman Institute for Fluid Dynamics, Lecture Series. 1990-06. (UNCLASSIFIED)
- Perkey, D. J., and C. W. Kreitzberg, 1976: A Time-Dependent Lateral Boundary Scheme for Limited-Area Primitive Equation Models. *Mon. Wea. Rev.*, **104**, 744-755. (UNCLASSIFIED)

- Pielke, R. A., 1974: A three-dimensional model of the sea breezes over south Florida. *Mon. Wea. Rev.*, **102**, 115-139. (UNCLASSIFIED)
- Pielke, R. A., W. A. Lyons, R. T. McNider, M. D. Moran, D. A. Moon, R. A. Stocker, R. L. Walko, and M. Uliasz, 1991: Regional and mesoscale meteorological modeling as applied to air quality studies. In *Air Pollution Modeling and its Application VIII*, p259-289, H. van Dop and D. G. Steyn (eds), Plenum Press, New York. (UNCLASSIFIED)
- Pitts, R. O., and T. J. Lyons, 1992: A coupled mesoscale/particle model applied to an urban area. *Atmos. Env.*, **26B**, 279-289. (UNCLASSIFIED)
- Proctor, F. H., 1987: The Terminal Area Simulation System / Volume I: Theoretical Formulation, NASA Contractor Report 4046. (UNCLASSIFIED)
- Pruppacher, H. R., and J. D. Klett, 1978: *Microphysics of Clouds and Precipitation*. D. Reidel, 714 pp. (UNCLASSIFIED)
- Robert, A. J., 1969: The integration of a spectral model of the atmosphere by the implicit method. *Proceedings of WMO/IUGG Symposium on Numerical Weather Prediction*, Tokyo, 1969. (UNCLASSIFIED)
- Rausch, R. D., 1992: Time-Marching Aeroelastic and Spatial Adaptation Procedures on Triangular and Tetrahedral Meshes using an Unstructured-Grid Euler Method. *PhD Dissertation*. Purdue University.(UNCLASSIFIED)
- Sasamori T., 1972: A linear harmonic analysis of atmospheric motion with radiative dissipation. *J. Meteor. Soc. of Japan*. **50**, 505-518. (UNCLASSIFIED)
- Schnack, D. D., I. Lottati, Z. Mikic, and P. Satyanarayana, 1993: MHD simulation on an unstructured, adaptive mesh (abstract). *EOS, Trans. of Am. Geophys., Union* **74**, SH11A-16 (fall meeting). (UNCLASSIFIED)
- Schweitzer, P.N., 1993: *Modern Average Global Sea-Surface Temperature*. CD-ROM, U.S. Geological Survey Digital Data Series DDS-10. (UNCLASSIFIED)
- Sellers, W. D., 1965: *Physical Climatology*, University of Chicago Press, Chicago, 272 pp. (UNCLASSIFIED)
- Sherman, C. A., 1978: A mass-consistent model for wind fields over complex terrain. *J. Appl. Meteor.*, **17**, 312-319. (UNCLASSIFIED)
- Skamarock, W. C., and J. B. Klemp, 1992: Adaptive grid refinement for two-dimensional and three-dimensional nonhydrostatic atmospheric flow. *Mon. Wea. Rev.*, **121**, 788-804. (UNCLASSIFIED)
- Smeda M. S., 1979: Incorporation of planetary boundary layer process into numerical forecasting models. *Boundary-Layer Meteor.*, **16**, 115-129. (UNCLASSIFIED)
- Smolarkiewicz, P. K., 1984: A fully multidimensional positive definite advection transport algorithm with small implicit diffusion. *J. Comput. Phys.*, **54**, 325. (UNCLASSIFIED)
- Smolarkiewicz, P. K., and T. L. Clark, 1986: The multidimensional positive definite advection transport algorithm: Further development and application., *J. Comput. Phys.*, **67**, 396. (UNCLASSIFIED)
- Smolarkiewicz, P. K., and W. W. Gradowski, 1990: The multidimensional positive advection transport algorithm: Nonoscillatory option. *J. Comput. Phys.*, **86**, 355. (UNCLASSIFIED)

- Someshwar Das, U. C. Mohanty, and O. P. Sharma., 1988: Study of Kuo-type cumulus parameterizations during different epochs of the Asian summer monsoon. *Mon. Wea. Rev.*, **116**, 715-729. (UNCLASSIFIED)
- Stackpole, J. D., 1994: The WMO Format for the Storage of Weather Product information and the Exchange of weather Product Messages in Gridded Binary Form. NOAA Technical note number 388. (UNCLASSIFIED)
- Tiedtke, M., 1986: The parameterization of moist processes. Part 2: Parameterization of cumulus convection. ECMWF Lecture Note No. 3.3, 53 pp. (UNCLASSIFIED)
- Uliasz, M., 1990: Development of the Mesoscale Dispersion Modeling System Using Personal Computers Part I: Models and Computer Implementation. *Z. Meteorol.*, **40**, 110-120. (UNCLASSIFIED)
- Walko, R. L., C. J. Tremback, and R.F.A. Hertenstein, 1995: RAMS - The Regional Atmospheric Modeling System: User's guide. Published by MRC/ASTeR, Fort Collins, Colorado. (UNCLASSIFIED)
- Webb, R. S., C. E. Rosenzweig, and E. R. Levine, 1992: A Global Data Set of Soil Particle Size Properties. Digital raster data on a 1-degree geographic (lat/long) 180x360 grid. In: *Global Ecosystems Database Version 1.0: Disc A*. Boulder, CO: NOAA National Geophysical Data Center. Two independent and one derived spatial layer with 65 attributes, on CD-ROM, 16.5 MB. [first published in 1991]. (UNCLASSIFIED)
- Wexler, A., 1977: Vapor pressure formulation for ice. *J. Res. Natl. Bur. Stand.*, **81a**, 5-20. (UNCLASSIFIED)
- Wexler, A., 1976: Vapor pressure formulation for water in the range 0° to 100°C -- A Revision. *J. Res. Natl. Bur. Stand.*, **80a**, p. 775 ff. (UNCLASSIFIED)
- Wisner, C. H., H. D. Orville, and C. Meyers, 1972: A numerical model of a hail-bearing cloud. *J. Atmos. Sci.*, **29**, 1160-1181. (UNCLASSIFIED)
- Zienkiewicz, O.C., 1977: *The Finite Element Method*. 3rd edition, McGraw-Hill. (UNCLASSIFIED)

## DISTRIBUTION LIST

### DEPARTMENT OF DEFENSE

DEFENSE TECHNICAL INFORMATION CENTER  
8725 JOHN J. KINGMAN ROAD, SUITE 0944  
FORT BELVOIR, VA 22060-6218  
ATTN: DTIC/OCP

DEFENSE THREAT REDUCTION AGENCY  
6801 TELEGRAPH ROAD  
ALEXANDRIA, VA 22310-3398  
ATTN: CPW, MAJ T. SMITH  
ATTN: CPWCT  
ATTN: CPWE, D. MYERS  
ATTN: CPWE, MAJ C. WELLS  
ATTN: CPWT, DR L. WITWER

DEFENSE THREAT REDUCTION AGENCY  
ALBUQUERQUE OPERATIONS  
1680 TEXAS ST. SE  
KIRTLAND AFB, NM 87117-5669  
ATTN: CPT-D, DR G. BALADI  
ATTN: CPTO  
ATTN: CPX, LTC D. R. LITTLE

JOINT CHIEFS OF STAFF  
DIRECTOR FOR FORCE STRUCTURE,  
RESOURCES & ASSESSMENT, J-8  
8000 DEFENSE PENTAGON  
WASHINGTON, DC 20318-8000  
ATTN: J8 WAR FIGHTING DIV

### DEPARTMENT OF DEFENSE CONTRACTORS

APPLIED RESEARCH ASSOCIATES, INC.  
4300 SAN MATEO BLVD, NE, SUITE A220  
ALBUQUERQUE, NM 87110-1260  
ATTN: R. NEWELL

ITT INDUSTRIES  
ITT SYSTEMS CORPORATION  
ATTN: AODTRA/DASIAC  
1680 TEXAS STREET, SE  
KIRTLAND AFB, NM 87117-5669  
ATTN: DASIAC  
ATTN: DASIAC/DARE

LOGICON - RDA  
6940 S. KINGS HIGHWAY, SUITE 202  
ALEXANDRIA, VA 22310  
ATTN: R. POPE  
ATTN: T. MAZOLLA

MESO INC.  
185 JORDAN ROAD  
TROY, NY 12180  
ATTN: JOHN ZACK  
ATTN: K. WAIGHT  
ATTN: P. E. PRICE  
ATTN: S. YOUNG

MISSION RESEARCH CORPORATION  
ASTER DIVISION  
2629 REDWING DRIVE, SUITE 310  
FORT COLLINS, CO 80526  
ATTN: C. TREMBACK  
ATTN: M. WEISSBLUTH

MISSION RESEARCH CORPORATION  
P. O. BOX 1257  
HUNTSVILLE, AL 35807  
ATTN: B. BAUER

PACIFIC-SIERRA RESEARCH CORPORATION  
2901 28TH STREET  
SANTA MONICA, CA 90405-2938  
ATTN: H. BRODE

SCIENCE APPLICATIONS INT'L CORPORATION  
2111 EISENHOWER AVENUE, SUITE 303  
ALEXANDRIA, VA 22314  
ATTN: J. COCKAYNE

SCIENCE APPLICATIONS INTL CORP  
10260 CAMPUS POINT DRIVE  
SAN DIEGO, CA 92121-1578  
ATTN: T. JARRETT

SCIENCE APPLICATIONS INT'L CORPORATION  
1100 FIRST AVENUE, SUITE 300  
KING OF PRUSSIA, PA 19406  
ATTN: J. SONTOWSKI

SCIENCE APPLICATIONS INT'L CORPORATION  
2109 AIR PARK ROAD, SE  
ALBUQUERQUE, NM 87106  
ATTN: J. MANSHIP



SCIENCE APPLICATIONS INT'L CORPORATION  
P. O. BOX 1303  
MCLEAN, VA 22102  
ATTN: A. SARMA  
ATTN: C. AGRITELLIS  
ATTN: D. BACON  
ATTN: D. E. MAYS  
ATTN: J. COCKAYNE  
ATTN: J. MCGAGHAN  
ATTN: M. HALL  
ATTN: M. TURNER  
ATTN: N. AHMAD  
ATTN: P. L. R. MADALA  
ATTN: P. LEE  
ATTN: T. J. DUNN

SCIENCE APPLICATIONS INT'L CORPORATION  
P. O. BOX 1303  
MCLEAN, VA 22102  
ATTN: T. WAIT  
ATTN: Y. JIN  
ATTN: Z. BOYBEYI

THE AEROSPACE CORPORATION  
P. O. BOX 92957  
LOS ANGELES, CA 90009  
ATTN: DR M. PLONSKI, MS M8/719

THE TITIAN CORPORATION  
TITAN RESEARCH & TECHNOLOGY DIVISION  
P. O. BOX 2229  
PRINCETON, NJ 08543-2229  
ATTN: I. SYKES

TITAN CORPORATION (THE)  
TITAN RESEARCH & TECHNOLOGY DIVISION  
9410 TOPANGO CANYON BOULEVARD,  
SUITE 104  
CHATSWORTH, CA 91311-5771  
ATTN: R. ENGLAND

TRW S. I. G.  
STRATEGIC SYSTEMS DIVISION  
P. O. BOX 1310  
SAN BERNARDINO, CA 92402-1310  
ATTN: N. LIPNER

VISIDYNE, INC.  
P. O. BOX 1399  
GOLETA, CA 93116-1399  
ATTN: J. DEVORE

## DEPARTMENT OF ENERGY

UNIVERSITY OF CALIFORNIA  
LAWRENCE LIVERMORE NATIONAL  
LABORATORY  
P. O. BOX 808  
LIVERMORE, CA 94551-9900  
ATTN: L-030, A. KUHL

LOS ALAMOS NATIONAL LABORATORY  
P. O. BOX 1663  
LOS ALAMOS, NM 87545  
ATTN: MS J514, A. S. MASON  
ATTN: MS670, J. NORMAN  
ATTN: R. W. WHITAKER, ESS-5MS/F665  
ATTN: WX-1, B. SHAFER

## DEPARTMENT OF THE AIR FORCE

AF WEATHER TECHNICAL LIBRARY  
151 PATTON AVENUE  
ASHEVILLE, NC 28802  
ATTN: K. MARSHALL

HEADQUARTERS  
AIR FORCE SPACE COMMAND  
DIRECTOR OF OPERATIONS  
150 VANDENBERG STREET  
PETERSON AFB, CO 80914-4120  
ATTN: AFSPC/DO

AIR FORCE WEATHER AGENCY/DNXM  
106 PEACEKEEPER DRIVE, SUITE 2N3  
OFFUTT AFB, NE 68113-4039  
ATTN: MAJ R. LEFEVRE

AIR UNIVERSITY LIBRARY  
600 CHENNAULT CIRCLE  
BLDG 1405 - ROOM 160  
MAXWELL AFB, AL 36112-6424  
ATTN: AUL-LSE

HQ USAF/XOWX  
1490 AIR FORCE PENTAGON  
WASHINGTON, DC 20330-1490  
ATTN: XOWX

**DEPARTMENT OF THE ARMY**

DEPARTMENT OF THE ARMY  
DEPUTY CHIEF OF STAFF FOR  
OPERATIONS AND PLANS  
PENTAGON  
WASHINGTON, DC 20310-0460  
ATTN: DAMO-NCZ

US ARMY RESEARCH LABORATORY  
AMSRL-SL-CS E3331  
5101 HOADLEY ROAD  
ABERDEEN PROVING GROUND, MD 21010-5423  
ATTN: SLCBR-SS-T, TECHNICAL LIBRARY

US ARMY RESEARCH LABORATORIES  
2800 POWDER MILL ROAD  
ADELPHI, MD 20783-1197  
ATTN: AMSRL-SL-CE  
ATTN: J. MARTIN  
ATTN: R. CIONCO

COMMANDER  
WEST DESERT TEST CENTER  
ATTN: STEDP-WD-M  
DUGWAY, UT 84022-5000  
ATTN: C. BILTOFT  
ATTN: J. BOWERS

**DEPARTMENT OF THE NAVY**

DEPUTY CHIEF OF NAVAL OPERATIONS  
(PLANS, POLICY & OPERATIONS)  
2000 NAVY PENTAGON ROOM  
ROOM 4E592, N3/N5  
WASHINGTON, DC 20350-2000  
ATTN: BRANCH HEAD, N514

NAVAL RESEARCH LABORATORY  
4555 OVERLOOK AVENUE, SW  
WASHINGTON, DC 20375-5000  
ATTN: CODE 5227, RESEARCH REPORT  
ATTN: S. CHANG

COMMANDER  
NAVAL SURFACE WARFARE CENTER  
DAHLGREN DIVISION  
17320 DAHLGREN ROAD  
DAHLGREN, VA 22448-5000  
ATTN: CODE BSI, T. BAUER